EXPERIMENTAL OBSERVATIONS AND MODELING OF THE SOUTHERN KĀNEʻOHE WATERSHED AND BAY: IMPLICATIONS OF CLIMATE CHANGE ON NUTRIENT EXPORT

A THESIS SUBMITTED TO THE GRADUATE DIVISION OF THE UNIVERSITY OF HAWAIʻI AT MĀNOA IN PARTIAL FULFILLMENT OF THE REQUIREMENTS FOR THE DEGREE OF

MASTER OF SCIENCE

IN

OCEANOGRAPHY

DECEMBER 2016

By

Sara L. Coffey

Thesis Committee:

Eric De Carlo, Chairperson
Fred Mackenzie
Kyle Edwards

Acknowledgements

Many thanks are owed to everyone that helped me complete this thesis. I would like to thank Eric De Carlo and Fred Mackenzie for co-advising me and helping me to pursue a project that coupled geochemistry and my engineering background. Thank you to Kyle Edwards for statistical and modeling help with this thesis, and thank you to Seth Travis for the help with Matlab and troubleshooting code error.

Thank you to the Fall 2013 Oceanography cohort: Kaitlan Prugger, Emma Nuss, Astrid Leitner, Gerianne Terlouw, Seth Travis, and Gabi Weiss. Your friendship and support throughout the past three years has been valued beyond words and I truly appreciate each and every one of you. Thanks for the laughs and entertaining lunch periods.

Thank you to the Ocean office staff and Van Tran for their assistance throughout the past few years. I would also like to acknowledge the financial support for this research provided by the University of Hawai‘i Sea Grant and the NOAA PMEL Carbon Group.

Thank you to all of my friends at Capoeira Senzala and the Honolulu Marathon Clinic for making my life outside of grad school enjoyable. Thank you to my parents for the constant support and encouragement after moving 5,000 miles from home. Finally, thank you to those that inspired me to continue my education in science: Andrew Calderwood, “Kumu” Alex Moore and the entire staff of the Cornell Earth and Environmental Systems field program.

Abstract

Climate change driven impacts on nutrient export of inorganic nitrogen and phosphorous were evaluated in the Southern Kāneʻohe Watershed and Bay, Oahu, Hawaii. Statistical analysis of precipitation, discharge, and suspended sediment and experimental results analyzing nutrient release associated with runoff were synthesized in the formation of a predictive biogeochemical model that analyzed the impacts of climate change on nutrient export. Anticipated changes for the study region were applied as perturbations to the model that analyzed export through the year 2100. These changes include decreasing precipitation, increasing temperature, and rising sea level. Model results suggest that phosphate and nitrate + nitrite export to Southern Kāneʻohe Bay will decrease by 3-13% from year 2015 to 2100, while ammonia export is projected to increase 3-11%. Nutrient limitation or reduction may decrease primary production in the Bay, ultimately limiting its potential for carbon sequestration.

Table of Contents

List of Tables

List of Figures

CHAPTER 1: INTRODUCTION

1.1 Rationale

Throughout the past two centuries, human activities have had a profound impact on the exchange of the bio-essential elements, carbon (C) and the nutrients nitrogen (N) and phosphorous (P), between the land, atmosphere, and the aquatic environment (Mackenzie et al., 2011; Regnier et al., 2013). This topic is of growing interest to scientists and the public alike due to the environmental concerns related to the enhanced greenhouse effect and complications that may arise from continued emissions of greenhouse gases through fossil fuel combustion and land-use activities. A growing population, the persistence of detrimental industrial, transportation and agricultural activities of humankind, and continued development of previously non-industrialized nations will continue to impact biogeochemical cycles (e.g., Mackenzie et al. 1993); therefore, it is important to analyze the effects of anthropogenic intervention on natural biogeochemical cycles and on global climate change.

Studying nutrient cycling is often challenging. This arises in part because it is necessary to distinguish between anthropogenic perturbations and natural transfers within the cycles of biogeochemically important elements, as well as predict future changes. As a well-studied region in Hawaii, the Kāneʻohe watershed and southern portion of Kāneʻohe Bay are an ideal ecosystem in which to model how interactions between the watershed and coastal ocean affect C-N-P cycles and dynamics using data from past and current studies. Experimental work and statistical analysis will also be performed to develop the model, as discussed in this thesis.

1.2 Site Description

The Kāneʻohe Bay watershed is located on the windward side of Oahu and is bound by the Ko'olau Mountains and Kāneʻohe Bay (Figure 1.1). The watershed spans an area of 97km^2 with 9 major perennial streams that carry surface runoff from the watershed to Kāneʻohe Bay (Smith et al., 1981). Approximately 13 km long by 4 km wide, the sheltered embayment hosts a variety of topographical features, watersheds, and marine geomorphic zones (Lowe, 2009).

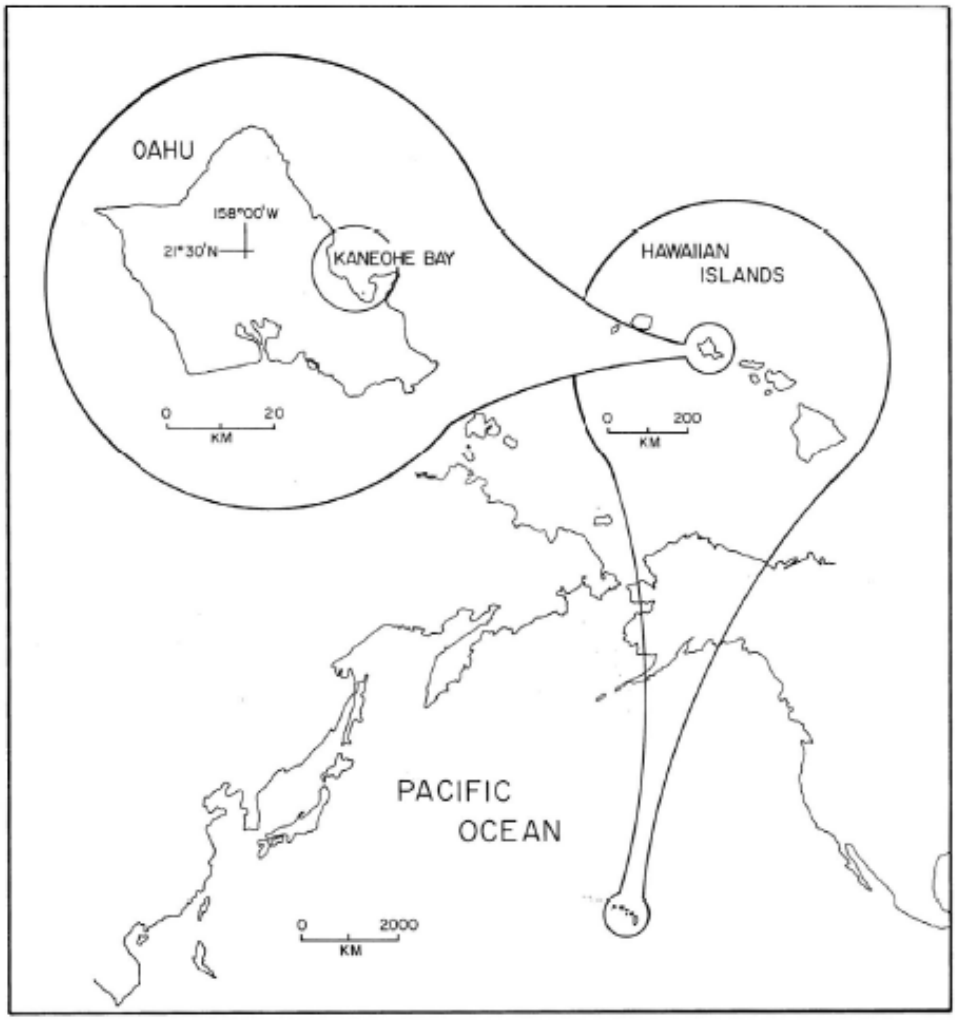

Figure 1.1: Study Location (Smith et al., 1981).

Kāneʻohe, Ahuimanu, and Waiahole are the primary streams draining into Kāneʻohe Bay. Waiahole Stream is located in the northern portion of the overall Kāneʻohe Bay watershed and feeds into the Northern portion of the Bay. Ahuimanu Stream is located in the central region, while Kāneʻohe Stream is the major stream draining into the southern portion of the Bay. This study focused specifically on the highly populated and urbanized Southern Kāneʻohe Watershed and the 8.37 km^2 semi-enclosed Southern portion of Kāneʻohe Bay.

The southeastern portion of the Bay is sheltered by Coconut Island and is bound by large reef areas that inhibit water circulation in this part of the Bay compared to the open and channelized northern portion of the Bay. While transport of seawater into the Bay is governed predominately by wave action, circulation patterns within the Bay are controlled by the bathymetry, evaporation, precipitation, and stream runoff and driven by the wind, with minor effects from tides (Jokiel 1993; Drupp et al. 2011).

Precipitation in the watershed varies as a function of location and time, with prevailing winds playing a large role in precipitation patterns. During the dry season (May-September), Northeast trade winds prevail causing orographic showers from the lifting and cooling of onshore air masses moving inland against the Koʻolau mountain range (Kinzie III et al., 2001). The wet season (October-April) is characterized by more frequent southerly (Kona) winds that cause intermittent storms. El Niño Southern Oscillation (ENSO) can also strongly impact annual variability in precipitation (Juvik and Juvik, 1998). Constant northeast trade winds encourage mixing within the Bay, especially when winter storms are present. However, stratification can occur during times of increased temperatures and low wind speeds (Smith et al 1981). Variation

in rainfall coupled with the steep topography of the Ko'olau mountains leads to large variations in watershed streamflow. USGS gage data analysis (Station 16272200) shows that within the Kāne'ohe Watershed, stream discharge can vary between 0.01 m^3/sec under base flow and over 100 m^3/sec under storm conditions.

Storms are responsible for transporting the majority of the sediment load that enters Kāne'ohe Bay, and stream runoff acts as a major source of nutrients to the coastal zone (Hoover and Mackenzie, 2009; De Carlo et al., 2007). Nutrient inputs via streams are vital to primary production within estuaries and coastal zones like Kāne'ohe Bay. The concentration and ratio of nutrients in a coastal region control primary production to a significant extent, in addition to the availability of light and other factors. Marine phytoplankton cells typically are composed of nitrogen and phosphorous in a molar 16:1 ratio (Redfield et al., 1934). However, stream nutrient export resulting from storms can increase the N:P water discharge ratio to values as high as 48, increasing phytoplankton growth and changing the limiting nutrient for primary production from N to P (Ringuet and Mackenzie, 2005; Drupp et al., 2011). Increased primary production can temporarily reduce pCO_2 and lead to a switch in the direction of the air-sea flux of CO_2. Nutrient inputs and sediment loading can also have adverse impacts on water quality such as eutrophication. This is of concern since estuarine environments, such as Kāne'ohe Bay, are highly productive ecosystems accounting for high concentrations of organic carbon capable of sequestering anthropogenic carbon (Ringuet and Mackenzie, 2005).

1.3 Research Hypotheses and Objectives

The purpose of this research is to do the following:

1) Determine primary nutrient reservoirs and fluxes within the Southern Kāne'ohe Bay and Watershed.
2) Determine relationships between precipitation, discharge, and suspended sediment within the study region. Use statistical analysis to develop a steady-state water and suspended sediment balance.
3) Experimentally determine nutrient uptake or release when suspended sediment reacts with fresh and marine waters.
4) Create a steady state model and force it with predicted temperature, precipitation and sea level rise to estimate the impact of climate change on nutrient export through 2100.

Changes in climate have been observed throughout Oahu over the past century including increases in atmospheric and oceanic temperature and CO_2, sea level rise, and a decrease in precipitation, runoff, and stream flow (IPCC FAR Annex I). This research will analyze the past, present, and future nutrient cycling of the Southern Kāne'ohe Bay region and proximal marine waters through the use of a mathematical biogeochemical model. Experimental results that evaluate nutrient uptake or release that occurs when suspended sediment reacts with fresh and marine waters as well as statistical relationships evaluating the relationships between precipitation, discharge, and suspended sediment will be added as inputs. The model will

describe the physical, chemical, and biological processes that affect the elements N and P and their coupled interactions and cycles.

While estimates vary, the latest Intergovernmental Panel on Climate Change (IPCC) report provides regional projections for rainfall across the planet under various scenarios. These suggest that precipitation will decrease 5-15% in Hawaii over the next 75 years (IPCC FAR Annex I). It is anticipated that by combining mathematical modeling with laboratory experimental work, projections will be made that may aid in determining how nutrient cycling throughout the Kāneʻohe Bay watershed and nearshore marine waters will change as a result of the IPCC predicted change in precipitation and temperature, which presumably will influence riverine water and sediment discharge into southern Kāneʻohe Bay.

A series of hypotheses were formulated to address the research goals. The following null hypotheses that are expected to be falsified will be tested:

1) There is no empirical relationship between total daily precipitation and mean daily water discharge for the Southern Kāneʻohe Bay watershed.

   When testing Hypothesis 1, it is expected that as mean annual precipitation decreases in the Southern Kāneʻohe Bay watershed, mean annual discharge will consequently decrease. There will likely be separate empirical relationships to address baseline precipitation conditions consisting of light rain and storm events.

2) There is no empirical relationship between mean daily water discharge and mean daily suspended sediment discharge for the Southern Kāneʻohe Bay watershed.

When testing Hypothesis 2, it is expected that as mean annual water discharge decreases in the Southern Kāneʻohe Bay watershed, mean annual suspended sediment discharge to the proximal coastal zone will consequently decrease. There will likely be separate empirical relationships to address baseline precipitation conditions and storm events.

3) There will be no release of N and P from terrestrial suspended matter entering the coastal ocean.

When testing Hypothesis 3, it is anticipated that there will be a release of nitrogen and phosphorous from terrestrial suspended matter entering the coastal ocean. Fluxes of terrestrially derived particulate organic matter and inorganic N and P into the coastal region of Southern Kāneʻohe Bay will decrease with climate change. It is also contended that proportionally more N will be released into Southern Kāneʻohe Bay through desorption from the suspended sediment riverine load than P, and that N will desorb at a faster rate, as seen in prior work by De Carlo and Dollar and discussed in Chapter 4 (Tech Report,1995).

The working hypothesis of this study is that:

4) As precipitation decreases due to climate change, a lower sediment load to Southern Kāneʻohe Bay will lead to a lesser release of inorganic nutrients from the suspended sediment riverine load.

By coupling the experimental work and statistical models with the mathematical model, it will be possible to quantify the impact of future climate change on nutrient fluxes to the proximal marine waters of Southern Kāneʻohe Bay thereby allowing the testing of Hypothesis 4. It is anticipated that as precipitation in Hawaii decreases as a result of predicted climate change, fewer inorganic nutrients will be released into Southern Kāneʻohe Bay from the suspended sediment riverine load.

Literature Cited:

De Carlo, E.H. and Dollar, S. (1995) Assessment of Suspended Solids and Particulate Nutrient Loading to Surface Runoff and the Coastal Ocean in the Honokowai Drainage Basin, Lahaina District, Maui. Final report to NOAA Algal Blooms Program.

De Carlo, E.H., Hoover, D.J., Young, C.W., Hoover, R.S., Mackenzie, F.T. (2007) Impact of storm runoff from subtropical watersheds on coastal water quality and productivity. Applied Geochemistry 22: 1777–1797.

Drupp, P., DeCarlo, E.H., Mackenzie, F.T., Bienfang, P., & Sabine, C.L. (2011) Nutrient inputs, phytoplankton response, and CO2 variations in a semi-enclosed subtropical embayment, Kāneʻohe Bay, Hawaii. Aquatic Geochemistry, 17, 473-498.

Hoover, D.J., Mackenzie, F.T. (2009) Fluvial Fluxes of Water, Suspended Particulate Matter, and Nutrients and Potential Impacts on Tropical Coastal Water Biogeochemistry: Oahu, Hawaiʻi. Aquat. Geochemistry 15: 547–570.

IPCC. (2013) Annex I: Atlas of Global and Regional Climate Projections [van Oldenborgh, G.J., M. Collins, J. Arblaster, J.H. Christensen, J. Marotzke, S.B. Power, M. Rummukainen and T. Zhou (eds.)]. In: Climate Change 2013: The Physical Science Basis. Contribution of Working Group I to the Fifth Assessment Report of the Intergovernmental Panel on Climate Change [Stocker, T.F., D. Qin, G.-K. Plattner, M. Tignor, S.K. Allen, J. Boschung, A. Nauels, Y. Xia, V. Bex and P.M. Midgley (eds.)]. Cambridge University Press, Cambridge, United Kingdom and New York, NY, USA.

Jokiel, P.L. (1993) Jokiel's Illustrated Scientific Guide to Kane'ohe Bay, O'ahu. Hawaii Institute of Marine Biology, 65 pp.

Juvik, S.P. and J.O. Juvik (1998) Atlas of Hawaii. Honolulu, University of Hawaii Press.

Kinzie III, R.A., Mackenzie, F.T., Smith, S.V. and Stimson, J. (2001) CISNet: Linkages between a tropical watershed and reef ecosystems. Project 98-NCERQA, NOAA, 23 pp.

Lowe, R. J., Falter, J. L., Monismith, S. G., & Atkinson, M. J. (2009) Wave-driven circulation of a coastal reef-lagoon system. *Journal of Physical Oceanography,* 39(4), 873-893.

Mackenzie, F.T. (2003) Our Changing Planet. Prentice-Hall. Upper Saddle River, NJ.

Mackenzie, F.T., De Carlo E.H, Lerman, A. (2011) Coupled C, N, P, and O Biogeochemical Cycling at the Land-Ocean Interface. In: Wolanski E and McLusky DS (eds.) Treatise on Estuarine and Coastal Sciences, Vol 5, Waltham: Academic Press, 317-342.

Mackenzie, F. T., Ver, L. M., Sabine, C., Lane, M., and Lerman, A., (1993) C, N, P, S biogeochemical cycles and global change. In: Interactions of C, N, P, and S Biogeochemical Cycles and Global Change, R. Wollast, F. T. Mackenzie, and L. Chou, eds., Springer-Verlag, Berlin, 1-61.

Redfield, A. (1934) On the proportions of organic derivatives in seawater and their relation to the composition of plankton.pdf. In: Daniel RJ (ed) James Johnstone Memorial Volume. University Press of Liverpool, pp 176–192.

Regnier et al. (2013) Anthropogenic perturbation of the carbon fluxes from land to ocean. Nature Geoscience, 6, 597-607, doi:10.1038/ngeo1830.

Ringuet S, Mackenzie F.T. (2005) Controls on nutrient and phytoplankton dynamics during normal flow and storm runoff conditions, Southern Kāneʻohe Bay, Hawaiʻi. Estuaries 28:327–337.

Shea, E.L., Dolcemascolo, G., Anderson, C.L., Barnston, A., Guard, C.P., Hamnett, M.P., Kubota, S.T., Lewis, N., Loschnigg, J., and G. Meehl (2001) *Preparing for a changing climate. The potential consequences of climate variability and change.* A report of the Pacific Islands Regional Assessment Group. East-West Center. 102pp.

Smith, S.V., W.J. Kimmerer, E.A. Laws, R.E. Brock, and T.M. Walsh (1981) Kāneʻohe Bay sewage diversion experiment: Perspectives on ecosystem responses to nutritional perturbation. Pacific Science 35: 279-395.

CHAPTER 2: METHODS

2.1 Field Methods

To address Hypothesis 3, nutrient release experiments were performed in the laboratory to evaluate the potential for release or uptake of nutrients when particulate materials enter surface waters. The soil map shown in Figure 2.1 (Ristvet, 1978) indicates that the Southern Kāneʻohe Watershed is primarily comprised of Lolekaʻa silty clay soil (Lo soil); however, Hanalei silty clay (Hn soil) and Kāneʻohe silty clay (Kg soil) soil types are also present.

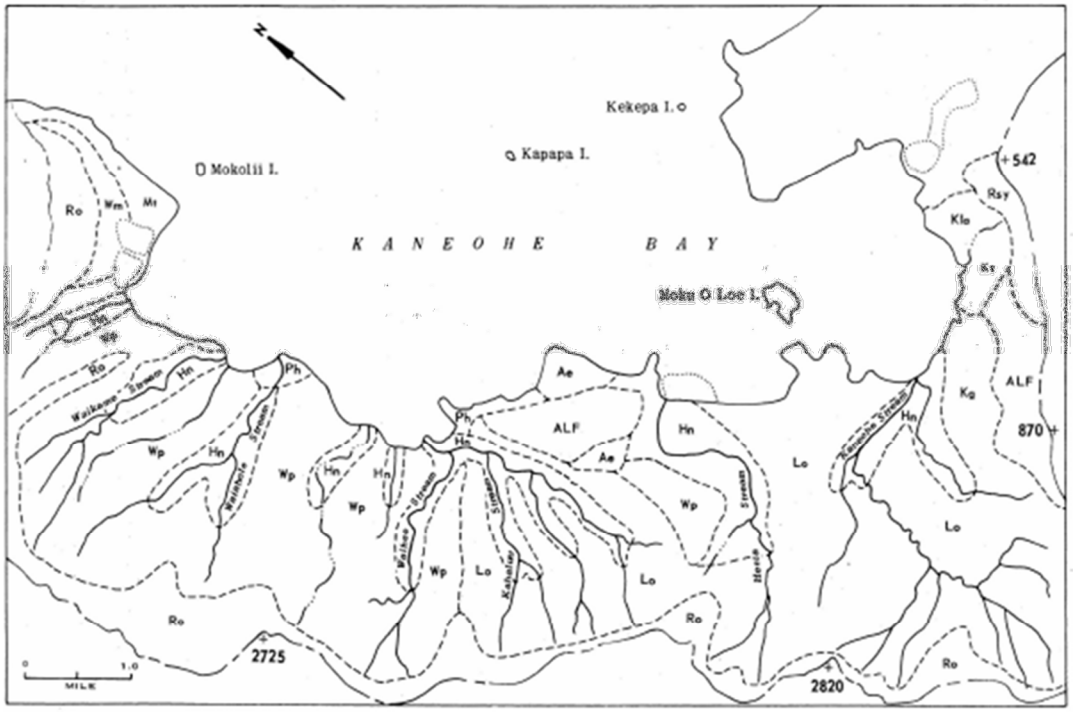

Figure 2.1: Soil types of the Kāneʻohe Bay watershed (Ristvet, 1978. Originally adapted from Foote et al., 1972).

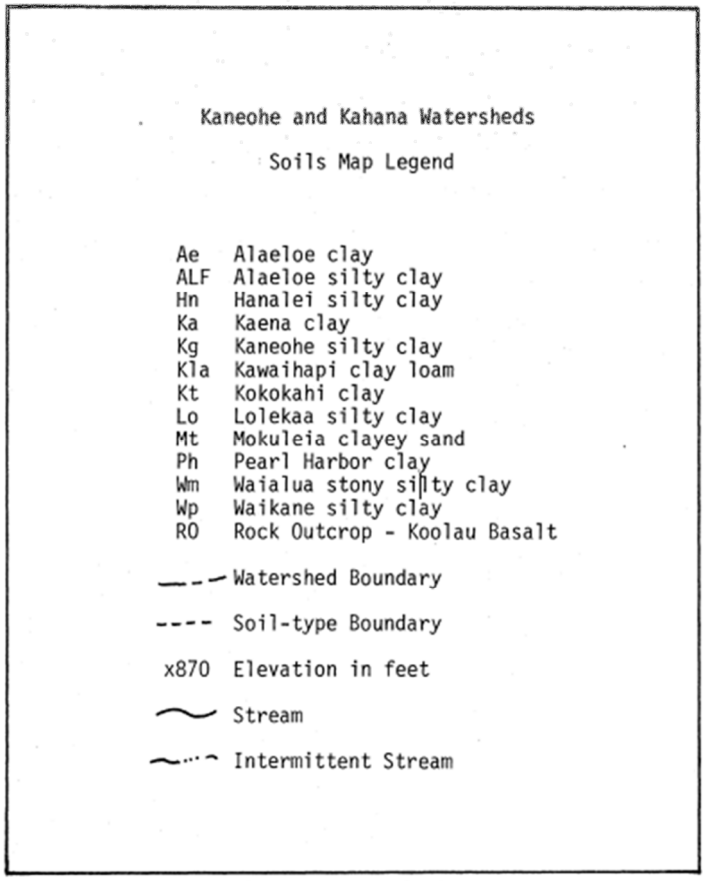

Figure 2.2B: Corresponding legend to Figure 2.1 (Ristvet, 1978. Originally adapted from Foote et al., 1972).

Samples of all three soil types were collected for laboratory analysis by collecting one gallon-sized bag of surficial soil in each region. Coordinates for each soil collection site are listed in Table 2.1 and shown graphically in Figure 2.2. Stream bed sediments, Luluku Stream water, and seawater were also collected from the Southern Kāneʻohe Bay region with locations also listed in Table 2.1 and displayed in Figure 2.2. Lo soil was collected adjacent to Luluku stream near USGS site 16270900, Hn soil was collected adjacent to Kāneʻohe Stream and Kāneʻohe Bay, and Kg soil was collected next to the Kokokahi YWCA along the shore. Stream

sediment and stream water were collected from Luluku Stream adjacent to the USGS site, and seawater was collected from the Coconut Island seawater intake pipe.

Table 2.1: GPS coordinates of collection sites for laboratory work.

Collection Site Locations	Latitude (N)	Longitude (W)
USGS site 16270900 (Stream water collection site + Lo Soil Collection Site)	21°23'42"	157°48'44"
Coconut Island seawater intake pipe (Seawater collection site)	21°26'00"	157°47'12"
Kg Soil Collection site	21°24'39"	157°46'44"
Hn Soil Collection site	21°24'39"	157°47'8"

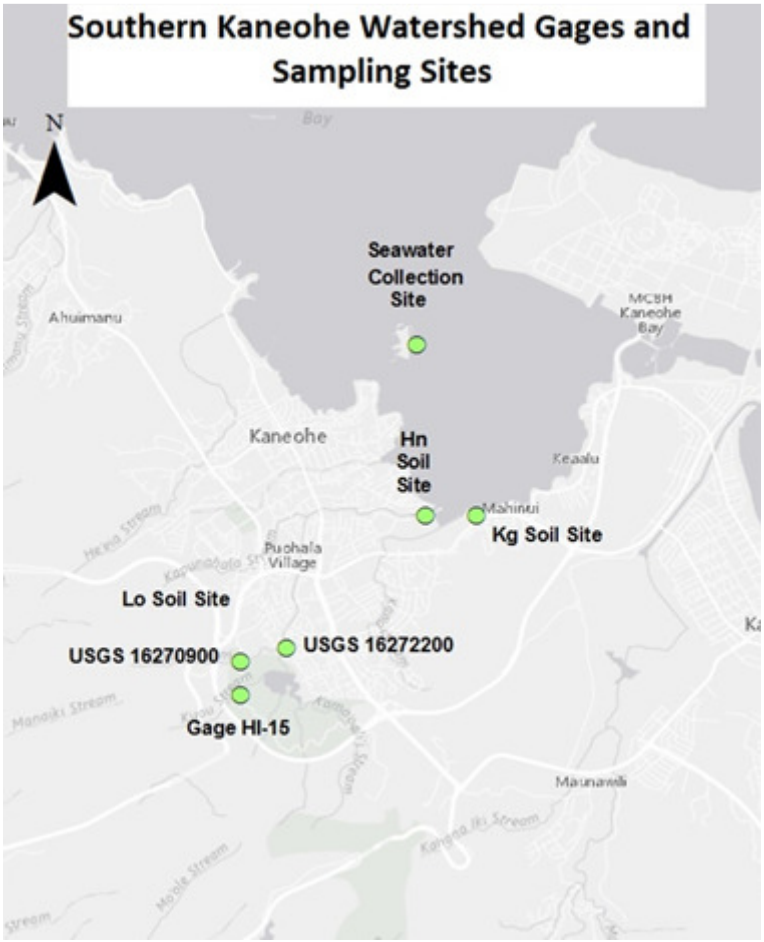

Figure 2.2: Locations of soil, sediment, marine and stream water sampling sites in Southern Kāne‘ohe Bay.

2.2 Laboratory Methods

The surficial soils and sediment were placed in separate plastic tubs to air dry at room temperature in the laboratory for a week before further analysis. Once dry, the soil and sediment were sieved and separated into various size fractions (<75 µm, 75-355 µm, 355 µm-2mm, and >2mm). The soil and sediment were then sterilized in the oven for 24 hours at 110 °C to inhibit biological activity from altering the soil throughout the course of the experiments. Seawater and stream water were collected in 20 L carboys and poisoned by addition of a saturated $HgCl_2$ solution and then filtered through a 0.2 µm membrane into separate acid-cleaned carboys. After experiment 19 the protocol was changed so that seawater and stream water were collected immediately before experimentation rather than filtering and poisoning the water. This modification is thought to simulate better natural stream and sea conditions.

A series of nutrient release experiments was conducted with water of varying salinities and concentrations of suspended particles shown in Figure 2.3.

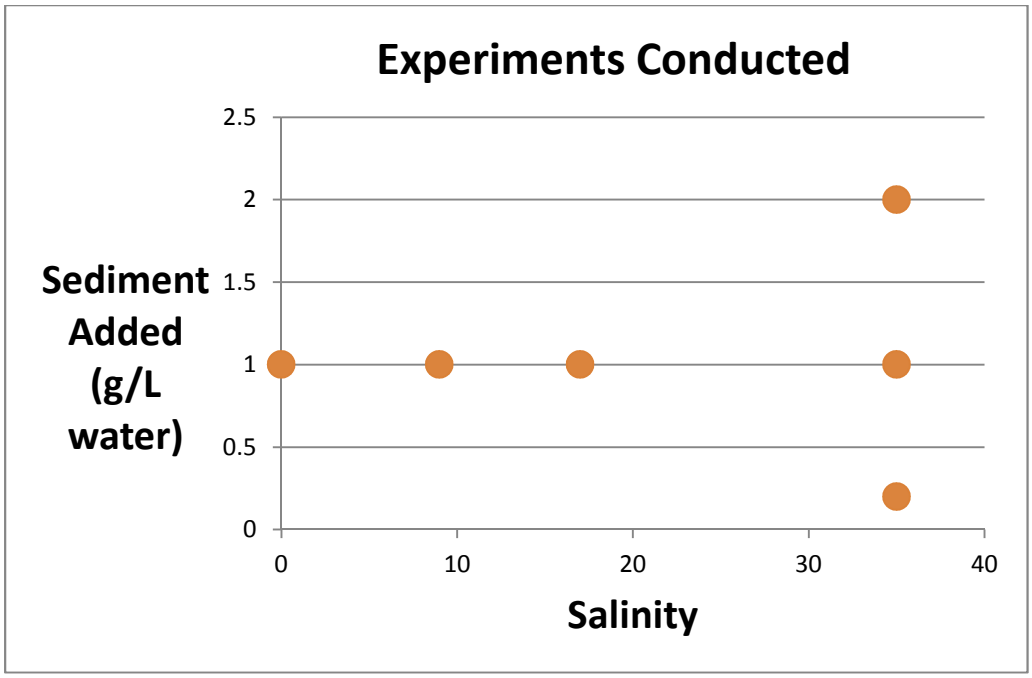

Figure 2.3: Experimental conditions analyzed.

The Lo soil type was used for all experiments since the watershed primarily consists of this soil type. These experiments were conducted in either pure stream water or pure seawater, and in mixtures of 75% stream water/25% seawater and 50% stream water/50% seawater. Most experiments were conducted with a suspended particle concentration of 1 g/L using the <75 µm fraction of the soil. Additional experiments were conducted in pure seawater with a varying suspended particle load of 2g/L and 0.2 g/L. During the experiments, the soil or sediment sample was mixed with 1 L of solution and stirred continuously to maintain the particulate matter in suspension for the duration of the experiment and to simulate stream water mixing with seawater in a near shore zone such as Southern Kāneʻohe Bay. The <75 µm size was selected because small particles exhibit a larger surface area to volume ratio and remain in suspension longer than coarser particles (Sposito, 2008; De Carlo and Dollar, Tech Report, 1995), therefore are most likely to react with seawater.

Experiments were carried out in a jacketed reactor with temperature kept constant at 25 °C with a recirculating water bath. Forty-milliliter aliquots of the experimental fluid (suspended particles + water) were collected with a syringe and filtered through a 0.2 µm membrane into 60 mL Nalgene bottles at predetermined time intervals of approximately 1, 3, 7, 15, 30 minutes and 1, 2, 4, 8, 12, 24 and 72 hours. The original solution with no particles was also collected before the start of each experiment.

A Thermo Scientific Orion Star A214 pH Meter was calibrated according to manufacturer's specifications using National Institute of Standards and Technology (NIST) buffers and was used to record pH every five minutes for the first hour of each experiment and at each sample collection time interval thereafter. Buffers were not used in order to simulare natural conditions. Duplicates of each experiment were conducted and filtered water samples were stored in the freezer until they were analyzed for phosphate, silicate, ammonia, and nitrate + nitrite (N+N). All labware and sampling bottles were acid cleaned in a 10% HCl solution and rinsed thoroughly with (18 M Ω-cm) deionized water.

Nutrient concentrations were determined on a Seal Analytical AA3 HR Nutrient Autoanalyzer in the SOEST Laboratory for Analytical Biogeochemistry. This instrument simultaneously measures dissolved inorganic nitrate, nitrite, ammonium, phosphate and silicate. Ammonium was measured fluorometrically following the method of Kerouel and Aminot (1997) that involves reacting the sample with o-phthalaldehyde (OPA) using a borate buffer and sodium sulfite to form a fluorescent species in a quantity proportional to the ammonium concentration (S-LAB website).

The concentrations of nitrate and nitrite were determined colorimetrically following methods described by Armstrong et al (1967) and Grasshoff (1983). Nitrate to nitrite reduction occurs through the use of a copper-cadmium reductor column followed by reaction with sulfanilamide to form a diazo compound. The compound couples with N-1-naphthylethylene diamine dihydrochloride to form a purple azo dye, and the absorption of the solution is measured at 550 nm.

Silicate concentrations were determined colorimetrically following the Grashoff and Kremling (1983) protocol. Ascorbic acid is used to reduce silicomolybdate in acidic solution to molybdenum with the absorbance of the solution measured at 820 nm.

The colorimetric protocol described by Murphy and Riley (1962) was used for the determination of orthophosphate. The reaction of orthophosphate, molybdate ion and antimony ion, followed by ascorbic acid reduction, creates a blue color, the absorbance of which can be determined at 880 nm.

Samples of all three soil types were sent to the Agricultural Diagnostic Service Center at the University of Hawai‘i at Mānoa to analyze for the following: pH, %N, %C, P, K, Ca, Mg, Nitrate, and Ammonium.

Soil particle size analysis was performed on all three soil types by sieving each soil into the following size fractions in mm: >2, 2-1.651, 1.651-1, 1-0.495, 0.495-0.351, 0.351-0.075, 0.075-0.0625, 0.0625-0.045. The decantation protocol outlined by Krumbein et al. (1988) was used to further separate the smaller size fractions of the soils (0.045-0.0156 mm, 0.0156-0.0078 mm, 0.0078-0.0039 mm, 0.0039-0.00195 mm, <0.00195 mm). Mean, median, kurtosis, and

skewness calculations were made for each soil type also following the Krumbein et al. (1988) protocol.

2.3 Modeling Methods

To address Hypothesis 1, a statistical model was created using the software R for statistical computing and graphical techniques. The model was constructed to determine if there is an empirical relationship between total daily precipitation and mean daily water discharge for the Southern Kāneʻohe Bay watershed, and what that relationship may be. Daily precipitation and discharge data collected from July 1994 to October 2005 were utilized. The precipitation data were obtained from the Hawaiʻi Archived Hydronet Data (http://www.prh.noaa.gov/hnl/hydro/hydronet/hydronet-data.php). For the purposes of this study, Gage "HI-15 Luluku" was used, as shown in Figure 2.2. Each station recorded precipitation measurements over 15 minute intervals; total daily precipitation values were obtained by subtracting the initial daily gage value from the final daily value. Discharge data were obtained from the USGS National Water Information System Mapper. Site Number 16272200 at Kamoʻoaliʻi Stream below Luluku Stream was used with mean daily surface water discharge reported in ft^3/sec. Table 2.2 lists the GPS coordinates of Site 16272200 and Gage "HI-15 Luluku."

Table 2.2: GPS coordinates of gages used for modeling purposes.

Gage locations	**Lat (N)**	**Long (W)**
Gage HI-15 Luluku (precipitation measurements location)	21°23'14.3"	157°48'35.3"
USGS Site Number 16272200 (discharge/suspended sediment data location)	21°23'36.2"	157°48'13.5"

A time series analysis was completed to assess major trends and periods of variability to determine what the empirical relationship is between precipitation and discharge.

Initially, a histogram of the discharge data was created to investigate the distributional properties of the response variable. A Shapiro test and density plot of the data disproved the null hypothesis that the discharge data are normally distributed. A lognormal error distribution was assumed since the data are highly skewed and constrained to be greater than or equal to zero. A generalized additive model (GAM) in the mgcv (Mixed GAM Computation Vehicle with GCV/AIC/REML Smoothness Estimation) package (Wood, 2011) was used initially to investigate the shape of the curve representing the relationship between precipitation and discharge. This is ideal methodology since a GAM can fit an arbitrary smooth function between a predictor and a response; however, a parametric function is preferred for its predictive capabilities to be applied to the biogeochemical model. A series of parametric fit approaches were additionally investigated including: generalized linear model (glm), linear model (lm), and a series of functions including: sigmoid, linear, exponential, and monomolecular using mle2 in the bblme package.

To address Hypothesis 2, another statistical model was created using R software to determine if there is an empirical relationship between mean annual water discharge and mean annual suspended sediment discharge, and what that relationship may be. Daily data from the USGS National Water Information System Mapper Site Number 1627220 ranging from November of 1976 to September of 1998 were utilized for this analysis.

Similar to Hypothesis 1, a histogram was made of the suspended sediment data to investigate the distributional properties of the response variable. A Shapiro test and density

plot of the data disproved the null hypothesis that the discharge data are normally distributed; rather, the data reflect a lognormal distribution. A GAM was first used to analyze the relationship between discharge and suspended sediment. A series of parametric fit approaches were then investigated including: glm, lm, cubic log-log polynomial, 4th order log-log polynomial, 5th order log-log polynomial, Modified Power, Exponential and Power functions.

To address Hypothesis 4, parameters that describe the reservoirs and fluxes comprising the biogeochemical cycles of inorganic nitrogen and phosphorous in the Southern Kāne'ohe Bay watershed surface environment and proximal coastal zone were first established. Diagrams of the processes impacting the water balance and suspended sediment balance are shown in Figures 2.4 and 2.5.

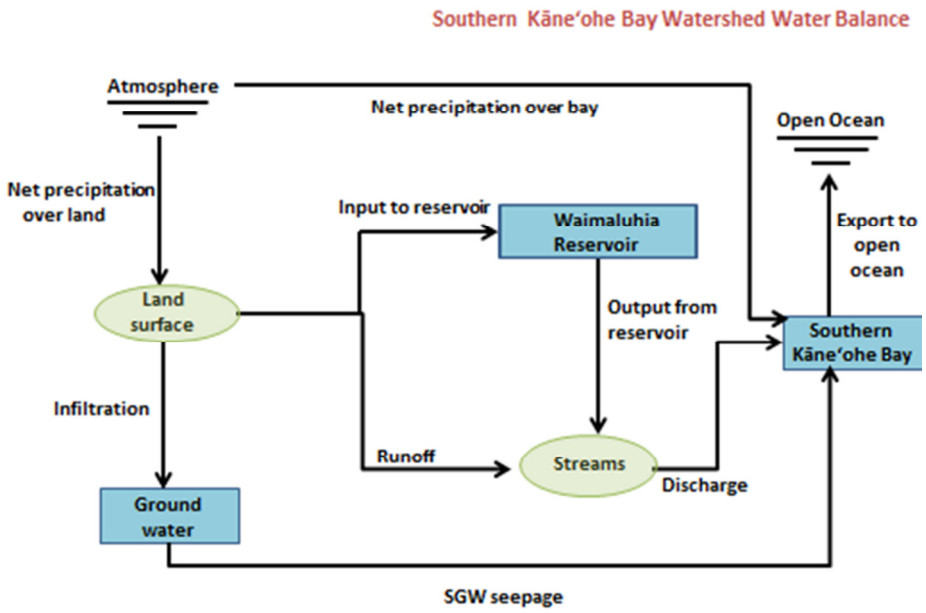

Figure 2.4: Schematic diagram of the conceptual water model of inorganic nitrogen and phosphorous for the Kāne'ohe Bay watershed and adjacent proximal marine coastal waters. Squares represent reservoirs, ovals represent transfer points, stacked lines represent sources and sinks, and arrows represent fluxes.

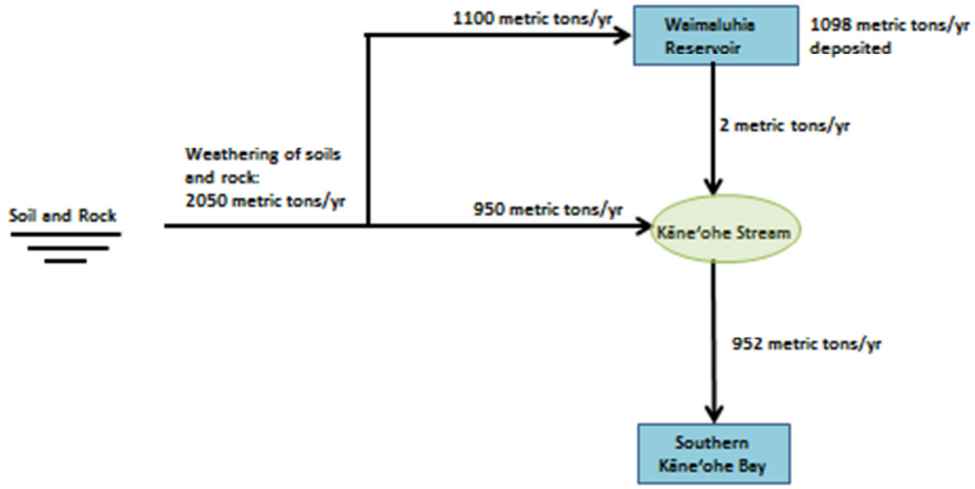

Figure 2.5: Schematic diagram of the conceptual suspended sediment model of inorganic nitrogen, and phosphorous for the Kāne'ohe Bay watershed and adjacent proximal marine coastal waters. Squares represent reservoirs, ovals represent transfer points, stacked lines represent sources, and arrows represent fluxes.

Previous studies of the Kāne'ohe Watershed, USGS gage data, and experimental work from this study were consulted to determine reservoir sizes and fluxes at the initial steady state condition for both the water and suspended sediment balance as discussed in Chapter 5. Once steady state balances were complete for the suspended sediment and water models, a combined water-suspended sediment biogeochemical box model of the Southern Kāne'ohe Watershed was formulated (Figure 2.6). The model was developed and run in MATLAB initially at steady state, and then run again using atmospheric CO_2 concentration as a proxy for temperature and precipitation as forcings to perturb the system. The Representative Concentration Pathway (RCP) emissions scenarios developed for the Intergovernmental Panel on Climate Change (IPCC) 5th Assessment Report were applied to the model in order to evaluate

how the Southern Kāne‘ohe Bay watershed and adjacent coastal marine waters will respond to variations in temperature and flow under future climate change scenarios.

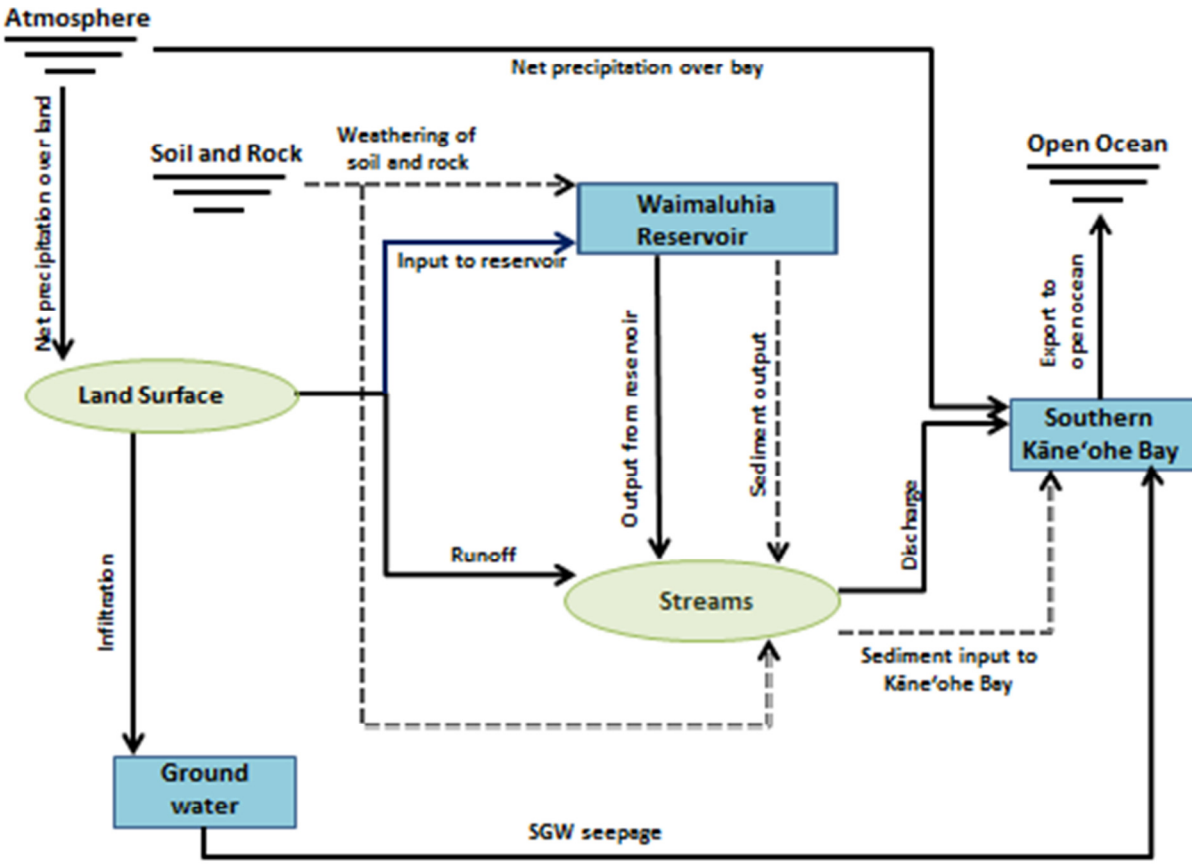

Figure 2.6: Schematic diagram of the conceptual combined water and suspended sediment model of inorganic nitrogen and phosphorous for the Kāne‘ohe Bay watershed and adjacent proximal marine coastal waters. Squares represent reservoirs, ovals represent transfer points, stacked lines represent sources and sinks, and arrows represent fluxes. Solid arrows represent water transfer and dashed arrows represent sediment transfer.

Literature Cited:

Armstrong, F.A.J., Sterns, C.R. and Strickland, J.D.H. (1967) The measurement of upwelling and subsequent biological processes by means of the Technicon AutoAnalyzer and associated equipment. *Deep Sea Res. 14, 381-389.*

De Carlo, E.H., and Dollar, S. (1995) Assessment of Suspended Solids and Particulate Nutrient Loading to Surface Runoff and the Coastal Ocean in the Honokowai Drainage Basin, Lahaina District, Maui.

Foote, D.E., Hill, E.l., Sakuichi, N. and Stephens, F. (1972) Soil survey of the islands of Kaui, Oahu, Maui, Molokai and lanai, State of Hawai'i. U.S. Dept. of Agriculture, Soil Conservation Service, U.S. Govt. Printing Office, Washington, D.C.: 232pp.

Grasshoff K., Ehrhardt M., and Kremling K. (1983) Methods of Seawater Analysis, second revised and extended edition.

Kerouel, R. and Aminot, A. (1997) Fluorometric determination of ammonia in sea and estuarine waters by direct segmented flow analysis. Marine Chemistry Vol. 57, no. 3-4, pp. 265-275.

Krumbein, W.C. and Pettijohn F.J. (1988) Manual of Sedimentary Petrography. SEPM Classic Facsimile Edition of the 1938 original; SEPM Reprint Series. Tulsa: Society for Economic Paleontologists and Mineralogists (SEPM)

Murphy J. and Riley I. P. (1962) A modified single solution method for the determination of phosphate in natural waters. Anal. Chim. Acta 27:31-6.

Ristvet, Byron L. (1978) Reverse Weathering Reactions within Recent Nearshore Marine Sediments, Kāne'ohe Bay, Oahu. Chicago: Northwestern University.

Wood, S.N. (2011) Fast stable restricted maximum likelihood and marginal likelihood estimation of semiparametric generalized linear models. Journal of the Royal Statistical Society (B) 73(1):3-36.

Chapter 3: Statistical Analysis of Rainfall, Discharge and Suspended Sediment Trends in the Kāneʻohe Watershed

3.1 Introduction

The primary goal of this thesis is to analyze the past, present, and predict future nutrient cycling of the Southern Kāneʻohe Bay watershed and proximal marine waters through the use of a mathematical biogeochemical model. In order to do this, it was first necessary to test the following null hypotheses:

1) There is no empirical relationship between total daily precipitation and mean daily water discharge for the Southern Kāneʻohe Bay watershed.
2) There is no empirical relationship between mean daily water discharge and mean daily suspended sediment discharge for the Southern Kāneʻohe Bay watershed.

The first hypothesis was addressed using Hawaiʻi Archived Hydronet Data (Gage 15 at Luluku Stream) for precipitation values in inches and USGS data (Station 16272200 at Kamooalii Stream below Luluku Stream) for discharge values in cubic feet per second. Average daily values were used for each data set for the overlapping time period of July 1994-October 2005.

The second hypothesis was addressed using data from the aforementioned USGS gage for daily mean discharge in cubic feet per second and suspended sediment discharge in tons per day. Average daily values were used for data from November 1976- September 1998.

A generalized additive model (GAM) in the mgcv (Mixed GAM Computation Vehicle with GCV/AIC/REML Smoothness Estimation) package was used initially to investigate the shape of

the curve representing the relationship between precipitation and discharge and discharge and suspended sediment. This is ideal since GAMs make no assumptions about the relationship between the predictor and response variables; however, parametric functions are preferred for predictive modeling because GAM models do not have extrapolative capabilities. A series of parametric fits was investigated for Hypothesis 1 and Hypothesis 2 to determine the most accurate model for each data set.

3.2 Results

Hypothesis 1

Parametric models were fit using maximum likelihood estimation and evaluated in terms of Akaike Information Criterion (AIC) and root mean square error (RMSE). AIC is used to select the model that provides the best predictive performance, and RMSE is reported to quantify the typical error between predictions and observed values. Smaller numbers indicate better model performance. Model results were presented in ∂AIC, where ∂AIC = model AIC – lowest model AIC value. Linear, exponential, monomolecular and sigmoid parametric functions were investigated to fit the precipitation-discharge data set. Based on visual assessment of residuals, the assumption was made that the data were log-normally distributed.

Model type, function equation, ∂AIC and RMSE values are presented in Table 3.1. A visual comparison is provided in Figure 3.1.

Table 3.1: AIC and RMSE value model comparison for precipitation-discharge relationship. The most accurate model is represented by: Discharge=$121/1+e^{(-0.9(Precip-3.3)}$. Discharge values are in ft^3/sec (1 ft^3/sec=0.028 m^3/sec).

Model Type	Equation Used	∂AIC	RMSE
Sigmoid	$Discharge = L/(1+e^{-k*(Precip-x0)})$	0	6.7
Linear	Discharge = (n+m*Precip)	99	7.7
Monomolecular	$Discharge = a(1 - e^{-b*Precip}))$	107	7.8
Exponential	$Discharge = e^{f-(g*Precip)}$	109	71

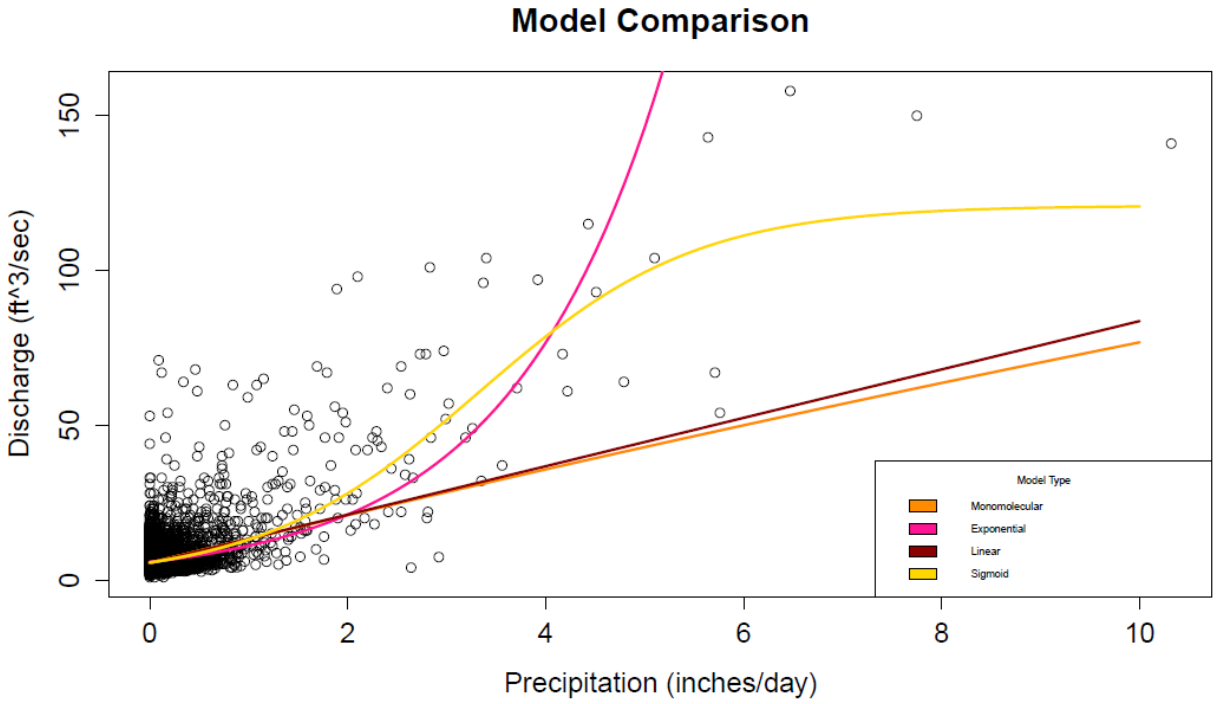

Figure 3.1: Model comparison for precipitation-discharge relationship.

Figure 3.1 indicates that the models follow similar trends in the 0-1 inch (0-2.54 cm) precipitation range, but then start to diverge under higher precipitation ranges. The exponential model's predicted values exceed observed discharge at precipitation values higher

than 5 inches (12.7 cm). This model also has the highest AIC value and a RMSE value of 71 cubic feet for second (Table 3.1), indicating that there is a high discrepancy between observed and predicted values. The monomolecular and linear models follow similar trends where predicted values are much smaller than observed discharge at precipitation values higher than 3 inches. The monomolecular model yields ðAIC and RMSE values of 107 and 7.8 cubic feet per second, respectively. The linear model yields ðAIC and RMSE values of 99 and 7.7 cubic feet per second, respectively. The sigmoid model has the lowest error with a RMSE value of 6.7 cubic feet per second (0.19 m^3/sec). Visual comparison also suggests that the sigmoid model is most accurate as the data fit the high precipitation data better than the other models.

Visually comparing the sigmoid model with a GAM model indicates how well the sigmoid function fits the data compared to a nonparametric curve. Figure 3.2 indicates that the sigmoid model captures data trends well in the precipitation range of less than 2 inches/day (5 cm/day), as the model values are nearly identical. The models deviate slightly at values higher than 2 inches per day, but the sigmoid model lies almost entirely within the GAM standard error, indicated by the dashed lines. This suggests that the sigmoid model adequately captures the trends in this data set.

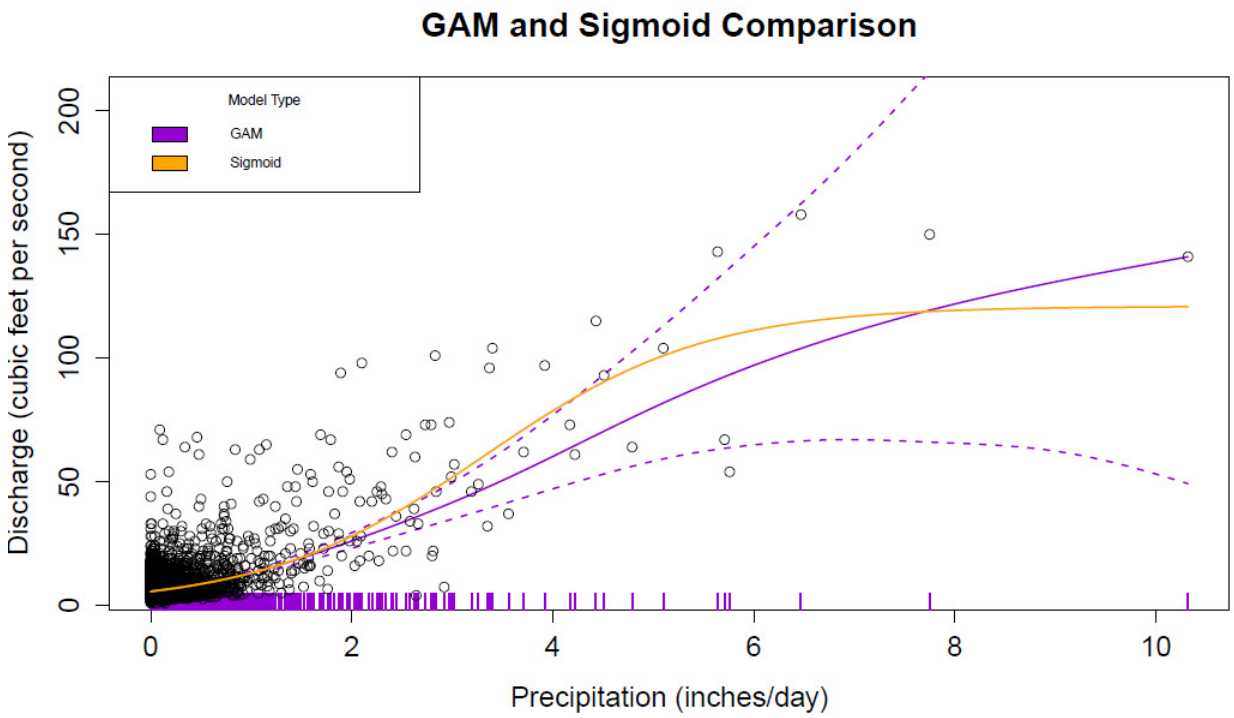

Figure 3.2: Sigmoid model compared with GAM model.

The data frame used for this analysis contains 3,964 data points with an average precipitation of 0.19 inches/day (0.48 cm/day). This indicates that the majority of the data points are in the low precipitation range. Figure 3.3 plots the sigmoid model at low precipitation values of less than 1 inch/day (2.54 cm/day), and Figure 3.4 shows the model plotted on log scale for better visualization of the points.

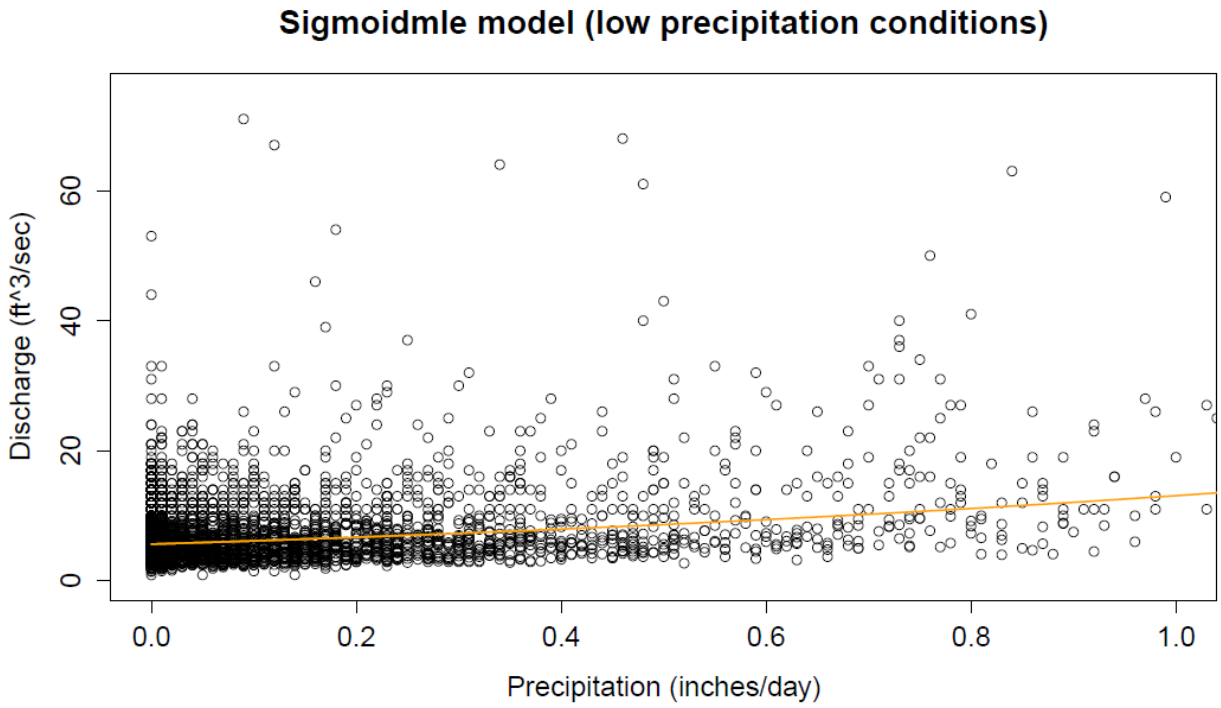

Figure 3.3: Sigmoid model fit at low precipitation values.

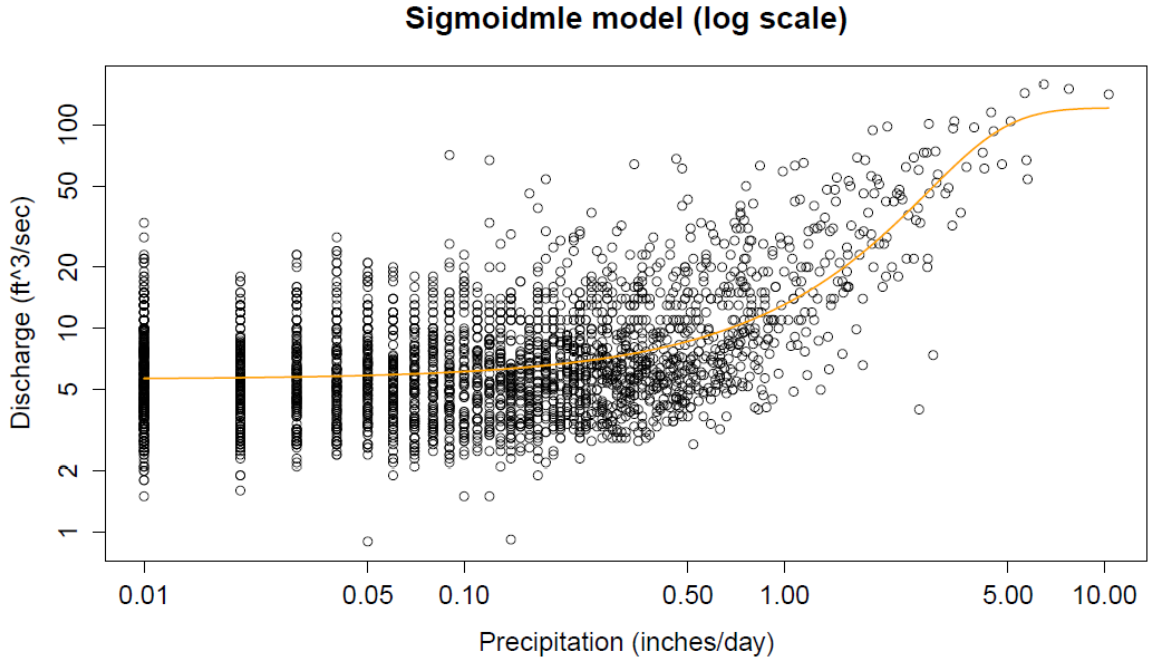

Figure 3.4: Sigmoid model plotted on log scale.

Both Figures 3.3 and 3.4 suggest that there is less of an empirical relationship between precipitation and discharge at lower precipitation values, particularly below the average daily precipitation of 0.19 inches per day. The correlation coefficient of the data below the average daily precipitation values is 0.04; however, it is 0.8 for values greater than the average daily precipitation, suggesting there is a strong relationship between precipitation and discharge at values greater than 0.19 inches per day.

The segmented package identifies breakpoints in generalized linear models that have segmented relationships by detecting locations where the relationship between the variables changes. This was applied to a log-linear model of discharge vs. precipitation, and the breakpoint was determined to be 1.83 inches per day (4.6 cm/day). The correlation coefficient below the breakpoint is 0.42 and the correlation above the breakpoint is 0.7. This suggests that there is an empirical relationship between precipitation and discharge data at low and high precipitation, but the relationship is stronger at precipitation values above 1.8 inches/day.

Hypothesis 2

A similar approach was taken to evaluate the discharge-suspended sediment relationship in Southern Kāneʻohe Bay. Exponential, power, modified power, and polynomial functions on a log-log scale (3rd, 4th, and 5th order) were investigated using maximum likelihood estimation. In order to evaluate the polynomial functions on a log scale, it was necessary to convert the 13 suspended sediment values of 0 tons per day from the data frame to a nonzero number. These values were changed to 0.01 tons per day (0.009 metric tons/day), reflecting the smallest nonzero suspended sediment value registered. This change introduced minimal bias since the data frame consists of 8,003 points.

Model type, function equation, AIC values and RMSE values are presented in Table 3.2. A visual comparison is provided in Figures 3.5 and on the log-log scale in Figure 3.6 for enhanced visualization.

Table 3.2: AIC and RMSE value model comparison for discharge-suspended sediment relationship. The most accurate model is represented by: Suspended Sediment = $\exp(-0.02 \log(x)^4 + 0.24 \log(x)^3 + -0.39 \log(x)^2 + 0.75 \log(x) - 2.95)$, where x= discharge values. Suspended sediment values are in tons/day (1 ton/day=0.9 metric tons/day).

Model Type	Equation Used	∂AIC	RMSE
Log-log polynomial (4th order)	Suspended Sediment = $\exp(a*\log(x)^4 + b*\log(x)^3 + c*\log(x)^2 + d*\log(x) + e)$; x=Discharge	0	22.6
Log-log polynomial (5th order)	Suspended Sediment = $\exp(a*\log(x)^5 + b*\log(x)^4 + c*\log(x)^3 + d*\log(x)^2 + e*\log(x) + f)$; x=Discharge	1	22.9
Log-log polynomial (3rd order)	Suspended Sediment = $\exp(a*\log(x)^3 + b*\log(x)^2 + c*\log(x) + d)$; x=Discharge	87	74.9
Modified power	Suspended Sediment = $a*\text{Discharge}^{(1+b*\exp(-c*\text{Discharge}))}$	483	33.4
Power	Suspended Sediment = $p*\text{Discharge}^{z}$	717	31.5
Exponential	Suspended Sediment = $e^{f-(g*\text{Discharge})}$	2736	2363813

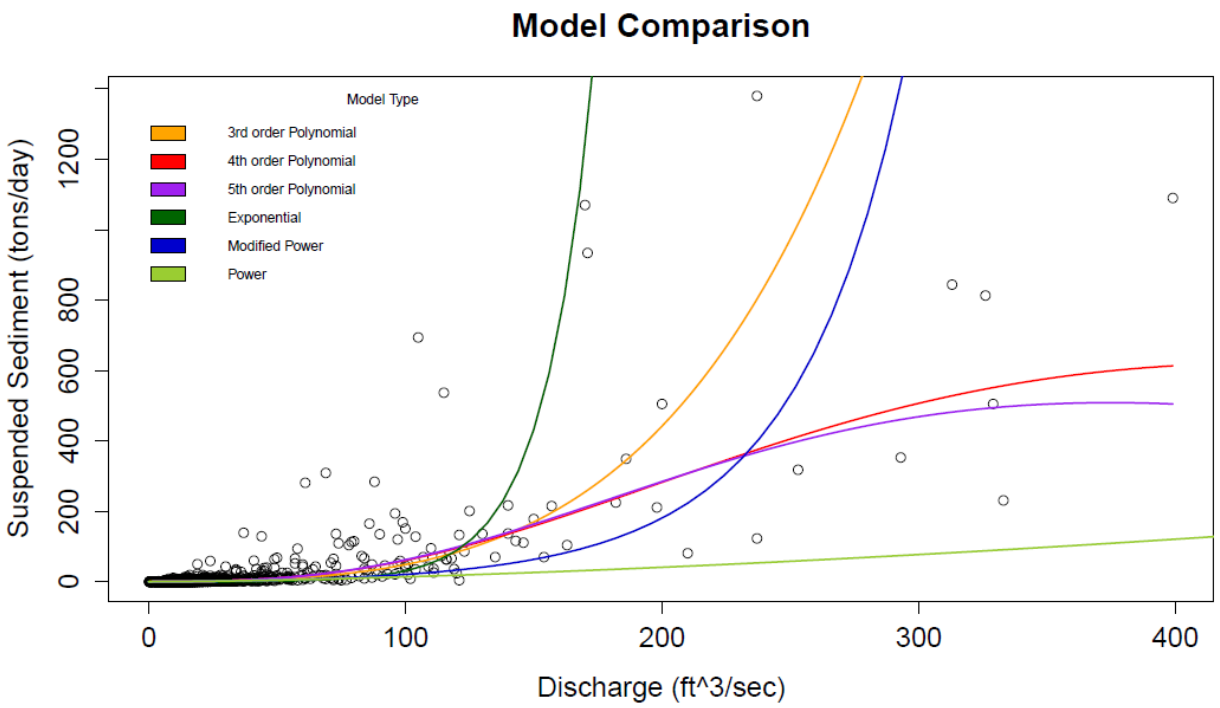

Figure 3.5: Model comparison for the discharge-suspended sediment relationship.

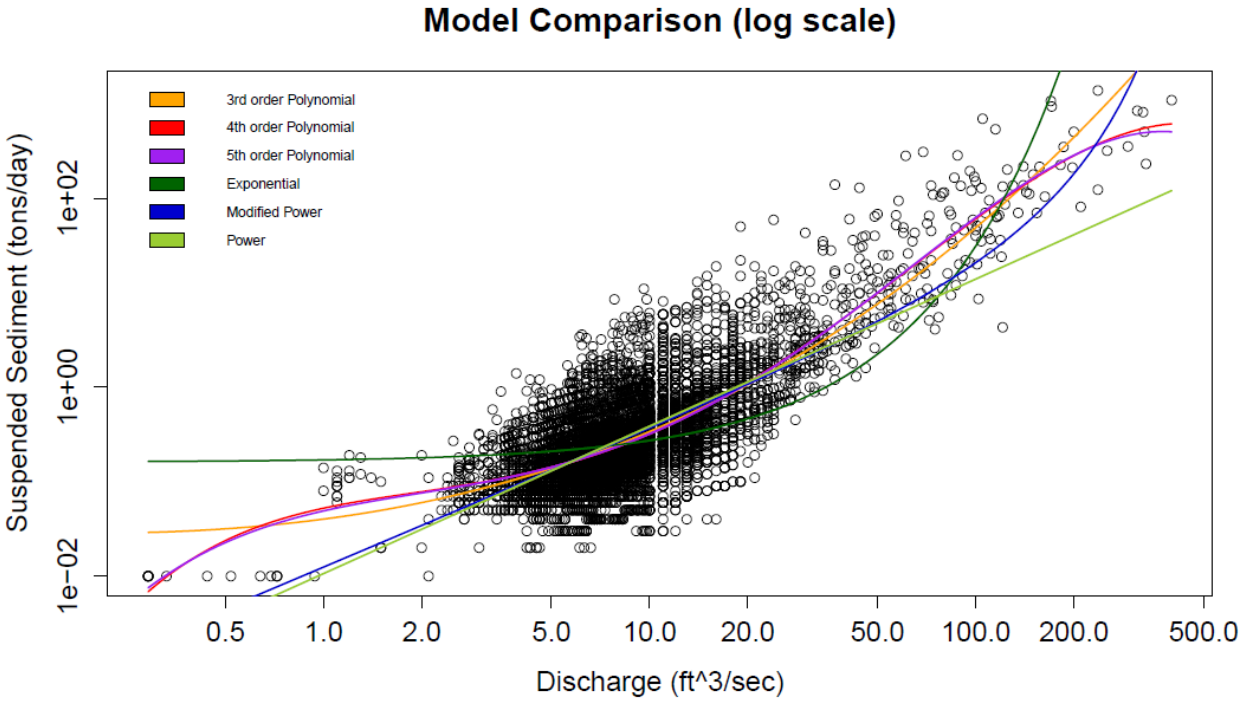

Figure 3.6: Model comparison on a log-log scale for the discharge-suspended sediment relationship.

Figures 3.5 and 3.6 indicate that all models follow similar trends in the 5-50 cubic feet per second (0.14-1.4 m^3/sec) discharge range, but then start to diverge in higher and lower discharge ranges. The exponential model predicted values exceed observed suspended sediment at discharge values above the 170 ft^3/sec (4.8 m^3/sec) range. This model has the highest ∂AIC at 2736 and a RMSE of 2363813 tons/day (Table 3.2), indicating that the model is not a good representation of the data. The power and modified power models have ∂AIC values of 871 and 637 and RMSE values of 31.5 and 33.4 tons/day, respectively, indicating that there is a high discrepancy between the observed and predicted values for both models. All three polynomial models were fit to a log-log scale since the data approximate a polynomial fit under these conditions. The third order polynomial has a ∂AIC of 87 and a RMSE of 74.9 tons/day. The fourth and fifth order polynomial models had the lowest AIC and the fourth order had the lowest RMSE of 22.6 tons/day (20.5 metric tons/day), indicating that this model fits the data best. Likewise, visual comparison of the models in Figures 3.5 and 3.6 indicates that the fourth order polynomial is most representative of the data set.

Figure 3.7 indicates that the fourth order polynomial model follows similar trends to the GAM below 100 cubic feet per second (2.8 m^3/sec), although predicted suspended sediment values are slightly smaller. Unlike the fourth order polynomial, the GAM model oscillates at discharge values higher than 100 cubic feet per second; however this region represents a scattered portion of the data set and includes few data points.

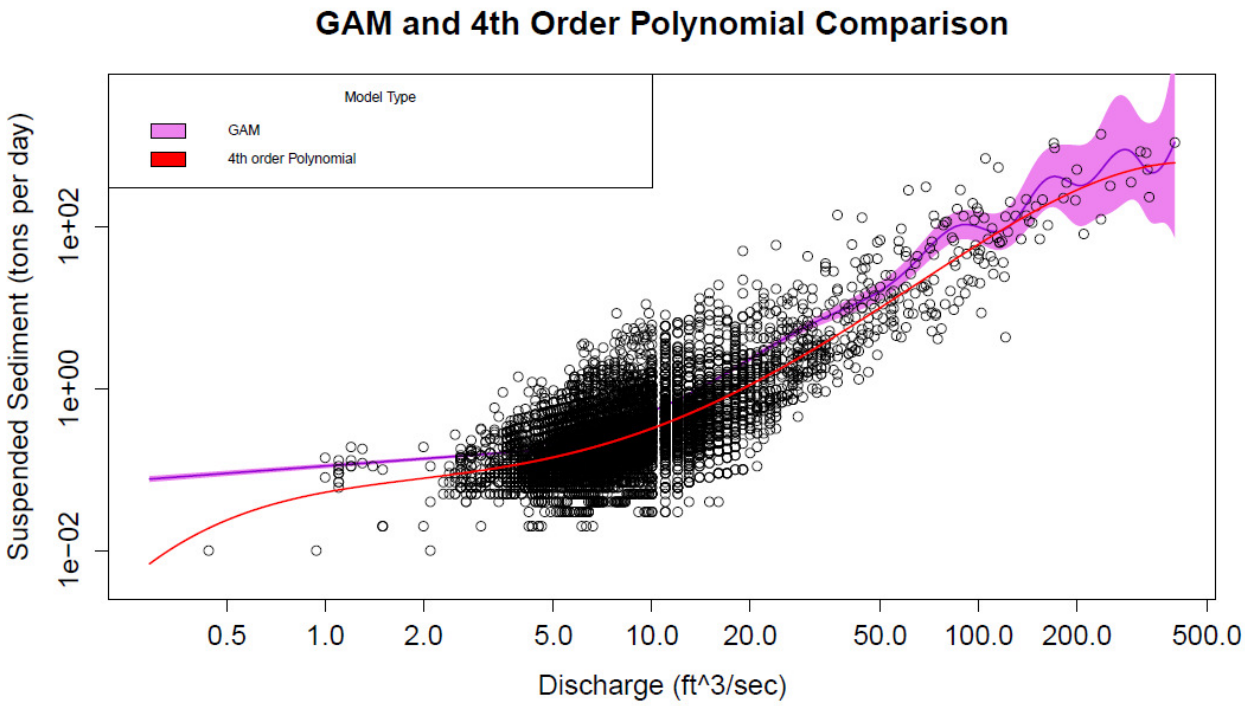

Figure 3.7: Polynomial (4th order) model compared with GAM model.

The data frame used for this analysis contains 8,003 data points with an average discharge of 10.8 cubic feet per second (0.8 m^3/sec) and median discharge of 7.5 cubic feet per second (0.21 m^3/sec), indicating that the majority of the data points are in the low discharge range. Figure 3.8 shows a plot of the fourth order polynomial model at discharge values less than 40 cubic feet per second (1.1 m^3/sec).

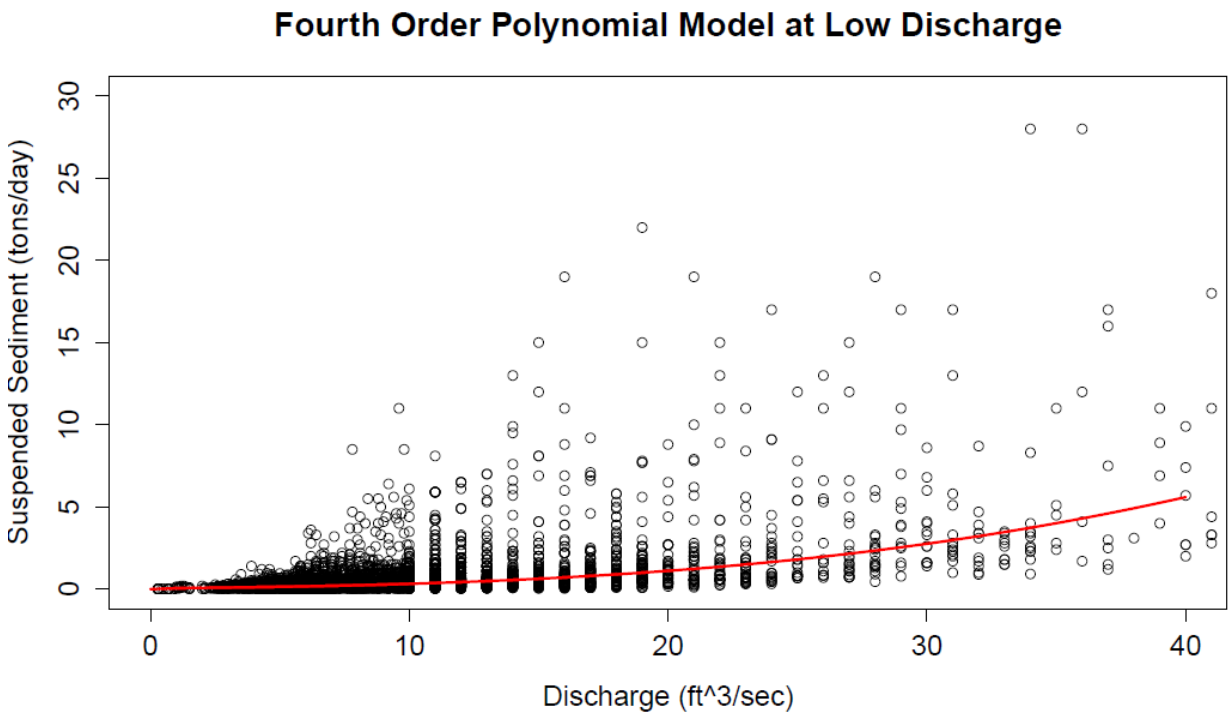

Figure 3.8: Fourth order polynomial model fit at low discharge values.

Figure 3.8 suggests that there is a lower correlation between discharge and suspended sediment at lower discharge values. The correlation coefficient of the data below the median discharge value of 7.5 cubic feet per second is 0.2, while it is 0.72 for values above the median discharge value indicating a stronger relationship between discharge and suspended sediment above 7.5 cubic feet per second.

The segmented package was applied to a log-linear model, and the breakpoint was determined to be 30.8 cubic feet per second (0.87 m^3/sec). The correlation coefficient below the breakpoint is 0.38 and the correlation above the breakpoint is 0.72. This suggests that there is an empirical relationship between discharge and suspended sediment data represented by a fourth order log-log polynomial equation. The polynomial model correctly shows that the slope of the discharge-suspended sediment curve is steeper at higher discharge values, and the

breakpoint function verifies that there is a distinct change in slope at 30.8 cubic feet per second.

The Precipitation-Discharge relationship (Figure 3.2) and Discharge-Suspended Sediment relationship (Figure 3.7) were synthesized to determine a relationship between precipitation and suspended sediment release into Kāneʻohe Stream shown in Figure 3.9.

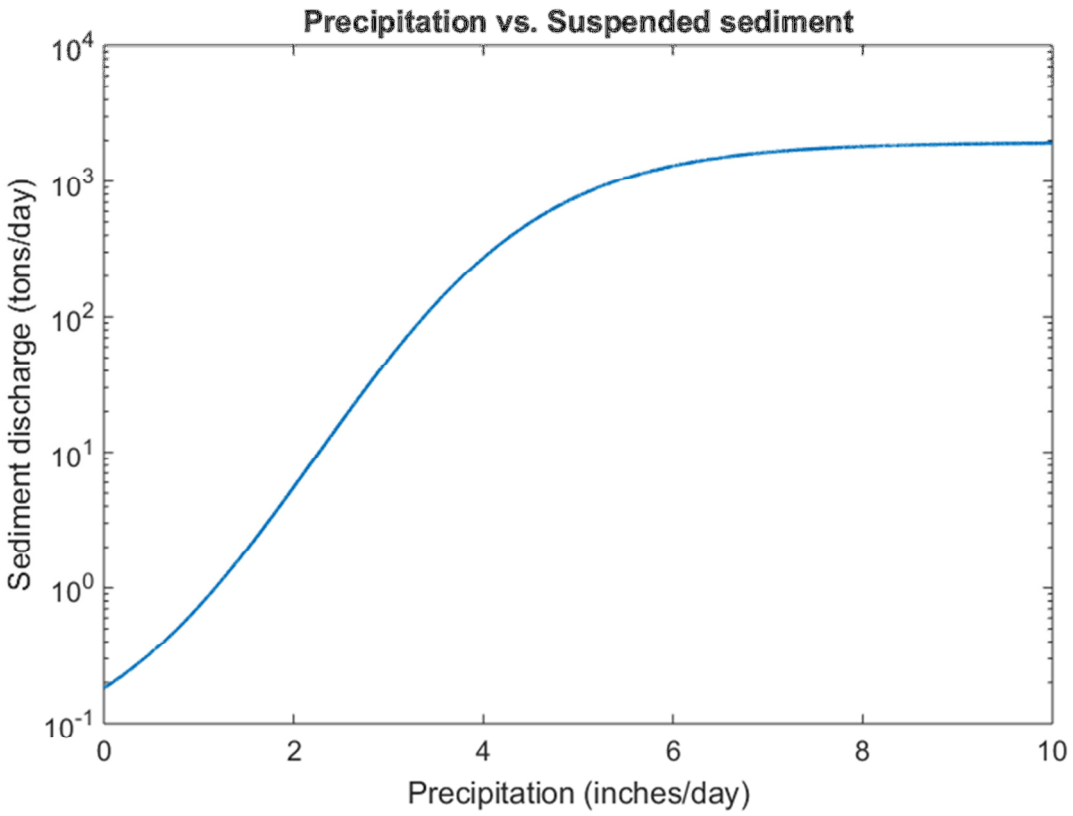

Figure 3.9: Precipitation-Suspended Sediment relationship.

This relationship shows that there is an approximately linear relationship between precipitation and suspended sediment below the 4 inches/day precipitation range. When precipitation exceeds 4 inches per day the relationship saturates. This relationship will be used as a forcing in the mathematical model (Chapter 5) to determine the impact of decreased precipitation on sediment discharge.

3.3 Discussion

Understanding small coastal watershed dynamics is crucial to biogeochemical studies, as Milliman and Syvitski (1992) posited that over half of the sediment discharged to the sea originates from the cumulative discharge of watersheds smaller than 10,000 km^2. The Hawai'ian Islands present unique geography consisting of steep mountainous regions; the Southern Kāne'ohe watershed varies in elevation from 2,792 feet (851 m) in the Ko'olaupoko Mountains to sea level over an area of 3,641 acres ($1.4x10^7$ m^2)(DOH, 2007), making the region prone to flash flooding due to the possibility of intense precipitation coupled with steep topography (Guzman et al., 2013). Brief precipitation events have the potential to produce surface runoff and eroding slopes and stream banks produce suspended sediment that enters the streams and ultimately Southern Kāne'ohe Bay over time periods of minutes to hours (Tomlinson and De Carlo, 2003).

Sediment delivery via streams varies as a function of discharge, the onset of rainfall, land use, and land cover (Guzman et al., 2013). The gage data analyzed suggest that at low precipitation ranges (1.8 inches/day or less) discharge values are low because soil infiltration rates exceed rainfall intensity, resulting in rainfall absorbance and low runoff and erosion rates (Bayabil et al., 2010). Once precipitation exceeds 1.8 inches/day, soil becomes saturated which leads to surface runoff, erosion, and the deposition of suspended sediment into Kāne'ohe Stream.

Storm runoff and sediment that enter Kāne'ohe Bay via Kāne'ohe Stream alter considerably the water quality of the Bay and can have a lasting impact since the semi-enclosed

Southern Kāneʻohe Bay has a residence time of ~13 days (Smith et al., 1981). High precipitation results in storm discharge and freshwater pulses from Kāneʻohe Stream that lead to stratification and the formation of turbid low salinity plumes. These plumes can persist up to a week depending on wind and weather patterns (Ringuet and Mackenzie, 2005). Effects of storm inputs to the Bay typically occur within a day of inputs; the input of nutrients leads to primary production and has the potential to change seawater N:P ratios and shift community structure (De Carlo et al., 2007). However, this process can have lasting impacts for periods of weeks to months as remineralization of terrestrial organic matter deposited during a storm event can provide continued nutrient inputs through remineralization, impacting marine species and the Bay ecosystem as a whole.

Land use, soil porosity, distribution of rainfall over the watershed, and moisture content of the soil are factors that could potentially explain the substantial variation in the response variables of discharge and suspended sediment. Despite this variation, models were fit that adequately captured average nonlinear relationships for precipitation-discharge and discharge-suspended sediment. Mean discharge and suspended sediment values were also used to determine mean annual fluxes. These model equations will be used as inputs for the biogeochemical model in Chapter 5.

4.4 Summary and Conclusion

Precipitation-discharge data spanning 11 years and discharge-suspended sediment data spanning 22 years were analyzed for the Southern Kāneʻohe watershed region in order to quantify patterns and trends of base flow and storm dynamics. The watershed is characterized

by average discharge values of 10.8 cubic feet/sec and suspended sediment fluxes of 2.8 tons/day, while storm conditions produce variable water discharge rates reaching up to 399 cubic feet/ sec and suspended sediment fluxes of up to 1380 tons/day.

Statistical analysis disproved both null hypotheses. There are empirical relationships representative of precipitation-discharge and discharge-suspended sediment represented by a sigmoid function and log-log fourth order polynomial function, respectively. However, these relationships tend to be stronger under storm conditions (precipitation > 1.8 inches/day, discharge> 30.8 cfs) when soil saturation leads to increased runoff and soil erosion than under low flow conditions. These relationships with be applied to the biogeochemical model in Chapter 5 to assess how decreasing precipitation and increasing temperature will impact nutrient export to Southern Kāneʻohe Bay.

Literature Cited:

Bayabil, H. K., Tilahun, S. A., Collick, A. S., and Steenhuis, T. S. (2010) Are runoff processes ecologically or topographically driven in the Ethiopian Highlands? The case of the Maybar. Ecohydrology, 3, 457–466.

Bolker, B.M. (2008) Ecological Models and Data in R. Princeton University Press.

De Carlo E.H., Hoover D.J., Young C.W., Hoover R.S., Mackenzie F.T. (2007) Impact of storm runoff from subtropical watersheds on coastal water quality and productivity. Applied Geochemistry 22: 1777–1797.

Guzman, C. D., Tilahun, S. A., Zegeye, A. D., and Steenhuis, T. S. (2013) Suspended sediment concentration-discharge relationships in the (sub-) humid Ethiopian highlands, Hydrol. Earth Syst. Sci., 17, 1067–1077.

Hawai‘i State Department of Health (DOH) (2007) Ko’olaupoko Watershed Restoration Action Strategy. Kailua Bay Advisory Council Finalized Plan ASO Log 05-080.

Milliman, J.D. and Syvitski, J.P.M. (1992) Geomorphic/tectonic control of the sediment discharge to the ocean: The importance of small mountainous rivers. Journal of Geology, 100(5), 525–544.

Ringuet, S., Mackenzie, F.T. (2005) Controls on nutrient and phytoplankton dynamics by storm runoff events southern Kāne‘ohe Bay, Hawai‘i, Estuaries 28, 327–337.

Smith, S.V., Kimmerer, W.J., Laws, E.A., Brock, R.E., Walsh, T.W. (1981) Kāne‘ohe Bay sewage experiment: perspectives on ecosystem responses to nutritional perturbation. Pacific Sci. 35, 379–395.

Tomlinson, M.S., De Carlo, E.H. (2003) The need for high resolution time series data to characterize Hawai‘ian streams. J. Am. Water Resour. Assoc. (JAWRA) 39, 113–123.

CHAPTER 4: ASSESSMENT OF SUSPENDED SOLIDS AND PARTICULATE NUTRIENT LOADING TO SURFACE RUNOFF AND THE COASTAL OCEAN IN THE KĀNE'OHE WATERSHED

4.1 Introduction

The purpose of this chapter is to address the following null hypothesis (Hypothesis 3): There will be no release of nitrogen and phosphorous from terrestrial suspended matter entering the coastal ocean.

Soil samples representative of the three dominant soil types present in the Kāne'ohe watershed (Figures 2.1 and 2.1B) were collected and analyzed for a variety of parameters discussed in this chapter. The locations of the soil sample sites are listed in Table 4.1.

Table 4.1: Locations of soil collection sites in the Southern Kāne'ohe watershed.

Soil Collection Site Locations	Latitude (N)	Longitude (W)
Lolekaa (Lo) Soil collection site	21°23'42"	157°48'44"
Kāne'ohe (Kg) Soil Collection site	21°24'39"	157°46'44"
Hanalei (Hn) Soil Collection site	21°24'39"	157°47'8"

Soil samples were analyzed for nutrient composition, grain size distribution and soil properties. Stokes' settling velocity calculations were also performed to assess the potential fate of suspended sediment particles entering the ocean.

Stream water and seawater samples were collected to evaluate preexisting nutrient concentrations and to perform nutrient release experiments that evaluate the release or uptake of nutrients from suspended sediments in fresh and marine waters. Sampling site coordinates are listed in Table 4.2.

Table 4.2: Locations of stream and seawater collection sites in the Southern Kāneʻohe Watershed and Bay.

Water Collection Site Locations	Latitude (N)	Longitude (W)
USGS site 16270900 (Stream water collection site)	21°23'42"	157°48'44"
Coconut Island seawater intake pipe (Seawater collection site)	21°26'00"	157°47'12"

4.2 Results

Southern Kāneʻohe Watershed Soil Types

The Southern Kāneʻohe Watershed consists of three soil types. (Ristvet, 1978. Originally adapted from Foote et al., 1972). Soil maps (Figures 2.1 and 2.1B) indicate that the Southern Kāneʻohe watershed is composed of silty clays including Hanalei silty clay (Hn), Lolekaa silty clay (Lo), and Kāneʻohe silty clay (Kg). Each soil type was analyzed for nutrient content, and grain size distribution. However, only the Lolekaa silty clay soil sample was used for nutrient release experiments since the majority of the watershed consists of this soil type.

Nutrient Composition of Soils

Each soil sample was analyzed for pH, Ca, Mg, P, K, NO_3^-, NH_4^+, total carbon, and total nitrogen at the Agricultural Diagnostic Service Center at the University of Hawaiʻi at Mānoa. Results are listed in Table 4.3.

Table 4.3: Composition of Kāneʻohe watershed soils.

				<--------µg/g----		---------->			
	pH	% N	%C	P	K	Ca	Mg	NO_3^-N	NH_4^-N
Hn Soil	7.9	0.08	3.80	32	495	6844	489	5.9	3.8
Lo Soil	4.8	0.07	1.40	6.0	575	802	344	15	1.4
Kg soil	4.2	0.32	4.00	31	816	1668	642	108	4.0

The focus of this thesis is inorganic phosphorous and inorganic nitrogen. Phosphorous concentrations ranged from 6 μg /g (Lo soil) to 32 μg /g (Hn soil). Nitrate concentrations ranged from 5.9 μg/g (Hn soil) to 108 μg/g (Kg soil), with a concentration of 15 μg/g for the Lolekaa soil sample (Lo soil). Ammonium concentrations ranged from 1.4 μg/g (Lo soil) to 4.0 μg/g (Kg soil). Compared to the Hn soil sample, the Lo and Kg samples are very acidic and low in calcium.

Nutrient Composition of Stream and Marine Waters

Prior to the start of each experiment, a water sample was filtered and collected to determine preexisting nutrient concentrations of the aqueous phase. These results are located in Appendix 4.1, with the sample ending in "00" indicating the initial water sample composition. Figure 4.1 shows the duplicate initial inorganic phosphate, N+N, and ammonia concentrations across the various salinities used for experimentation.

Preexisting phosphate concentrations decreased as salinity increased; initial concentrations for freshwater experiments were 1.15-1.26 μmol/L (Experiments 27 and 28) and 0.21-0.22 μmol/L for seawater experiments (Experiments 23 and 24). Likewise, nitrate + nitrite (N+N) concentrations decreased with increasing salinity. Initial concentrations for freshwater experiments were 10.4-10.8 μmol/L (Experiments 27 and 28) and 1.42-1.45 μmol/L for seawater experiments (Experiments 23 and 24). Preexisting ammonia concentrations did not exhibit an apparent correlation with salinity, although concentrations tended to be higher at high salinities. Ammonia values ranged between 1.34 and 3.94 μmol/L across the salinity values.

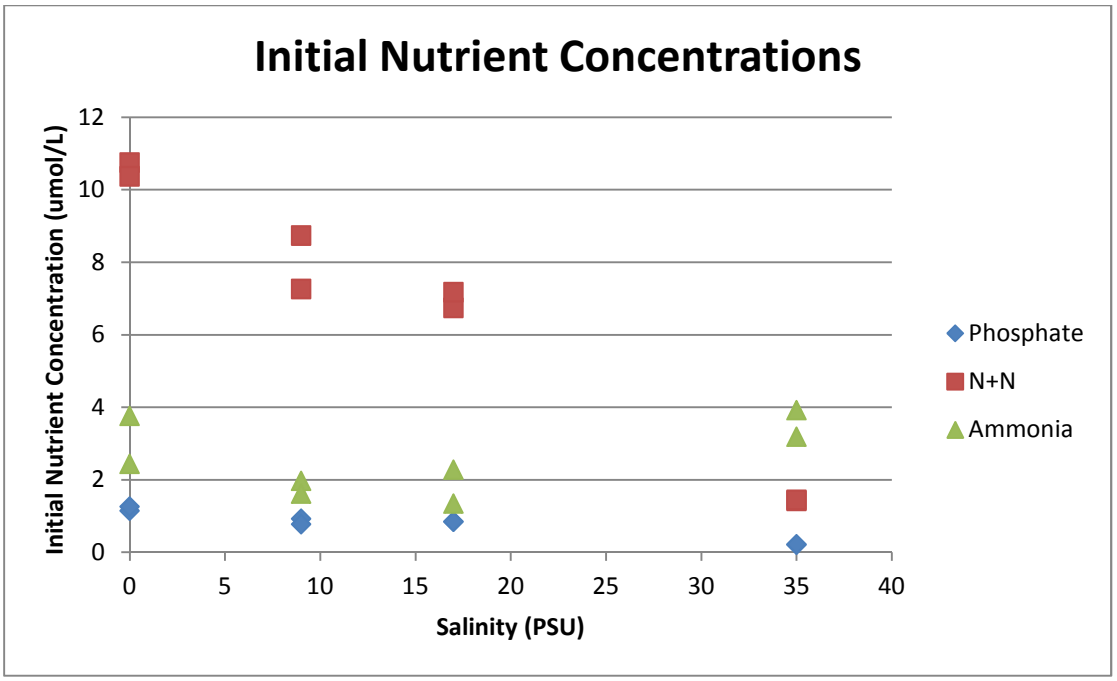

Figure 4.1: Initial nutrient concentrations across varying salinities.

Grain Size Distribution

All three dominant soil types in the Kāneʻohe watershed are classified as silty clays (Ristvet, 1978). Silty clays are defined by a composition of at least 40% clay and 40% silt (Soil Survey Manual, 1993). Grain size analysis was performed on each soil type to determine if the sample matched its classification.

Samples were collected from the three areas (coordinates in Table 4.1) and analyzed to determine their particle size distribution. Tables 4.4-4.6 and Figure 4.2 show results of the analyses.

Table 4.4: Grain size distribution of soil collected adjacent to Luluku Stream from the Lo region of soil map (Ristvet, 1978. Originally adapted from Foote et al., 1972).

Lo Soil

Weight of Test Sample (g)	**600.98**

Method	**Screen Openining/Particle Diameter (mm)**	**Velocity (cm/sec)**	**Settling time at 10 cm (min)**	**Grade Size (mm)**	**Weight Retained (g)**	**Weight %**	**Cumulative %**
Sieving	2	-	-	>2	32.05	5.33%	5.3%
Sieving	1.651	-	-	2-1.651	28.46	4.74%	10.1%
Sieving	1	-	-	1.651-1	99.02	16.48%	26.5%
Sieving	0.495	-	-	1-.495	34.51	5.74%	32.3%
Sieving	0.351	-	-	.495-.351	32.05	5.33%	37.6%
Sieving	0.075	-	-	.351-.075	48.11	8.01%	45.6%
Sieving	0.0625	-	-	.075-.0625	3.82	0.64%	46.3%
Sieving	0.045	-	-	.0625-.045	72.09	12.00%	58.3%
Decantation	0.0156	0.0217	7.73	.045-.0156	88.12	14.66%	72.9%
Decantation	0.0078	0.00543	31	.0156-.0078	100.11	16.66%	89.6%
Decantation	0.0039	0.00136	123	0.0078-0.0039	20.88	3.47%	93.1%
Decantation	0.00195	0.00034	490	0.0039-0.00195	26.32	4.38%	97.4%
Decantation	0.00098	0.000085	981	<0.00195	14.72	2.45%	99.9%
					600.26		99.9%
				Total	600.98		100.0%
				Sieve loss	***0.72***		***0.1%***

Table 4.5: Grain size distribution of soil collected adjacent to Kāneʻohe Bay from Kg region of soil map (Ristvet, 1978. Originally adapted from Foote et al., 1972).

Kg Soil

Weight of Test Sample (g)	**630.98**

Method	**Screen Openining/Particle Diameter (mm)**	**Velocity (cm/sec)**	**Settling time at 10 cm (min)**	**Grade Size (mm)**	**Weight Retained (g)**	**Weight %**	**Cumulative %**
Sieving	2	-	-	>2	11.01	1.74%	1.7%
Sieving	1.651	-	-	2-1.651	70.46	11.17%	12.9%
Sieving	1	-	-	1.651-1	109.71	17.39%	30.3%
Sieving	0.495	-	-	1-.495	72.13	11.43%	41.7%
Sieving	0.351	-	-	.495-.351	38.97	6.18%	47.9%
Sieving	0.075	-	-	.351-.075	84.22	13.35%	61.3%
Sieving	0.0625	-	-	.075-.0625	9.27	1.47%	62.7%
Sieving	0.045	-	-	.0625-.045	66.54	10.55%	73.3%
Decantation	0.0156	0.0217	7.73	.045-.0156	43.43	6.88%	80.2%
Decantation	0.0078	0.00543	31	.0156-.0078	29.7	4.71%	84.9%
Decantation	0.0039	0.00136	123	0.0078-0.0039	49.32	7.82%	92.7%
Decantation	0.00195	0.00034	490	0.0039-0.00195	31.11	4.93%	97.6%
Decantation	0.00098	0.000085	981	<0.00195	13.21	2.09%	99.7%
					629.08		99.7%
				Total	630.98		100.0%
				Sieve loss	***1.9***		***0.3%***

Table 4.6: Grain size distribution of soil collected adjacent to Kāneʻohe Bay and Luluku Stream from Hn region of soil map (Ristvet, 1978. Originally adapted from Foote et al., 1972).

Hn Soil

Weight of Test Sample (g)	**885.73**

Method	**Screen Openining/Particle Diameter (mm)**	**Velocity (cm/sec)**	**Settling time at 10 cm (min)**	**Grade Size (mm)**	**Weight Retained (g)**	**Weight %**	**Cumulative %**
Sieving	2	-	-	>2	6.06	0.68%	0.7%
Sieving	1.651	-	-	2-1.651	100.08	11.30%	12.0%
Sieving	1	-	-	1.651-1	208.45	23.53%	35.5%
Sieving	0.495	-	-	1-.495	78.42	8.85%	44.4%
Sieving	0.351	-	-	.495-.351	71.91	8.12%	52.5%
Sieving	0.075	-	-	.351-.075	84.22	9.51%	62.0%
Sieving	0.0625	-	-	.075-.0625	9.27	1.05%	63.0%
Sieving	0.045	-	-	.0625-.045	97.65	11.02%	74.1%
Decantation	0.0156	0.0217	7.73	.045-.0156	83.11	9.38%	83.5%
Decantation	0.0078	0.00543	31	.0156-.0078	76.66	8.66%	92.1%
Decantation	0.0039	0.00136	123	0.0078-0.0039	22.8	2.57%	94.7%
Decantation	0.00195	0.00034	490	0.0039-0.00195	37.11	4.19%	98.9%
Decantation	0.00098	0.000085	981	<0.00195	8.34	0.94%	99.8%
					884.08		99.8%
				Total	885.73		100.0%
				Sieve loss	***1.65***		***0.2%***

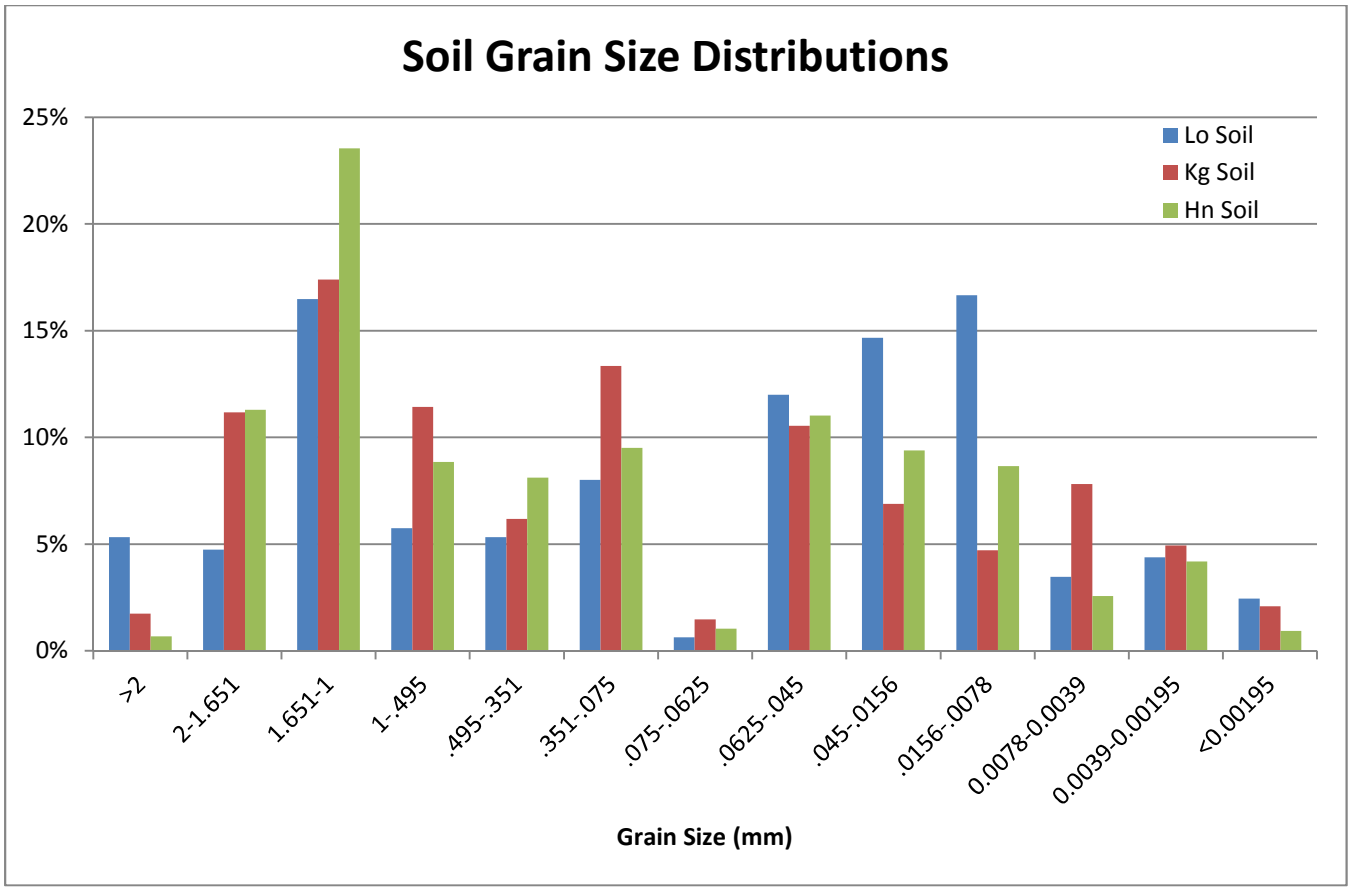

Figure 4.2: Histogram of grain size distribution of soil collected adjacent to Luluku Stream from the Lolekaa (Lo), Hanalei (Hn) and Kāneʻohe (Kg) regions of the soil map (Ristvet, 1978. Originally adapted from Foote et al.,1972).

Standard soil convention classifies sand as particles in the 0.063-2 mm range, silt in the 0.002-0.063 mm range, and clay as particles smaller than 0.002 mm (Soil survey manual, 1993). Based on this classification, the Lo soil sample collected consists of 58.3% sand, 39.1% silt, and 2.5% clay. The Kg soil sample is comprised of 73.3% sand, 24.3% silt, and 2.1% clay, and the Hn soil is comprised of 74.1% sand, 24.8% silt, and 0.9% clay. The cumulative frequency plots in Figures 4.3 show these distributions graphically. The Lo soil has a lower frequency of larger particles compared to the Kg and Hn soils.

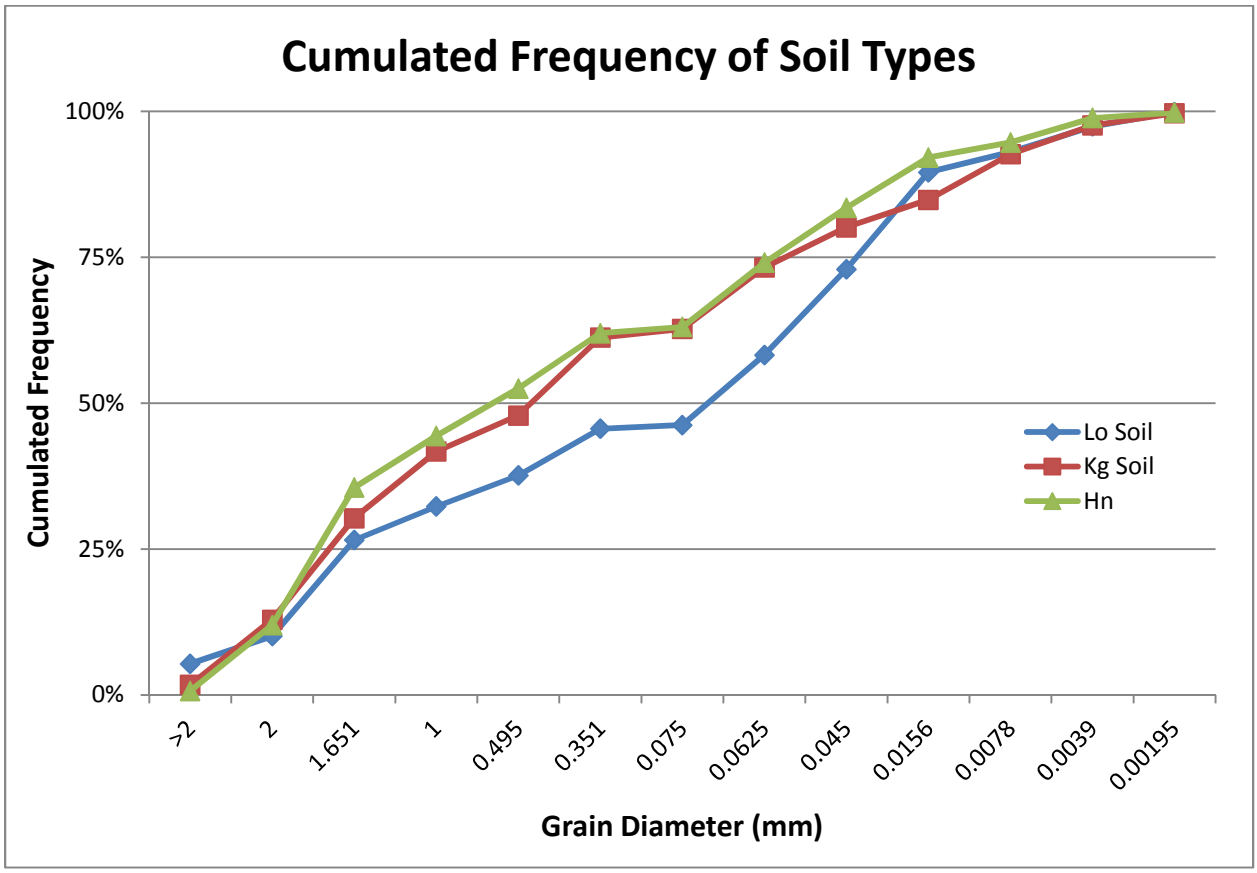

Figure 4.3: Cumulative frequency plot for soil types.

Grain size distributions were used to calculate mean and median particle size following the methods of Krumbein and Pettijohn (1988). Mean particle size calculations are shown in Tables 4.7-4.9. The first column in these tables lists the grain size in mm, the second column lists the weight percentage frequency, and the third column lists the grade size midpoint. The final column lists the multiplication of the frequency and midpoint columns. The sum of this column divided by the total frequency is the arithmetic mean value. The median particle size is the diameter that is larger than 50% of the diameters in the distribution and smaller than the other 50%. This was determined by analyzing the cumulative distribution graphs and identifying the point at which the 50-per cent line intersects with the cumulative curve as indicated in Tables 4.7-4.9.

Analysis indicates that the Lo soil sample had the smallest values of arithmetic mean and median particle size at 0.56 and 0.07 mm respectively. The Kg soil sample had a mean particle size of 0.64 mm and a median particle size of 0.48 mm. The Hn soil sample had similar mean and median particle sizes of 0.67 and 0.65 mm, respectively.

Table 4.7: Mean and median particle size calculations for Lo soil.

Lo-Arithmetic mean	(Krumbein and Pettijohn, 1988) method		
Grade Size (mm)	f: Weight Percentage Frequency (%)	m: Grain Midpoint (mm)	f*m
>2	5.33	3	16.0
2-1.651	4.7	1.8255	8.64
1.651-1	16.5	1.3255	21.8
1-.495	5.74	0.7475	4.29
.495-.351	5.33	0.423	2.26
.351-.075	8.01	0.213	1.71
.075-.0625	0.64	0.06875	0.04
.0625-.045	12.0	0.05375	0.64
.045-.0156	14.7	0.0303	0.444
.0156-.0078	16.7	0.0117	0.195
0.0078-0.0039	3.47	0.00585	0.020
0.0039-0.00195	4.38	0.002925	0.013
<0.00195	2.45	0.001465	0.004
Totals	99.9		56.1
	Mean=Sum/total frequency (mm)		**0.56**
	Median (mm)		**0.07**

Table 4.8: Mean and median particle size calculations for Kg soil.

Kg-Arithmetic mean (Krumbein and Pettijohn, 1988) method			
Grade Size (mm)	f: Weight Percentage Frequency (%)	m: Grain Midpoint (mm)	f*m
>2	1.74	3	5.23
2-1.651	11.2	1.8255	20.4
1.651-1	17.4	1.3255	23.0
1-.495	11.4	0.7475	8.54
.495-.351	6.18	0.423	2.61
.351-.075	13.3	0.213	2.84
.075-.0625	1.47	0.06875	0.10
.0625-.045	10.5	0.05375	0.57
.045-.0156	6.88	0.0303	0.21
.0156-.0078	4.71	0.0117	0.06
0.0078-0.0039	7.82	0.00585	0.05
0.0039-0.00195	4.93	0.002925	0.01
<0.00195	2.09	0.001465	0.00
Totals	99.7		63.7
	Mean=Sum/total frequency (mm)		**0.64**
	Median (mm)		**0.48**

Table 4.9: Mean and median particle size calculations for Hn soil.

Hn-Arithmetic mean (Krumbein and Pettijohn, 1988) method			
Grade Size (mm)	f: Weight Percentage Frequency (%)	m: Grain Midpoint (mm)	f*m
>2	0.68	3	2.05
2-1.651	11.30	1.8255	20.6
1.651-1	23.53	1.3255	31.2
1-.495	8.85	0.7475	6.62
.495-.351	8.12	0.423	3.43
.351-.075	9.51	0.213	2.03
.075-.0625	1.05	0.06875	0.07
.0625-.045	11.02	0.05375	0.593
.045-.0156	9.38	0.0303	0.284
.0156-.0078	8.66	0.0117	0.101
0.0078-0.0039	2.57	0.00585	0.015
0.0039-0.00195	4.19	0.002925	0.012
<0.00195	0.94	0.001465	0.001
Totals	99.8		67.0
	Mean=Sum/total frequency (mm)		**0.67**
	Median (mm)		**0.65**

Skewness and kurtosis calculations were also performed for each soil type. Skewness is a measure of the degree of asymmetry of frequency curves, or a measure of the tendency of the data to spread on one side or the other of the average (Krumbein et al., 1988). Kurtosis is the measure of the degree of peakedness in a frequency curve. The following equations were used for kurtosis and skewness calculations (Folk et al., 1957):

Skewness= $(\varphi_{84} + \varphi_{16} - 2\varphi_{50})/2(\varphi_{84}-\varphi_{16}) + (\varphi_{95} + \varphi_{5} -2\varphi_{50})/2(\varphi_{95}-\varphi_{5})$ **(Equation 4.1)**

Kurtosis= $(\varphi_{95} - \varphi_{5})/2.44(\varphi_{75}-\varphi_{25})$, **(Equation 4.2)**

where φ indicates the particle size at the corresponding frequency percentage.

Table 4.10 lists skewness and kurtosis values for each soil type, as well as the φ values derived from Figure 4.3.

Table 4.10: Skewness and kurtosis values for each soil type.

Skewness and Kurtosis Calculations	**Lo Soil**	**Kg Soil**	**Hn Soil**
φ_5	2	2	2
φ_{16}	1.88	1.94	1.94
φ_{25}	1.68	1.76	1.81
φ_{50}	0.07	0.48	0.65
φ_{75}	0.041	0.058	0.061
φ_{84}	0.026	0.010	0.043
φ_{95}	0.006	0.006	0.008
Skewness	-0.94	-0.52	-0.36
Kurtosis	1.3	1.4	1.4

Skewness values between -0.3 and -1 are classified as strongly coarse-skewed (Folk et al., 1957), and a value of 0 represents symmetry. The Lo soil sample exhibited the least symmetry with a skewness value of -0.94, followed by Kg and Hn soils with values of -0.52 and -

0.36 respectively. Each soil type fits this classification of coarse-skewed; however, the Lo soil sample is most strongly coarse-skewed.

Normal curves have a kurtosis value of 1 and leptokurtic curves have a kurtosis value larger than 1, as seen in the Kāneʻohe watershed soils. The Lo soil sample has a kurtosis value of 1.3 and both the Kg and Hn soil samples have a kurtosis value of 1.4. This means that the distribution has a high peak compared to a normal distribution.

Stokes' Settling Velocity

Stokes' Settling Velocity calculations were performed to evaluate the potential fate of suspended solid particles entering the ocean. Calculations (Krumbein et al., 1988) were performed in order to estimate how long suspended sediment particles remain in suspension in the Kāneʻohe Stream estuary and Bay before settling out.

Assumptions were made that under storm conditions (2 inches or more of precipitation in a 24 hour period), flow through the streams would be high enough to keep silt and clay particles suspended until reaching the estuarine region indicated in Figure 4.4.

Figure 4.4: Google maps image of the mouth of Kāneʻohe Stream. Yellow lines indicate the estuarine region where flow velocity decreases and particles begin to settle.

Calculations were performed to estimate the amount of time it would take water to pass through the estuarine region denoted in Figure 4.4, and the distribution of particles that would settle out during the transit.

Hypothesis 1 analysis indicates that during storm events stream flow can vary from 0.85 m^3/sec to 4.25 m^3/sec, while flow is in the 0.4 m^3/sec range during base flow conditions. Velocity of water passing through the estuary was calculated using the formula velocity=flow/cross-sectional area. Google maps indicated that the average width of the estuary region is 27 m, and an average depth of 1 m was assumed indicating a cross-sectional area of 27 m^2. The estuary length is approximately 370 m. Table 4.11 shows calculations performed to estimate the amount of time it will take water to transit through the estuary under different flow conditions.

Table 4.11: Calculations to determine amount of time it would take water to pass through the estuary under different flow scenarios.

	Flow (m3/sec)	Area (m2)	Velocity (m/s)	Estuary distance (m)	Transit time (min)
Base	0.4	27	0.01	370	416
Storm (low)	0.85	27	0.03	370	196
Storm (high)	4.25	27	0.16	370	39

Equation 4.3 can be used to calculate Stokes' settling velocity (Krumbein et al., 1988):

Velocity= Cr^2 (**Equation 4.3**)

Where C is a constant = $2 (\rho_s - \rho_f)g/9\eta$

ρ_s=density of the sphere
ρ_f=density of the fluid
g= acceleration due to gravity (980 cm/sec^2)
η= viscosity of the fluid
r= radius of the sphere in cm

There are several limitations to these calculations, namely the assumption that particles are spheres while most suspended sediment particles are not perfect spheres. However, these calculations can provide an estimate for how long particles will remain suspended. A "C value" of 3.57×10^4 was used as it reflects water at a temperature of 20 ^oC, and the average particle specific gravity was taken as that of quartz of 2.65 (Krumbein et al., 1988), comparable to feldspar values of 2.55-2.75. Settling velocities calculated from Equation 4.3 are listed in Table 4.12 and depicted in Figure 4.5.

Table 4.12: Stokes' Settling Velocity calculations for Kāne'ohe Stream particles.

Diameter Size (mm)	Settling velocity (cm/sec)
0.00195	0.0003
0.0039	0.001
0.0078	0.005
0.0156	0.022
0.045	0.181
0.0625	0.349
0.075	0.502
0.351	11.0
0.495	21.9
1	89.3
1.651	243
2	357

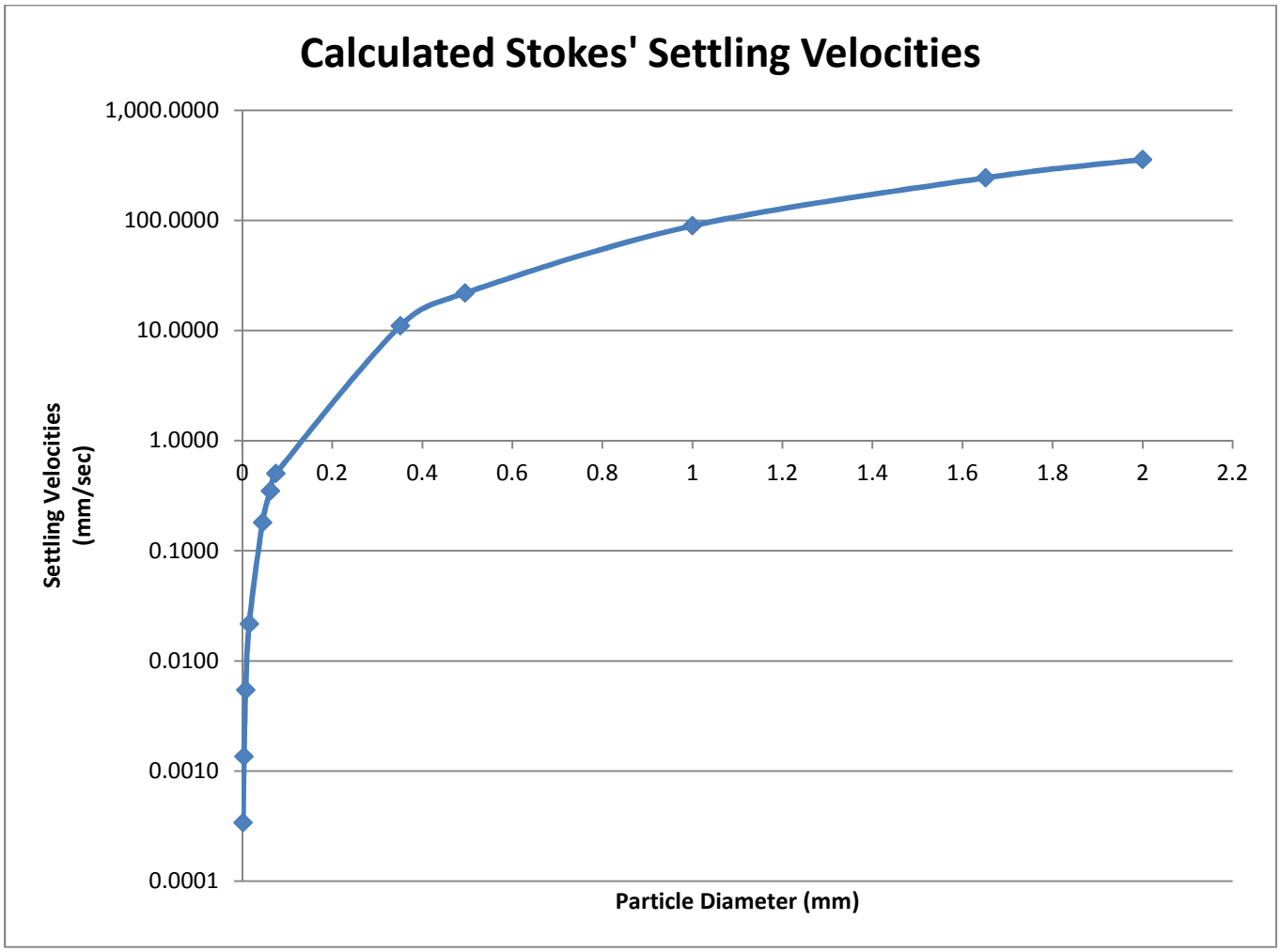

Figure 4.5: Stokes' settling velocities for a series of particle sizes in the Kāne'ohe watershed.

Based on these calculations, the 2 mm particles would settle at a velocity of 357 cm/sec and the smallest particles (0.00195 mm diameter) would settle at 0.0003 cm/ sec. Table 4.11 indicates that the estimated transit time through the estuary during base flow conditions is 416 minutes. Under these conditions, particles with a diameter of 0.0078 mm or larger will have settled in the estuary since (0.005 cm/sec) x (416 min) x (60 mins/sec) = 136 cm, or 1.36 m which exceeds the estimated estuary depth of 1 m. Particles smaller than the 0.0078 mm diameter have the potential to enter Southern Kāneʻohe Bay.

With a mean depth of 9.5 m (Smith, 1981), silts may remain suspended in the Bay for several days. However, it is more likely that silts will coagulate as a result seawater ions neutralizing the charge on hydrophobic colloidal soil particles, allowing for aggregation and settling (Kotz et al., 2015). The majority of the particles will have left suspension within a 12-hour period. For these reasons, twelve-hour experiment duration was considered suitable to capture the major effects of suspended sediments on nutrient concentrations in water.

Nutrient Release Potential of Suspended Soils

An initial set of experiments was run for approximately 3 days to evaluate the release or uptake of nutrients from suspended sediments over time. Results of these experiments are shown in Figures 4.7-4.8. The data were discarded due to the likelihood that the lack of air flow through the experimental system during the course of the experiments caused suboxic to anoxic conditions in the reaction vessel, leading to a buildup of ammonia. Ammonia plots are not provided for this experiment because the concentrations were far above the analytical range of the method used to quantify ammonia for the majority of the collected samples, as seen in Appendix 4.1, and are meaningless in terms of application to particle nutrient release in

natural solutions. This experiment, however, showed that the rate of nutrient release decreased and eventually stopped within nearly 12 hours. Figure 4.7 indicates that phosphate values for Experiment 5 level off in the 0.5 umol/L range by the 480 minute sample and the N+N values level off in the 14-15 umol/L range between the 480 and 1440 minute samples. Likewise, when the x-axis of these figures is changed to 1/square root (time) as seen in Figure 4.8, the y-axis intercept shows that a pseudo-equilibrium is reached within 12 hours of experimentation. Subsequent experiments were only carried out to approximately 720 minutes to capture the extent of change of nutrient concentrations in solution before reaching pseudo-equilibrium.

The following experiments shown in Table 4.13 and Figure 4.6 were conducted in duplicates.

Table 4.13: Nutrient release experiments.

Quantity of Luluku Stream Water (ml)	Quantity of Ocean Water (ml)	Quantity of Soil added (g)	Experiment Numbers	Corresponding Figure(s)
1000	0	1	27,28	4.9
750	250	1	21,22	4.10, 4.11
500	500	1	18,19	4.12
0	1000	1	23,24	4.13
0	1000	0.2	25,26	4.14
0	1000	2	29,30	4.15

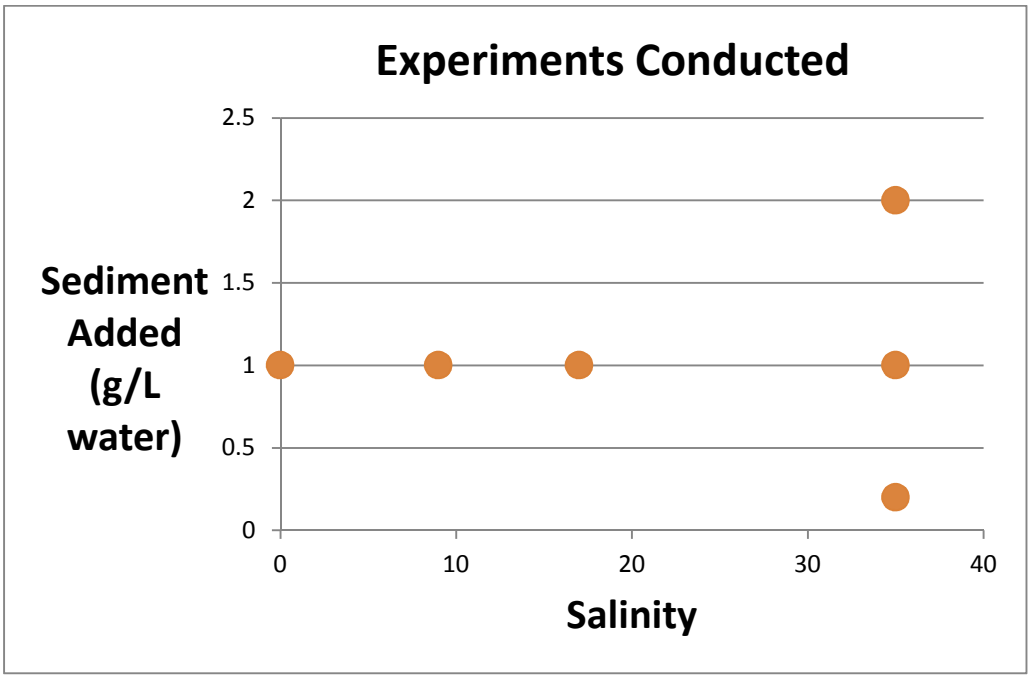

Figure 4.6:Experimental conditions.

Figures 4.7-4.15 show experimental results.

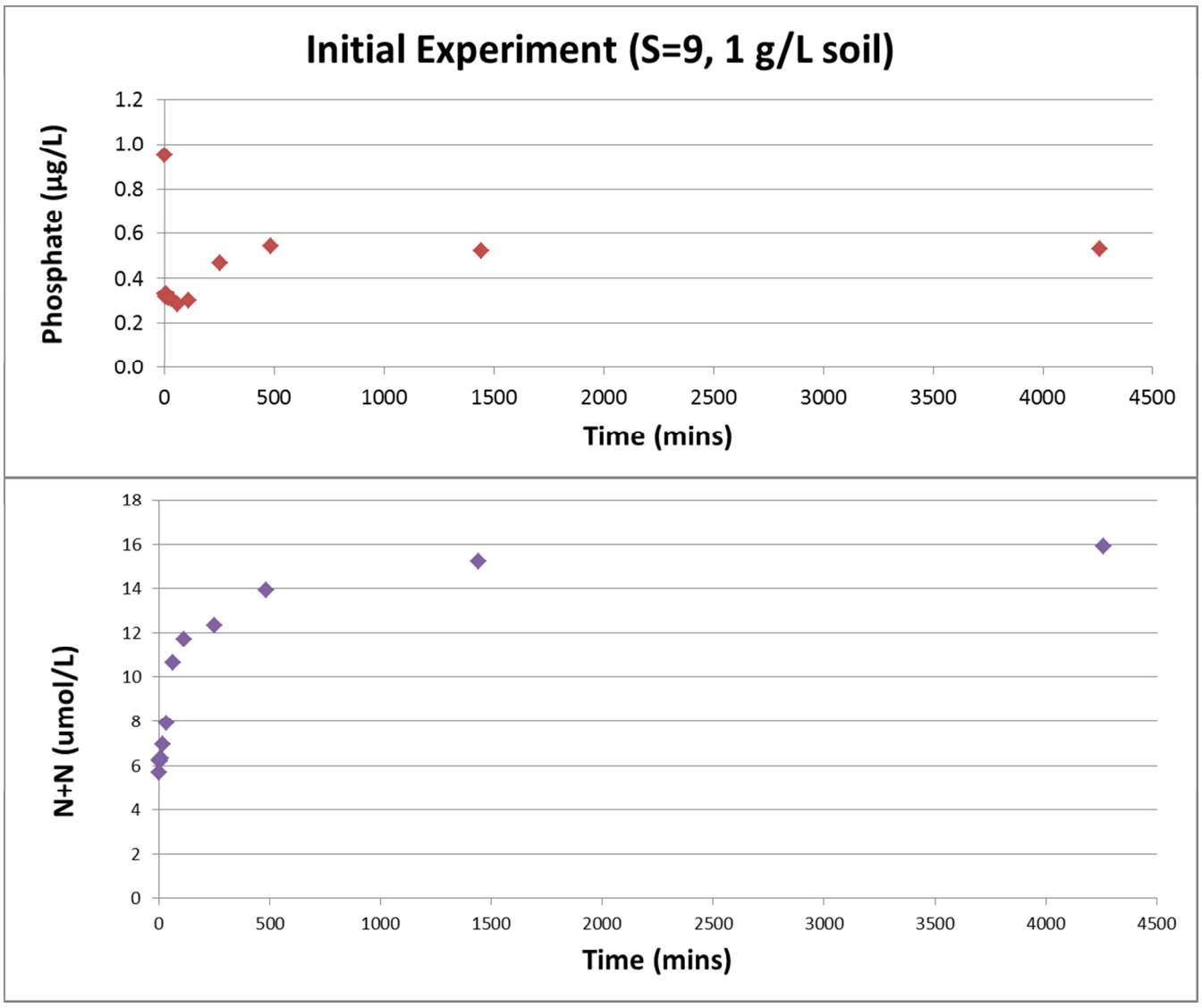

Figure 4.7: Phosphate and N+N uptake and release to S=9 water.

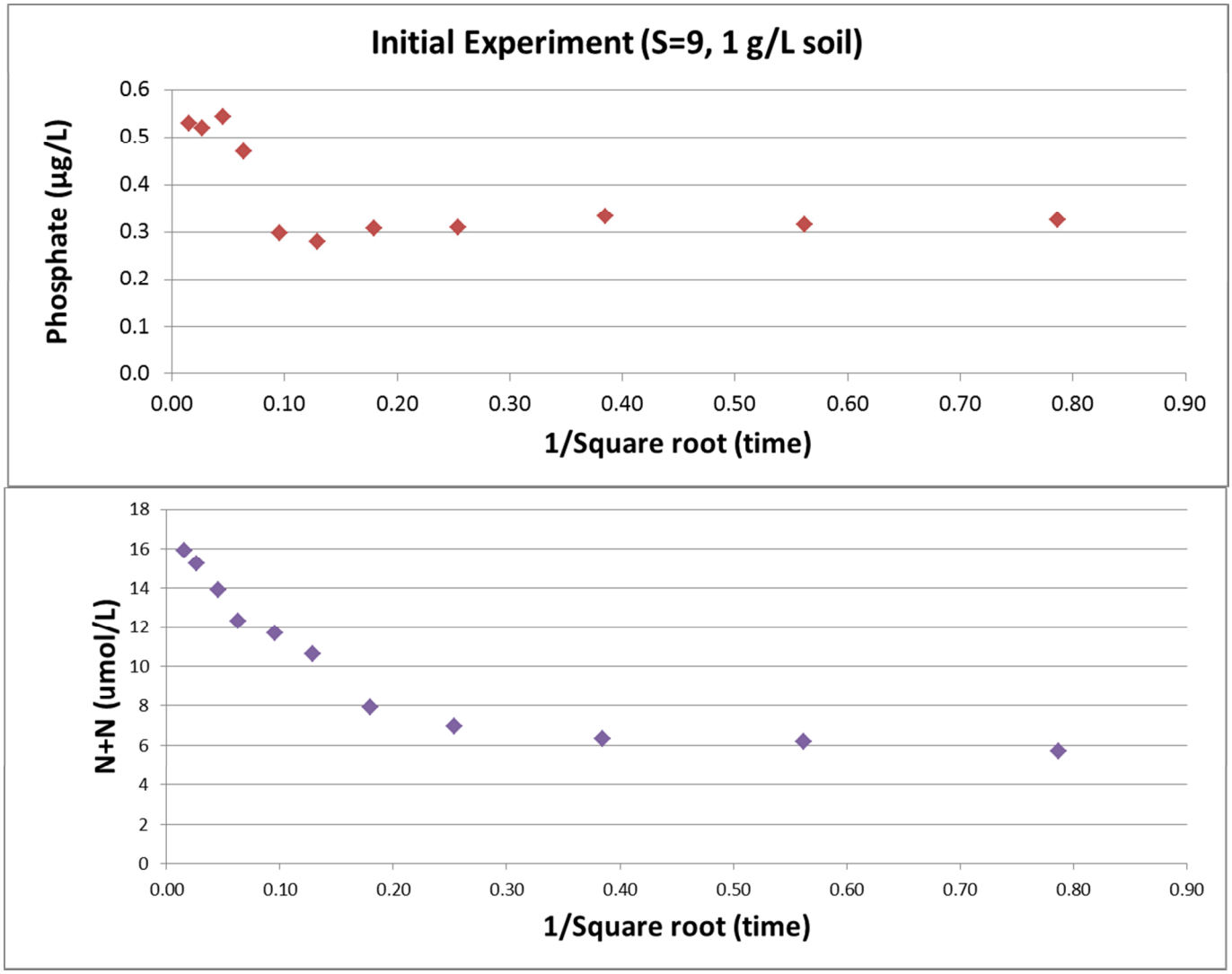

Figure 4.8: Phosphate and N+N uptake and release to S=9 water plotted over 1/square root(time).

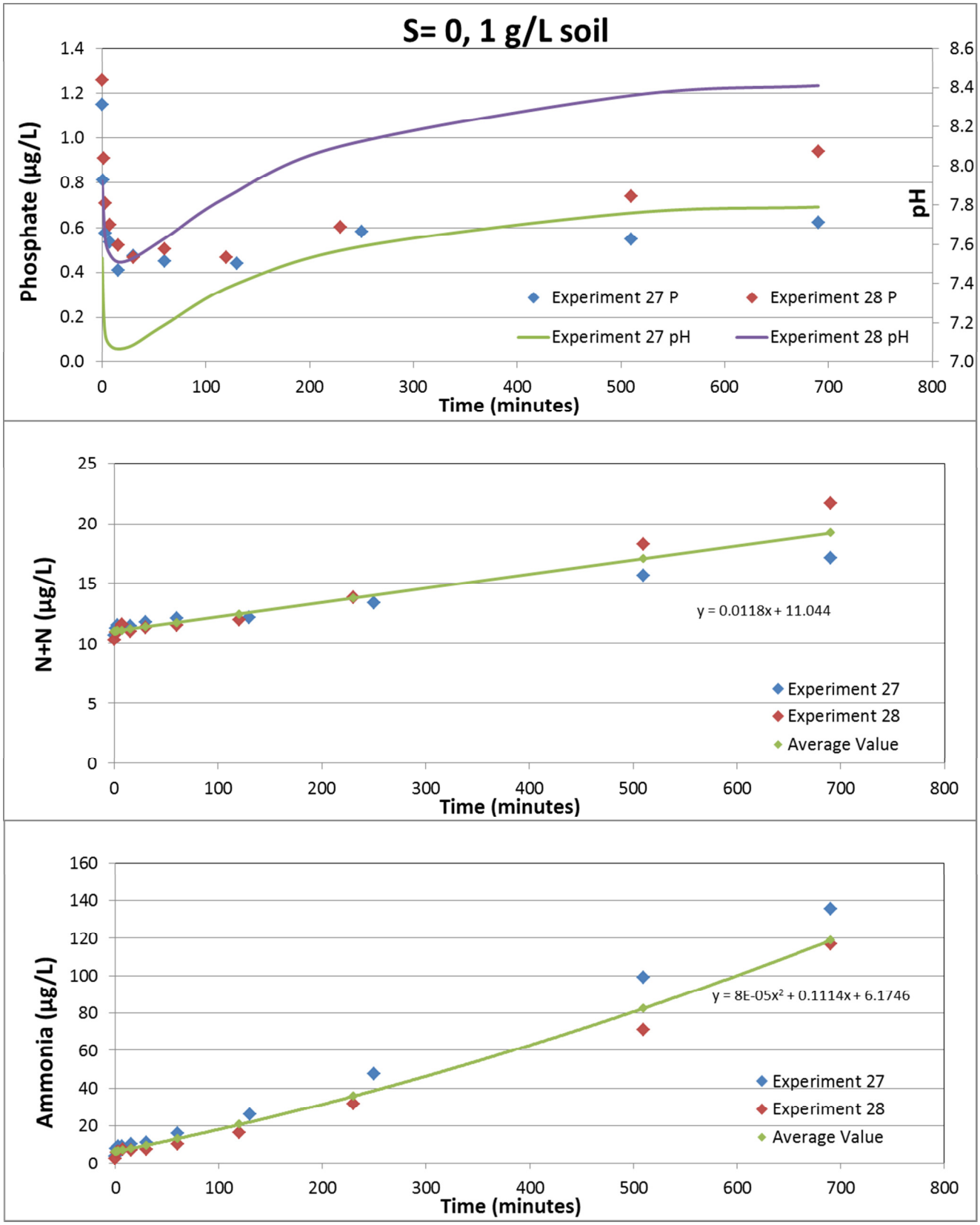

Figure 4.9: S=0, 1 g/L Experimental results.

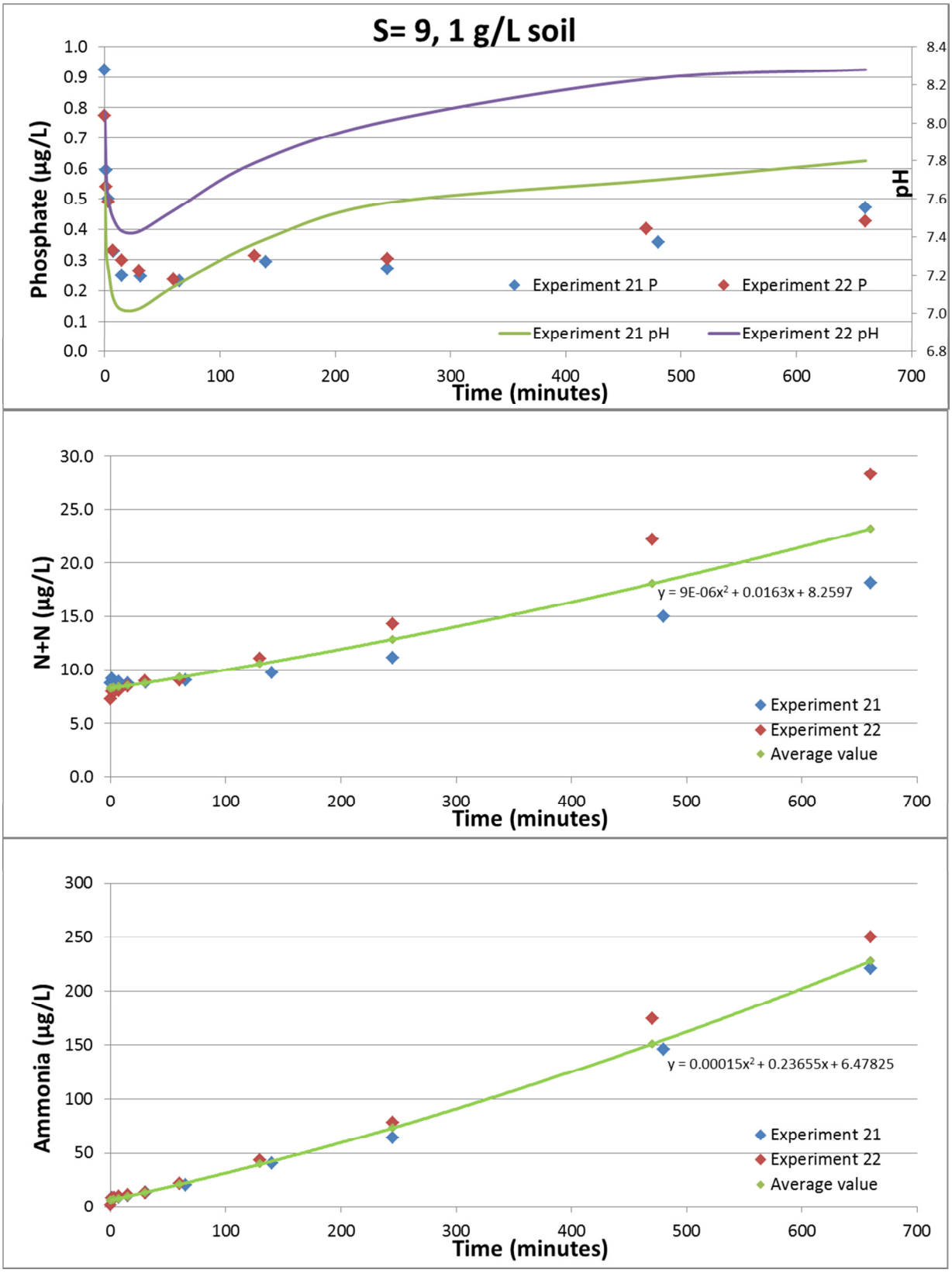

Figure 4.10: S=9, 1 g/L Experimental results.

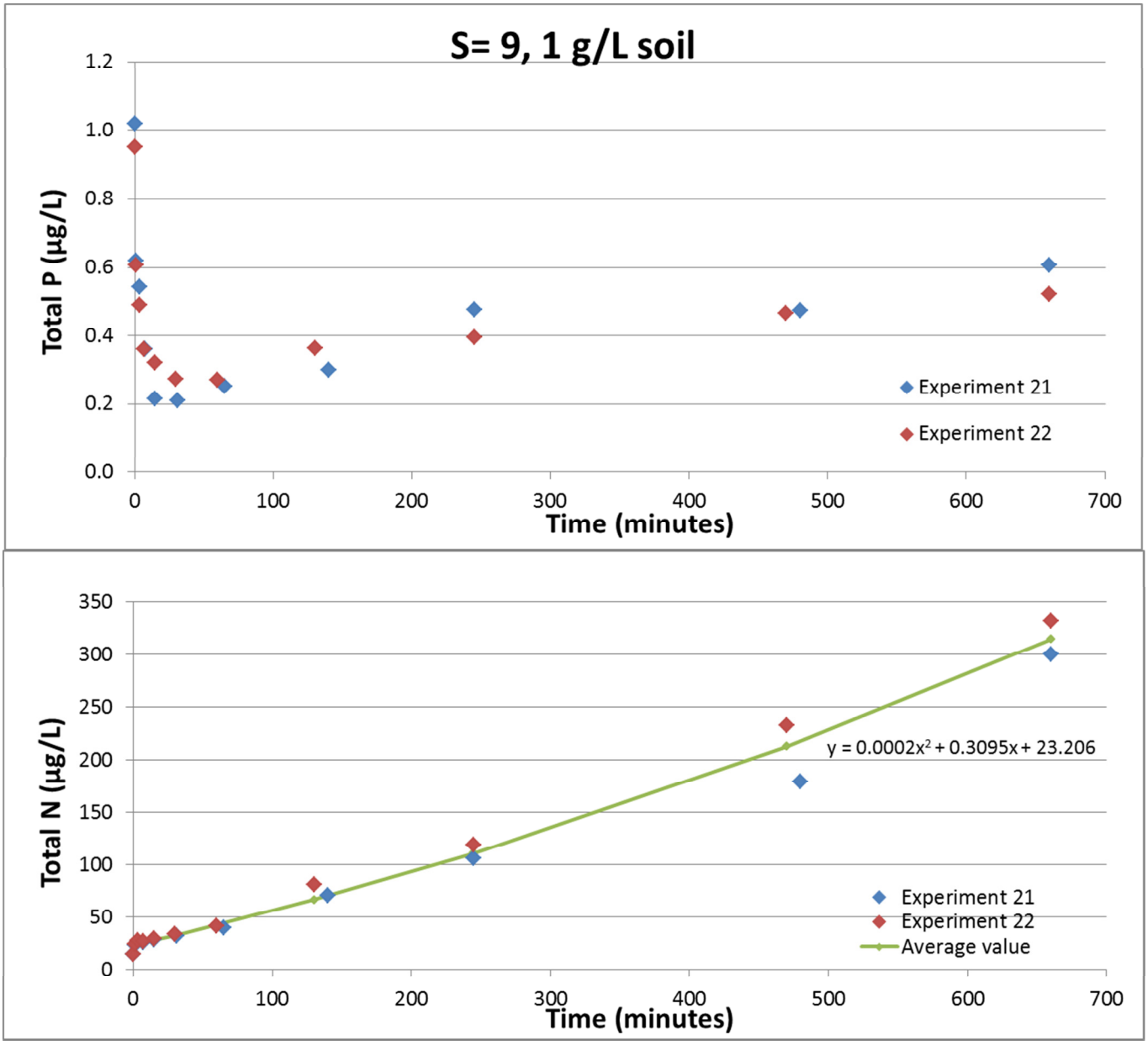

Figure 4.11: S=9, 1 g/L Experimental results.

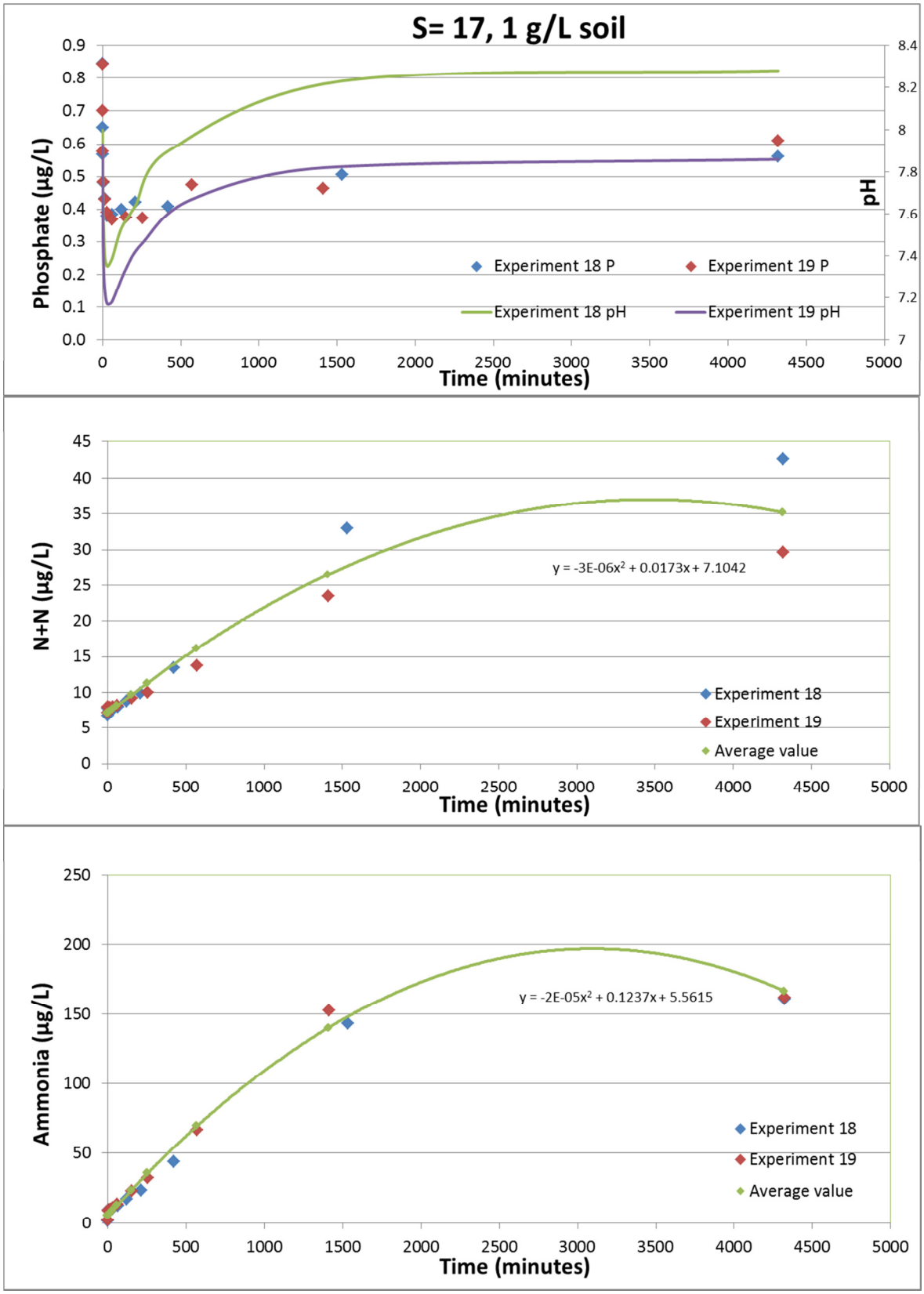

Figure 4.12: S=17, 1 g/L Experimental results.

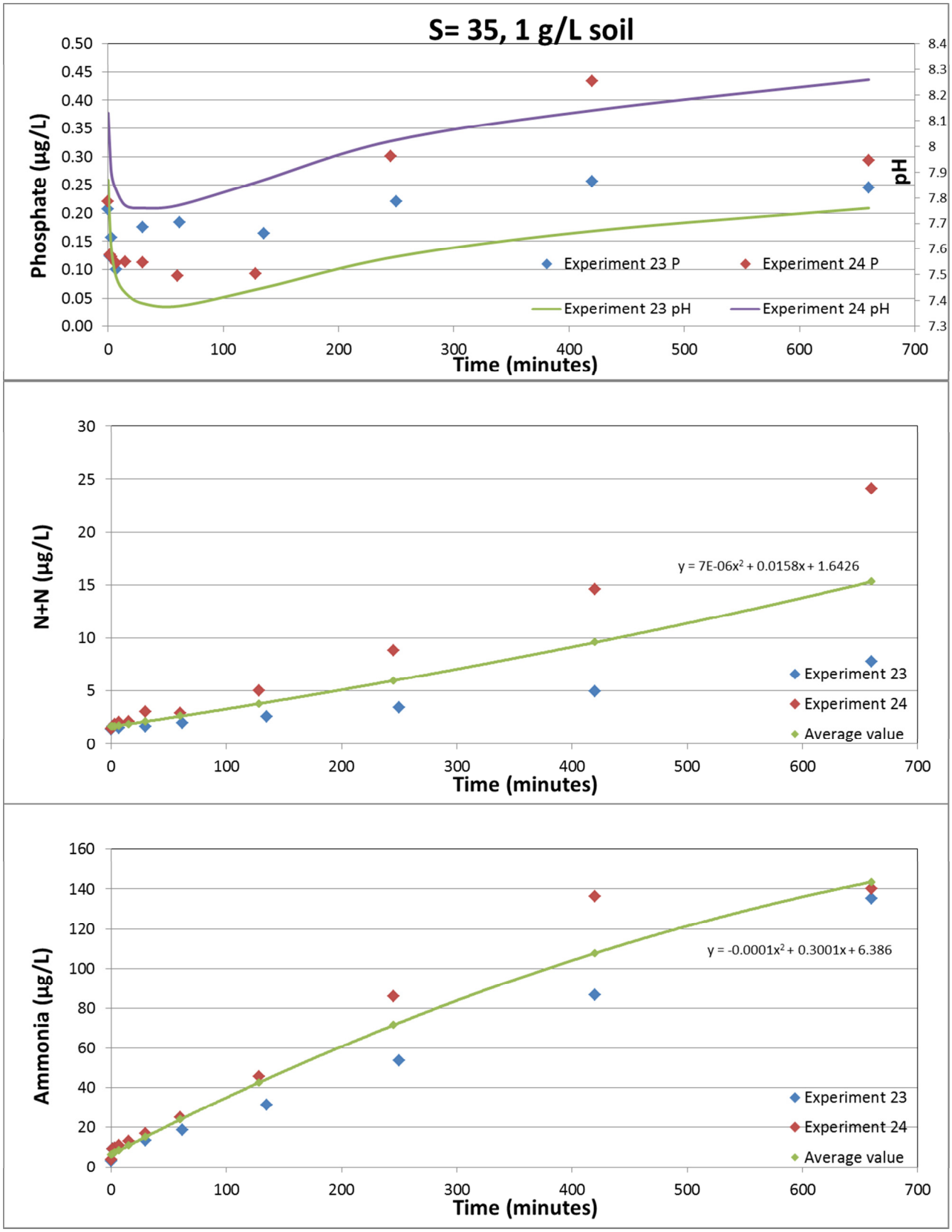

Figure 4.13: S=35, 1 g/L Experimental results.

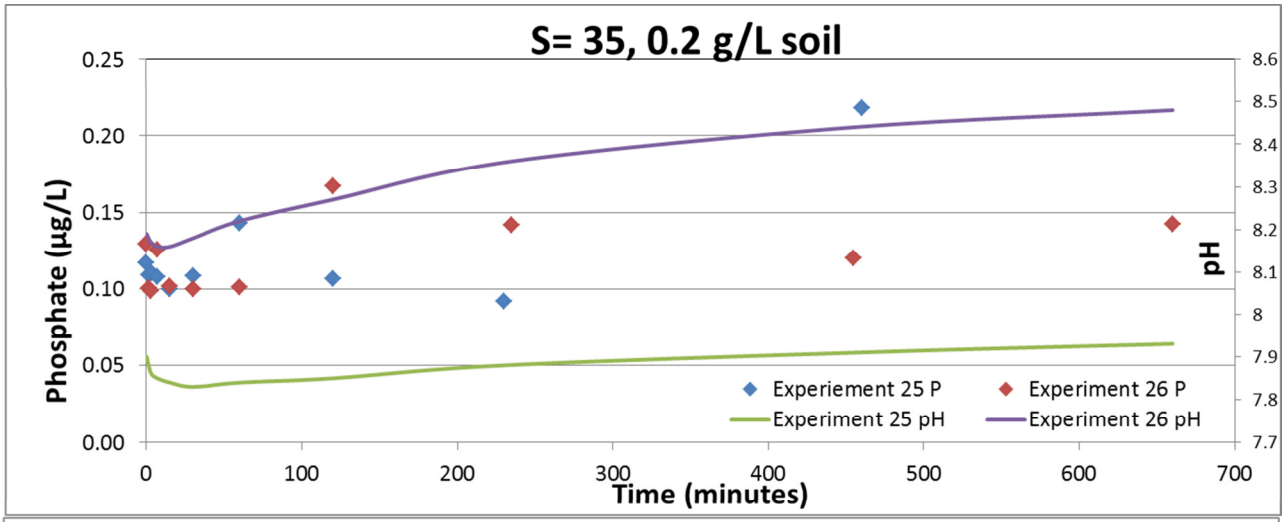

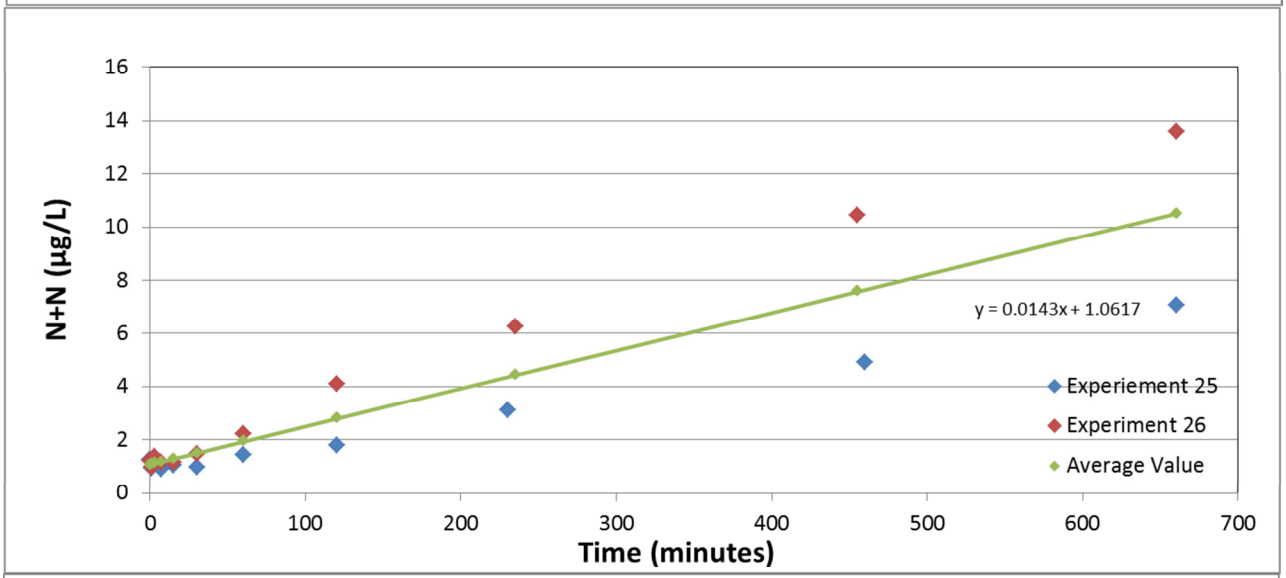

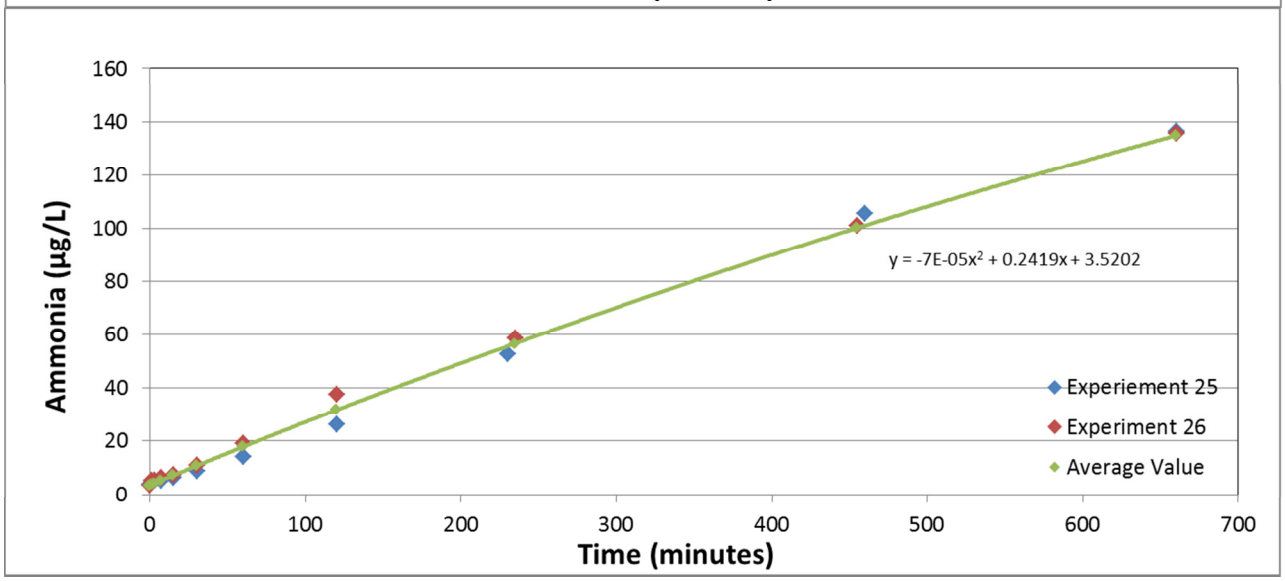

Figure 4.14: S=35, 0.2 g/L Experimental results.

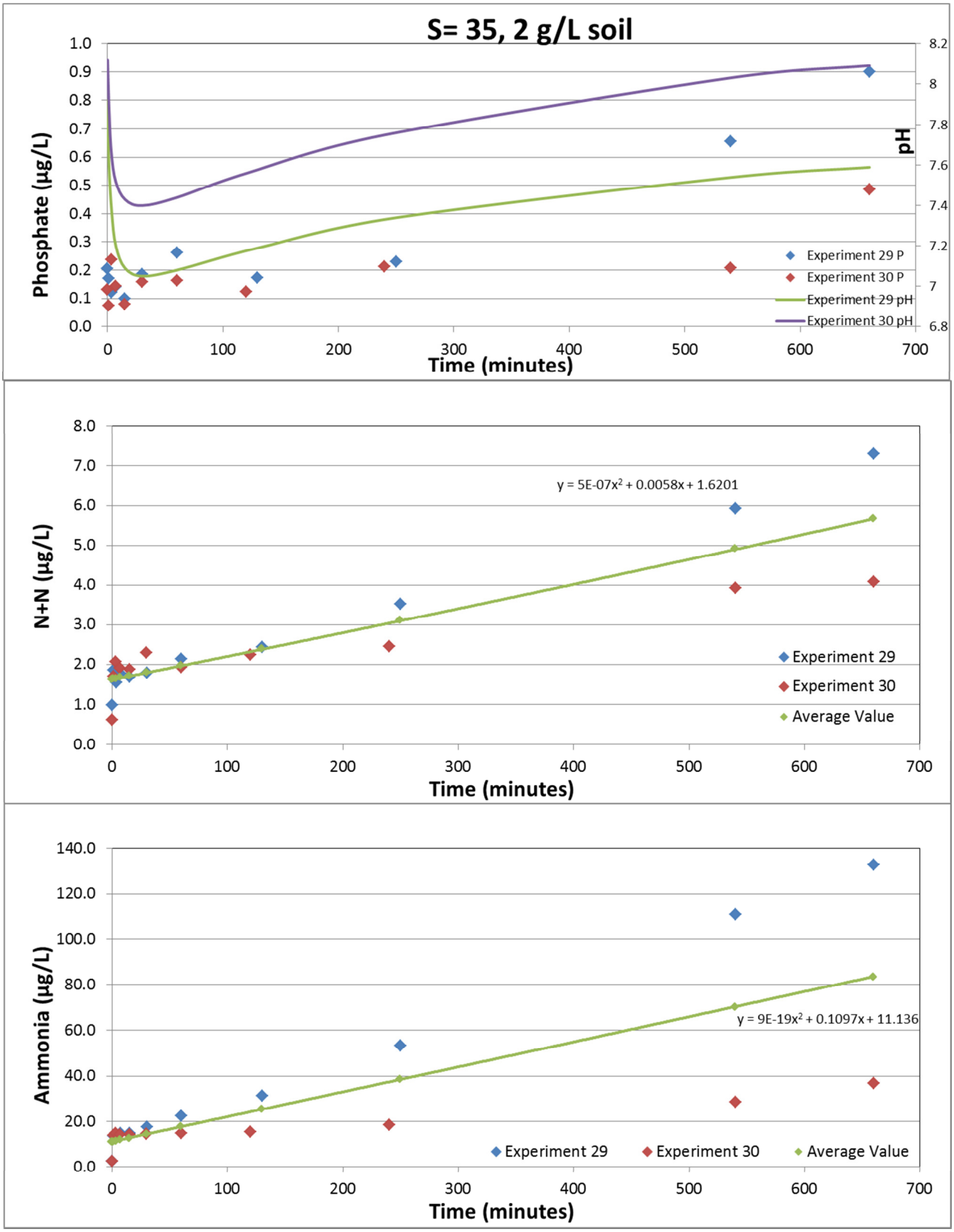

Figure 4.15: S=35, 2 g/L Experimental results.

While the exact amount of nutrients released in each experiment differed, trends for all experiments were generally similar (Figures 4.9-4.15). Variation between experiments of the same salinity and soil composition may be explained by the fact that natural suspended sediment particles consisting of a mixture of many different phases were used. Different soil composition may explain variation between experiments run under the same conditions.

The behavior of phosphate was characterized by an initial rapid uptake from solution within the first hour of experimentation followed by a slower release throughout the duration of the experiment. Unlike phosphate, ammonia and N+N exhibited similar trends, with both nutrients being only released from the particles. Table 4.14 shows the extent of nutrient release or uptake for each experiment.

Table 4.14: Extent of uptake or release of nutrients during experiments.

Experiment Number	Salinity and Soil Composition	Initial Phosphate Uptake (µmol/L)	Subsequent Phosphate release (µmol/L)	Net uptake/release (µmol/L)	N + N release (µmol/L)	Ammonia release (µmol/L)
27	S=0, 1 g soil	0.74	0.21	-0.53	6.4	132
28	S=0, 1 g soil	0.79	0.47	-0.32	11.3	115
27/28 average		***0.77***	***0.34***	***-0.42***	***8.8***	***123***
21	S=9, 1 g soil	0.69	0.24	-0.45	9.4	219
22	S=9, 1 g soil	0.54	0.19	-0.35	21.0	248
21/22 average		***0.61***	***0.21***	***-0.40***	***15.2***	***234***
18	S=17, 1 g soil	0.46	0.18	-0.28	35.9	160
19	S=17, 1 g soil	0.47	0.24	-0.23	22.5	160
18/19 average		***0.47***	***0.21***	***-0.26***	***29.2***	***160***
23	S=35, 1 g soil	0.11	0.15	0.04	6.3	132
24	S=35, 1 g soil	0.13	0.21	0.07	22.7	136
23/24 average		***0.12***	***0.18***	***0.05***	***14.5***	***134***
25	S=35, 0.2 g soil	0.02	0.12	0.10	5.8	133
26	S=35, 0.2 g soil	0.03	0.04	0.01	12.4	132
25/26 average		***0.02***	***0.08***	***0.06***	***9.1***	***132***
29	S=35, 2 g soil	0.11	0.80	0.69	6.3	130
30	S=35, 2 g soil	0.05	0.40	0.35	3.5	34
29/30 average		***0.08***	***0.60***	***0.52***	***4.9***	***82***

Total Nitrogen and Total Phosphorous were also analyzed for Experiments 21 and 22 and results are listed in Table 4.15.

Table 4.15: Extent of uptake or release of Total P and Total N during experiments.

Experiment Number	Salinity and Soil Composition	Initial Total P Uptake (µmol/L)	Subsequent Total P release (µmol/L)	Net Uptake of Total P (µmol/L)	Total N release (µmol/L)
21	S=9, 1 g soil	0.80	0.40	-0.41	285
22	S=9, 1 g soil	0.68	0.25	-0.43	317

Initial phosphate uptake was greatest with the freshwater experiments (average of 0.77 umol/L) and least with the pure seawater experiments (average of 0.12 umol/L). Likewise, subsequent phosphate release was greatest in freshwater experiments (average of 0.34 umol/L) and least with seawater experiments (0.18 umol/L). All experiments exhibited a net uptake of phosphate from solution by the particles except for those conducted in pure

seawater. An average net phosphate release of 0.05 umol/L and 0.06 umol/L occurred for seawater experiments conducted with 1 g and 0.2 g of sediment, respectively, while there was a 0.52 umol/L average phosphate released for the seawater experiment conducted with 2 g of sediment.

N + N release varied with salinity and sediment load. Maximum average release occurred under the S=17 experiment (29.2 umol/L), and minimum average release occurred under the S=35, 2 g soil experiment (4.9 umol/L). Average ammonia release was greatest under the S=9, 1 g soil experimental conditions (234 umol/L). All other experiments yielded an average ammonia release of 82-160 umol/L. Ammonia and N+N release exhibited a linear trend initially; however, the rate of release slowed in the latter half of some experiments, particularly in Experiments 18 and 19.

Tables 4.16-4.17 list the equations obtained for the N+N and Ammonia fits to experimental data that are applied in the following modeling chapter. All equations are approximately linear; however, polynomial equations were used in instances where a stronger coefficient of determination (R^2) was fit.

Table 4.16: Equations used to fit N+N nutrient release curves.

N+N	Equation	Equation form	R^2 value
Experiment 21, S=9	$y = 1E\text{-}05x^2 + 0.0071x + 8.743$	Polynomial	0.996
Experiment 22, S=9	$y = 9E\text{-}06x^2 + 0.0256x + 7.776$	Polynomial	0.998
Average (21/22)	$y = 9.5E\text{-}06x^2 + 0.01635x + 8.259$	Polynomial	-
Experiment 18, S=17	$y = -3E\text{-}06x^2 + 0.021x + 6.7959$	Polynomial	0.995
Experiment 19, S=17	$y = -2E\text{-}06x^2 + 0.0136x + 7.4126$	Polynomial	0.996
Average (18/19)	$y = -2.5E\text{-}06x^2 + 0.0173x + 7.1042$	Polynomial	-
Experiment 23, S=35	$y = 5E\text{-}06x^2 + 0.0063x + 1.5705$	Polynomial	0.997
Experiment 24, S=35	$y = 1E\text{-}05x^2 + 0.0252x + 1.7146$	Polynomial	0.998
Average (23/24)	$y = 7.5E\text{-}06x^2 + 0.01575x + 1.64255$	Polynomial	-
Experiment 25, S=35	$y = 0.009x + 0.9499$	Linear	0.99
Experiment 26, S=35	$y = 0.0196x + 1.1735$	Linear	0.994
Average (25/26)	$y=.0143x + 1.0617$	Linear	-
Experiment 27, S=0	$y = 0.0084x + 11.329$	Linear	0.985
Experiment 28, S=0	$y = 0.0152x + 10.759$	Linear	0.988
Average (27/28)	$y=.0118x + 11.044$	Linear	-
Experiment 29, S=35, 2g	$y = 2E\text{-}06x^2 + 0.0071x + 1.5553$	Polynomial	0.987
Experiment 30, S=35, 2g	$y = -1E\text{-}06x^2 + 0.0045x + 1.6849$	Polynomial	0.829
Average (29/30)	$y = .5E\text{-}06x^2 + 0.0058x + 1.6201$	Polynomial	-

Table 4.17: Equations used to fit Ammonia nutrient release curves.

Ammonia	Equation	Equation form	R^2 value
Experiment 21, S=9 Equation	$y = 0.0002x^2 + 0.1938x + 7.0486$	Polynomial	0.999
Experiment 22, S=9 Equation	$y = 0.0001x^2 + 0.2793x + 5.9079$	Polynomial	0.999
Average (21/22)	$y = 0.00015x^2 + 0.2365x + 6.4783$	Polynomial	-
Experiment 18, S=17	$y=-2E-05x^2 + 0.1158x + 5.3604$	Polynomial	0.995
Experiment 19, S=17	$y = -2E-05x^2 + 0.1315x + 5.7625$	Polynomial	0.996
Average (18/19)	$y = -2E-05x^2 + 0.1237x + 5.5615$	Polynomial	-
Experiment 23, S=35	$y = 2E-05x^2 + 0.178x + 7.5324$	Polynomial	0.998
Experiment 24, S=35	$y = -0.0003x^2 + 0.4222x + 5.2395$	Polynomial	0.99
Average (23/24)	$y= 1.4E-04x^2 + .3001x + 6.386$	Polynomial	-
Experiment 25, S=35	$y = -4E-05x^2 + 0.2297x + 2.7242$	Polynomial	0.997
Experiment 26, S=35	$y = -9E-05x^2 + 0.2542x + 4.3161$	Polynomial	0.999
Average (25/26)	$y = -6.5E-05x^2 + 0.2419x + 3.5202$	Polynomial	-
Experiment 27, S=0	$y = 5E-05x^2 + 0.1506x + 6.8554$	Polynomial	0.999
Experiment 28, S=0	$y = 0.0001x^2 + 0.0721x + 5.4937$	Polynomial	0.997
Average (27/28)	$y = 7.5E-05x^2 + 0.1114x + 6.1746$	Polynomial	-
Experiment 29, S=35, 2g	$y = 0.1845x + 10.418$	Linear	0.994
Experiment 30, S=35, 2g	$y = 0.0348x + 11.853$	Linear	0.843
Average (29/30)	$y=.1097x + 11.136$	Linear	-

4.3 Discussion

Grain Size Analysis

As mentioned previously, the Lo soil sample collected consists of 58.3% sand, 39.1% silt, and 2.5% clay. The Kg soil sample consists of 73.3% sand, 24.3% silt, and 2.1% clay and the Hn soil consists of 74.1% sand, 24.8% silt, and 0.9% clay. Grain size analysis suggests that the soils analyzed here are more representative of a silty sand than a silty clay (Soil Survey Manual, 1993). Mean and median particle sizes for each soil sediment type also fall under sand classifications. While only one surficial soil sample was collected per soil region, these results suggest a high abundance of sands in the Kāneʻohe watershed soils. Since larger particles settle faster than small particles (Table 4.12 and Figure 4.8), it is likely that the majority of sand sized particles carried by streams during storms are deposited in the estuarine region denoted in Figure 4.7. The silt and clay sized particles are more likely to react with seawater since they exhibit a larger surface area to volume ratio and remain in suspension longer than coarser particles (Sposito, 2008; De Carlo and Dollar, Tech Report, 1995). Since the Lo soil has the highest silt and clay composition, it is likely to have the most impact on stream and Bay marine water composition in terms of nutrient release.

Nutrient Release Potential

Nutrient release experiments performed as a function of varying salinities and sediment quantities (Figures 4.9-4.15) were designed to simulate the interaction of land runoff delivered to streams and estuaries. Chemical sorption reactions in soils are typically rapid and can operate on time scales of minutes or hours as readily exchangeable ions adsorb or desorb from solid surfaces (Sposito, 2008). The common sequence of steps for heterogeneous reactions includes: adsorption of aqueous or gas species onto a surface, reaction of adsorbed species among themselves or with the surface atoms, and desorption of product species (Lasaga, 1998). N+N and ammonia results suggest that nonspecific (electrostatic) interaction is the major mechanism involving the reaction of these species with solid surfaces, while phosphate

experimental results suggest that specific adsorption (chemisorption) followed by electrostatic desorption is the dominant mechanism.

The pH trend observed during experimentation was an initial drop of 0.5-1 pH units in the first hour, followed by a subsequent increase in pH throughout the rest of experiments (Figures 4.9-4.15, Appendix 4.1). Iron oxides are a highly abundant phase in Hawaiian soils (Irving, 1998). It is likely that the initial pH drop occurred as iron, a hydrolysis-inducing ion, equilibrated with the liquid solution and phosphate molecules rapidly adsorbed to soil particles following H^+ ions release from $Fe\text{-}OH_2^+$ groups at the particle surfaces.

This trend continued, leading to the enhanced sorption of phosphate from the water mixtures onto the particles since the tendency of phosphate to complex with iron oxides is greater than the tendency to form solution $Fe(OH)_x$-phosphate complexes (Stumm and Morgan, 1995; Sposito, 2008). Additionally, as the solution pH decreased due to the inherent acidity of the soil, there is stronger tendency for phosphate anions to form surface complexes with the soil particles. After this initial interaction, surface charge decreased and the pH approached and exceeded the pzc, allowing for slow phosphate release from soil particles to occur, likely through electrostatic interactions. The presence of abundant anions such as sulfate in seawater, that can displace phosphate, is a possible reason for the net longer term phosphate release in seawater while the absence of this species in stream waters a net phosphate uptake in the freshwater samples. Yet, had the experiments been carried out longer we anticipate that there could have been a net phosphate release for freshwater samples also.

Previous experiments by De Carlo and Dollar (Tech Report, 1995) were run using the same protocol but using synthetic stream water and soils from West Maui. The authors' experiments showed phosphorous release throughout at least the first eight hours of interaction between soil particles and stream water. Differing trends in phosphate release between the two studies are likely due to the fact that their study used synthetic stream and sea water without nutrients as well as a potentially different soil composition.

In both this study and that of De Carlo and Dollar (1995), soils interacting with stream or marine waters showed a rapid release of nitrogen. Initial experiments run for several days

indicated that nitrate + nitrite (N+N) behavior was characterized by a rapid release over 10-12 hours followed by a leveling off to a near steady state condition (Figure 4.10). Adsorption reactions can exhibit "tails" extending for days to weeks (Sposito, 2008), so this study assumed that full release occurred within 12 hours. Ammonia exhibited a comparable trend. Similar to the De Carlo and Dollar (Tech Report, 1995) study, it is likely that little surface charge should remain on the particles due to the proximity of the suspension to the pH-zpc of iron oxyhydroxides. These conditions do not favor N+N or ammonia attraction to soil surfaces, and if the solution pH is above the pzc, there would also be repulsion of anions (e.g., nitrate, nitrite), thereby allowing for nutrient release into the liquid suspension. Ion exchange between NH_4^+ and potassium (K^+) in seawater involving clay minerals is likely to have facilitated the release of ammonia into water.

As discussed previously, all experiments were run using the acidic Lo soil type with a pH of 4.8 (Table 4.3). The Kg soil is also acidic with a sample pH of 4.2; however, the Hn soil had a pH of 7.9. Further experimentation could determine how nutrient release dynamics change with different soils as well as under varying pH and different nutrient concentrations in the experimental fluids.

Near Shore Ocean Implications

Previous studies have suggested that under baseline conditions primary productivity in Southern Kāneʻohe Bay is nitrogen limited (e.g., Smith et al. 1981; Laws and Allen, 1996; Hoover, 2002; Ringuet and Mackenzie, 2005). Ringuet and Mackenzie (2005) determined that following storm events, Southern Kāneʻohe Bay waters were driven toward phosphorous limitation with observed dissolved inorganic nitrogen (DIN): dissolved inorganic phosphorous (DIP) ratios of 25-29 due to fluxes of runoff nutrients, exceeding the commonly observed Redfield Ratio of 16. Recovery times to standard DIN:DIP ratios ranged from 3 to 8 days in their study.

Similarly, the current study suggests that inputs of suspended sediment to Southern Kāneʻohe Bay have the potential to alter nutrient ratios through seawater-particle interactions. Experiments 21-22 in Appendix 4.1 show that by the end of the time of experimentation,

DIN:DIP reached 492 for Experiment 21 and 638 for Experiment 22. This suggests that Southern Kāneʻohe Bay can become phosphorous limited under a variety of sediment loads since DIN:DIP ratios greater than 16 were observed for experiments using varying salinities and sediment loads 0.2, 1, and 2 g of soil, hence supporting the original hypothesis of Ringuet and Mackenzie (2005).

Potential nutrient loadings to the ocean can be estimated by coupling sediment load projections with experimental nutrient release estimates. A predictive model to address how the Kāneʻohe watershed nutrient export varies in response to climate change is presented in the next chapter.

4.4 Summary and Conclusion

Soil analysis and nutrient release experiments conducted in this study have demonstrated that:

1) Surficial soils in the Kāneʻohe watershed are predominately composed of sand sized particles. Under baseline conditions these particles will deposit into the Kāneʻohe Stream estuarine region.

2) There will be a release of nitrogen from terrestrial suspended matter entering the coastal ocean due to rapid surface electrostatic (ion exchange) reactions.

3) Phosphate behavior is dependent upon salinity; in pure seawater there is a net release of phosphorous into the coastal ocean, but in lower salinity water there is a net uptake of phosphorous because of its propensity for strong surface complexation reactions.

Ringuet and Mackenzie (2005) previously determined that intermittent effects of P limitation occur following storms, demonstrating that nutrient limitation status in Kāneʻohe Bay waters and other coastal marine waters is subject to change on short time scales. Similarly, this research determined that the input of suspended sediments to Southern Kāneʻohe Bay has the

potential to lead to phosphorous limitation rather than the normally observed nitrogen limitation. This is due in large measure to the strong and sustained release of N from stream-borne particles. Experimental nutrient release results will be applied to the biogeochemical model in Chapter 5 to evaluate how decreasing precipitation and increasing temperature will impact nutrient export to Southern Kāneʻohe Bay.

Literature Cited:

De Carlo, E.H., and Dollar, S. (1995): Assessment of Suspended Solids and Particulate Nutrient Loading to Surface Runoff and the Coastal Ocean in the Honokowai Drainage Basin, Lahaina District, Maui.

Folk, R. L. & Ward, W. C. (1957) Brazos River bar: a study in the significance of grain size parameters. J. Sediment. Petrol. 27:3-26.

Foote, D.E., Hill, E.l., Sakuichi, N. and Stephens, F. (1972) Soil survey of the islands of Kaui, Oahu, Maui, Molokai and lanai, State of Hawai'i. U.S. Dept. of Agriculture, Soil Conservation Service, U.S. Govt. Printing Office, Washington, D.C.: 232pp.

Hoover, D.J. (2002) Fluvial nitrogen and phosphorus inputs to Hawai'ian coastal waters: storm loading, particle-solution transformations and ecosystem impacts. Department of Oceanography. Honolulu, University of Hawai'i.

Irving, M.M. (1998) An investigation of reactions among heavy metals and naturally occurring minerals in synthetic and natural stream waters. Dissertation, Department of Chemistry, University of Hawai'i at Mānoa , Honolulu.

Kotz, J. C., Treichel, P., Townsend, J. R., & Treichel, D. A. (2015). Chemistry & chemical reactivity (9th ed.). Cengage Learning.

Krumbein, W.C. and Pettijohn F.J. (1988) Manual of Sedimentary Petrography. SEPM Classic Facsimile Edition of the 1938 original; SEPM Reprint Series. Tulsa: Society for Economic Paleontologists and Mineralogists (SEPM).

Lasaga, A. C.(2014). Kinetic Theory in the Earth Sciences. Princeton: Princeton University Press.

Laws, E.A., and Allen, C.B. (1996) Water quality in a subtropical embayment more than a decade after diversion of sewage discharges. Pacific Science, 50(2):194-210.

Ringuet, S. and Mackenzie, F.T. (2005) "Controls on Nutrient and Phytoplankton Dynamics During Normal Flow and Storm Runoff Conditions, Southern Kāne'ohe Bay, Hawai'i." Estuaries 28(3):327-337.

Ristvet, B.L. (1978) Reverse weathering reactions within recent nearshore marine sediments, Kāne'ohe Bay, Oahu. Test Directorate Field Command, Kirtland AFB, New Mexico, 314 pp.

Smith, S.V., W.J. Kimmerer, E.A. Laws, R.E. Brock, and T.M. Walsh. (1981) Kāne'ohe Bay sewage diversion experiment: Perspectives on ecosystem responses to nutritional perturbation. Pacific Science **35**: 279-395.

Soil Survey Staff. (1993) Soil Survey Manual. United States Dept. of Agri. U. S. Government Printing Office, Washington, D. C. 20402. pp. 136-146.

Sposito, G. (2008) The chemistry of soils. 2nd edition. Oxford University Press, New York.

Stumm, W. and Morgan, J.J. Aquatic Chemistry: Chemical Equilibria and Rates in Natural Waters, 3rd ed., Wiley, New York, 1995.

CHAPTER 5: Increased Atmospheric CO_2 and Temperature and Decreased Precipitation Effects on the Southern Kāneʻohe Watershed and Southern Kāneʻohe Bay

5.1 Introduction

A water-suspended sediment biogeochemical box model (Southern Kāneʻohe WAtershed and Offshore Nutrient Export Model, hereafter referred to as SKWANEM) of the Southern Kāneʻohe Watershed and Southern Kāneʻohe Bay, Hawaii was created to evaluate how increasing temperatures and decreased precipitation may impact nutrient export in the study region. SKWANEM includes 3 reservoirs, two transfer points, and 11 fluxes accounting for water and weathering cycles. A steady state model designed for year 2015 of initial conditions was formulated first from literature data for reservoir masses and fluxes between reservoirs. Data from previous studies and USGS gages in the Kāneʻohe Bay region were used to determine the initial reservoirs and fluxes. Perturbations were then applied to the model using projections of atmospheric CO_2 and precipitation using the Intergovernmental Panel on Climate Change (IPCC) Representative Concentration Pathway (RCP) Scenarios (2013) through the year 2100. Precipitation projections for the island of Oahu based on statistical downscaling of rainfall changes from the IPCC were used (Elison Timm et al., 2015) and regional CO_2 concentration projections for the island of Oahu specifically were applied to SKWANEM to address the working hypothesis, which states that:

As precipitation decreases due to climate change, a lower sediment load to Southern Kāneʻohe Bay will lead to a lesser release of inorganic nutrients from the suspended sediment riverine load.

This chapter addresses model formulation and anticipated changes in nutrient export as a result of predicted changes in precipitation and CO_2 concentrations. Figure 5.1 illustrates the study region for the SKWANEM Model. The Kāneʻohe watershed spans 11.3 km^2 (Hoover, 2002) and the southern portion of Kāneʻohe Bay encompasses 8.37 km^2 of land area (Smith et al., 1981). Groundwater, Waimaluhia Reservoir, and the southern portion of Kāneʻohe Bay are the three reservoirs in SKWANEM within the Southern Kāneʻohe region. Land surface and streams act as transfer points that relocate water and sediment from one reservoir to another. External sources for the system are the atmosphere and soil and rock, and in addition there is an external sink for the open ocean.

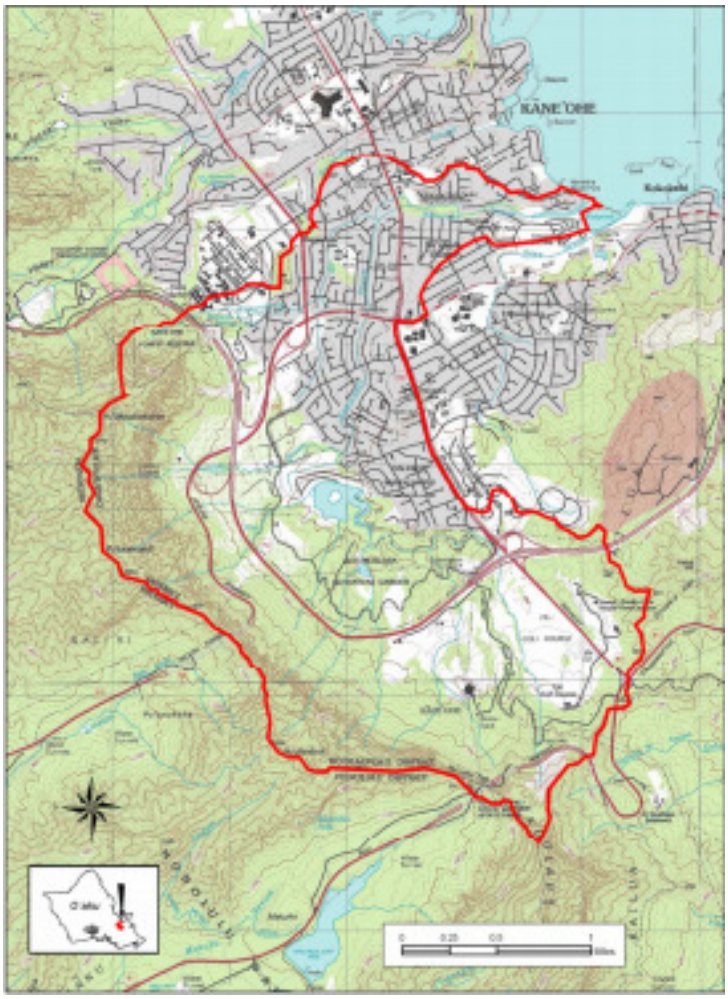

Figure 5.1: Kāne‘ohe Watershed location map
(Executive Summary – State of Hawaii Department of Health, 2009).

Waimaluhia reservoir is a 26-acre artificial water body created by a dam located within Kāne‘ohe Watershed that was designed as a flood control measure (Wong, 2001). An assumption in SKWANEM is that all water from the tributaries upstream of the reservoir enter the reservoir. Of the five streams that flow into the reservoir, two are intermittent (Kuou Stream and Piho Stream), while Hooleinaiwa, Kamooalii, and Right Branch Kamooalii Streams are perennial. Figure 5.2 depicts stream locations.

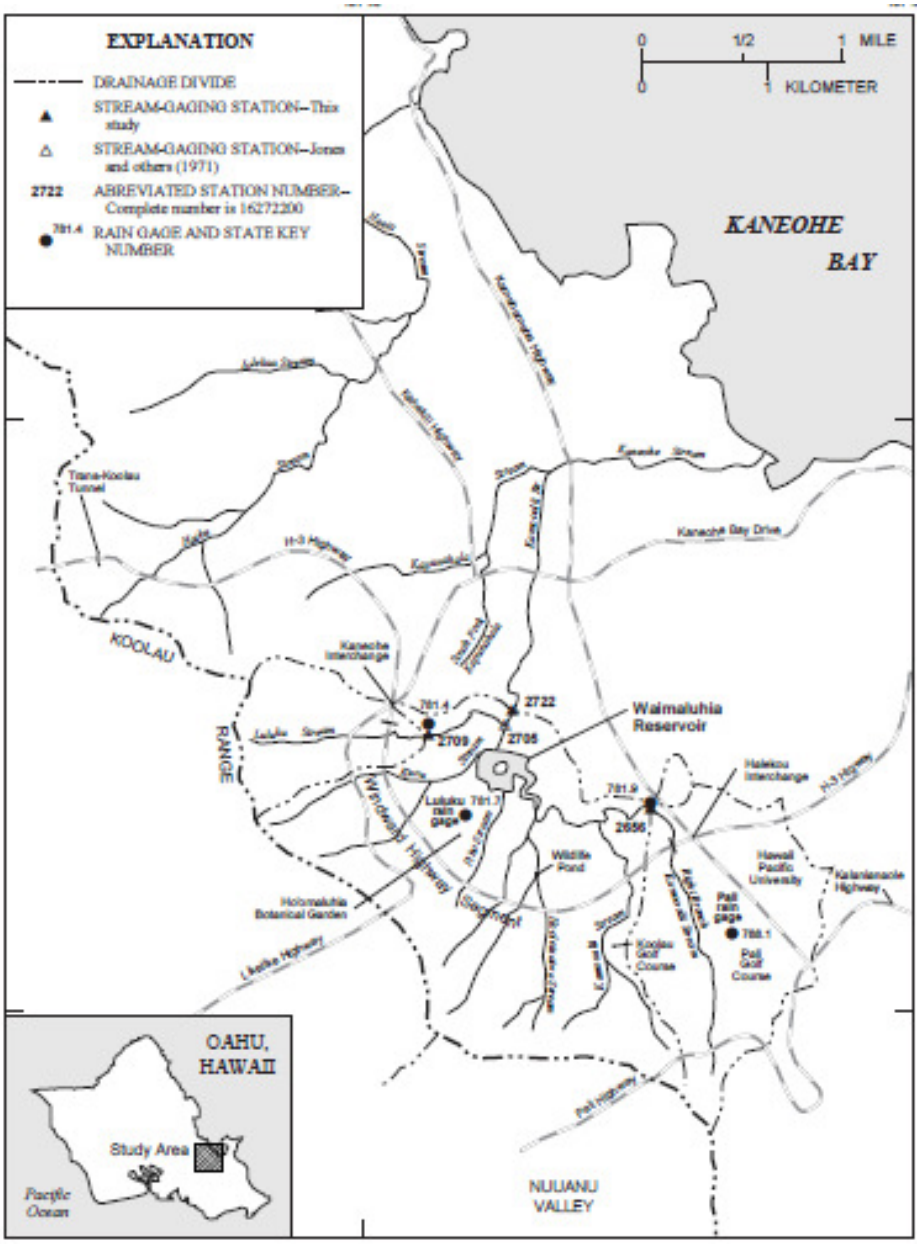

Figure 5.2: Waimaluhia Reservoir study region (Wong, 2001).

5.2 SKWANEM Model Development

SKWANEM was developed and run in Matlab using ODE23, a solver function designed to solve nonstiff differential equations. The following assumptions and procedures were followed that are common to biogeochemical box modeling (e.g. Lerman et al., 1975; Ver et al., 1999; Andersson et al., 2003; Drupp, 2015):

Equation 5.1 was the standard mass balance equation solved in box modeling approaches, where M_i is the mass of the reservoir in question and CF_{ji} is the flux from reservoir *j* to *i*, and CF_{ij} is the flux from reservoir *i* to *j.*

$$\frac{dM_i}{dt} = \sum_j CF_{ji} - \sum_i CF_{ij} \qquad \textbf{(Equation 5.1)}$$

The assumption was made that the system originates at a steady state condition with no net fluxes. These steady state values were approximated using literature and experimental work from the Kāneʻohe Bay region, or surrounding region if necessary. Initial steady state conditions were run for 85 years (the point at which the changes in reservoir sizes and fluxes was negligible) to ensure a steady state before perturbing the system with projected changes in precipitation and CO_2 concentration as a function of temperature.

5.3 Water and Sediment Balances- domain and initial conditions

Steady-state water and suspended sediment balances were first assembled for the study region to approximate current watershed conditions.

Steady State Water Balance

SKWANEM's water domain is composed of the following reservoirs: ground water, Waimaluhia Reservoir, and Kāne'ohe Bay, and the following fluxes depicted in Figure 5.3: net precipitation over land, net precipitation over Bay, infiltration, submarine ground water (SGW) seepage, input to Waimaluhia Reservoir, runoff, output from the reservoir, discharge, and marine water export to the open ocean.

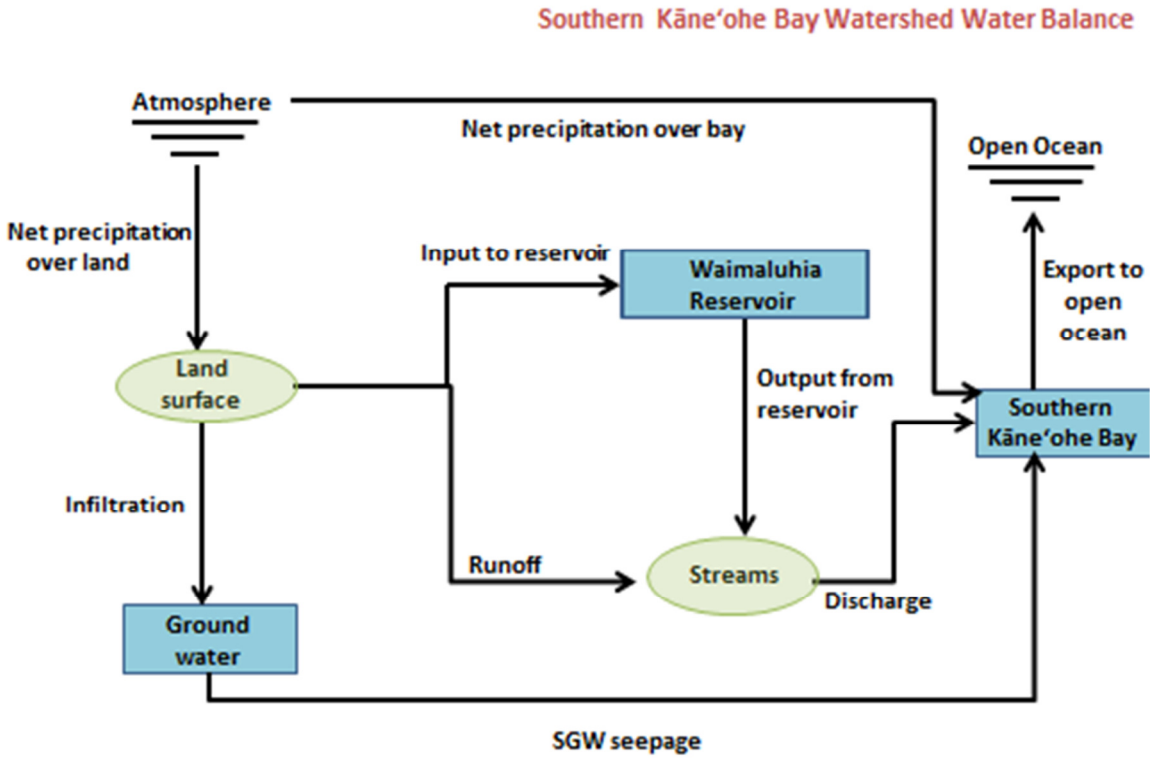

Figure 5.3: Schematic diagram of the conceptual water model of inorganic nitrogen and phosphorous for the Kāne'ohe watershed and adjacent proximal marine coastal waters. Squares represent reservoirs, ovals represent transfer points, stacked lines represent sources and sinks, and arrows represent fluxes.

Steady state reservoir volumes and justifications for the values taken are listed in Table 5.1. Individual volumes spanned five orders of magnitude, with Waimaluhia Reservoir at 2.1 x 10^5 m^3, and the ground water estimate at 1.13 x 10^{10} m^3.

Table 5.1: SKWANEM Initial steady state reservoir volumes.

Water reservoirs at steady state	Reservoir notation in model code	Volume in m^3	Remarks
Ground Water	GW	1.13 x 10^{10}	Using the assumption that freshwater extends 2 km below sea level (the depth at which porosity is typically reduced) and rock porosity is 50% (Oki, 2016), groundwater volume = watershed area x freshwater thickness x rock porosity = 11.3 km^2 (Hoover, 2002) x 2 km x 0.5 x ($10^9 m^3$/ km^3)= 1.13 x 10^{10} m^3.
Waimaluhia Reservoir	WR	2.1 x 10^5	The reported volume in July 1998 was 209.3 acre-ft (Wong, 2001). The reservoir has a design loss rate of 2 acre-ft/yr. With no reports of dredging to the reservoir, it is assumed that 36 acre-ft of sediment have deposited since July 1998 and the current reservoir water volume is 173.3 acre-ft. 173.3 acre-ft x 1233.5 m^3/acre-ft=2.10 x 10^5 m^3.
Kaneohe Bay (Southern portion)	KB	7.96 x 10^7	Based on the Inner Kaneohe Bay Southern Basin Volume consisting of outfall + southeast sectors (Smith et al., 1981).

Steady state fluxes were also estimated using USGS gage data and available literature for Kāne‘ohe Bay and neighboring regions. All values in units of m^3/yr and corresponding justifications are provided in Table 5.2.

Table 5.2: Initial steady state fluxes for water in m^3/year.

Water fluxes at steady state	Flux notation in model code	Rate in m^3/yr	Remarks
Flux of net precipitation into Kaneohe Watershed	Npland	1.28×10^7	**Precipitation**: The average precipitation for the Kaneohe Watershed is 204 cm/yr and the watershed area is 11.3 km^2 (Hoover, 2002). Precipitation over Kaneohe watershed = precipitation rate x watershed area= 2.04m/yr x 1.13×10^7 m^2= 2.31×10^7 m^3/yr **Evapotranspiration**: Evapotranspiration= 45% of precipitation (Cox at al., 1973) = 1.03×10^7 m^3/yr. **Net Precipitation**=Precipitation-Evapotranspiration= 1.28×10^7 m^3/yr.
Flux of net precipitation into Southern Kaneohe Bay	NPOcean	9.47×10^6	Same calculations as those for net precipitation intro Kaneohe Watershed using the Southern basin area of 8.37 km^2 (Smith at al., 1981).
Flux of infiltration to groundwater through the land surface	Infiltration	2.98×10^6	Cox et al. (1973) estimated 2.27×10^7 L/day of submarine groundwater discharge; 36% enters the southern portion of the bay (McGowan, 2004). The assumption is made that at steady state infiltration = flux of water out of groundwater reservoir. 2.27×10^7 L/day x 0.36 x 365 days/yr x $1 m^3/1000$ L = 2.98×10^6 m^3/yr.
Flux of runoff from the land surface	LandRunoff	1.02×10^6	Depending on annual precipitation and land use runoff rates can vary between 4% and upward of 30% (Giambelluca, 1986). A rate of 8% was used for this study because the majority of the watershed is classified as having moderately low runoff potential (State of Hawaii Department of Health Executive Summary, 2009).
Flux of output from Waimaluhia Reservoir	OutputWR	8.8×10^6	The average reservoir outflow for years 1985-1997 was 3600 ft^3/s-days/year (Wong, 2001). 3600 ft3/s-days/year x $1 m^3/35.3$ ft^3 x 86400 s-days = 8.8×10^6 m^3.
Flux of input to Waimaluhia Reservoir	InputWR	8.8×10^6	At steady state the assumption is made that the flux of input to Waimaluhia Reservoir = the output flux from Waimaluhia Reservoir.
Flux of stream water entering Kaneohe Bay	StreamDischarge	9.82×10^6	USGS Gage 16272200 data from 1978-2005 yielded an average discharge of 10.31 cfs. This is equivalent to 9.2×10^6 m^3/yr. This value was modified to 9.82×10^6 m^3/yr in order for the system to balance at steady state.
Flux of groundwater entering Kaneohe Bay	SGWSeepage	2.98×10^6	Cox et al. (1973) estimated 2.27×10^7 L/day of submarine groundwater discharge; 36% enters the southern portion of the bay (McGowan, 2004). 2.27×10^7 L/day x 0.36 x 365 days/yr x $1 m^3/1000$ L = 2.98×10^6 m^3/yr.
Flux of water exiting Kaneohe Bay to the open ocean	OcnExport	2.27×10^7	The assumption was made that the bay volume will remain constant at steady state. OcnExport = SGWSeepage + NPOcean + StreamDischarge

Precipitation fluxes into the watershed and Southern Kāne'ohe Bay were the largest fluxes at 1.28 x 10^7 and 9.47 x 10^6 m^3/yr, respectively. Precipitation has a strong impact on the water balance since it is the originating water flux and the subsequent fluxes are a function of precipitation, all are in the 10^6 order of magnitude. Figure 5.4 depicts the water balance schematic with the corresponding flux values in m^3/yr incorporated into the diagram.

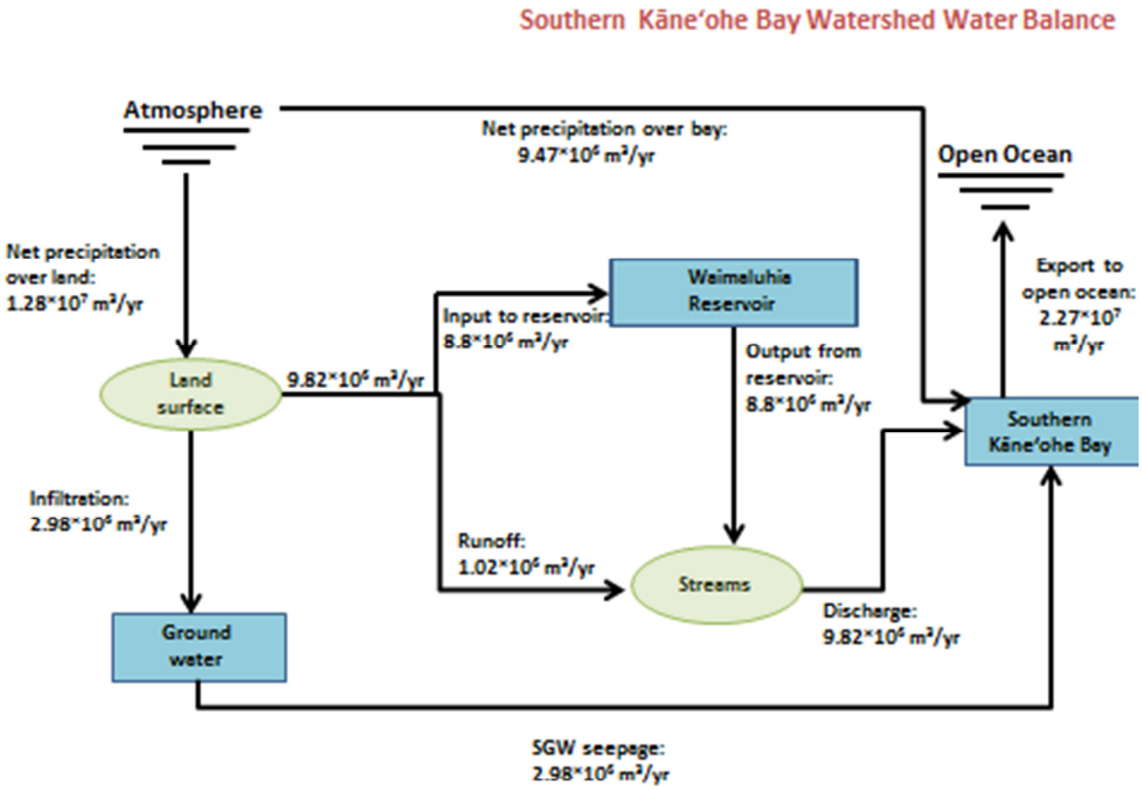

Figure 5.4: Schematic diagram of the conceptual water model of inorganic nitrogen and phosphorous for the Kāne'ohe watershed and adjacent proximal marine coastal waters with corresponding flux values. Squares represent reservoirs, ovals represent transfer points, stacked lines represent sources and sinks, and arrows represent fluxes.

Steady State Sediment Balance

SKWANEM's suspended sediment domain is composed of the reservoirs Waimaluhia Reservoir and Kāne'ohe Bay and the following fluxes depicted in Figure 5.5: sediment input to Waimaluhia Reservoir, sediment input to Kāne'ohe Stream, sediment output from Waimaluhia Reservoir, and sediment input into Kāne'ohe Bay. Sediment deposition in Waimaluhia Reservoir is considered as a sink.

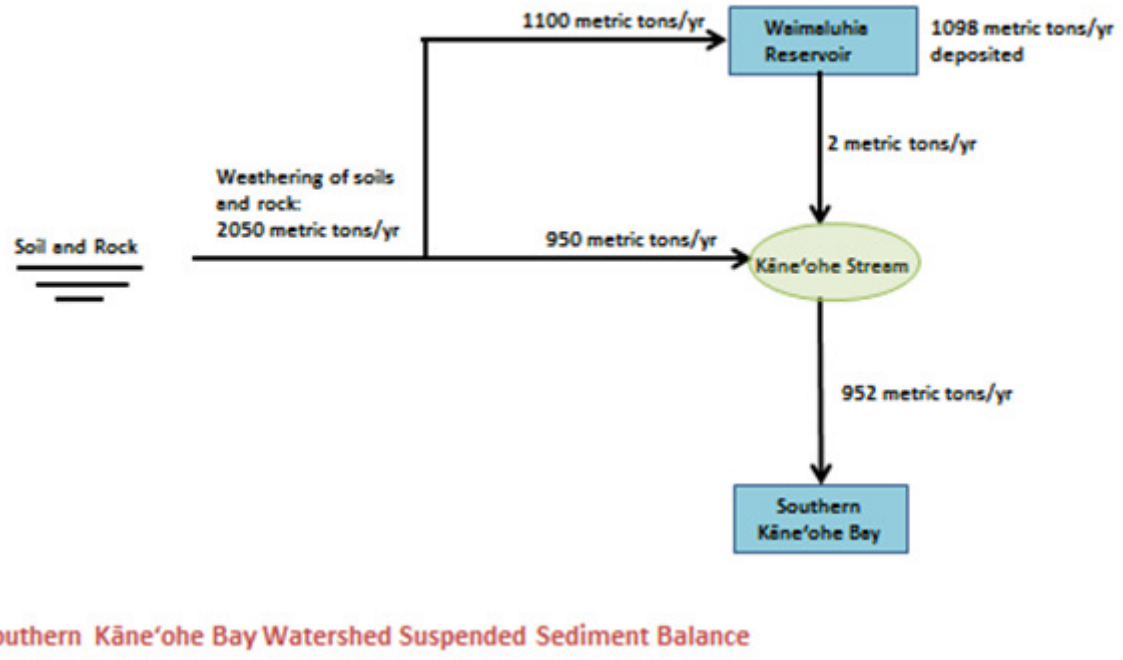

Figure 5.5: Schematic diagram of the conceptual suspended sediment model of inorganic nitrogen and phosphorous for the Kāne'ohe watershed and adjacent proximal marine coastal waters. Squares represent reservoirs, ovals represent transfer points, stacked lines represent sources and sinks, and arrows represent fluxes.

SKWANEM is a box model that considers fluxes into and out of the reservoirs but not reactions within the reservoirs, such as diagenesis. For this reason the assumption was made that the suspended sediment particles already deposited into Waimaluhia Reservoir and Southern Kāneʻohe Bay were nonreactive in terms of inorganic phosphorous and nitrogen at steady state conditions. Soil volumes of Waimaluhia Reservoir and Southern Kāneʻohe Bay and their corresponding nutrient concentrations were not calculated; the assumption was made that the corresponding water nutrient concentrations would reflect the input of nutrients from these sediments. For this reason, only the input of new suspended sediment via weathering was considered. Table 5.3 lists the suspended sediment fluxes in metric tons/yr and justification for these values.

Table 5.3: Initial steady state suspended sediment fluxes in metric tons/year.

Suspended sediment fluxes at steady state	Flux notation in model code	Rate in metric tons/yr	Remarks
Sediment input to Waimaluhia Reservoir	SedInputWR	1100	Waimaluhia reservoir was designed for a sediment accumulation rate of 2 acre-ft/year (Wong, 2001). The average bulk density of deposited sediments between 1983 and 1998 was 29 pounds per cubic foot. Annual accumulation= 2 acre-ft/year x 1233 cubic meter/1 acre-foot x 29 lbs/ft^3 x 1 cubic foot/0.028 cubic meter x 1 metric ton/2204.6 lbs= 1159 metric tons/yr. This value was rounded down slightly to 1100 metric tons/yr to account for the fact that several years during the study window had accumulation rates lower than 2 acre-ft/year.
Sediment input to Kaneohe Stream	SedInputKS	950	Daily suspended sediment data from the USGS National Water Information System Mapper Site Number 1627220 ranging from November of 1976 to September of 1998 were utilized for this analysis (Hypothesis 2 data used in Chapter 2). The mean daily suspended sediment discharge during this period was 2.9 tons per day, or 2.6 metric tons. 2.6 metric tons/day x 365 days/year= 950 metric tons/yr
Sediment deposited in Waimaluhia Reservoir or along the bank	N/A	1098	The assumption was made that the majority of the sediment entering Waimaluhia was trapped in the reservoir or deposited along stream banks.
Sediment output from Waimaluhia Reservoir	N/A	2	The assumption was made that the majority of the sediment entering Waimaluhia was trapped in the reservoir or deposited along the bank.
Sediment input to Kaneohe Bay	N/A	952	Sediment entering Kaneohe Bay is the sum of the suspended sediment in Kaneohe Stream and the suspended sediment exiting Waimaluhia Reservoir.

The steady state suspended sediment schematic of Figure 5.5 assumes that physical weathering is the sum of steady state sediment input to Waimaluhia Reservoir and steady state sediment input to Kāne‘ohe Stream. The values in Table 5.3 indicate that, based on this assumption, there are approximately 2050 metric tons/year of physical weathering in the watershed. There is a wide range of estimates for physical weathering rates on Oahu from previous denudation studies. Li (1988) estimated a range of 6-30 mg/cm^2/yr for physical

weathering on Oahu. Over the 11.3 km^2 area of the watershed, this is equivalent to 678-3390 metric tons/yr. Nelson et al. (2013) conducted a more recent study and calculated denudation rates that overlap with lower ranges of previous estimates (Li, 1988; Rad et al., 2007; Navarre-Sitchler and Brantley, 2007). Their physical weathering estimate for windward Oahu is 0.009-0.013 m/ka. When calculated over the watershed region and assuming a basaltic rock density of 2.6 g/cm^3 (Li, 1988), this estimate translates to 294-381 metric tons/yr. The steady state suspended sediment balance estimate of 2050 metric tons/year of physical weathering falls within the literature's estimated range of 294-3390 metric tons/year, suggesting the SKWANEM estimate is reasonable. Figure 5.6 lists the steady state suspended sediment values with corresponding fluxes listed in metric tons/yr. The sediment flux terms for inputs to Waimaluhia Reservoir and Kāneʻohe Stream were used in the coupled water-sediment model discussed in the next section.

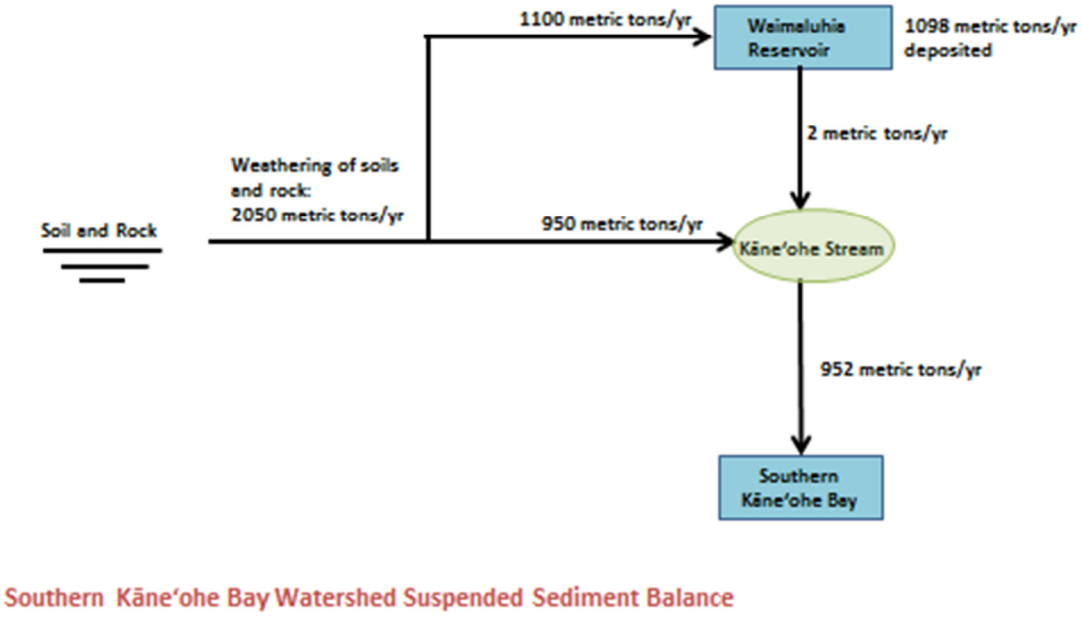

Figure 5.6: Schematic diagram of the conceptual suspended sediment model of inorganic nitrogen and phosphorous for the Kāne'ohe watershed and adjacent proximal marine coastal waters with corresponding flux values. Squares represent reservoirs, ovals represent transfer points, stacked lines represent sources and sinks, and arrows represent fluxes.

5.4 Combined Balance and Equations

The variables of the water balance schematic (Figures 5.3 and 5.4) and suspended sediment schematic (Figures 5.5 and 5.6) were combined to create a coupled water-suspended sediment model to evaluate inorganic nitrogen and phosphorous export in the Kāne'ohe watershed and adjacent proximal marine waters. This schematic for the SKWANEM model is depicted in Figure 5.7.

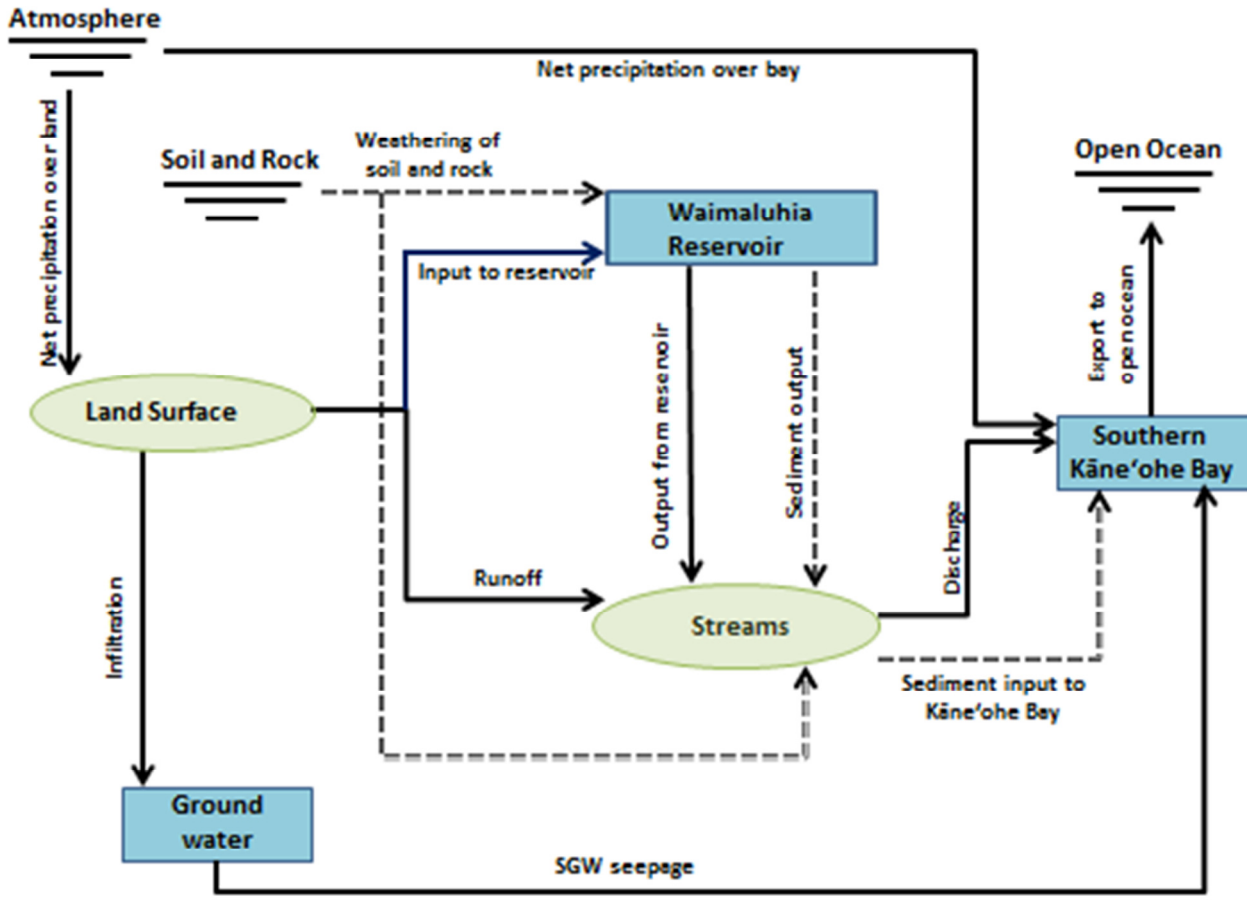

Figure 5.7: Schematic diagram of the conceptual combined water and suspended sediment model of inorganic nitrogen and phosphorous for the Kāne'ohe Bay watershed and adjacent proximal marine coastal waters. Squares represent reservoirs, ovals represent transfer points, stacked lines represent sources and sinks, and arrows represent fluxes. Solid arrows represent water transfer and dashed arrows represent sediment transfer.

Water calculations

Nutrient export for the water domain was evaluated by solving standard mass balance equations (Equation 5.1) and multiplying each water flux by the nutrient concentration of the originating reservoir or source to obtain the magnitudes of the nutrient fluxes (in µmol). Inorganic nutrient concentration values for groundwater, Kāneʻohe Bay, and precipitation were assessed from recent literature in the Kāneʻohe Bay region. For the Waimaluhia Reservoir nutrient concentrations used in calculation of fluxes, samples were collected from the outflow region of the reservoir over several days under low flow conditions, and the mean value was used for the model (Table 5.4). Mean phosphate values for Waimaluhia Reservoir were 0.6 µmol/L, and N+N and ammonia values were 20.8 and 2.5 µmol/L respectively.

Table 5.4: Waimaluhia Reservoir nutrient concentrations.

Sample Name	**Total N**	**Total P**	**Phosphate**	**Silicate**	**N+N**	**Ammonia**
	µmol/L	**µmol/L**	**µmol/L**	**µmol/L**	**µmol/L**	**µmol/L**
SC-WR-1	43.24	1.37	0.74	368.25	21.28	2.54
SC-WR-2	37.44	1.19	0.51	296.01	20.94	2.32
SC-WR-3	43.14	1.54	0.66	375.99	20.10	2.59
Average	*41.3*	*1.4*	*0.6*	*346.8*	*20.8*	*2.5*

Table 5.5 lists all inorganic nutrient concentrations used in the SKWANEM model, with supporting remarks and justification for values.

Table 5.5: Inorganic nutrient concentrations for reservoirs and sources.

Reservoir	Phosphate	N+N	Ammonia	Remarks
	µmol/L	µmol/L	µmol/L	
Groundwater	1.5	10	10	Hoover (2009) estimates phosphate, N+N, and ammonium groundwater concentrations in the Kaneohe Bay sub-watersheds to be 0.5 -1.2 µmol, 5-10 µmol, and 8-12 µmol, respectively. Dulai et al. (2016) estimate phosphate and N+N concentrations to be 1.6 +/- 0.5 µmol and 12.1 +/- 2.9 µmol respectively. Estimates were made based on these averages, and the assumption was made that ammonia concentrations are equivalent to ammonium concentrations.
Waimaluhia Reservoir	0.6	20.8	2.5	The average value of the 3 samples collected from Waimaluhia Reservoir was used(Table 5.4).
Ocean (S. Kaneohe Bay)	0.07	0.19	0.1	Averages values from 1998-2001 monitoring studies of Southern Kaneohe Bay were used (Kinzie III et al., 2001). The assumptions were made that ammonia concentrations are equivalent to ammonium concentrations N+N concentrations are equivalent to nitrate concentrations.
Precipitation	0	3.6	0.05	Phosphate and N+N values were taken from Root et al. (2004). N+N was converted from 0.22 mg/L to 3.6 µmol/L. Ammonia values were taken from the National Atmospheric Deposition program website's value for Hawaii Volcanoes National Park since no Oahu data was available (http://nadp.sws.uiuc.edu/nadpdata/register.asp). Annual average ammonium concentrations were available for the period of 2000-2005. These 5 values were averaged to obtain an average annual ammonium concentration of 0.02 mg/L. This value was converted to 0.57 µmol/L. The assumption was made that ammonia concentrations are equivalent to ammonium concentrations, and that Oahu Ammonia precipitation concentrations are equivalent to approximately 10% of that at Hawaii Volcanoes National Park.

Suspended sediment calculations

Several assumptions were made in the implementation of the suspended sediment nutrient fluxes:

While the suspended sediment diagram (Figure 5.6) shows 4 sediment fluxes, only sediment fluxes into Waimaluhia Reservoir and Kāneʻohe stream were considered in the model since the Kāneʻohe stream flux represents the sum of the fluxes into Kāneʻohe stream. Likewise, nutrient fluxes involving sediment leaving Waimaluhia Reservoir were not considered because of the assumption that all suspended sediment-water reactions had likely occurred during the long residence time of the water in the reservoir, and that the nutrient concentrations of the water leaving the reservoir would account of reactions taking place within the reservoir.

The fluxes of nutrients associated with suspended sediment into Waimaluhia Reservoir were calculated by multiplying the quantity of suspended sediment entering the reservoir (Table 5.3) by the soil nutrient concentrations listed in Table 4.3 of Chapter 4 and in Table 5.6. As described previously, only the Luluku soil type was considered for model calculations and nutrient release experiments since the vast majority of the Kāneʻohe watershed is composed of this soil type (Figures 2.1 and 2.1B). Calculations were also performed to convert nutrient concentration values to µmol/metric tons by dividing by the molecular weight and converting grams to metric tons as shown in Table 5.6.

Table 5.6: Soil inorganic nutrient concentrations in µmol/metric tons.

	Soil concentration (µg/g)	Inverse Molecular Weight (mol/g)	Gram-metric tons conversion (g/metric tons)	**Nutrient input concentration (µmol/metric tons)**
Phosphate	6	1/30.971	10^6	2.E+05
N+N	15	1/62.005	10^6	2.E+05
Ammonia	1.4	1/18.039	10^6	8.E+04

The fluxes of nutrients associated with suspended sediment input to Kāneʻohe Stream were calculated by multiplying the quantity of suspended sediment entering Kāneʻohe Stream by the estimated magnitude of uptake or release derived from the Chapter 4 experimental results. Table 4.14 lists the net uptake and release of nutrients from experiments with various salinities and nutrient loads. The average nutrient release or uptake from Experiments 27 and 28 (S=0, 1 g sediment added) was used for model calculations. This experiment showed a net uptake of phosphorous (0.42 µmol/L). Previous research has shown that storm conditions can lead to phosphorous limitation in Kāneʻohe Bay (Ringuet and Mackenzie, 2005), but this tends to be a short-term effect. For this reason, and due to the fact that stream water in the watershed ultimately reaches Kāneʻohe Bay, the average phosphorous release from Experiments 23 and 24 (S=35, 1 g sediment added) of 0.05 µmol/L was used in the model calculations. Table 4.14 values listed in µmol/L were multiplied by 10^6 g/metric tons and the experimental conditions of 1 g of soil/1 L of water to yield the potential uptake or release of nutrients from soil in units of µmol/metric tons (Table 5.7).

Table 5.7: Potential nutrient release of inorganic nutrients in µmol/metric tons.

	Net release of nutrients from experiments (µmol/L)	**Potential uptake or release in µmol/metric tons**
Phosphate	0.05	5.00E+04
N+N	8.8	8.80E+06
Ammonia	123	1.23E+08

Physical and chemical weathering

The processes involving physical and chemical weathering were considered in the formulation of the SKWANEM model. Berner et al. (1983) and Arvidson et al. (2006) presented a series of equations that predict weathering rates for the effect of temperature on runoff and rates of mineral dissolution. This was done through a temperature correction factor, $f_B(T)$, given as:

$$f_B(T) = k_w(T)/k_w(T_0) = [c(T)/c(T_0)][R(T)/R(T_0)] \quad \textbf{(Equation 5.2)}$$

where: k_w = first order rate constant for weathering
c = concentration in river water of an element resulting from weathering
R = runoff
T = worldwide mean annual surface air temperature (°C)
T_0 = present worldwide mean annual surface air temperature

Equation 5.3 was also used to convert air temperature to atmospheric CO_2 content:

$$A_{CO2}(t)/A_{CO2}(o)=\exp[0.347(T-T_0)] \quad \textbf{(Equation 5.3)}$$

where: $A_{CO2}(t)$ = mass of atmospheric CO_2 at time t
$A_{CO2}(o)$= mass of atmospheric CO_2 today
T= mean annual global air surface temperature in degrees Celsius at time t

Berner et al. combined Equations 5.2 and 5.3 to determine the relationship between weathering flux and atmospheric CO_2 concentration, as follows:

$$f_B(CO_2) = 1.0 + 0.252 \ln [A_{CO2}/A_{CO2o}] + 0.0156 \{ \ln [A_{CO2}/A_{CO2o}]\}^2 \text{ (**Equation 5.4**)}$$

where: A_{CO2} = new atmospheric CO_2 content
A_{CO2o} = current CO_2 content

In the SKWANEM model, Equation 5.4 was multiplied by each suspended sediment flux to account for chemical weathering. Values of 399 µatm were used for both A_{CO2} and A_{CO2o} at T_0 for steady state calculations. Physical weathering was also accounted for by using the Kāne'ohe Stream precipitation-suspended sediment relationship derived in Chapter 3 (Figure 3.9) coupled with precipitation projections discussed in Section 5.5.

Steady state equations

Initial steady state equations are provided in Appendix 5.1 based on the aforementioned assumptions and model schematic conceptual diagram (Figure 5.7).

5.5 Perturbations

After solving for the initial SKWANEM steady-state conditions, perturbations were applied to the model to reflect estimated changes in CO_2 concentrations, precipitation, and volume of Kāne'ohe Bay to reflect rising sea level. The Hawaiian Islands have already experienced a drying trend in recent decades (Diaz and Giambelluca, 2012) and the Intergovernmental Panel on Climate Change (IPCC) 5th Assessment Report (Intergovernmental Panel on Climate Change, 2013) predicts this trend will continue. The concentration of atmospheric CO_2 and sea level will also continue to rise.

The time period of 2015-2100 was analyzed for this study since this is the period of projection analysis used in the IPCC 5th Assessment Report on which the forcings are based. Similarly to previous work (Drupp, 2015), RCP emissions scenarios developed for the IPCC 5th Assessment Report were applied to the model as forcings. The scenarios applied to SKWANEM in this study were Representative Concentration Pathways RCP 4.5 and RCP 8.5, where 4.5 and 8.5 represent the global radiative forcing in W/m^2 at year 2100. RCP 4.5 represents a mitigation scenario where greenhouse gas emissions are reduced to stabilize radiative forcings in 2100 through explicit action (Thomson et al., 2011). RCP 8.5 represents a high-emission "business as usual" scenario that is consistent with heavy reliance on fossil fuels and that nearly triples current CO_2 emissions by 2100 (Riahi et al., 2011).

Atmospheric temperature and CO_2 concentration perturbation values specific to the Hawaiian Islands chain were obtained from the Coupled Model Intercomparison Project (CMIP) 5 model outputs accessed online (http://climexp.knmi.nl/). Figure 5.8 shows the predicted atmospheric temperature and CO_2 concentrations under RCP 4.5 and RCP 8.5 emissions scenarios.

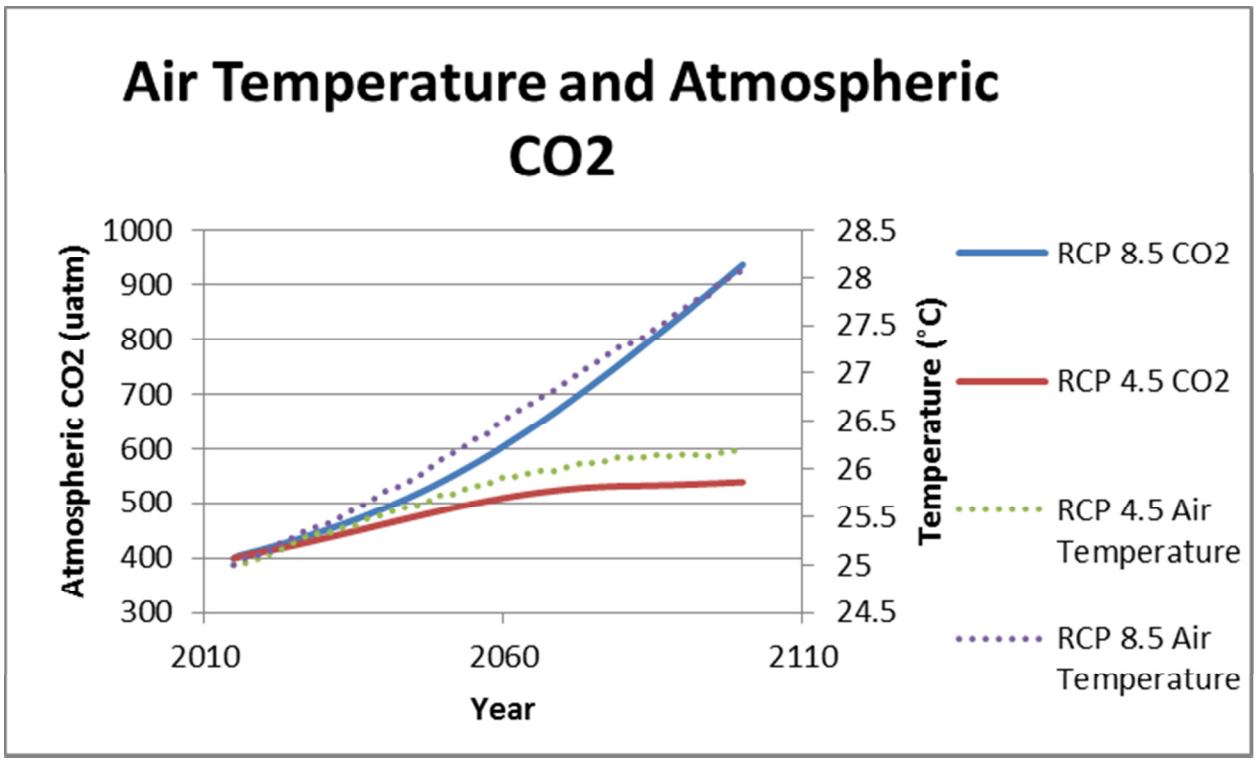

Figure 5.8: Predicted atmospheric Temperature and CO_2 concentrations under RCP 4.5 and RCP 8.5 scenarios.

Precipitation values were derived from statistical downscaling of rainfall changes in Hawai'i based on the CMIP5 global model projections (Elison Timm et al., 2015). These values were derived through the use of spatially extensive and high quality monthly rainfall data coupled with climate predictor information including: moisture transport to the middle of the atmosphere, vertical temperature gradients, and geopotential height fields. At the time of model formulation and writeup, the complete data set from this study was not available due to an error found in the dry season data (data are typically available at http://apdrc.soest.hawaii.edu/datadoc/sd5.php). For this reason, estimates of the magnitude of changes in precipitation were made from Figure 5.9 (from Elison Timm et al., 2015) that approximated the estimated average precipitation changes for wet and dry seasons over the

time periods of 2041-2071 and 2071-2099 under both RCP 4.5 and 8.5. Personal correspondence with the lead author of the precipitation study suggested that amplitude from the mid 21st century (2041-2071) change patterns could be reduced by 50% to crudely estimate changes for the 2015-2040 time period.

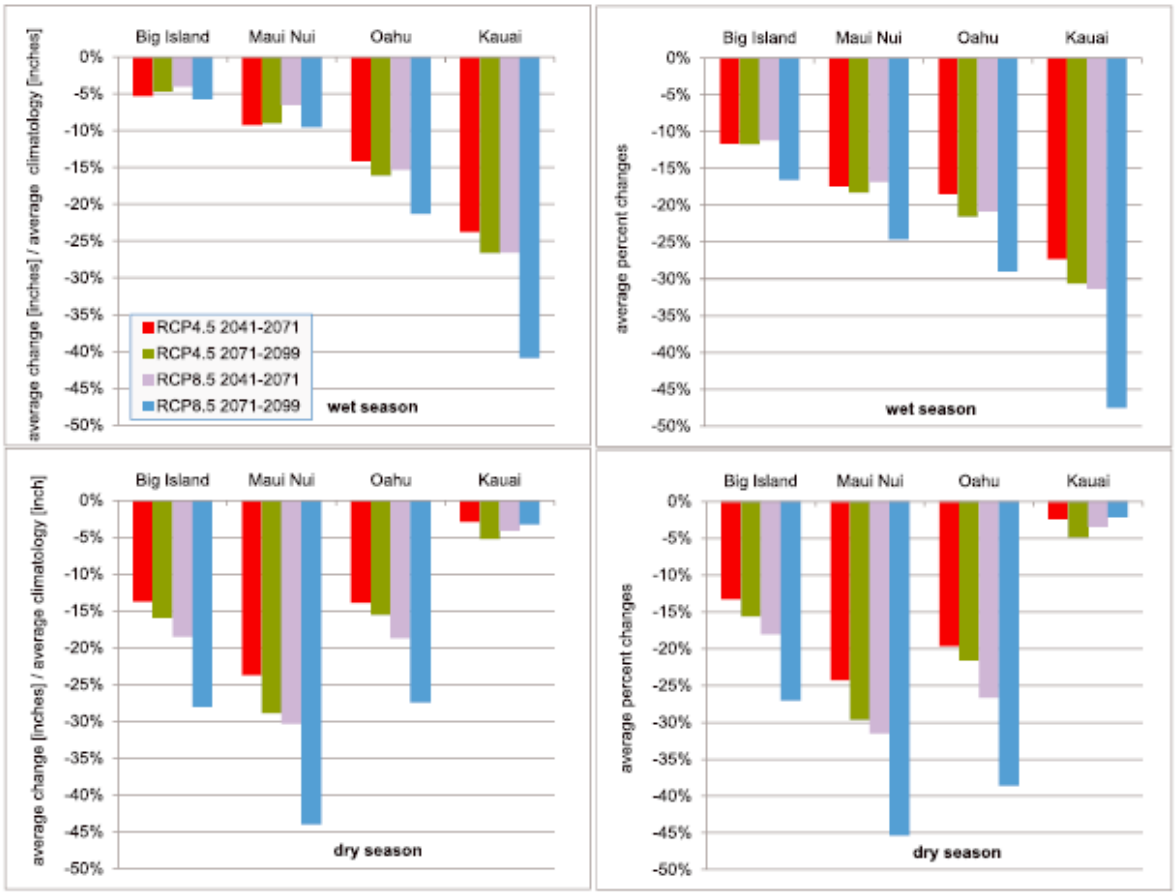

Summary statistics for the four islands groups. The top charts show the percentage changes averaged over the islands for the wet season (using interpolated maps). Bottom row shows the statistic for the dry season. Each island has four scenarios (RCP4.5 and RCP8.5 for the middle and late 21st century; see color legend). Right figures present for comparison the area-averaged precipitation anomalies when averaging the percentage changes (as shown in Figure 13) directly. Left figures show for comparison area-averaged precipitation changes expressed in percent of the island-average seasonal rainfall climatology from the Rainfall Atlas of Hawai'i [*Giambelluca et al.*, 2013]. Note that for that purpose, we first converted the local percentage anomalies into absolute anomalies (in units of mm).

Figure 5.9: Estimated changes in precipitation over the Hawaiian Islands (figure and caption from Elison Timm et al., 2015).

The assumption was made that annual change could be approximated by averaging the wet and dry season change for each time period. This study also made the assumption that the annual percent change occurred linearly; values were interpolated linearly at intervals of 1 year to create forcing files. Figure 5.9 shows the estimated precipitation changes for RCP 4.5 and RCP 8.5.

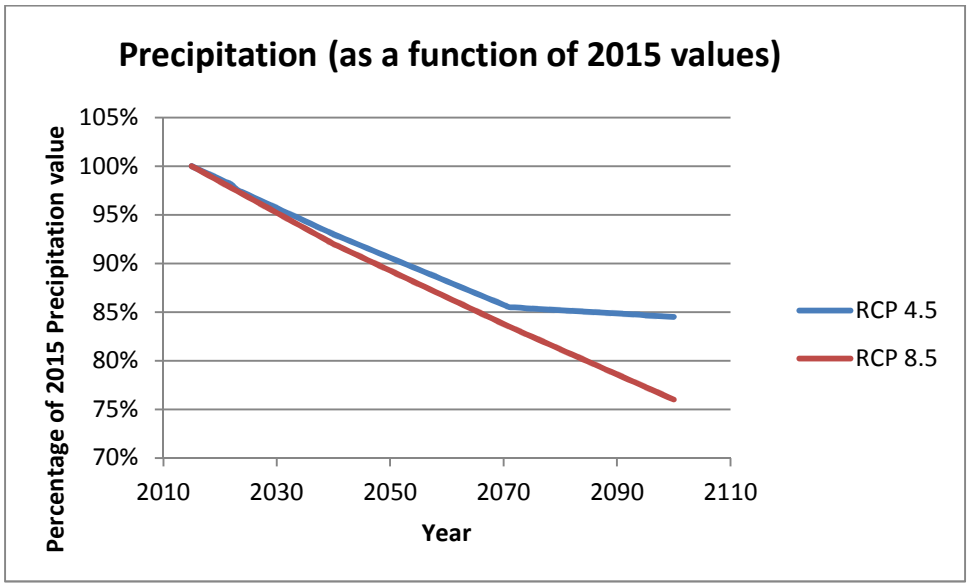

Figure 5.10: Predicted change in precipitation under RCP 4.5 and RCP 8.5 scenarios.

The predicted sea level rise for Oahu through 2100 is greater than global average sea level rise. Annual increases in sea level were derived from the projection value at the 50th percentile of certainty for the year 2100 using RCP 4.5 and RCP 8.5 scenario data (Kopp et al., 2014). These data produced an expected average sea level rise of 0.87 cm/year for RCP 8.5 and 0.65 cm/year for RCP 4.5. These values were applied to the volume of Southern Kāneʻohe Bay for the forcing scenarios. Potential change in the volume of Southern Kāneʻohe Bay is plotted in Figure 5.11. Steady state, RCP 4.5 and RCP 8.5 forcing files with values of pCO_2, precipitation, and Kāneʻohe Bay volume are provided in Appendix 5.2.

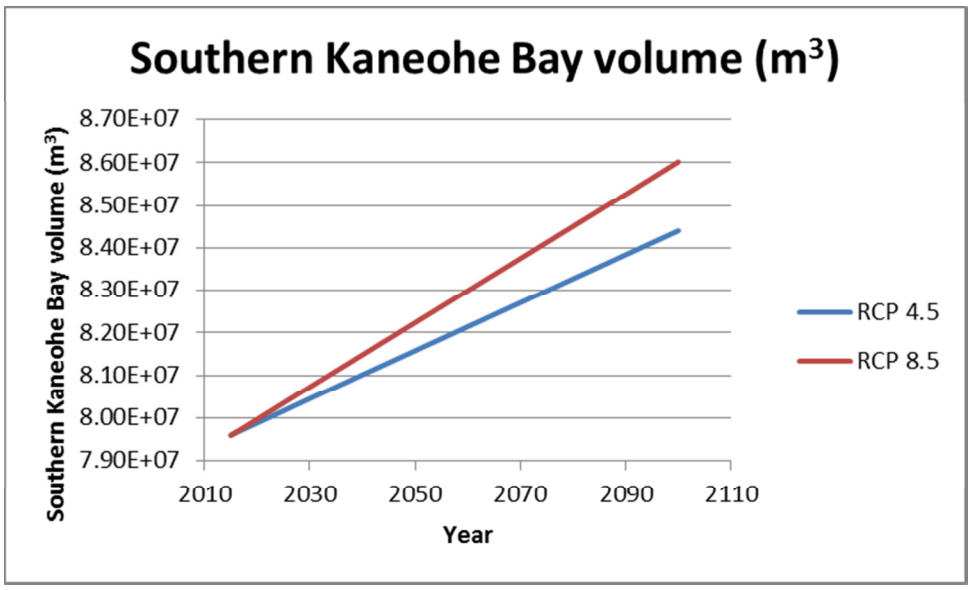

Figure 5.11: Estimated change in volume of Southern Kāneʻohe Bay.

5.6 Results and Discussion

Estimated water flux rates derived from the SKWANEM model at year 2100 under RCP 4.5 and 8.5 are listed in Table 5.8.

Table 5.8: Estimate change in flux rates under RCP 4.5 and RCP 8.5.

Water Flux Rates (m3/yr)	**2015**	**2100 (RCP 4.5)**	**2100 (RCP 8.5)**
Infiltration	2.98E+06	2.52E+06	2.28E+06
Percent reduction		*15%*	*23%*
SGWSeepage	2.98E+06	2.97E+06	2.97E+06
Percent reduction		*0.3%*	*0.3%*
InputWR	8.80E+06	7.44E+06	6.73E+06
Percent reduction		*15%*	*24%*
OutputWR	8.80E+06	7.44E+06	6.73E+06
Percent reduction		*15%*	*24%*
OcnExport	2.23E+07	1.93E+07	1.77E+07
Percent reduction		*13%*	*20%*
LandRunoff	1.02E+06	8.62E+05	7.80E+05
Percent reduction		*15%*	*24%*
StreamDischarge	9.82E+06	8.30E+06	7.51E+06
Percent reduction		*15%*	*24%*

Under both forcing scenarios, groundwater seepage (SGW) has a negligible decrease in flux rate of 0.3% from year 2015 (initial state of SKWANEM) to 2100 for both RCP 4.5 and RCP 8.5. This suggests that decreased precipitation as a result of climate change may have a smaller impact on the groundwater reservoir since it is orders of magnitude larger than the other water reservoirs in the region (Table 5.1). All other water fluxes exhibit a 13-15% decrease from 2015 to 2100 under RCP 4.5, and an estimated 20-24% decrease under RCP 8.5 (Table 5.8 and Figure 5.12), indicating that decreased precipitation will substantially lower water export to Southern Kāneʻohe Bay.

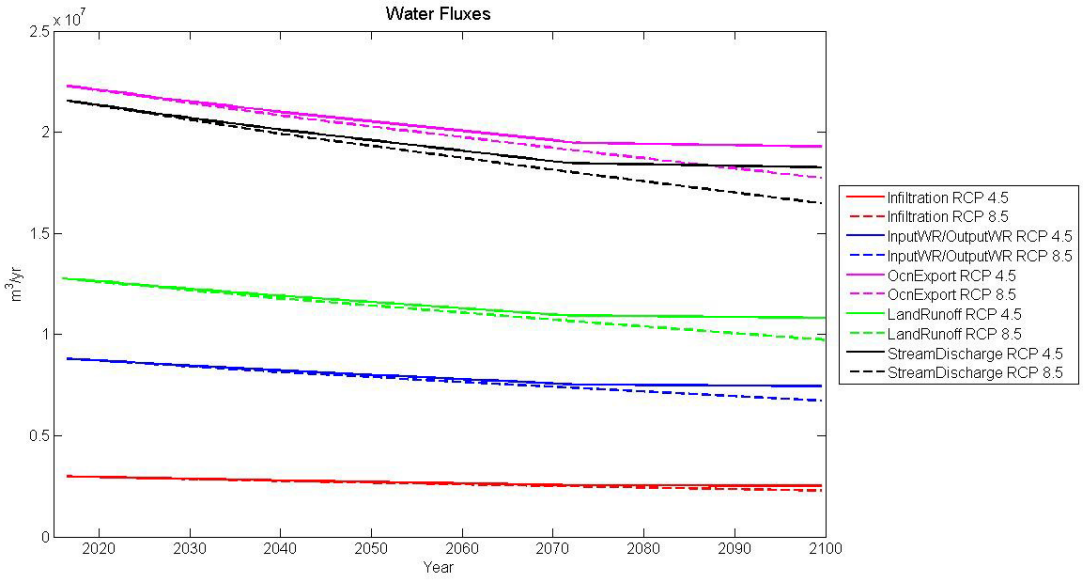

Figure 5.12: Estimated change in water flux rates under RCP 4.5 and RCP 8.5.

Sediment fluxes are listed in Table 5.9 and depicted in Figure 5.13.

Table 5.9: Estimated change in sediment flux rates under RCP 4.5 and RCP 8.5.

Sediment Flux Rates (metric tons/yr)	**2015**	**2100 (RCP 4.5)**	**2100 (RCP 8.5)**
SedInputWR	1.10E+03	1.06E+03	1.14E+03
Percent increase		*-3%*	*3%*
SedInputKS	9.50E+02	9.19E+02	9.80E+02
Percent increase		*-3%*	*3%*

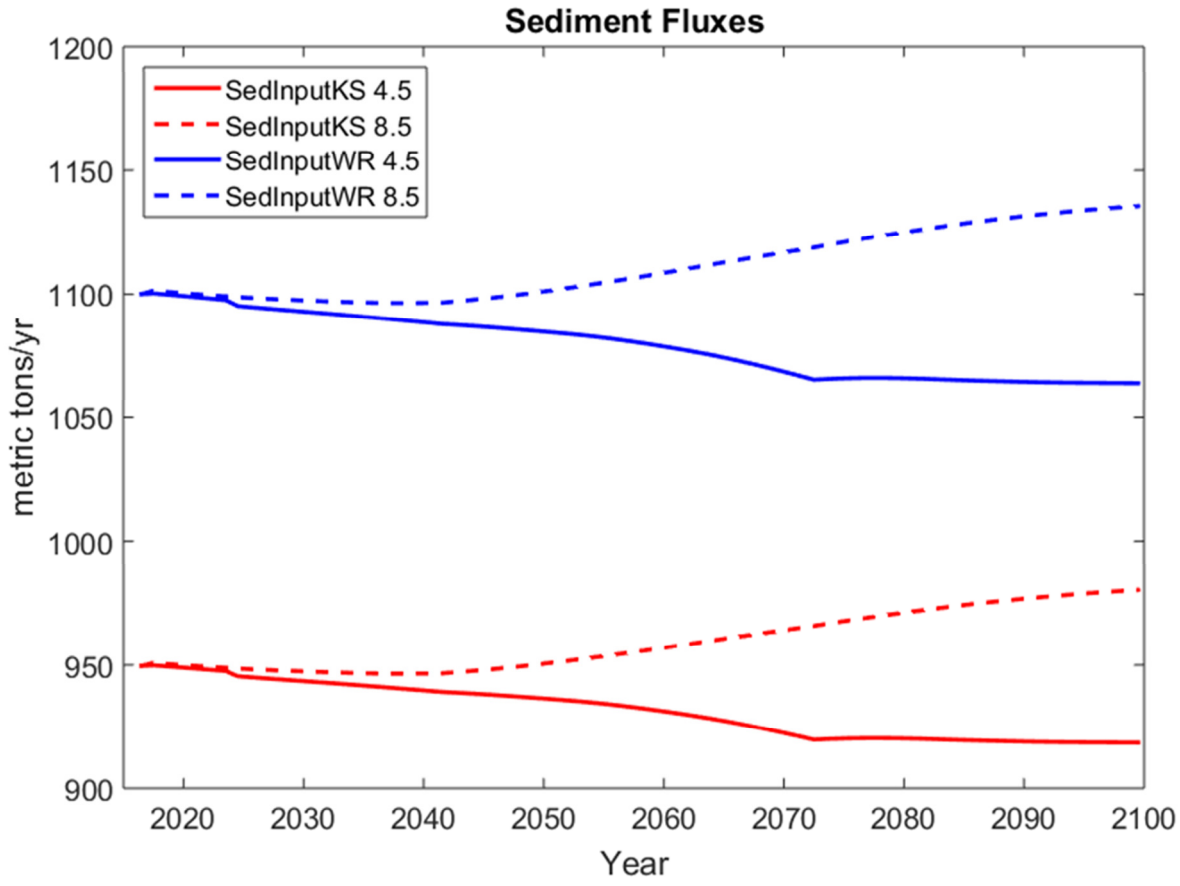

Figure 5.13: Estimated change in sediment flux rates under RCP 4.5 and RCP 8.5.

Table 5.9 and Figure 5.13 suggest that suspended sediment input to both Waimaluhia Reservoir and Kāneʻohe Stream will decrease as a result of decreased precipitation and increased atmospheric CO_2 as a function of temperature under RCP 4.5. Under RCP 8.5

suspended sediment fluxes are anticipated to increase. A sensitivity analysis was performed (Figure 5.14) to determine how precipitation and temperature & CO_2 impact the sediment input to Waimaluhia Reservoir.

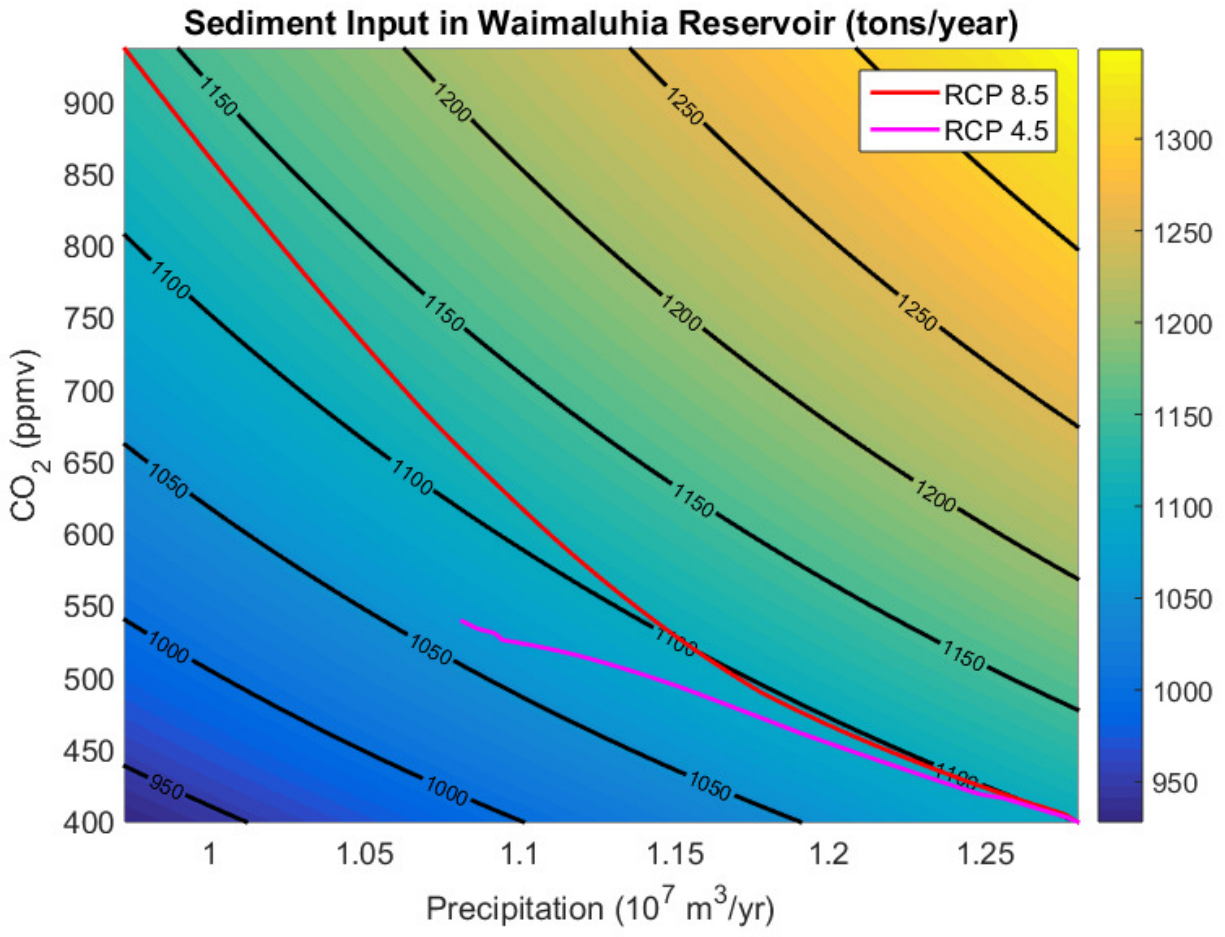

Figure 5.14: Sensitivity analysis of the impact of precipitation and temperature & CO_2 change to sediment input to Waimaluhia Reservoir under RCP 4.5 and RCP 8.5.

Figure 5.14 shows how the opposing effects of a decrease in precipitation and increase in temperature & CO_2 impact weathering in the Southern Kāneʻohe region. Under the RCP 4.5 scenario projections, the anticipated decrease in precipitation has a stronger impact on the system than increase in temperature and CO_2, leading to a projected decrease in sediment

input to Waimaluhia Reservoir. On the contrary, under RCP 8.5 scenario projections the anticipated decrease in precipitation has a weaker impact on the system than increase in temperature and CO_2, leading to a projected increase in sediment input to Waimaluhia Reservoir.

Decreases in water fluxes and varying changes in suspended sediment fluxes under the different scenarios translate to varying changes in inorganic nutrient fluxes from the year 2015 to 2100. Phosphate, N+N, and ammonia fluxes under RCP 4.5 and 8.5 are listed in Tables 5.10-5.12.

Table 5.10: Estimated change in phosphate flux rates under RCP 4.5 and RCP 8.5.

Phosphate Fluxes (µmol/yr)	**2015 Rate**	**2100 Rate RCP 4.5**	**2100 Rate RCP 8.5**
Infiltration	0	0	0
Percent change		*0%*	*0%*
SGWSeepage	3.50E+09	3.43E+09	3.43E+09
Percent change		*-2%*	*-2%*
InputWR	0	0	0
Percent change		*0%*	*0%*
OutputWR	2.13E+08	2.21E+08	2.46E+08
Percent change		*4%*	*15%*
OcnExport	3.77E+09	3.66E+09	3.63E+09
Percent change		*-3%*	*-4%*
LandRunoff	0	0	0
Percent change		*0%*	*0%*
StreamDischarge	2.13E+08	2.21E+08	2.45E+08
Percent change		*4%*	*15%*
SedInputWR	2.13E+08	2.21E+08	2.45E+08
Percent change		*4%*	*15%*
SedInputKS	4.75E+07	4.93E+07	5.49E+07
Percent change		*4%*	*16%*

Table 5.11: Estimated change in N+N flux rates under RCP 4.5 and RCP 8.5.

N+N Fluxes (µmol/yr)	**2015 Rate**	**2100 Rate RCP 4.5**	**2100 Rate RCP 8.5**
Infiltration	1.07E+10	9.07E+09	8.20E+09
Percent change		*-15%*	*-23%*
SGWSeepage	2.57E+10	2.53E+10	2.53E+10
Percent change		*-1%*	*-1%*
InputWR	3.16E+10	2.67E+10	2.42E+10
Percent change		*-16%*	*-23%*
OutputWR	3.19E+10	2.70E+10	2.44E+10
Percent change		*-15%*	*-24%*
OcnExport	1.09E+11	9.90E+10	9.45E+10
Percent change		*-9%*	*-13%*
LandRunoff	3.89E+10	3.31E+10	3.00E+10
Percent change		*-15%*	*-23%*
StreamDischarge	7.08E+10	6.60E+10	5.96E+10
Percent change		*-7%*	*-16%*
SedInputWR	2.66E+08	2.76E+08	3.07E+08
Percent change		*4%*	*15%*
SedInputKS	1.44E+10	1.50E+10	1.67E+10
Percent change		*4%*	*16%*

Table 5.12: Estimated change in ammonia flux rates under RCP 4.5 and RCP 8.5.

Ammonia Fluxes (µmol/yr)	**2015 Rate**	**2100 Rate RCP 4.5**	**2100 Rate RCP 8.5**
Infiltration	1.49E+08	1.26E+08	1.14E+08
Percent change		*-15%*	*-23%*
SGWSeepage	2.34E+10	2.29E+10	2.29E+10
Percent change		*-2%*	*-2%*
InputWR	4.40E+08	3.72E+08	3.36E+08
Percent change		*-15%*	*-24%*
OutputWR	5.25E+08	4.60E+08	4.35E+08
Percent change		*-12%*	*-17%*
OcnExport	2.46E+11	2.53E+11	2.74E+11
Percent change		*3%*	*11%*
LandRunoff	1.80E+08	1.57E+08	1.49E+08
Percent change		*-12%*	*-17%*
StreamDischarge	9.81E+08	9.13E+08	8.23E+08
Percent change		*-7%*	*-16%*
SedInputWR	8.53E+07	8.87E+07	9.88E+07
Percent change		*4%*	*16%*
SedInputKS	2.20E+11	2.31E+11	2.57E+11
Percent change		*5%*	*17%*

Since Oahu rainwater does not contain phosphate (Table 5.5), there are no infiltration, InputWR, or LandRunoff phosphate fluxes. Groundwater seepage phosphate fluxes decreased slightly (2%) under both scenarios from 2015 to 2100. Sediment phosphate fluxes increased 4% under RCP 4.5 and 15-16% under RCP 8.5, and the OcnExport phosphate flux decreased 3% and 4% under RCP 4.5 and 8.5 (Table 5.10).

Similar to phosphate, groundwater seepage N+N fluxes decreased slightly (1%) under both scenarios from 2015 to 2100. All other N+N water fluxes decreased 7-15% under RCP 4.5 and 13-24% under RCP 8.5 and N+N sediment fluxes increased 4-16% (Table 5.11). Groundwater seepage ammonia fluxes decreased 2% under both scenarios. Sediment fluxes increased 4-5% under RCP 4.5 and 16-17% under RCP 8.5 from 2015 to 2100 and the OcnExport flux increases 3-11% (Table 5.12).

Since marine phytoplankton cells typically contain nitrogen and phosphorous in a 16:1 molar ratio (Redfield et al., 1934; Cox et al., 2006), it is also important to model predicted inorganic N: inorganic P to see what nutrient may limit phytoplankton growth. Figure 5.15 suggests that under both scenarios both Waimaluhia Reservoir and Kāneʻohe Bay will be phosphorous limited, as N:P ratios far exceed 16:1 under all scenarios. This suggests that freshwater has a strong impact on the waters of Kāneʻohe Bay since phosphorous limitation is commonly observed in freshwater systems (Smith et al., 1999).

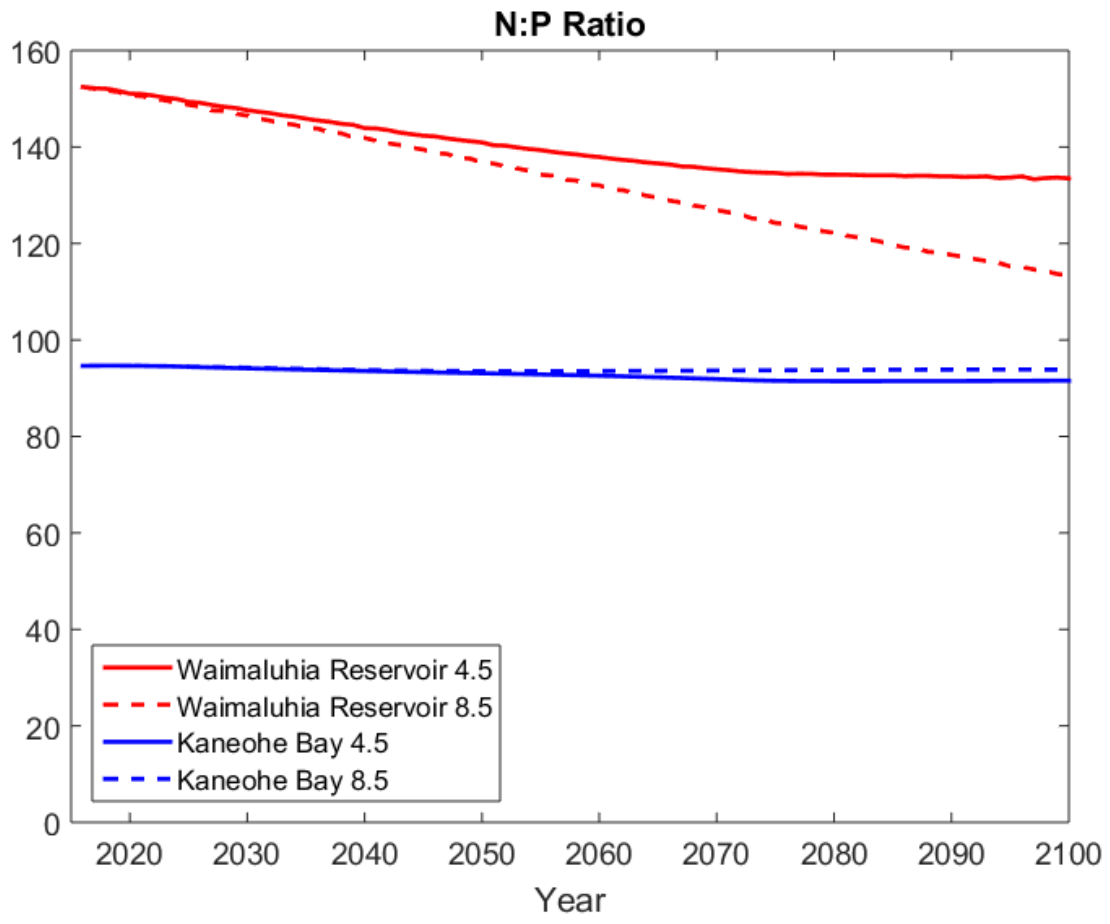

Figure 5.15: Estimated Inorganic N: Inorganic P under RCP 4.5 and RCP 8.5.

Most of the reservoirs, fluxes, and nutrient values used in this model are well constrained because Kāneʻohe Bay is a highly studied region (e.g. Cox et al., 1973; Smith et al., 1981; Jokiel et al., 1993; Laws and Allen, 1996; Kinzie et al., 2001; Ringuet and Mackenzie, 2005; Tanaka and Mackenzie, 2005; Hoover et al., 2006; De Carlo et al., 2007; Fagan and Mackenzie, 2007; Hoover and Mackenzie, 2009; Drupp et al. 2011); however, limited data existed to determine the size and nutrient concentrations of the groundwater reservoir. A sensitivity analysis was performed to see how model results may vary as a result of modifying groundwater parameters (Figure 5.16).

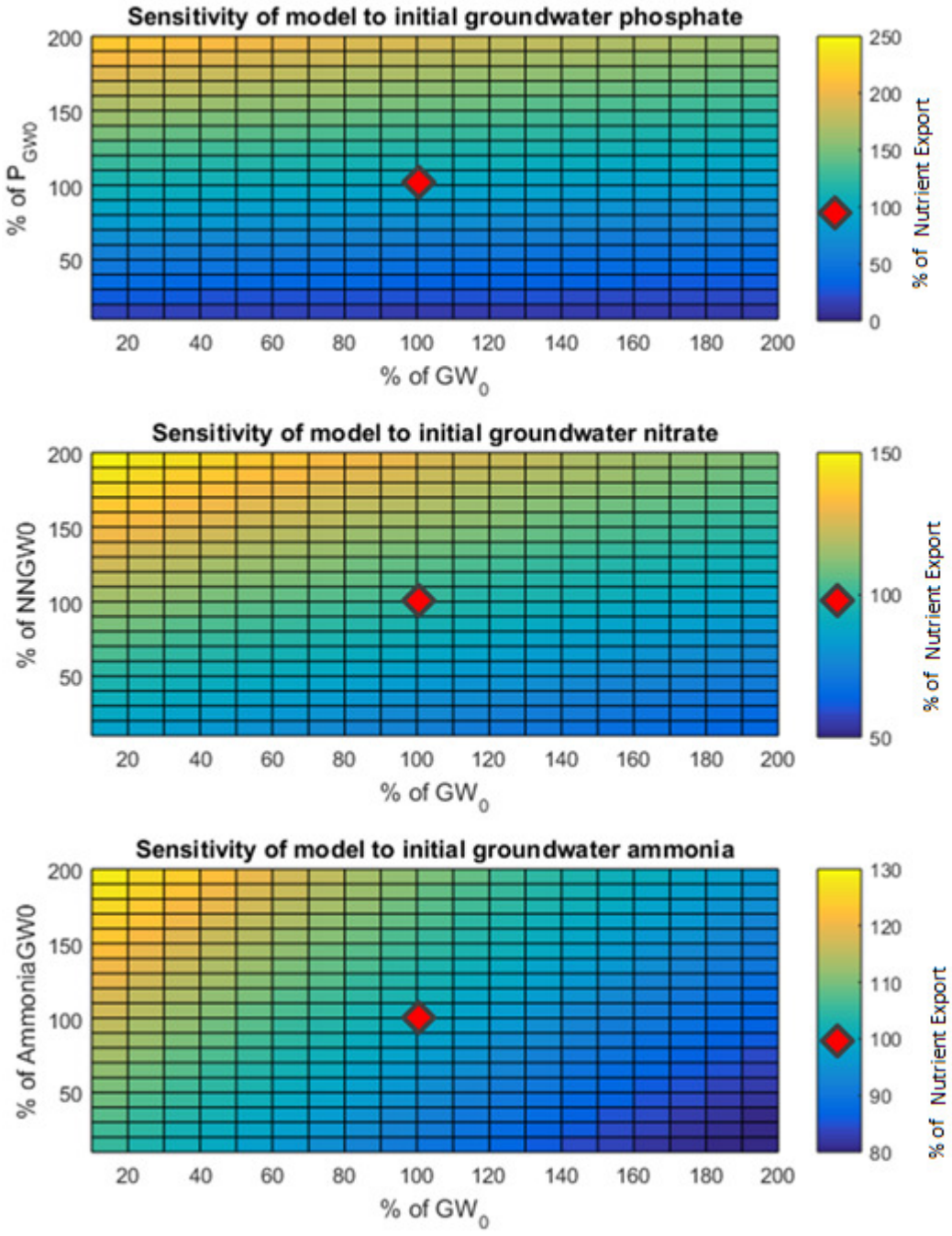

Figure 5.16: Sensitivity analysis of groundwater parameters under RCP 8.5.

Figure 5.16 assesses how the mass of phosphate, N+N and ammonia may vary depending on the initial groundwater reservoir size and nutrient concentrations. The x-axis varies by percentage of the initial groundwater reservoir (m^3), and the y-axis varies as percentage of the respective nutrient concentration used for the groundwater reservoir. The red symbols indicate the values applied to the model, and the nutrient concentrations used for the model were 1.5 µmol/L phosphate, 10 µmol/L N+N and 10 µmol/L ammonia.

The first plot shows that the phosphate reservoir size has a minimal impact on nutrient export since increasing or decreasing the reservoir size does not impact the net export. However, increasing the phosphate concentration approximately 50% increases the nutrient export approximately 50%. The N+N and ammonia plots show that if the groundwater reservoir size was overestimated or nutrient concentrations were underestimated, nutrient export to Southern Kāneʻohe Bay may be underestimated. On the contrary, if the groundwater reservoir size was underestimated or nutrient concentrations were overestimated, nutrient export to Southern Kāneʻohe Bay may be overestimated. Further studies of the groundwater reservoir will allow more robust estimates of nutrient export to be made since this sensitivity analysis shows that changing the nutrient concentrations or reservoir sizes could have a strong impact on net export.

5.7 Summary and Conclusion

Oahu has shown a drying trend over the past century and this trend is expected to continue through 2100 (Ellison Timm et al., 2015). All of the major Hawaiian Islands have exhibited a tendency toward dryer periods since the mid-20th century (Chu et al., 2010; Keener

et al., 2012). Coinciding with the downward trend in precipitation, long-term streamflow gauge monitoring indicates a statistically significant reduction in base flow over the past century (Oki, 2004; Keener et al., 2012). This indicates that the groundwater contribution to stream flow is decreasing, suggesting a decline in groundwater recharge and storage (Gingerich & Oki, 2000).

A continued reduction of stream flow has the potential to have a large impact on ecosystems since stream nutrient loads are an important source of nutrient delivery to Southern Kāneʻohe Bay. The SKWANEM model results suggest that phosphate and N+N export to Southern Kāneʻohe Bay will decrease by 3-13% from year 2015 to 2100, while ammonia export is projected to increase 3-11%. Nutrient limitation or reduction may decrease primary production in the Bay, ultimately limiting the potential for carbon sequestration, since the transfer of carbon dioxide into organic carbon by photosynthetic plankton is a process by which atmospheric CO_2 can be transferred to the deep ocean and sequestered for long periods of time (Street et al., 2005).

Chu et al. (2010) determined that extreme precipitation events are more likely to occur during La Niña years and less likely to occur during El Niño years. The authors also determined that there has been an increase in extreme precipitation events in recent years that is likely to continue with increasing water vapor in the atmosphere, air temperature, and circulation strength in a warming background. This study did not take extreme precipitation events into consideration and future work should consider these events. Extreme precipitation events facilitate the mass transport of nutrients and sediment into the Bay, allowing for algae growth and inhibition of photosynthesis, respectively.

Literature Cited:

Andersson, A., Mackenzie, F., Ver, L. (2003) Solution of shallow-water carbonates: An insignificant buffer against rising atmospheric CO2. Geology 31: 513–516.

Arvidson, R.S., Guidry, M., Mackenzie, F.T. (2006) MAGic: a Phanerozoic model for thegeochemical cycling of major rock-forming components. Am. J. Sci. 306: 135–190.

Berner, R., Lasaga, A., Garrels, R. (1983) The Carbonate-Silicate Geochemical Cycle and its Effect on Atmospheric Carbon Dioxide over the Past 100 Million Years. American Journal of Science 283: 641–683.

Chu, P.S., Chen, Y. R., & Schroeder, T. A. (2010). Changes in precipitation extremes in the Hawaiian Islands in a warming climate. Journal of Climate, 23(18), 4881–4900. doi:10.1175/2010JCLI3484.1

Cox, D.C. Fan, P. F., and Chave K.E. (1973) Estuarine pollution in the State of Hawaii; Volume 2: Kāneʻohe Bay study. University of Hawaii Water Resources Research Center.

Cox, E., Ribes, M., Kinzie, R.A. (2006) Temporal and spatial scaling of planktonic responses to nutrient inputs into a subtropical embayment. Mar Ecol Prog Ser 324:19–35. doi: 10.3354/meps324019

De Carlo, E.H., Hoover, D.J., Young, C.W., Hoover, R.S., Mackenzie, F.T. (2007) Impact of storm runoff from subtropical watersheds on coastal water quality and productivity. Applied Geochemistry 22: 1777–1797.

Diaz, H. F., and T. W. Giambelluca (2012) Changes in atmospheric circulation patterns associated with high and low rainfall regimes in the Hawaiian Islands region on multiple time scales, Global Planet. Change, 98–99: 97–108.

Drupp, P. S. (2015) Observations and modeling of the CO2-carbonic acid system on Hawaiian coral reefs: implications of future ocean acidification and climate change. Ph.D. dissertation, University of Hawaii at Manoa, 298 p.

Dulai, H., Kleven, H., Ruttenberg, K. (2016) Evaluation of Submarine Groundwater Discharge as Coastal Nutrient Source and Its Role in Coastal Groundwater Quality and Quantity. Chapter submitted for publication in *Emerging Issues in Groundwater Resources*, Advances in Water Security. Springer International Publishing Switzerland.

Elison Timm, O., Giambelluca, T.W., and Diaz, H.F. (2015) Statistical downscaling of rainfall changes in Hawaiʻi based on the CMIP5 global model projections. Journal of Geophysical Research: Atmospheres. 120: 92-112.

Elison Timm, O. (2016, June 22.) Email correspondence.

Executive Summary – State of Hawaii Department of Health. (2009) Total Maximum Daily Loads for Total Suspended Solids, Nitrogen and Phosphorous in Kāneʻohe Stream Kāneʻohe, Hawaii. Retrieved from Environmental Health Administration of Hawaii.

Fagan, K.E., Mackenzie, F.T. (2007) Air-sea CO2 exchange in a subtropical estuarine-coral reef system, Kaneohe Bay, Oahu, Hawaiʻi. Marine Chemistry 106:174–191

Giambelluca, T.W. (1986) Land use effects on the water balance of a tropical island, National Geographic Research 2(2):125-151.

Gingerich, S. B., & Oki, D. S. (2000). Ground water in Hawaii (US Geological Survey Fact Sheet No. 126-00). Retrieved from http://hi.water.usgs.gov/publications/pubs/fs/fs126-00.pdf

Hoover, D.J. (2002) Fluvial nitrogen and phosphorus in Hawaii: storm runoff, land use, and impacts on coastal waters. Ph. D. dissertation, University of Hawaii at Manoa, Honolulu, Hawaii. 437 pages.

Hoover, D.J., Mackenzie, F.T. (2009) Fluvial Fluxes of Water, Suspended Particulate Matter, and Nutrients and Potential Impacts on Tropical Coastal Water Biogeochemistry: Oahu, Hawaiʻi. Aquat. Geochemistry 15: 547–570.

Jokiel, P.L. (1993) Jokiel's Illustrated Scientific Guide to Kane'ohe Bay, O'ahu. Hawaii Institute of Marine Biology, 65 pp.

Keener, V. W., Marra, J. J., Finucane, M. L., Spooner, D., & Smith, M. H. (2012). Climate Change and Pacific Islands: Indicators and Impacts. Report for The 2012 Pacific Islands Regional Climate Assessment. Washington, DC: Island Press.

Kinzie III, R.A., Mackenzie, F.T., Smith, S.V. and Stimson, J. (2001) CISNet: Linkages between a tropical watershed and reef ecosystems. Project 98-NCERQA, NOAA, 23 pp.

Kopp, R. E., Horton, R. M., Little, C.M., Mitrovica, J. X., Oppenheimer, M. , Rasmussen, D. J., Strauss, B. H., Tebaldi, C. (2014) Probabilistic 21st and 22nd century sea-level projections at a global network of tide-gauge sites, Earth's Future, 2: 383–406. doi:10.1002/2014EF000239.

Laws. E.A., Allen, C.B. (1996) Water quality in a subtropical embayment more than a decade after diversion of sewage discharges. Pacific Science 50:194–210.

Lerman, A., Mackenzie, F.T., Garrels, R.M. (1975) Modeling of geochemical cycles. Phosphorus as an example. Geol. Soc. Am. Mem. 142: 205–218.

Li, Y. (1988) Denudation rates of the Hawaiian Islands by rivers and groundwaters. Pacific Sci. 42: 253–266.

McGowan, M. (2004) Submarine groundwater discharge: Freshwater and nutrient input into Hawaii's coastal zone, MS thesis, Dep. of Geol. and Geophys., Univ. of Hawai'i at Mānoa, Honolulu.

Navarre-Sitchler A. and Brantley S. (2007) Basalt weathering across scales. Earth Planet. Sci. Lett. 261(1–2): 321–334.

Nelson, S.T., Tingey, D.G., and Selck, B. (2013) The denudation of ocean islands by ground and surface waters: The effects of climate, soil thickness, and water contact times on Oahu, Hawaii. Geochimica et Cosmochimica Acta, 103 : 276–294.

Oki, D. (2016, March 30.) Email correspondence.

Oki, D. S. (2004) Trends in streamflow characteristics at long-term gaging stations, Hawaii (US Geological Survey Scientific Investigations Report No. 2004-5080). Retrieved from http://pubs.usgs.gov/sir/2004/5080/

Rad S. D., Allegre C. J. and Louvat P. (2007) Hidden erosion on volcanic islands. Earth Planet. Sci. Lett. 262(1–2): 109–124.

Redfield, A. (1934) On the proportions of organic derivatives in seawater and their relation to the composition of plankton.pdf. In: Daniel RJ (ed) James Johnstone Memorial Volume. University Press of Liverpool. 176–192.

Riahi, K., Rao, S., Krey, V. et al. (2011) RCP 8.5—A scenario of comparatively high greenhouse gas emissions. Climatic Change. 109: 33. doi:10.1007/s10584-011-0149-y

Root, E., Jones, W., Schwarz, B., and Gibbons, J. (2004) Rainwater chemistry across the United States. http://www.people.carleton.edu/bhaileab/environmentalgeology/RainWater.

Smith, S.V., W.J. Kimmerer, E.A. Laws, R.E. Brock, and T.M. Walsh. (1981) Kāneʻohe Bay sewage diversion experiment: Perspectives on ecosystem responses to nutritional perturbation. Pacific Science 35: 279-395.

Smith, V.H., Tilman, G.D. & Nekola, J.C. (1999) Eutrophication: impacts of excess nutrient inputs on freshwater, marine, and terrestrial ecosystems. Environ. Pollut., 100: 179–196.

Street, J.H., Paytan, A. (2005) Iron, phytoplankton growth, and the carbon cycle. Met Ions Biol Syst. 43: 153-93.

Tanaka, Kk, Mackenzie, F.T. (2005) Statistical and stability analysis of subtropical ecosystem dynamics in Southern Kaneohe Bay. Hawaiʻi Ecol Model 188:296–326.

Thomson, A.M., Calvin, K.V., Smith, S.J., Kyle, G.P., Volke, A., Patel, P., Delgado-Arias, S., Bond-Lamberty, B., Wise, M.A., Clarke, L.E. and Edmonds, J.A. (2011) RCP4.5: a pathway for stabilization of radiative forcing by 2100. Climatic Change 109: 77–94.

Ver, L.M., Mackenzie, F.T., Lerman, A. (1999) Biogeochemical Responses of the Carbon Cycle to Natural and Human Perturbations: Past, Present, and Future. Am. J. Sci. 299: 762–801.

Wong, M. F. (2001) Sedimentation History of Waimaluhia Reservoir during Highway Construction, Oahu, Hawaii, 1983-98. Honolulu, Hawaii : Denver, CO :U.S. Dept. of the Interior, U.S. Geological Survey ; Branch of Information Services [distributor]. Print.

CHAPTER 6: CONCLUSIONS

Throughout the past two centuries, human activities have had a profound impact on the exchange of the bio-essential elements, carbon (C) and the nutrients nitrogen (N) and phosphorous (P), between the land, atmosphere, and the aquatic environment (Regnier et al., 2013). A growing population, the persistence of detrimental industrial, transportation and agricultural activities of humankind, and continued development of previously non-industrialized nations will continue to impact biogeochemical cycles (e.g., Mackenzie et al. 1993).

This research was conducted to analyze the past, present, and predict future nutrient cycling of the Southern Kāneʻohe Bay watershed and proximal marine waters through the use of a mathematical biogeochemical model. The model describes the physical, chemical, and biological processes that affect the elements N and P and their coupled interactions and cycles, and may aid in determining how nutrient cycling throughout the Kāneʻohe Bay watershed and nearshore marine waters will change as a result of the IPCC predicted decrease in precipitation and increase in atmospheric CO_2.

The following hypotheses were tested, with a summary of results listed:

Hypothesis 1: There is no empirical relationship between total daily precipitation and mean daily water discharge for the Southern Kāneʻohe Bay watershed.

Precipitation-discharge data spanning 11 years were analyzed for the Southern Kāneʻohe watershed region in order to quantify patterns and trends of base flow and storm dynamics.

The watershed is characterized by average discharge values of 10.8 cubic feet/sec, while storm conditions produce variable water discharge rates reaching up to 399 cubic feet/ sec. Statistical analysis disproved this hypothesis. The empirical relationship representative of precipitation-discharge is represented by a sigmoid function. However, this relationship tends to be stronger under storm conditions (precipitation > 1.8 inches/day), when soil saturation leads to increased runoff and soil erosion, than under low flow conditions.

Hypothesis 2: There is no empirical relationship between mean daily water discharge and mean daily suspended sediment discharge for the Southern Kāneʻohe Bay watershed.

Discharge-suspended sediment data spanning 22 years were analyzed for the Southern Kāneʻohe watershed region in order to quantify patterns and trends of base flow and storm dynamics. The watershed is characterized by average suspended sediment fluxes of 2.8 tons/day, while storm conditions produce variable suspended sediment fluxes of up to 1380 tons/day. Statistical analysis disproved the null hypotheses. The empirical relationship representative of discharge-suspended sediment is represented by a log-log fourth order polynomial function. However, this relationship tends to be stronger under storm conditions (discharge> 30.8 cfs) when soil saturation leads to increased runoff and soil erosion than under low flow conditions.

Hypothesis 3: There will be no release of N and P from terrestrial suspended matter entering the coastal ocean.

Soil analysis and nutrient release experiments conducted in this study have demonstrated that surficial soils in the Kāneʻohe watershed are predominately composed of sand sized particles. Under baseline conditions these particles will deposit into the Kāneʻohe Stream estuarine region and there will be a release of nitrogen from terrestrial suspended matter entering the coastal ocean. Phosphate behavior is dependent upon salinity; in pure seawater there is a net release of phosphorous into the coastal ocean, but in lower salinity water there is a net uptake of phosphorous. Ringuet and Mackenzie (2005) previously determined that intermittent effects of P limitation following storms demonstrate that nutrient limitation status in Bay waters is subject to change on short time scales. Similarly, this research determined that the input of suspended sediment to Southern Kāneʻohe Bay can lead to phosphorous limitation rather than the normally observed nitrogen limitation.

Hypothesis 4: As precipitation decreases due to climate change, a lower sediment load to Southern Kāneʻohe Bay will lead to a lesser release of inorganic nutrients from the suspended sediment riverine load.

Oahu has shown a drying trend over the past century expected to continue through 2100 (Ellison Timm et al., 2015). Model results indicate that all water and sediment fluxes will decrease substantially as a result of decreased precipitation, ultimately lessening the nutrient loads entering Southern Kāneʻohe Bay by 3-13% for phosphate and N+N, and increasing ammonia loads by 3-11%. Experimental work coupled with model results indicate that P release

will occur at a slower rate, causing the Inorganic N: Inorganic P ratio to exceed 16:1 in Southern Kāneʻohe Bay. This may limit primary production in the Bay, ultimately limiting the potential for carbon sequestration.

APPENDICES

Appendix 3.1 Hypothesis 1 code

```
#Sara Coffey
#Research Hypothesis 1

#clear workspace
rm(list=ls()) #clear all variables
#set working directory
setwd("C:/Users/Sara/Documents/Final Project R/Precip Data/Precip
Data/HSTmonths/HI15")
getwd()     #verify that it's accurate

#----------------Introductory Comments-------------------------------------#
#Sara Coffey
#06 May 2015
#Code analyses of Hawai'i Archived Hydronet Data, Gage 15 (Luluku Stream)
#Monthly data sets from July 1994-October 2005
#Each file is a comma delimited text file which should contain 96 rows
(measurements taken every 15 minutes)
#Values are running totals in inches
#number of columns correspond to the amount of days there are in a particular
month
#For the purpose of compiling daily precipitation data and analyzing with
average discharge data to look for effect of precipitation on discharge
#-------------------------------------------------------------------------#

#First load all monthly Precipitation files into R from 1994-2005

#Name Months for vector
MonthNames<-
c("Jan","Feb","Mar","Apr","May","Jun","Jul","Aug","Sep","Oct","Nov","Dec")
#Compile years
Years<-c(1994:2005)

#Create vector of all file names
fileNames<-paste("15_",
                 rep(Years, each=12),
                 rep(MonthNames, times=length(Years)),
                 ".csv", sep="")

fileNames<-fileNames[7:142] #crop vector so that dates align with available
data

nFiles<-length(fileNames)

#Create empty data frame to store all data from 1994-2005
AllData<-data.frame()

#Create for loop to import all data
for (fileName in fileNames){
 #fileName<- '15_1995Jul.csv' # to test
  fileNow = as.matrix(read.csv(fileName)) # bring data in as matrix so
everything is same class
  fileNow[which(fileNow == "   .   ")] = NA # Converting bad data from '   .   '
to NA
```

```
  dailyPrecip<-as.numeric(fileNow[nrow(fileNow),])-as.numeric(fileNow[1,])
#calculate precipitation by subtracting final value from initial, convert
back to numeric

#adjust calculation for instances where the counter is reset (yielding
negative precipitation value)
whereNegs<-which(dailyPrecip<0)
if (length(whereNegs)>0) {

totalrows<-nrow(fileNow)

for (k in c(1:length(whereNegs))){
j<-which(as.numeric(fileNow[,whereNegs[k]])==0)[1]
dailyPrecip[whereNegs[k]]<-(as.numeric(fileNow[j-1,whereNegs[k]])-
as.numeric(fileNow[1,whereNegs[k]]))+as.numeric(fileNow[totalrows,whereNegs[k
]])
}
}

#add checkpoint to ensure all negative precipitation values have been removed
if (length(which(dailyPrecip<0)) >0) {
print('we have a problem here')
print(fileName)
print(dailyPrecip)
readline()}

  dailyPrecip<-round(dailyPrecip,4)     #round value
  dataNow<-data.frame(RainGage=rep(15,ncol(fileNow)),  #create columns for
Gage, Year, Day, Precip value for day
                      Year=rep(substr(fileName, start = 4, stop = 7),
ncol(fileNow)),
                      Month = rep(substr(fileName, start = 8, stop = 10),
ncol(fileNow)),
                      Day=c(1:ncol(fileNow)),
                      Precip=as.numeric(dailyPrecip))
AllData<-rbind(AllData,dataNow)
}       #Add to AllData and repeat



#--------------------------- Comments-----------------------------------#
#Code analyses of USGS Station 16272200 Kamooalii Str below Luluku Str near
Kāne‘ohe
#Monthly data sets from 1994-2005
#Daily mean discharge reported in cubic feet per second
#Create data frame of discharge data to be merged with precipitation data for
analysis of precipitation vs. discharge
#-----------------------------------------------------------------------#
#Now add in USGS discharge data

#change wd to import data
setwd("C:/Users/Sara/Documents/Final Project R/Discharge")
getwd()     #verify that it's accurate

#import data file
DischargeData<-read.csv("DischargeData.csv")  #Readme file
```

```
#name columns
colnames(DischargeData)<-
c("DischargeSource","Station","Date","Discharge","Approval")

#convert Date column to format of AllData columns so that data frame can be
merged with precipitation data
#Extract needed information from "FullData" to create new DF that can be
merged with AllData

DischargeData$Date<-strptime(DischargeData$Date, format="%m/%d/%Y") # Make
Date into a year month day object
DischargeData$Year<-format(DischargeData$Date, "%Y") # extract year
class(DischargeData$Year) # check class of year
DischargeData$Year<-as.numeric(DischargeData$Year) # convert year to numeric

DischargeData$Month<-format(DischargeData$Date, "%m") # extract month
class(DischargeData$Month) # check class of month
DischargeData$Month<-as.numeric(DischargeData$Month) # convert month to
numeric
DischargeData$Month<-format(DischargeData$Date, format="%b",tz="")  #change
month from decimal to abbreviated month


DischargeData$Day<-format(DischargeData$Date, "%d") # extract day
class(DischargeData$Day) # check class of Day
DischargeData$Day<-as.numeric(DischargeData$Day) # convert day to numeric


#Now combine AllData and DischargeData by Year, Month,Day to make new df
called CombinedData
CombinedData<-merge(AllData,DischargeData,by=c("Year", "Month", "Day"))

#Remove "Date" column since we already have month, day, and year
CombinedData<-CombinedData[, !(colnames(CombinedData) %in% c("Date"))]

#convert to numeric
CombinedData$Precip<-as.numeric(CombinedData$Precip)
CombinedData$Discharge<-as.numeric(CombinedData$Discharge)

#remove outlying point since it's value is triple the next highest value and
likely erroneous
CombinedData[-which.max(CombinedData$Discharge),]->CombinedData

#Add a counter to the data frame that can be used as a predictor for the time
series analysis
CombinedData$Counter<-c(1:4119)

#Verify Data
head(CombinedData)

#remove na values
CombinedData2=subset(CombinedData,!is.na(Precip))


################################################################################
                          #Analysis
################################################################################
```

```
#take histogram of response and investigate distributional properties
hist(log(CombinedData2$Discharge),breaks=20)
shapiro.test(CombinedData2$Discharge)
plot(density(CombinedData2$Discharge))
#reject null hypothesis that samples come from normal distribution
#Appears to be a lognormal distribution


##################Models#############################################################

#Start with linear model of just discharge and precipitation
GLM1<-glm(formula=Discharge~Precip, data=CombinedData2,
family=Gamma(link='log'))    #try linear fit
summary(GLM1)

#RMS calculation
predictedvaluesGLM1<-predict(GLM1,type='response')
observedvalues<-CombinedData2$Discharge
rmsGLM1<-sqrt(mean((observedvalues-predictedvaluesGLM1)^2))

#Add month as a predictor
GLM2<-glm(formula=Discharge~Precip + Month, data=CombinedData2,
family=Gamma(link='log'))    #try linear fit
summary(GLM2)
plot(GLM2)

#RMS calculation
predictedvaluesGLM2<-predict(GLM2,type='response')
observedvalues<-CombinedData2$Discharge
rmsGLM2<-sqrt(mean((observedvalues-predictedvaluesGLM2)^2))

#Add square root of precipitation
GLM3<-glm(formula=Discharge~sqrt(Precip) + Month, data=CombinedData2,
family=Gamma(link='log'))  #try linear fit
summary(GLM3)
plot(GLM3)

#RMS calculation
predictedvaluesGLM3<-predict(GLM3,type='response')
observedvalues<-CombinedData2$Discharge
rmsGLM3<-sqrt(mean((observedvalues-predictedvaluesGLM3)^2))


#Plot GLM1
plot(CombinedData2$Precip,CombinedData2$Discharge,xlab='Precipitation
(inches)',ylab='Discharge (ft^3/sec)',main='GLM1')
curve(exp(coef(GLM1)[1]+coef(GLM1)[2]*x),add=T)


#Plot GLM2
plot(CombinedData2$Precip,CombinedData2$Discharge,xlab='Precipitation
(inches)',ylab='Discharge (ft^3/sec)',main='GLM2')
curve(exp(coef(GLM2)[1]+coef(GLM2)[2]*x),add=T)


#Plot GLM3
```

```
plot(CombinedData2$Precip,CombinedData2$Discharge,xlab='Precipitation
(inches)',ylab='Discharge (ft^3/sec)',main='GLM3')
curve(exp(coef(GLM3)[1]+coef(GLM3)[2]*x),add=T)


##Enhanced view GLM 2 since it has the best AIC
plot(CombinedData2$Precip,CombinedData2$Discharge,xlab='Precipitation
(inches)',ylab='Discharge (ft^3/sec)',main='Axis change of
GLM2',xlim=c(0,1),ylim=c(0,40),xaxs='i',yaxs='i')
curve(exp(coef(GLM2)[1]+coef(GLM2)[2]*x),add=T)

###################Linear model with lm#################################
LinFit<-lm(Discharge~Precip,data=CombinedData2)
plot(CombinedData$Precip,CombinedData$Discharge,xlab='Precipitation
(inches)',ylab='Discharge (ft^3/sec)',main='LinFit')
abline(LinFit)

#RMS calculation
predictedvaluesLinFit<-predict(LinFit,type='response')
observedvalues<-CombinedData2$Discharge
rmsLinFit<-sqrt(mean((observedvalues-predictedvaluesLinFit)^2))

#add month
LinFit2<-lm(Discharge~Precip + Month,data=CombinedData2)
plot(CombinedData$Precip,CombinedData$Discharge,xlab='Precipitation
(inches)',ylab='Discharge (ft^3/sec)',main='LinFit2')
abline(LinFit2)

#RMS calculation
predictedvaluesLinFit2<-predict(LinFit2,type='response')
observedvalues<-CombinedData2$Discharge
rmsLinFit2<-sqrt(mean((observedvalues-predictedvaluesLinFit2)^2))

################################Michaelis Menten model#########################
#Load nlme
library(nlme)

MM2 <- nls(Discharge ~ Vm * Precip/(K+Precip), data = CombinedData2,
                  start = list(K = max(CombinedData2$Discharge)/2, Vm =
max(CombinedData2$Discharge)))

funx2<-function(x)predict(MM2,list(Precip=x))

plot(CombinedData$Precip,CombinedData$Discharge,xlab='Precipitation
(inches)',ylab='Discharge (ft^3/sec)',main='MM2')
curve(funx2,from=0,to=10,add=T)

#RMS calculation
predictedvaluesMM2<-predict(MM2,list(Precip=CombinedData2$Precip))
observedvalues<-CombinedData2$Discharge
rmsMM2<-sqrt(mean((observedvalues-predictedvaluesMM2)^2))

#########################Monomolecular#########################################
library(bbmle)
#write a function for the likelihood of the discharge data

discharge.NLL <- function(Discharge, Precip, a, b, c, sigma) {
```

```
  mean.discharge <- c + a*(1 - exp(-b*Precip))
  -sum(dlnorm(Discharge, meanlog <- log(mean.discharge), sdlog = sigma, log =
TRUE))
}


MonoM1 <- mle2(discharge.NLL, start = list(c = 6, a = 390, b = 1, sigma = 1),
data = CombinedData2)


plot(CombinedData$Precip,CombinedData$Discharge,xlab='Precipitation
(inches)',ylab='Discharge (ft^3/sec)',main='Monomolecular')
a=coef(MonoM1)[1]
b=coef(MonoM1)[2]
c=coef(MonoM1)[3]
curve(c + a*(1 - exp(-b*x)),from=0,to=10,add=T)

#RMS calculation
predictedvaluesMonoM1<-c + a*(1 - exp(-b*CombinedData2$Precip))
observedvalues<-CombinedData2$Discharge
rmsMonoM1<-sqrt(mean((observedvalues-predictedvaluesMonoM1)^2))

###################Sigmoid#############################################################

Sigmoid<- nls(Discharge ~ L/(1+exp(-k*(Precip-x0))), data = CombinedData2,
              start=list(L=160,x0=1,k=1))


funxs<-function(x)predict(Sigmoid,list(Precip=x))

plot(CombinedData$Precip,CombinedData$Discharge,xlab='Precipitation
(inches)',ylab='Discharge
(ft^3/sec)',main='Sigmoid',xlim=c(0,2),ylim=c(0,30))
curve(funxs,from=0,to=10,add=T,col='blue')                #sigmoid


#RMS calculation
predictedvaluesSigmoid<-predict(Sigmoid,type='response')
observedvalues<-CombinedData2$Discharge
rmsSigmoid<-sqrt(mean((observedvalues-predictedvaluesSigmoid)^2))


#######################sigmoid using mle#################################
discharge.NLL <- function(Discharge, Precip, L,x0,k, sigma) {
  mean.discharge <- L/(1+exp(-k*(Precip-x0)))
  -sum(dlnorm(Discharge, meanlog <- log(mean.discharge), sdlog = sigma, log =
TRUE))
}


Sigmoidmle <- mle2(discharge.NLL, start = list(L = 121, x0 = 3, k = 1, sigma
= 1), data = CombinedData2)


plot(CombinedData2$Precip,CombinedData2$Discharge,xlab='Precipitation
(inches)',ylab='Discharge (ft^3/sec)',main='Sigmoid mle')
L=coef(Sigmoidmle)[1]
```

```
x0=coef(Sigmoidmle)[2]
k=coef(Sigmoidmle)[3]
curve(L/(1+exp(-k*(x-x0))),from=0,to=10,add=T)

#RMS calculation
predictedvaluesSigmoidmle<-L/(1+exp(-k*(CombinedData2$Precip-x0)))
observedvalues<-CombinedData2$Discharge
rmsSigmoidmle<-sqrt(mean((observedvalues-predictedvaluesSigmoidmle)^2))

#######################Exponential using mle############################
discharge.NLL <- function(Discharge, Precip,f,g,sigma) {
  mean.discharge <- exp(f-g*Precip)
  -sum(dlnorm(Discharge, meanlog <- log(mean.discharge), sdlog = sigma, log =
TRUE))
}


Expmle <- mle2(discharge.NLL, start = list(f = 1.7, g=.7, sigma = 1), data =
CombinedData2)


plot(CombinedData$Precip,CombinedData$Discharge,xlab='Precipitation
(inches)',ylab='Discharge (ft^3/sec)',main='Exponential mle')
f=coef(Expmle)[1]
g=coef(Expmle)[2]
curve(exp(f-g*x),from=0,to=10,add=T,col='red')

#RMS calculation
predictedvaluesExpmle<-exp(f-(g*CombinedData2$Precip))
observedvalues<-CombinedData2$Discharge
rmsExpmle<-sqrt(mean((observedvalues-predictedvaluesExpmle)^2))


#################################linear using mle#################################
discharge.NLL <- function(Discharge, Precip,n,m,sigma) {
  mean.discharge <-(n+m*Precip)
  -sum(dlnorm(Discharge, meanlog <- log(mean.discharge), sdlog = sigma, log =
TRUE))
}


Linmle <- mle2(discharge.NLL, start = list(n = 5.5, m=15, sigma = 1), data =
CombinedData2)


plot(CombinedData2$Precip,CombinedData2$Discharge,xlab='Precipitation
(inches)',ylab='Discharge (ft^3/sec)',main='Linear mle')
n=coef(Linmle)[1]
m=coef(Linmle)[2]
curve(n+(m*x),from=0,to=10,add=T)

#RMS calculation
predictedvaluesLinmle<-(n+(m*CombinedData2$Precip))
observedvalues<-CombinedData2$Discharge
rmsLinmle<-sqrt(mean((observedvalues-predictedvaluesLinmle)^2))

##############################Gams#############################################
```

```
#precip as predictor
library(mgcv)    #load mgcv package
M2<-gam(Discharge~s(Precip), data=CombinedData2, family=Gamma(link='log'))
summary(M2)
plot(M2, shift=coef(M2)[1],trans=exp,xlab="Precipitation
(inches)",ylab="Discharge (cubic feet per second)",main='M2',xlim=c(0,2))
points(CombinedData$Precip,CombinedData$Discharge)
#several families were investigated for these models (identity, inverse, log,
etc.) and the log family produced the lowest AIC values
#therefore, the log family was used in the following models

#RMS calculation
predictedvaluesM2<-predict(M2,type='response')
observedvalues<-CombinedData2$Discharge
rmsM2<-sqrt(mean((observedvalues-predictedvaluesM2)^2))

#precip and month as predictors
M3<-gam(Discharge~s(Precip)+ Month, data=CombinedData2,
family=Gamma(link='log'))
summary(M3)
plot(M3, shift=coef(M3)[1],trans=exp,main="Precipitation effect on Discharge
(M3)",xlab="Precipitation (inches)",ylab="Discharge (cubic feet per
second)",xlim=c(0,2))
points(CombinedData$Precip,CombinedData$Discharge)
xrange<-seq(0,10,0.01)
newdata<-data.frame(Precip=xrange,Month='Feb')
y<-predict(Lin3,newdata,type='response')
lines(xrange,y,col='red')

#RMS calculation
predictedvaluesM3<-predict(M3,type='response')
observedvalues<-CombinedData2$Discharge
rmsM3<-sqrt(mean((observedvalues-predictedvaluesM3)^2))

#square root of precip and month as predictors
M4<-gam(Discharge~s(sqrt(Precip))+ Month, data=CombinedData2,
family=Gamma(link='log'))
summary(M4)
plot(M4, shift=coef(M4)[1],trans=exp,main="Precipitation effect on Discharge
(M4)",xlab="Square Root of Precipitation (inches)",ylab="Discharge (cubic
feet per second)")
points(CombinedData$Precip,CombinedData$Discharge)

#RMS calculation
predictedvaluesM4<-predict(M4,type='response')
observedvalues<-CombinedData2$Discharge
rmsM4<-sqrt(mean((observedvalues-predictedvaluesM4)^2))

############################Analysis#########################################
#use AIC to compare all models
AIC(GLM1,GLM2,GLM3,LinFit,LinFit2,MM2,MonoM1,Sigmoid,Sigmoidmle,Expmle,Linmle
,M2,M3,M4)


#######Plotting#################################################################
#Plot all models together (part 1)
```

```
plot(CombinedData2$Precip,CombinedData2$Discharge,xlab='Precipitation
(inches)',ylab='Discharge (ft^3/sec)',main='Model Comparison')
curve(exp(coef(GLM1)[1]+coef(GLM1)[2]*x),add=T, col='darkgreen',lwd=2) #GLM1
curve(exp(coef(GLM2)[1]+coef(GLM2)[2]*x),add=T, col='darkorange',lwd=2) #GLM2
curve(exp(coef(GLM3)[1]+coef(GLM3)[2]*x),add=T, col='darkmagenta',lwd=2)
#GLM3
abline(LinFit,add=T, col='deeppink',lwd=2)  #Linfit
abline(LinFit2,add=T, col='darkred',lwd=2) #Linfit2
curve(L/(1+exp(-k*(x-x0))),from=0,to=10,add=T, col='gold',lwd=2) #Sigmoidmle
leg.txt<-c("GLM1","GLM2","GLM3", "Linfit", "Linfit2", "Sigmoidmle")
legend("bottomright", legend=leg.txt,title = "Model
Name",cex=0.5,fill=c("darkgreen","darkorange","darkmagenta","deeppink","darkr
ed","gold"))

#Plot all models together (part 2)
plot(CombinedData2$Precip,CombinedData2$Discharge,xlab='Precipitation
(inches)',ylab='Discharge (ft^3/sec)',main='Model Comparison')
curve(funx2,from=0,to=10,add=T,col='darkgreen',lwd=2) #MM2
curve(c + a*(1 - exp(-b*x)),from=0,to=10,add=T,col='darkorange',lwd=2)
#MonoM1
curve(funxs,from=0,to=10,add=T,col='darkmagenta',lwd=2)     #Sigmoid
curve(exp(f-g*x),from=0,to=10,add=T,col='deeppink',lwd=2) #Expmle
curve(n+(m*x),from=0,to=10,add=T,col='darkred',lwd=2) #Linmle
curve(L/(1+exp(-k*(x-x0))),from=0,to=10,add=T,col='gold',lwd=2) #Sigmoidmle
leg.txt<-c("MM2","MonoM1","Sigmoid", "Expmle", "Linmle", "Sigmoidmle")
legend("bottomright", legend=leg.txt,title = "Model
Name",cex=0.5,fill=c("darkgreen","darkorange","darkmagenta","deeppink","darkr
ed","gold"))

#Plot predictive mle models together
plot(CombinedData2$Precip,CombinedData2$Discharge,xlab='Precipitation
(inches)',ylab='Discharge (ft^3/sec)',main='Model Comparison')
curve(c + a*(1 - exp(-b*x)),from=0,to=10,add=T,col='darkorange',lwd=2)
#MonoM1
curve(exp(f-g*x),from=0,to=10,add=T,col='deeppink',lwd=2) #Expmle
curve(n+(m*x),from=0,to=10,add=T,col='darkred',lwd=2) #Linmle
curve(L/(1+exp(-k*(x-x0))),from=0,to=10,add=T,col='gold',lwd=2) #Sigmoidmle
leg.txt<-c("MonoM1","Expmle", "Linmle", "Sigmoidmle")
legend("bottomright", legend=leg.txt,title = "Model
Name",cex=0.5,fill=c("darkorange","deeppink","darkred","gold"))


#Plot over 0-1 inch Precip range
plot(CombinedData2$Precip,CombinedData2$Discharge,xlab='Precipitation
(inches)',ylab='Discharge (ft^3/sec)',main='Sigmoidmle model (low
precipitation conditions)',xlim=c(0,1),ylim=c(0,75))
L=coef(Sigmoidmle)[1]
x0=coef(Sigmoidmle)[2]
k=coef(Sigmoidmle)[3]
curve(L/(1+exp(-k*(x-x0))),from=0,to=10,add=T,col='orange',lwd=1.5)

#Plot model on log scale for enhanced visibility
plot(CombinedData2$Precip,CombinedData2$Discharge,xlab='Precipitation
(inches)',ylab='Discharge (ft^3/sec)',main='Sigmoidmle model (log
scale)',log='xy')
curve(L/(1+exp(-k*(x-x0))),add=T,col='orange',lwd=1.5)
```

```
###Standard plot of Sigmoidmle
plot(CombinedData$Precip,CombinedData$Discharge,xlab='Precipitation
(inches)',ylab='Discharge (ft^3/sec)',main='Sigmoid mle')
L=coef(Sigmoidmle)[1]
x0=coef(Sigmoidmle)[2]
k=coef(Sigmoidmle)[3]
curve(L/(1+exp(-k*(x-x0))),from=0,to=10,add=T,col='blue')

#####plot sigmoid mle against M3######
plot(M3, shift=coef(M3)[1],trans=exp,main="GAM(M3) and Sigmoidmle
comparison",xlab="Precipitation (inches)",ylab="Discharge (cubic feet per
second)",col='darkviolet',lwd=1.5,ylim=c(0,3.5))
points(CombinedData$Precip,CombinedData$Discharge)
curve(L/(1+exp(-k*(x-x0))),add=T,col='orange',lwd=1.5) #sigmoid
leg.txt<-c("M3","Sigmoidmle")
legend("topleft", legend=leg.txt,title = "Model
Name",cex=0.5,fill=c("darkviolet","orange"))


##############Correlation Analysis#################################################
#Number of data points
length(CombinedData2$Precip)

#Range of precipitation values
range(CombinedData2$Precip)

#Range of discharge values
range(CombinedData2$Discharge)

#Average precipitation value
mean(CombinedData2$Precip)

#Median precipitation value
median(CombinedData2$Precip)

#Low precipitation data frame
LowPrecipData<-subset(CombinedData2,CombinedData2$Precip < 0.2)

#High precipitation data frame2
HighPrecipData<-subset(CombinedData2,CombinedData2$Precip >= 0.2)

#Correlation coefficient LowPrecipData
cor(LowPrecipData$Precip,LowPrecipData$Discharge)

#Correlation coefficient HighPrecipData
cor(HighPrecipData$Precip,HighPrecipData$Discharge)

#Correlation coefficient CombinedData2
cor(CombinedData2$Precip,CombinedData2$Discharge)

#find the breakpoint in the data
library(segmented)
segmented(GLM2, seg.Z =~Precip, psi = 0.2)

#Below the breakpoint data frame
Belowbp<-subset(CombinedData2,CombinedData2$Precip < 1.83)
```

```r
#Above the breakpoint data frame
Abovebp<-subset(CombinedData2,CombinedData2$Precip >= 1.83)

#Correlation coefficient Belowbp
cor(Belowbp$Precip,Belowbp$Discharge)

#Correlation coefficient Abovebp
cor(Abovebp$Precip,Abovebp$Discharge)
```

Appendix 3.2 Hypothesis 2 code

```
#Sara Coffey
#Research Hypothesis 2

#clear workspace
rm(list=ls()) #clear all variables
#set working directory
setwd("C:/Users/Sara/Documents/Final Project R/Sediment")
getwd()     #verify that it's accurate

#---------------Introductory Comments-------------------------------------
---------------#
#Sara Coffey
#26 May 2015
#Code analyses of USGS Station 16272200 Kamooalii Str below Luluku Str near
Kāne'ohe
#Monthly data sets from 1976-1998
#Daily mean discharge reported in cubic feet per second and suspended
sediment discharge in tons per day
#-----------------------------------------------------------------------
---------------#

#import data file
CombinedData<-read.csv(file.choose(),header=T)

#Separate date into Year, Day, Month
CombinedData$Date<-strptime(CombinedData$Date, format="%m/%d/%Y") # Make Date
into a year month day object
CombinedData$Year<-format(CombinedData$Date, "%Y") # extract year
class(CombinedDischargeData$Year) # check class of year
CombinedData$Year<-as.numeric(CombinedData$Year) # convert year to numeric

CombinedData$Month<-format(CombinedData$Date, "%m") # extract month
class(CombinedData$Month) # check class of month
CombinedData$Month<-as.numeric(CombinedData$Month) # convert month to numeric
CombinedData$Month<-format(CombinedData$Date, format="%b",tz="")  #change
month from decimal to abbreviated month

CombinedData$Day<-format(CombinedData$Date, "%d") # extract day
class(CombinedData$Day) # check class of Day
CombinedData$Day<-as.numeric(CombinedData$Day) # convert day to numeric

#Remove na values and likely erroneous value at discharge=623
CombinedData2<-subset(CombinedData,!is.na(Discharge))
CombinedData2<-subset(CombinedData2,!is.na(Susp.Sed))
CombinedData2 = CombinedData2[!CombinedData2$Discharge > 600,]

##############################Analysis#####################################

#take histogram of response and investigate distributional properties
hist(log(CombinedData2$Susp.Sed),breaks=20)
plot(density(CombinedData2$Susp.Sed))
#reject null hypothesis that samples come from normal distribution
#Appears to be a lognormal distribution
```

```
#######Modify data to remove Suspended Sediment 0 values#########
#find number of non-zeros
sum(CombinedData2$Susp.Sed==0)

#find smallest nonzero value
min(CombinedData2$Susp.Sed[CombinedData2$Susp.Sed>0])

#change the 13 zeros to .01
CombinedData2$Susp.Sed[CombinedData2$Susp.Sed==0] <- .01
#################################################################

#Start with linear model of just discharge and Susp Sed
GLM1<-glm(formula=Susp.Sed~Discharge,
data=CombinedData2,family=Gamma(link='log'))  #try linear fit
summary(GLM1)

#Plot GLM1
xrange<-seq(0,600,0.1)
y<-predict(GLM1,list(Discharge=xrange),type='response')
plot(CombinedData2$Discharge,CombinedData2$Susp.Sed,xlab='Discharge
(ft^3/sec)',ylab='Suspended Sediment (tons/day)',main='GLM1')
lines(xrange,y)

#Plot GLM1 zoomed in
xrange<-seq(0,50,0.1)
y<-predict(GLM1,list(Discharge=xrange),type='response')
plot(CombinedData2$Discharge,CombinedData2$Susp.Sed,xlab='Discharge
(ft^3/sec)',ylab='Suspended Sediment (tons/day)',main='GLM1 zoomed
in',xlim=c(0,50),ylim=c(0,40),xaxs='i',yaxs='i')
lines(xrange,y)

#Plot GLM2 with month as a predictor
GLM2<-glm(formula=Susp.Sed~Discharge + Month,
data=CombinedData2,family=Gamma(link='log'))  #try linear fit
summary(GLM2)
plot(GLM2)

#Plot GLM2
plot(CombinedData2$Discharge,CombinedData2$Susp.Sed,xlab='Discharge
(ft^3/sec)',ylab='Suspended Sediment (tons/day)',main='GLM2')
curve(exp(coef(GLM2)[1]+coef(GLM2)[2]*x),add=T)

#Plot GLM3- Add square root of precipitation
GLM3<-glm(formula=Susp.Sed~sqrt(Discharge) + Month, data=CombinedData2,
family=Gamma(link='log'))  #try linear fit
summary(GLM3)
plot(GLM3)

#Plot GLM3
plot(CombinedData2$Discharge,CombinedData2$Susp.Sed,xlab='Discharge
(ft^3/sec)',ylab='Suspended Sediment (tons/day)',main='GLM3')
curve(exp(coef(GLM3)[1]+coef(GLM3)[2]*x),add=T)

###################Linear model with lm#################################
LinFit<-lm(Susp.Sed~Discharge,data=CombinedData2)
```

```
plot(CombinedData2$Discharge,CombinedData2$Susp.Sed,xlab='Discharge
(ft^3/sec)',ylab='Suspended Sediment (tons/day)',main='LinFit')
abline(LinFit)

#add month
LinFit2<-lm(Susp.Sed~Discharge + Month,data=CombinedData2)
plot(CombinedData2$Discharge,CombinedData2$Susp.Sed,xlab='Discharge
(ft^3/sec)',ylab='Suspended Sediment (tons/day)',main='LinFit2')
abline(LinFit2)

########################Cubic polynomial#####################################
CubPoly<-lm(log(Susp.Sed) ~ log(Discharge) + I(log(Discharge)^2) +
I(log(Discharge)^3),data=CombinedData2)
funxCP<-function(x)predict(CubPoly,list(Discharge=x))

plot(log(CombinedData2$Discharge),log(CombinedData2$Susp.Sed),main="Cubic
Polynomial")
curve(coef(CubPoly)[1]+coef(CubPoly)[2]*x + coef(CubPoly)[3]*x^2 +
coef(CubPoly)[4]*x^3,add=T,col='orange')

#RMSE calculation
x<-CombinedData2$Discharge
predictedvaluesCubPoly<-(coef(CubPoly)[1]+coef(CubPoly)[2]*x +
coef(CubPoly)[3]*x^2 + coef(CubPoly)[4]*x^3)
observedvalues<-CombinedData2$Susp.Sed
rmsCubPoly<-sqrt(mean((observedvalues-predictedvaluesCubPoly)^2))

###################Cubic Polynomial with mle2#############################
library(bbmle)
susp.sed.NLL <- function(Susp.Sed, Discharge, aa,bb,cc,dd, sigma) {
  mean.susp.sed <- exp(dd+cc*log(Discharge) + bb*log(Discharge)^2
+aa*log(Discharge)^3)
  -sum(dlnorm(Susp.Sed, meanlog <- log(mean.susp.sed), sdlog = exp(sigma),
log = TRUE))
}

CubPolynomial <- mle2(susp.sed.NLL, start = list(dd=-3,cc=0.4,bb=0.1,aa=0.01,
sigma = log(1)), data = CombinedData2, trace = TRUE)

plot(log(CombinedData2$Discharge),log(CombinedData2$Susp.Sed),main="Cubic
Polynomial")
aa<-coef(CubPolynomial)[1]
bb<-coef(CubPolynomial)[2]
cc<-coef(CubPolynomial)[3]
dd<-coef(CubPolynomial)[4]
curve(dd+cc*x + bb*x^2 + aa*x^3,add=T,col='orange')

#RMSE calculation
x<-CombinedData2$Discharge
predictedvaluesCubPolynomial<-exp(dd+cc*log(x) + bb*log(x)^2 +aa*log(x)^3)
observedvalues<-CombinedData2$Susp.Sed
rmsCubPolynomial<-sqrt(mean((observedvalues-predictedvaluesCubPolynomial)^2))
#################4th order polynomial with lm#################################
Poly4<-lm(log(Susp.Sed) ~ log(Discharge) + I(log(Discharge)^2) +
I(log(Discharge)^3) + I(log(Discharge)^4),data=CombinedData2)
```

```
plot(log(CombinedData2$Discharge),log(CombinedData2$Susp.Sed),main="4th order
Polynomial")
curve(coef(Poly4)[1]+coef(Poly4)[2]*x + coef(Poly4)[3]*x^2 +
coef(Poly4)[4]*x^3 + coef(Poly4)[5]*x^4,add=T,col='orange')

##########4th order Polynomial with mle2###################################
library(bbmle)
susp.sed.NLL <- function(Susp.Sed, Discharge, a1,b1,c1,d1,e1,sigma) {
  mean.susp.sed <- exp(e1+d1*log(Discharge)+c1*log(Discharge)^2 +
b1*log(Discharge)^3 +a1*log(Discharge)^4)
  -sum(dlnorm(Susp.Sed, meanlog <- log(mean.susp.sed), sdlog = exp(sigma),
log = TRUE))
}

Polynomial4 <- mle2(susp.sed.NLL, start = list(e1=-2.9 ,d1=0.7,c1=-
0.4,b1=0.2,a1=0.01, sigma = log(1)), data = CombinedData2, trace = TRUE)

plot(log(CombinedData2$Discharge),log(CombinedData2$Susp.Sed),main="4th order
Polynomial")
a1<-coef(Polynomial4)[1]
b1<-coef(Polynomial4)[2]
c1<-coef(Polynomial4)[3]
d1<-coef(Polynomial4)[4]
e1<-coef(Polynomial4)[5]
curve(e1+d1*x+c1*x^2 + b1*x^3 + a1*x^4,add=T,col='orange')

#RMSE calculation
x<-CombinedData2$Discharge
predictedvaluesPolynomial4<-exp(e1+d1*log(x) + c1*log(x)^2 +b1*log(x)^3 +
a1*log(x)^4)
observedvalues<-CombinedData2$Susp.Sed
rmsPolynomial4<-sqrt(mean((observedvalues-predictedvaluesPolynomial4)^2))
#################5th order polynomial with lm#####################################
Polyfive<-lm(log(Susp.Sed) ~ log(Discharge) + I(log(Discharge)^2) +
I(log(Discharge)^3) + I(log(Discharge)^4) +
I(log(Discharge)^5),data=CombinedData2)

plot(log(CombinedData2$Discharge),log(CombinedData2$Susp.Sed),main="5th order
Polynomial")
curve(coef(Polyfive)[1]+coef(Polyfive)[2]*x + coef(Polyfive)[3]*x^2 +
coef(Polyfive)[4]*x^3 + coef(Polyfive)[5]*x^4 +
coef(Polyfive)[6]*x^5,add=T,col='orange')

#################5th order Polynomial with mle2##############################
susp.sed.NLL <- function(Susp.Sed, Discharge, a2,b2,c2,d2,e2,f2,sigma) {
  mean.susp.sed <-
exp(f2+e2*log(Discharge)+d2*log(Discharge)^2+c2*log(Discharge)^3 +
b2*log(Discharge)^4 +a2*log(Discharge)^5)
  -sum(dlnorm(Susp.Sed, meanlog <- log(mean.susp.sed), sdlog = exp(sigma),
log = TRUE))
}

Poly5 <- mle2(susp.sed.NLL, start = list(f2=-3,e2=0.7,d2=-
0.3,c2=0.2,b2=0.01,a2=0.01, sigma = log(1)), data = CombinedData2, trace =
TRUE)

a2<-coef(Poly5)[1]
```

```
b2<-coef(Poly5)[2]
c2<-coef(Poly5)[3]
d2<-coef(Poly5)[4]
e2<-coef(Poly5)[5]
f2<-coef(Poly5)[6]

plot(log(CombinedData2$Discharge),log(CombinedData2$Susp.Sed),main="5th order
Polynomial")
curve(f2 + e2*x +d2*x^2 + c2*x^3 + b2*x^4 + a2*x^5,add=T,col='orange')

#RMSE calculation
x<-CombinedData2$Discharge
predictedvaluesPoly5<-exp(f2 + e2*log(x) +d2*log(x)^2 + c2*log(x)^3 +
b2*log(x)^4 + a2*log(x)^5)
observedvalues<-CombinedData2$Susp.Sed
rmsPoly5<-sqrt(mean((observedvalues-predictedvaluesPoly5)^2))
##############Qplot#########################################################

require(ggplot2)
qplot(log(Discharge), log(Susp.Sed), group = Discharge > 38.55, geom =
c('point', 'smooth'),
      method = 'lm', se = F, data = CombinedData2)

#################sigmoid using mle#######################################
susp.sed.NLL <- function(Susp.Sed, Discharge, L,x0,k, sigma) {
  mean.susp.sed <- L/(1+exp(-k*(Discharge-x0)))
  -sum(dlnorm(Susp.Sed, meanlog <- log(mean.susp.sed), sdlog = sigma, log =
TRUE))
}

Sigmoidmle <- mle2(susp.sed.NLL, start = list(L = 1, x0 = 158, k = .03, sigma
= 1), data = CombinedData2)

#plot
plot(CombinedData2$Discharge,CombinedData2$Susp.Sed,xlab='Discharge
(ft^3/sec)',ylab='Suspended Sediment (tons/day)',main='Sigmoidmle')
L=coef(Sigmoidmle)[1]
x0=coef(Sigmoidmle)[2]
k=coef(Sigmoidmle)[3]
curve(L/(1+exp(-k*(x-x0))),from=0,to=700,add=T, col='red')

#enhanced
plot(CombinedData2$Discharge,CombinedData2$Susp.Sed,xlab='Discharge
(ft^3/sec)',ylab='Suspended Sediment
(tons/day)',main='Sigmoidmle',xlim=c(0,50),ylim=c(0,30))
L=coef(Sigmoidmle)[1]
x0=coef(Sigmoidmle)[2]
k=coef(Sigmoidmle)[3]
curve(L/(1+exp(-k*(x-x0))),from=0,to=700,add=T,col='red')
######################Exponential using mle################################
library(bbmle)
susp.sed.NLL <- function(Susp.Sed, Discharge,f,g, sigma) {
  mean.susp.sed <- exp(f-g*Discharge)
  -sum(dlnorm(Susp.Sed, meanlog <- log(mean.susp.sed), sdlog = sigma, log =
TRUE))
}
```

```
Expmle2 <- mle2(susp.sed.NLL, start = list(f = -1.7, g=.09, sigma = 1), data
= CombinedData2)

plot(CombinedData2$Discharge,CombinedData2$Susp.Sed,xlab='Discharge
(ft^3/sec)',ylab='Suspended Sediment (tons/day)',main='Expmle')
f=coef(Expmle2)[1]
g=coef(Expmle2)[2]
curve(exp(f-g*x),from=0,to=600,add=T)

#RMSE calculation
predictedvaluesExpmle2<-(exp(f-(g*CombinedData2$Discharge)))
observedvalues<-CombinedData2$Susp.Sed
rmsExpmle2<-sqrt(mean((observedvalues-predictedvaluesExpmle2)^2))
############################linear using mle############################
susp.sed.NLL <- function(Susp.Sed, Discharge,n,m, sigma) {
  mean.susp.sed <- (exp(n+m*Discharge))
  -sum(dlnorm(Susp.Sed, meanlog <- log(mean.susp.sed), sdlog = sigma, log =
TRUE))
}

Linmle2 <- mle2(susp.sed.NLL, start = list(n =-10, m=1.3, sigma = 1), data =
CombinedData2)

plot(CombinedData2$Discharge,CombinedData2$Susp.Sed,xlab='Discharge
(ft^3/sec)',ylab='Suspended Sediment (tons/day)',main='Linmle')
n=exp(coef(Linmle2)[1])
m=coef(Linmle2)[2]
curve(n+(m*x),from=0,to=700,add=T) #linear

#RMS calculation
predictedvaluesLinmle2<-(n+(m*CombinedData2$Discharge))
observedvalues<-CombinedData2$Susp.Sed
rmsLinmle2<-sqrt(mean((observedvalues-predictedvaluesLinmle2)^2))
##################Modified power using mle#####################################
susp.sed.NLL <- function(Susp.Sed, Discharge,a,b,c,sigma) {
  mean.susp.sed <- a*Discharge^(1+b*exp(-c*Discharge))
  -sum(dlnorm(Susp.Sed, meanlog <- log(mean.susp.sed), sdlog = sigma, log =
TRUE))
}

MPmle <- mle2(susp.sed.NLL, start = list(a =.01, b=.5,c=.001, sigma = 1),
data = CombinedData2)

plot(CombinedData2$Discharge,CombinedData2$Susp.Sed,xlab='Discharge
(ft^3/sec)',ylab='Suspended Sediment (tons/day)',main='MPmle')
a=coef(MPmle)[1]
b=coef(MPmle)[2]
c=coef(MPmle)[3]
curve(a*x^(1+b*exp(-c*x)),from=0,to=700,add=T,col='red')

#RMSE calculation
predictedvaluesMPmle<-(a*CombinedData2$Discharge)^(1+b*exp(-
c*CombinedData2$Discharge))
observedvalues<-CombinedData2$Susp.Sed
rmsMPmle<-sqrt(mean((observedvalues-predictedvaluesMPmle)^2))
#########################power using mle##################################
susp.sed.NLL <- function(Susp.Sed, Discharge,p,z, sigma) {
```

```
  mean.susp.sed <- (p*Discharge^z)
  -sum(dlnorm(Susp.Sed, meanlog <- log(mean.susp.sed), sdlog = sigma, log =
TRUE))
}

Powermle <- mle2(susp.sed.NLL, start = list(p=10^-2,z=1, sigma = 1), data =
CombinedData2)

plot(CombinedData2$Discharge,CombinedData2$Susp.Sed,xlab='Discharge
(ft^3/sec)',ylab='Suspended Sediment (tons/day)',main='Powermle')
p=coef(Powermle)[1]
z=coef(Powermle)[2]
curve(p*x^z,from=0,to=600,add=T,col='red')

#RMSE calculation
predictedvaluesPowermle<-p*CombinedData2$Discharge^z
observedvalues<-CombinedData2$Susp.Sed
rmsPowermle<-sqrt(mean((observedvalues-predictedvaluesPowermle)^2))
###################Gams#############################################################
library(mgcv)    #load mgcv package

M2<-gam(Susp.Sed~s(Discharge), data=CombinedData2, family=Gamma(link='log'))
summary(M2)
plot(M2, shift=coef(M2)[1],trans=exp,main="Discharge vs. Susp Sed
(M2)",xlab="Discharge",ylab="Suspended Sediment",xlim=c(0,50))
points(CombinedData2$Discharge,CombinedData2$Susp.Sed)

#RMSE calculation
predictedvaluesM2<-predict(M2,type='response')
observedvalues<-CombinedData2$Susp.Sed
rmsM2<-sqrt(mean((observedvalues-predictedvaluesM2)^2))

#M3 model
M3<-gam(Susp.Sed~s(Discharge)+ Month, data=CombinedData2,
family=Gamma(link='log'))
summary(M3)
plot(M3, shift=coef(M3)[1],trans=exp,main="Discharge vs. Susp Sed
(M3)",xlab="Discharge",ylab="Suspended Sediment")
points(CombinedData2$Discharge,CombinedData2$Susp.Sed)

###change axis###
M3<-gam(Susp.Sed~s(Discharge)+ Month, data=CombinedData2,
family=Gamma(link='log'))
summary(M3)
plot(M3, shift=coef(M3)[1],trans=exp,main="Discharge vs. Susp Sed
(M3)",xlab="Discharge",ylab="Suspended Sediment")
points(CombinedData2$Discharge,CombinedData2$Susp.Sed)

#RMSE calculation
predictedvaluesM3<-predict(M3,type='response')
observedvalues<-CombinedData2$Susp.Sed
rmsM3<-sqrt(mean((observedvalues-predictedvaluesM3)^2))

#################################Plot together#################################
plot(CombinedData2$Discharge,CombinedData2$Susp.Sed,xlab='Discharge
(ft^3/sec)',ylab='Suspended Sediment (tons/day)',main='Model Comparison')
```

```
curve(exp(dd+cc*log(x) + bb*log(x)^2 +
aa*log(x)^3),add=T,col='orange',lwd=1.5)
#CubPolynomial
curve(exp(e1+d1*log(x)+c1*log(x)^2 + b1*log(x)^3 +
a1*log(x)^4),add=T,col='red',lwd=1.5)                    #Polynomial4
curve(exp(f2 + e2*log(x) +d2*log(x)^2 + c2*log(x)^3 + b2*log(x)^4 +
a2*log(x)^5),add=T,col='purple',lwd=1.5) #Polyfive
curve(exp(f-g*x),from=0,to=600,add=T, col='darkgreen',lwd=1.5)
#Expmle2
curve(a*x^(1+b*exp(-c*x)),from=0,to=700,add=T,col='mediumblue',lwd=1.5)
#MPmle
curve(p*x^z,from=0,to=600,add=T,col='yellowgreen',lwd=1.5)  #Powermle
leg.txt<-c("3rd order Polynomial","4th order Polynomial","5th order
Polynomial","Exponential","Modified Power","Power")
legend("topleft",cex=0.5, bty='n',legend=leg.txt,title = "Model
Type",fill=c("orange","red","purple","darkgreen","mediumblue","yellowgreen"))

#Enhanced view
plot(CombinedData2$Discharge,CombinedData2$Susp.Sed,xlab='Discharge
(ft^3/sec)',ylab='Suspended Sediment (tons/day)',main='Model
Comparison',xlim=c(0,20),ylim=c(0,15))
curve(exp(dd+cc*log(x) + bb*log(x)^2 + aa*log(x)^3),add=T,col='orange',lwd=2)
#CubPolynomial
curve(exp(e1+d1*log(x)+c1*log(x)^2 + b1*log(x)^3 +
a1*log(x)^4),add=T,col='red',lwd=2)                    #Polynomial4
curve(exp(f2 + e2*log(x) +d2*log(x)^2 + c2*log(x)^3 + b2*log(x)^4 +
a2*log(x)^5),add=T,col='purple',lwd=2) #Polyfive
curve(exp(f-g*x),from=0,to=600,add=T, col='darkgreen',lwd=2)          #Expmle2
curve(a*x^(1+b*exp(-c*x)),from=0,to=700,add=T,col='mediumblue',lwd=2)  #MPmle
curve(p*x^z,from=0,to=600,add=T,col='yellowgreen',lwd=2)  #Powermle
leg.txt<-c("3rd order
Polynomial","Polynomial4","Polyfive","Expmle2","MPmle","Powermle")
legend("topleft",cex=0.5, legend=leg.txt,title = "Model
Name",fill=c("orange","red","purple","darkgreen","mediumblue","yellowgreen"))

#Plot over log scale
plot(CombinedData2$Discharge,CombinedData2$Susp.Sed,log='xy',xlab='Discharge
(ft^3/sec)',ylab='Suspended Sediment (tons/day)',main='Model Comparison (log
scale)')
curve(exp(dd+cc*log(x) + bb*log(x)^2 +
aa*log(x)^3),add=T,col='orange',lwd=1.5)
#CubPolynomial
curve(exp(e1+d1*log(x)+c1*log(x)^2 + b1*log(x)^3 +
a1*log(x)^4),add=T,col='red',lwd=1.5)                    #Polynomial4
curve(exp(f2 + e2*log(x) +d2*log(x)^2 + c2*log(x)^3 + b2*log(x)^4 +
a2*log(x)^5),add=T,col='purple',lwd=1.5) #Polyfive
curve(exp(f-g*x),add=T, col='darkgreen',lwd=1.5)          #Expmle2
curve(a*x^(1+b*exp(-c*x)),add=T,col='mediumblue',lwd=1.5)  #MPmle
curve(p*x^z,add=T,col='yellowgreen',lwd=1.5)  #Powermle
leg.txt<-c("3rd order Polynomial","4th order Polynomial","5th order
Polynomial","Exponential","Modified Power","Power")
legend("topleft",cex=0.5,bty='n',legend=leg.txt,fill=c("orange","red","purple
","darkgreen","mediumblue","yellowgreen"))

#####plot sigmoid mle against M2######
```

```
plot(M2, shift=coef(M2)[1],trans=exp,main="GAM(M2) and Poly4
Comparison",xlab="Discharge (cfs)",ylab="Suspended Sediment (tons per
day)",col='darkviolet',lwd=1.5)
points(CombinedData$Discharge,CombinedData$Susp.Sed)
curve(exp(e1+d1*log(x)+c1*log(x)^2 + b1*log(x)^3 +
a1*log(x)^4),add=T,col='red',lwd=1.5)            #Polynomial4
leg.txt<-c("M2","Poly4")
legend("topleft", legend=leg.txt,title = "Model
Name",cex=0.5,fill=c("darkviolet","orange"))

plot(M2, shift=coef(M2)[1], trans = function(x) exp(x), main="GAM and 4th
Order Polynomial Comparison",xlab="Discharge (ft^3/sec)",ylab="Suspended
Sediment (tons per day)",col='darkviolet',lwd=1.5, log = 'xy', shade = TRUE,
shade.col = 'violet', ylim = log(c(1e-2, 1e4)), rug = FALSE)
points(CombinedData$Discharge,I(CombinedData$Susp.Sed))
curve(exp(e1+d1*log(x)+c1*log(x)^2 + b1*log(x)^3 +
a1*log(x)^4),add=T,col='red',lwd=1.5)            #Polynomial4
leg.txt<-c("GAM","4th order Polynomial")
legend("topleft", legend=leg.txt,title = "Model Type",cex=0.5,
fill=c("violet","red"))

#chosen plot
plot(CombinedData2$Discharge,CombinedData2$Susp.Sed,main="Poly4
model",xlab="Discharge (cfs)",ylab="Suspended Sediment (tons per day)")
curve(exp(e1+d1*log(x)+c1*log(x)^2 + b1*log(x)^3 +
a1*log(x)^4),add=T,col='red',lwd=1.5)            #Polynomial4

#Enhanced view of chosen plot
plot(CombinedData2$Discharge,CombinedData2$Susp.Sed,xlab='Discharge
(ft^3/sec)',ylab='Suspended Sediment (tons/day)',main='Fourth Order
Polynomial Model at Low Discharge',xlim=c(0,40),ylim=c(0,30))
curve(exp(e1+d1*log(x)+c1*log(x)^2 + b1*log(x)^3 +
a1*log(x)^4),add=T,col='red',lwd=2)                  #Polynomial4
##########Analysis#########################

#use AIC to compare all models
AIC(GLM1,GLM2,GLM3,LinFit,LinFit2,Expmle2,CubPolynomial,Polynomial4,Poly5,Lin
mle2,MPmle,Powermle,M2,M3)

##############Correlation Analysis#############################################
#Number of data points
length(CombinedData2$Discharge)

#Range of discharge values
range(CombinedData2$Discharge)

#Range of suspended sediment values
range(CombinedData2$Susp.Sed)

#Average discharge value
mean(CombinedData2$Discharge)

#Median discharge value
median(CombinedData2$Discharge)

#Low discharge data frame
LowDischargeData<-subset(CombinedData2,CombinedData2$Discharge < 7.5)
```

```
#High discharge data frame
HighDischargeData<-subset(CombinedData2,CombinedData2$Discharge >= 7.5)

#Correlation coefficient LowDischargeData
cor(LowDischargeData$Discharge,LowDischargeData$Susp.Sed)

#Correlation coefficient HighDischargeData
cor(HighDischargeData$Discharge,HighDischargeData$Susp.Sed)

#Correlation coefficient CombinedData2
cor(CombinedData2$Discharge,CombinedData2$Susp.Sed)

#find the breakpoint in the data
library(segmented)
LinFit<-lm(Susp.Sed~Discharge,data=CombinedData2)
Segmented<-segmented(GLM1,seg.Z= ~Discharge,psi=10)

#Below the breakpoint data frame
Belowbp<-subset(CombinedData2,CombinedData2$Discharge < 30.84)

#Above the breakpoint data frame
Abovebp<-subset(CombinedData2,CombinedData2$Discharge >= 30.84)

#Correlation coefficient Belowbp
cor(Belowbp$Discharge,Belowbp$Susp.Sed)

#Correlation coefficient Abovebp
cor(Abovebp$Discharge,Abovebp$Susp.Sed)
```

Appendix 4.1 Experimental Raw Data.

*Data values highlighted in red were discarded due to probable experimental or analytical error.

Experiment 5, S=9, 1 g soil						
	Time	Phosphate	Silicate	N+N	Ammonia	pH
	mins	µmol/L	µmol/L	µmol/L	µmol/L	
SC-1-9-0	0	0.95	358.60	6.26	4.46**	7.69
SC-1-9-12	2	0.33	307.19	5.70	0.03	7.30
SC-1-9-14	7	0.33	307.45	6.33	1.46	7.24
SC-1-9-15	16	0.31	286.51	6.97	5.17	7.17
SC-1-9-16	31	0.31	303.87	7.93	HIGH	7.06
SC-1-9-17	60	0.28	266.86	10.64	HIGH	7.03
SC-1-9-18	110	0.30	271.04	11.71	HIGH	7.12
SC-1-9-19	250	0.47	271.96	12.31	HIGH	7.20
SC-1-9-20	482	0.54	265.65	13.91	HIGH	7.36
SC-1-9-21	1440	0.52	266.88	15.24	HIGH	7.48
SC-1-9-22	4260	0.53	238.66	15.91	HIGH	7.74
Experiment 27, S=0, 1 g soil						
	Time	Phosphate	Silicate	N+N	Ammonia	pH
	mins	µmol/L	µmol/L	µmol/L	µmol/L	
SC-1-73-0	0	1.15	480.87	10.75	3.76	7.53
SC-1-73-1	1	0.81	483.56	11.31	8.02	7.28
SC-1-73-2	3	0.58	431.55	11.52	8.94	7.14
SC-1-73-3	7	0.53	491.59	11.55	8.87	7.09
SC-1-73-4	15	0.41	441.81	11.50	10.22	7.07
SC-1-73-5	30	0.47	446.86	11.83	11.06	7.09
SC-1-73-6	60	0.45	473.93	12.10	15.84	7.19
SC-1-73-7	130	0.44	485.50	12.16	26.02	7.40
SC-1-73-8	250	0.58	473.66	13.39	47.55	7.59
SC-1-73-9	510	0.55	451.26	15.69	98.84	7.76
SC-1-73-10	690	0.62	430.82	17.14	135.45	7.79
Experiment 28, S=0, 1 g soil						
	Time	Phosphate	Silicate	N+N	Ammonia	pH
	mins	µmol/L	µmol/L	µmol/L	µmol/L	
SC-1-75-0	0	1.26	518.62	10.37	2.44	7.92
SC-1-75-1	1	0.91	526.63	10.98	5.71	7.76
SC-1-75-2	3	0.71	499.89	11.00	6.19	7.62
SC-1-75-3	7	0.61	482.96	11.61	7.23	7.55
SC-1-75-4	16	0.52	493.18	11.05	6.88	7.51
SC-1-75-5	30	0.47	481.81	11.36	7.37	7.53
SC-1-75-6	60	0.50	466.39	11.56	10.26	7.63
SC-1-75-7	120	0.47	433.16	12.01	16.41	7.84
SC-1-75-8	230	0.60	474.17	13.84	31.89	8.10
SC-1-75-9	510	0.74	463.85	18.26	71.02	8.36
SC-1-75-10	690	0.94	393.42	21.67	116.98	8.41

Experiment 21, S=9, 1 g soil								
	Time	Phosphate	Silicate	N+N	Ammonia	pH	Total N	Total P
	mins	µmol/L	µmol/L	µmol/L	µmol/L		µmol/L	µmol/L
SC-1-59-00	0	0.92	387.60	8.73	1.97	7.68	14.50	1.02
SC-1-59-01	1	0.59	376.35	9.14	8.59	7.32	23.68	0.62
SC-1-59-02	3	0.50	381.09	8.89	8.81	7.22	26.63	0.54
SC-1-59-03	7	0.33	366.83	8.85	9.48	7.08	26.42	0.36
SC-1-59-04	15	0.25	366.01	8.72	10.56	7.02	28.38	0.21
SC-1-59-05	31	0.25	359.12	8.80	13.58	7.03	31.72	0.21
SC-1-59-06	65	0.23	351.90	9.05	20.84	7.16	40.06	0.25
SC-1-59-07	140	0.29	322.24	9.74	40.45	7.39	71.24	0.30
SC-1-59-08	245	0.27	299.04	11.15	64.10	7.58	106.46	0.48
SC-1-59-09	480	0.36	324.16	14.99	145.94	7.70	179.24	0.47
SC-1-59-10	660	0.47	319.68	18.10	221.14	7.80	299.96	0.61
Experiment 22, S=9, 1 g soil								
	Time	Phosphate	Silicate	N+N	Ammonia	pH	Total N	Total P
	mins	µmol/L	µmol/L	µmol/L	µmol/L		µmol/L	µmol/L
SC-1-61-00	0	0.77	396.97	7.26	1.62	8.06	14.93	0.95
SC-1-61-01	1	0.54	377.87	7.94	8.78	7.72	24.15	0.61
SC-1-61-02	3	0.49	385.61	7.90	8.85	7.59	27.71	0.49
SC-1-61-03	7	0.33	372.43	8.03	9.80	7.50	27.07	0.36
SC-1-61-04	15	0.30	372.35	8.49	11.37	7.43	29.43	0.32
SC-1-61-05	30	0.26	365.21	8.96	13.96	7.43	33.38	0.27
SC-1-61-06	60	0.24	356.19	9.05	21.91	7.54	41.60	0.27
SC-1-61-07	130	0.31	325.07	11.08	43.81	7.79	81.15	0.36
SC-1-61-08	245	0.30	318.29	14.26	78.40	8.01	118.76	0.40
SC-1-61-09	470	0.40	326.38	22.18	174.78	8.23	233.07	0.47
SC-1-61-10	660	0.43	321.26	28.25	250.01	8.28	332.12	0.52
Experiment 18, S=17, 1 g soil								
	Time	Phosphate	Silicate	N+N	Ammonia	pH		
	mins	µmol/L	µmol/L	µmol/L	µmol/L			
SC-1-39-00	0	0.84	240.04	6.74	1.34	8.00		
SC-1-39-01	1	0.65	236.63	7.74	9.60	7.79		
SC-1-39-02	3.25	0.57	237.02	7.73	9.24	7.63		
SC-1-39-03	7	0.48	237.11	7.38	9.23	7.53		
SC-1-39-04	15	0.43	228.99	7.47	9.40	7.39		
SC-1-39-05	31	0.38	220.29	7.60	10.54	7.35		
SC-1-39-06	62	0.38	215.53	7.96	12.50	7.39		
SC-1-39-07	120	0.40	210.39	8.76	17.16	7.53		
SC-1-39-08	210	0.42	215.61	9.84	23.52	7.64		
SC-1-39-09	420	0.41	203.32	13.41	43.88	7.90		
SC-1-39-11	1530	0.51	196.40	32.95	143.11	8.23		
SC-1-39-12	4320	0.56	197.86	42.66	160.95	8.28		

Experiment 19, S=17, 1 g soil						
	Time	Phosphate	Silicate	N+N	Ammonia	pH
	mins	µmol/L	µmol/L	µmol/L	µmol/L	
SC-1-41-00	0	0.84	260.18	7.17	2.28	7.93
SC-1-41-01	1	0.70	254.90	7.98	9.64	7.65
SC-1-41-02	3	0.58	253.96	7.81	9.04	7.48
SC-1-41-03	7	0.48	253.96	7.89	9.52	7.33
SC-1-41-04	15	0.43	246.90	7.84	9.99	7.23
SC-1-41-05	30	0.39	243.91	7.92	11.12	7.17
SC-1-41-06	60	0.37	236.62	8.13	13.52	7.18
SC-1-41-07	150	0.38	223.97	9.14	23.03	7.34
SC-1-41-08	254	0.37	221.52	10.00	32.5	7.46
SC-1-41-09	570	0.48	214.15	13.69	66.42	7.67
SC-1-41-11	1410	0.46	185.73	23.43	152.59	7.82
SC-1-41-12	4320	0.61	240.07	29.65	161.83	7.86
Experiment 23, S=35, 1 g soil						
	Time	Phosphate	Silicate	N+N	Ammonia	pH
	mins	µmol/L	µmol/L	µmol/L	µmol/L	
SC-1-65-0	0	0.21	11.91	1.42	3.18	7.87
SC-1-65-1	1.33	0.12	3.48	1.66	9.21	7.71
SC-1-65-2	3	0.16	8.73	1.78	9.69	7.59
SC-1-65-3	7	0.10	2.31	1.52	9.91	7.49
SC-1-65-4	15	0.06	<0.05	0.36	1.96	7.43
SC-1-65-5	30	0.17	2.19	1.64	13.55	7.39
SC-1-65-6	62	0.18	3.95	2.01	18.69	7.38
SC-1-65-7	135	0.16	6.29	2.60	31.20	7.45
SC-1-65-8	250	0.22	4.97	3.43	53.59	7.57
SC-1-65-9	420	0.26	6.31	4.95	86.67	7.67
SC-1-65-10	660	0.25	19.19	7.74	135.21	7.76
Experiment 24, S=35, 1 g soil						
	Time	Phosphate	Silicate	N+N	Ammonia	pH
	mins	µmol/L	µmol/L	µmol/L	µmol/L	
SC-1-67-0	0	0.22	13.96	1.45	3.92	8.13
SC-1-67-1	1	0.13	5.23	1.57	9.34	8.00
SC-1-67-2	3	0.12	9.79	1.89	9.67	7.89
SC-1-67-3	7	0.11	3.56	2.06	11.06	7.83
SC-1-67-4	15	0.11	3.78	2.09	13.20	7.77
SC-1-67-5	30	0.11	3.36	3.04	16.89	7.76
SC-1-67-6	60	0.09	3.79	2.93	24.88	7.77
SC-1-67-7	128	0.09	4.25	5.04	45.76	7.86
SC-1-67-8	245	0.30	6.45	8.79	85.72	8.02
SC-1-67-9	420	0.43	7.05	14.61	136.39	8.14
SC-1-67-10	660	0.29	18.45	24.11	140.24	8.26

Experiment 25, S=35,0.2 g soil						
	Time	Phosphate	Silicate	N+N	Ammonia	pH
	mins	µmol/L	µmol/L	µmol/L	µmol/L	
SC-1-69-0	0	0.12	1.33	1.25	3.78	7.9
SC-1-69-1	1	0.11	1.99	0.94	4.61	7.88
SC-1-69-2	3	0.11	1.28	1.31	5.09	7.86
SC-1-69-3	7	0.21	2.61	0.92	5.26	7.85
SC-1-69-4	15	0.11	1.48	1.04	6.34	7.84
SC-1-69-5	30	0.10	1.65	0.99	8.55	7.83
SC-1-69-6	60	0.11	2.78	1.45	14.04	7.84
SC-1-69-7	120	0.14	4.82	1.78	26.06	7.85
SC-1-69-8	230	0.11	4.37	3.09	52.56	7.88
SC-1-69-9	460	0.09	5.98	4.90	105.44	7.91
SC-1-69-10	660	0.22	11.07	7.06	136.44	7.93
Experiment 26, S=35,0.2 g soil						
	Time	Phosphate	Silicate	N+N	Ammonia	pH
	mins	µmol/L	µmol/L	µmol/L	µmol/L	
SC-1-71-0	0	0.13	4.08	1.21	3.36	8.19
SC-1-71-1	1	0.10	3.64	0.99	5.03	8.18
SC-1-71-2	3	0.10	2.87	1.36	5.26	8.17
SC-1-71-3	7	0.13	4.62	1.14	6.28	8.16
SC-1-71-4	15	0.10	3.09	1.17	7.39	8.16
SC-1-71-5	30	0.10	3.45	1.48	10.79	8.18
SC-1-71-6	60	0.10	4.00	2.21	18.92	8.22
SC-1-71-7	120	0.17	5.54	4.09	37.55	8.27
SC-1-71-8	235	0.14	9.69	6.27	58.57	8.36
SC-1-71-9	455	0.12	13.89	10.46	100.76	8.44
SC-1-71-10	660	0.14	18.08	13.62	135.59	8.48
Experiment 29, S=35, 2 g soil						
	Time	Phosphate	Silicate	N+N	Ammonia	pH
	mins	µmol/L	µmol/L	µmol/L	µmol/L	
SC-1-77-0	0	0.21	3.20	0.98	2.41	7.92
SC-1-77-1	1	0.17	2.90	1.87	13.43	7.61
SC-1-77-2	4	0.12	2.20	1.54	13.77	7.37
SC-1-77-3	7	0.14	1.39	1.78	14.72	7.2
SC-1-77-4	15	0.10	1.89	1.68	14.64	7.09
SC-1-77-5	30	0.18	1.89	1.80	17.62	7.05
SC-1-77-6	60	0.26	5.76	2.15	22.36	7.08
SC-1-77-7	130	0.17	5.93	2.44	31.32	7.19
SC-1-77-8	250	0.23	10.81	3.52	53.46	7.34
SC-1-77-9	540	0.66	5.66	5.93	111.14	7.54
SC-1-77-10	660	0.90	6.36	7.31	132.88	7.59

Experiment 30, S=35, 2 g soil						
	Time	Phosphate	Silicate	N+N	Ammonia	pH
	mins	µmol/L	µmol/L	µmol/L	µmol/L	
SC-1-79-0	0	0.13	2.34	0.62	2.49	8.12
SC-1-79-1	1	0.07	2.52	1.71	13.94	7.9
SC-1-79-2	3	0.24	3.36	2.08	14.89	7.67
SC-1-79-3	7	0.14	1.94	1.91	14.29	7.52
SC-1-79-4	15	0.08	0.37	1.87	14.29	7.43
SC-1-79-5	30	0.16	2.27	2.29	14.48	7.4
SC-1-79-6	60	0.16	2.49	1.93	14.73	7.44
SC-1-79-7	120	0.12	1.05	2.25	15.52	7.56
SC-1-79-8	240	0.21	7.22	2.46	18.47	7.75
SC-1-79-9	540	0.21	5.78	3.92	28.68	8.03
SC-1-79-10	660	0.48	5.88	4.09	36.89	8.09

Appendix 5.1.1 Differential Equations and Fluxes

Groundwater volume

dGW(t)/dt = Infiltration(t) - SGWSeepage(t)

Waimaluhia Reservoir water volume

dWR(t)/dt = InputWR(t) – OutputWR(t)

Kāneʻohe Bay water volume

dKB(t)/dt = StreamDischarge(t) + SGWSeepage(t) + NPOcean(t) – OcnExport(t)

Groundwater phosphate

dPGW(t)/dt = Infiltration(t)*PPrecip – (SGWSeepage(t)*PGW)/GW(t)

Waimaluhia Reservoir phosphate mass

dPWR(t)/dt = InputWR(t)*PPrecip – (OutputWR(t)*PWR)/WR(t) + SedWRConc(t)

Kāneʻohe Bay phosphate mass

dPKB(t)/dt = (OutputWR(t)*PWR)/WR(t) + LandRunoff(t)*PPrecip + (SGWSeepage(t)*PGW)/GW(t) + NPOcean(t)*PPrecip – (OcnExport(t)*PKB)/KB(t) + (SGWSeepage(t)*PGW)/GW(t)

Groundwater N+N mass

dNNGW(t)/dt = Infiltration(t)*NNPrecip – (SGWSeepage(t)*NNGW)/GW(t)

Waimaluhia Reservoir N+N mass

dNNWR(t)/dt = InputWR(t)*NNPrecip – (OutputWR(t)*NNWR)/WR(t) + SedWRConc(t)

Kāneʻohe Bay N+N mass

dNNKB(t)/dt = (OutputWR(t)*NNWR)/WR(t) + LandRunoff(t)*NNPrecip + (SGWSeepage(t)*NNGW)/GW(t) + NPOcean(t)*NNPrecip – (OcnExport(t)*NNKB)/KB(t)

Groundwater Ammonia mass

dAmmoniaGW(t)/dt = Infiltration(t)*AmmoniaPrecip – (SGWSeepage(t)*AmmoniaGW)/GW(t)

Waimaluhia Reservoir Ammonia mass

dAmmoniaWR(t)/dt= InputWR(t) * AmmoniaPrecip – (OutputWR(t)*AmmoniaWR)/WR(t) + SedWRConc(t)

Kāneʻohe Bay Ammonia mass

dAmmoniaKB(t)/dt = (OutputWR(t)*AmmoniaWR)/WR(t) + LandRunoff(t)*AmmoniaPrecip + (SGWSeepage(t)*AmmoniaGW)/GW(t) + NPOcean*AmmoniaPrecip – (OcnExport*AmmoniaKB)/KB(t) + SedKBConc(t)

Appendix 5.1.2 Flux equations

Rate constant for SGWSeepage flux

kgw = (2.98e6) / (1.13e10)

Rate constant for OutputWR flux

kwr = (8.8e6) / (2.1e5)

Watershed net precipitation flux (m^3/yr)

NPland = 1.28e7 * Preciprun(t)

Where Preciprun= values for change in precipitation from the forcing file

Southern Kāne'ohe Bay net precipitation flux (m^3/yr)

NPOcean = 9.47e6 * Preciprun(t)

Infiltration through land surface flux (m^3/yr)

Infiltration = NPland(t)*(2.98/12.8)

Input to Waimaluhia Reservoir flux (m^3/yr)

InputWR = NPland(t)*(8.8/12.8)

Runoff from land surface flux (m^3/yr)

LandRunoff = NPland(t)*(1.02/12.8)

Output from Waimaluhia Reservoir flux (m^3/yr)

OutputWR = kwr*WR(t)

Stream discharge flux (m^3/yr)

StreamDischarge=LandRunoff(t)+OutputWR(t)

Groundwater flux (m^3/yr)

SGWSeepage = kgw*GW(t)

Export to open ocean flux (m^3/yr)

OcnExport = StreamDischarge(t) + SGWSeepage(t) + NPOcean(t)

Chemical Weathering adjustment term

$FCO2=1.0+0.252*\log(ACO2/ACO20(t)) + 0.0156*(\log(ACO2/ACO20(t)))^2$

where: ACO2=CO2 values from forcing file
ACO20=atmospheric CO2 at year 2015

Rate constant for suspended sediment flux to Waimaluhia Reservoir
k1 = 1.25e-4/FCO2

Rate constant for suspended sediment flux to Kāne‘ohe Stream
k2 = 9.31e-4/FCO2

Suspended sediment flux to Waimaluhia Reservoir (metric tons/yr)

SedInputWR = k1*InputWR(t)

Suspended sediment flux to Kāne‘ohe Stream (metric tons/yr)

SedInputKS = k2*LandRunoff(t)

Suspended sediment nutrient flux to Waimaluhia Reservoir (µmol/yr)

SedWRConc = SedInputWR(t)*SoilContentNut

where: SoilContentNut= the soil concentration of phosphate, N+N or ammonia

Suspended sediment nutrient flux to Kāne‘ohe Stream (µmol/yr)

SedKBConc = SedInputKS(t)*FreshWaterReleaseNut

where: FreshWaterReleaseNut = the release of phosphate, N+N, or ammonia derived from experiments

Appendix 5.2.1 Steady State Forcing File

Year	pCO2 (µatm)	Precipitation (%)	KB volume (m3)
2015	399	100%	79590000
2016	399	100%	79590000
2017	399	100%	79590000
2018	399	100%	79590000
2019	399	100%	79590000
2020	399	100%	79590000
2021	399	100%	79590000
2022	399	100%	79590000
2023	399	100%	79590000
2024	399	100%	79590000
2025	399	100%	79590000
2026	399	100%	79590000
2027	399	100%	79590000
2028	399	100%	79590000
2029	399	100%	79590000
2030	399	100%	79590000
2031	399	100%	79590000
2032	399	100%	79590000
2033	399	100%	79590000
2034	399	100%	79590000
2035	399	100%	79590000
2036	399	100%	79590000
2037	399	100%	79590000
2038	399	100%	79590000
2039	399	100%	79590000
2040	399	100%	79590000
2041	399	100%	79590000
2042	399	100%	79590000
2043	399	100%	79590000
2044	399	100%	79590000
2045	399	100%	79590000
2046	399	100%	79590000
2047	399	100%	79590000
2048	399	100%	79590000
2049	399	100%	79590000
2050	399	100%	79590000
2051	399	100%	79590000
2052	399	100%	79590000
2053	399	100%	79590000
2054	399	100%	79590000
2055	399	100%	79590000

2056	399	100%	79590000
2057	399	100%	79590000
2058	399	100%	79590000
2059	399	100%	79590000
2060	399	100%	79590000
2061	399	100%	79590000
2062	399	100%	79590000
2063	399	100%	79590000
2064	399	100%	79590000
2065	399	100%	79590000
2066	399	100%	79590000
2067	399	100%	79590000
2068	399	100%	79590000
2069	399	100%	79590000
2070	399	100%	79590000
2071	399	100%	79590000
2072	399	100%	79590000
2073	399	100%	79590000
2074	399	100%	79590000
2075	399	100%	79590000
2076	399	100%	79590000
2077	399	100%	79590000
2078	399	100%	79590000
2079	399	100%	79590000
2080	399	100%	79590000
2081	399	100%	79590000
2082	399	100%	79590000
2083	399	100%	79590000
2084	399	100%	79590000
2085	399	100%	79590000
2086	399	100%	79590000
2087	399	100%	79590000
2088	399	100%	79590000
2089	399	100%	79590000
2090	399	100%	79590000
2091	399	100%	79590000
2092	399	100%	79590000
2093	399	100%	79590000
2094	399	100%	79590000
2095	399	100%	79590000
2096	399	100%	79590000
2097	399	100%	79590000
2098	399	100%	79590000
2099	399	100%	79590000
2100	399	100%	79590000

Appendix 5.2.2. RCP 4.5 Forcing File.

Year	pCO2 (µatm)	Precipitation (%)	KB Volume
2015	399	100.0%	79600000
2016	402.18	99.7%	79656550
2017	404.41	99.5%	79713100
2018	406.64	99.2%	79769650
2019	408.88	98.9%	79826200
2020	411.13	98.7%	79882750
2021	413.38	98.4%	79939300
2022	415.64	98.1%	79995850
2023	417.94	97.6%	80052400
2024	420.27	97.3%	80108950
2025	422.66	97.0%	80165500
2026	425.08	96.8%	80222050
2027	427.54	96.5%	80278600
2028	430.02	96.2%	80335150
2029	432.52	96.0%	80391700
2030	435.05	95.7%	80448250
2031	437.59	95.4%	80504800
2032	440.13	95.2%	80561350
2033	442.66	94.9%	80617900
2034	445.21	94.6%	80674450
2035	447.77	94.3%	80731000
2036	450.36	94.1%	80787550
2037	452.96	93.8%	80844100
2038	455.59	93.5%	80900650
2039	458.22	93.3%	80957200
2040	460.84	93.0%	81013750
2041	463.48	92.8%	81070300
2042	466.09	92.5%	81126850
2043	468.68	92.3%	81183400
2044	471.23	92.0%	81239950
2045	473.78	91.8%	81296500
2046	476.33	91.5%	81353050
2047	478.88	91.3%	81409600
2048	481.44	91.1%	81466150
2049	483.99	90.8%	81522700
2050	486.54	90.6%	81579250
2051	489.06	90.3%	81635800
2052	491.54	90.1%	81692350
2053	493.93	89.9%	81748900
2054	496.24	89.6%	81805450
2055	498.47	89.4%	81862000

2056	500.65	89.1%	81918550
2057	502.77	88.9%	81975100
2058	504.85	88.6%	82031650
2059	506.88	88.4%	82088200
2060	508.87	88.2%	82144750
2061	510.8	87.9%	82201300
2062	512.65	87.7%	82257850
2063	514.4	87.4%	82314400
2064	516.06	87.2%	82370950
2065	517.63	87.0%	82427500
2066	519.1	86.7%	82484050
2067	520.49	86.5%	82540600
2068	521.82	86.2%	82597150
2069	523.09	86.0%	82653700
2070	524.3	85.7%	82710250
2071	525.45	85.5%	82766800
2072	526.51	85.5%	82823350
2073	527.46	85.4%	82879900
2074	528.3	85.4%	82936450
2075	529.03	85.4%	82993000
2076	529.64	85.3%	83049550
2077	530.14	85.3%	83106100
2078	530.55	85.3%	83162650
2079	530.88	85.2%	83219200
2080	531.14	85.2%	83275750
2081	531.32	85.2%	83332300
2082	531.49	85.1%	83388850
2083	531.7	85.1%	83445400
2084	531.94	85.1%	83501950
2085	532.2	85.0%	83558500
2086	532.49	85.0%	83615050
2087	532.78	84.9%	83671600
2088	533.07	84.9%	83728150
2089	533.39	84.9%	83784700
2090	533.74	84.8%	83841250
2091	534.13	84.8%	83897800
2092	534.56	84.8%	83954350
2093	535.01	84.7%	84010900
2094	535.48	84.7%	84067450
2095	535.95	84.7%	84124000
2096	536.44	84.6%	84180550
2097	536.92	84.6%	84237100
2098	537.4	84.6%	84293650
2099	537.87	84.5%	84350200
2100	538.36	84.5%	84406750

Appendix 5.2.3. RP 8.5 Forcing File.

Year	pCO2 (µatm)	Precipitation (%)	KB Volume
2015	399	100.0%	79590000
2016	404.33	99.7%	79665690
2017	407.1	99.4%	79741380
2018	409.93	99.0%	79817070
2019	412.82	98.7%	79892760
2020	415.78	98.4%	79968450
2021	418.8	98.1%	80044140
2022	421.86	97.8%	80119830
2023	424.99	97.4%	80195520
2024	428.2	97.1%	80271210
2025	431.47	96.8%	80346900
2026	434.83	96.5%	80422590
2027	438.24	96.2%	80498280
2028	441.72	95.8%	80573970
2029	445.25	95.5%	80649660
2030	448.83	95.2%	80725350
2031	452.47	94.9%	80801040
2032	456.18	94.6%	80876730
2033	459.96	94.2%	80952420
2034	463.85	93.9%	81028110
2035	467.85	93.6%	81103800
2036	471.96	93.3%	81179490
2037	476.18	93.0%	81255180
2038	480.51	92.6%	81330870
2039	484.93	92.3%	81406560
2040	489.44	92.0%	81482250
2041	494.03	91.7%	81557940
2042	498.73	91.5%	81633630
2043	503.53	91.2%	81709320
2044	508.43	90.9%	81785010
2045	513.46	90.6%	81860700
2046	518.61	90.4%	81936390
2047	523.9	90.1%	82012080
2048	529.32	89.8%	82087770
2049	534.88	89.5%	82163460
2050	540.54	89.3%	82239150
2051	546.32	89.0%	82314840
2052	552.21	88.7%	82390530
2053	558.21	88.4%	82466220
2054	564.31	88.2%	82541910
2055	570.52	87.9%	82617600

2056	576.84	87.6%	82693290
2057	583.3	87.3%	82768980
2058	589.91	87.1%	82844670
2059	596.65	86.8%	82920360
2060	603.52	86.5%	82996050
2061	610.52	86.2%	83071740
2062	617.61	86.0%	83147430
2063	624.76	85.7%	83223120
2064	631.99	85.4%	83298810
2065	639.29	85.1%	83374500
2066	646.65	84.9%	83450190
2067	654.1	84.6%	83525880
2068	661.64	84.3%	83601570
2069	669.3	84.0%	83677260
2070	677.08	83.8%	83752950
2071	684.95	83.5%	83828640
2072	692.9	83.2%	83904330
2073	700.89	83.0%	83980020
2074	708.93	82.7%	84055710
2075	717.02	82.5%	84131400
2076	725.14	82.2%	84207090
2077	733.31	81.9%	84282780
2078	741.52	81.7%	84358470
2079	749.8	81.4%	84434160
2080	758.18	81.2%	84509850
2081	766.64	80.9%	84585540
2082	775.17	80.7%	84661230
2083	783.75	80.4%	84736920
2084	792.37	80.1%	84812610
2085	801.02	79.9%	84888300
2086	809.71	79.6%	84963990
2087	818.42	79.4%	85039680
2088	827.16	79.1%	85115370
2089	835.96	78.8%	85191060
2090	844.8	78.6%	85266750
2091	853.73	78.3%	85342440
2092	862.73	78.1%	85418130
2093	871.78	77.8%	85493820
2094	880.86	77.6%	85569510
2095	889.98	77.3%	85645200
2096	899.12	77.0%	85720890
2097	908.29	76.8%	85796580
2098	917.47	76.5%	85872270
2099	926.67	76.3%	85947960
2100	935.87	76.0%	86023650

Appendix 5.3.1 SKWANEM Model Code: Precipitation-Suspended Sediment Relationship

```
%Plot of Precipitation-Suspended Sediment Relationship

close all

x = [0:0.001:10];

%discharge equation
disc = 121./(1+exp(-0.9*(x-3.3)));

%suspended sediment equation
sed = exp(-0.02 * log(disc).^4 + 0.24 * log(disc).^3 -...
    0.39 * log(disc).^2 + 0.75 * log(disc) - 2.95);

sed_old = exp(-0.02 * log10(disc).^4 + 0.24 * log10(disc).^3 -...
    0.39 * log10(disc).^2 + 0.75 * log10(disc) - 2.95);

%%
target_precip = 0.19 + 0.49;

xind = min(find(min(abs(x-target_precip)) == abs(x - target_precip)));
sed_lin = (sed(xind+1) - sed(xind))/(x(xind+1)-x(xind));
sed_linear = sed(1) + sed_lin*(x-x(1));

xlow = 0.16;
xhigh = 0.23;

xlow_ind = min(find(min(abs(x-xlow)) == abs(x-xlow)));
xhigh_ind = min(find(min(abs(x-xhigh)) == abs(x-xhigh)));

dx = x(2:end) - x(1:end-1);
dsed = sed(2:end) - sed(1:end-1);

%%
offset = -5;
xposmin = 0.1;
yposmin = 0.125;
height = 0.8125;
width = 0.85;

%Plots
figure
set(gcf, 'Units','inches', 'Position',[0 0 8 6])
set(gcf, 'PaperPositionMode','auto')
subplot('Position',[xposmin yposmin width height])
semilogy(x,sed,'LineWidth',2)
set(gca,'FontSize',14)
xlabel('Precipitation (inches/day)')
ylabel('Sediment discharge (tons/day)')
title('Precipitation vs. Suspended sediment','FontSize',16)

figure
set(gcf, 'Units','inches', 'Position',[0 0 8 6])
set(gcf, 'PaperPositionMode','auto')
```

```
subplot('Position',[xposmin yposmin width height])
plot(x,sed,x,sed_old,'LineWidth',2)
hold on
plot(x(xlow_ind),sed(xlow_ind),'*r',x(xhigh_ind),sed(xhigh_ind),'*r')
hold off
xlim([0 0.5])%,ylim([0.08 0.09])
set(gca,'FontSize',14)
xlabel('Precipitation (inches/day)')
ylabel('Sediment discharge (tons/day)')

figure
set(gcf, 'Units','inches', 'Position',[0 0 8 6])
set(gcf, 'PaperPositionMode','auto')
subplot('Position',[xposmin yposmin width height])
plot((x(2:end)+x(1:end-1))/2,dsed,'LineWidth',2)
xlim([0 0.5])
set(gca,'FontSize',14)
xlabel('d(Precipitation) (inches/day)')
ylabel('Sediment discharge (tons/day)')
```

Appendix 5.3.2 SKWANEM Model Code: Mass Balance Code

```
%SKOANEM:Southern Kāne‘ohe Offshore and Watershed Nutrient Export Model
clear all

curdir = pwd;

% cd('c:\Users\Sara\Desktop')

global GW WR KB NPland NPOcean kgw kwr PPrecip NNPrecip AmmoniaPrecip...
    k1 k2 k3 k4 Precip0

global CO2run
global Preciprun

%Load steady state and forcing data
%Steady state data
SS_data = csvread('SteadyStateValues.csv',1,1);
CO2SS = SS_data(:,1);
PrecipSS = SS_data(:,2);
KBSS = SS_data(:,3);

%RCP 4.5 forcing data
Forcing45_data = csvread('IPCCforcings45.csv',1,1);
CO245 = Forcing45_data(:,1);
Precip45 = Forcing45_data(:,2);
KB45 = Forcing45_data(:,3);

%RCP 8.5 forcing data
Forcing85_data = csvread('IPCCforcings85.csv',1,1);
CO285 = Forcing85_data(:,1);
Precip85 = Forcing85_data(:,2);
KB85 = Forcing85_data(:,3);

%Water Fluxes
NPland=1.28e7;                  %Flux of net precip into watershed in m^3/yr
NPOcean=9.47e6;                 %Flux of net precip into Southern Bay in
m^3/yr
Infiltration=NPland*(2.98/12.8);    %Flux of Infiltration through land surface
InputWR=NPland*(8.8/12.8);            %Flux of input to Waimaluhia Reservoir
LandRunoff=NPland*(1.02/12.8);      %Flux of runoff from land surface
OutputWR=kwr*WR;                %Flux of output from Waimaluhia Reservoir
StreamDischarge=LandRunoff+OutputWR;    %Flux of stream water entering ocean
SGWSeepage=kgw*GW;              %Flux of ground water entering ocean

%First run at steady state for 85 years
CO2run=CO2SS;
Preciprun=PrecipSS;
Precip0 = Preciprun(1);
KB = KBSS;

%Reservoirs
GW=1.13e10;                     %Groundwater Reservoir volume in m^3
WR=2.1e5;                       %Waimaluhia Reservoir volume in m^3
% KB=79.59e6;                     %Southern Kāne‘ohe Bay volume in m^3
```

```
%Rate constants for steady state first order fluxes
kgw=(2.98e6)/(1.13e10);                 %rate constant for SGWSeepage flux
kwr=(8.8e6)/(2.1e5);                    %rate constant for OutputWR flux

%Nutrient concentrations from experiments and literature
%multiply each value by 1000 to convert from \mumol/L to \mumol/m^3 and by
%volume to get mass in \mumol
PPrecip=0;                          %Precipitation phosphate mass
PWR=0.6 * 1000 * WR;                %Waimaluhia Reservoir phosphate mass
PGW=1.5 * 1000 * GW;                %Groundwater phosphate mass
PKB=0.07 *1000 * KB(1);                %Kāne‘ohe Bay phosphate mass

NNPrecip=3.6 * 1000;              %Precipitation N+N mass
NNWR=20.8 * 1000 * WR;                %Waimaluhia Reservoir N+N mass
NNGW=10 * 1000 * GW;                %Groundwater N+N mass
NNKB=0.19 * 1000 * KB(1);                %Kāne‘ohe Bay N+N mass

AmmoniaPrecip=0.05 * 1000;          %Precipitation Ammonia mass
AmmoniaWR=2.5 * 1000 * WR;          %Waimaluhia Reservoir Ammonia mass
AmmoniaGW=10 * 1000 * GW;           %Groundwater Ammonia mass
AmmoniaKB=0.1 * 1000 * KB(1);          %Kāne‘ohe Bay Ammonia mass


%%%%%%%%%%%%%%%%%%%%%%%%%Suspended Sediment %%%%%%%%%%%%%%%%%%%%%%%%%%%%%%%%

%Values to relate suspended sediment value to water value (based on steady
%state)

%Atmospheric CO2 content of atmosphere at t0 (in ppmv)
ACO20=399;
ACO2=399;

%Fco2 equation
FCO2=1.0+0.252*log(ACO2/ACO20) + 0.0156*(log(ACO2/ACO20))^2;

%Suspended sediment to WR
k1=1.25*10^-4 * FCO2;

%Suspended sediment to KS
k2=9.31*10^-4 *FCO2;

%Suspended sediment out of WR
k3=2.27*10^-7 * FCO2;

%Suspended Sdiment KS to KBay
k4=9.8*10^-5 * FCO2;

%Sediment Nutrient release relationships
global SoilContentP SoilContentNN SoilContentAmmonia FreshWaterReleaseP ...
    FreshWaterReleaseNN FreshWaterReleaseAmmonia

global ResSedRelease
ResSedRelease = 1;

%Soil Analysis values
%lab values reported in ug/g
```

```
%multiply by mw and 10^6 g/metric tons to get correct units
%mw in g/mol
%final product in \mumol/metric tons
SoilContentP=6 * 10^6 * (1/30.974);                 %phosporous mw
SoilContentNN=15 * 10^6 * (1/62.0049);              %nitrate mw
SoilContentAmmonia=1.4 * 10^6 * (1/18.03846);       %ammonium mw

%Nutrient Release Experiment Values
%experimental values in \mumol/L
%multiply by 10^6g/metric tons to convert g to metric tons
%multiply by 1L/1g since those were experimental conditions
%final product is \mumol/metric tons
FreshWaterReleaseP=0.05 * 10^6;
FreshWaterReleaseNN= 15.2 * 10^6;
FreshWaterReleaseAmmonia= 234 * 10^6;

%%%%%%%%%%%%%%%%%%%%%%%%end Susp. Sed stuff%%%%%%%%%%%%%%%%%%%%%%%%%%%%%%%%

%Inital reservoir volumes of GW, WR, KB and nutrient concentrations
y0=[GW WR KB(1) PGW PWR PKB NNGW NNWR NNKB AmmoniaGW AmmoniaWR AmmoniaKB,...
    0 0 0 0 0 0 0];


%Time span 2015-2100
tspan=[1:85];

% solve the problem using ODE45
[t, Y] = ode23(@MassBalance_derivs, tspan, y0);

steadyruns = 10;
for s = 1:steadyruns
    s
y0=[GW WR KB(1) Y(end,4) Y(end,5) Y(end,6) Y(end,7) Y(end,8) Y(end,9)...
    Y(end,10) Y(end,11) Y(end,12),...
    0 0 0 0 0 0 0];
% y0=[GW WR KB 0 0 0 0 0 0 0 0 0];
clear t, clear Y
%Time span 2015-2010
tspan=[1:85];

% solve the problem using ODE45
[t, Y] = ode23(@MassBalance_derivs, tspan, y0);
end

%Now change scenario
CO2run=CO245;
Preciprun=Precip45;
KB = KB45;

%Inital reservoir volumes of GW, WR, KB and nutrient concentrations
y0=[GW WR KB(1) Y(end,4) Y(end,5) Y(end,6) Y(end,7) Y(end,8) Y(end,9)...
    Y(end,10) Y(end,11) Y(end,12),...
    0 0 0 0 0 0 0];
% y0=[GW WR KB 0 0 0 0 0 0 0 0 0];
clear t, clear Y
%Time span 2015-2010
tspan=[1:85];
```

```
% solve the problem using ODE45
[t, Y] = ode23(@MassBalance_derivs, tspan, y0);

%%%%%%%%%%%%%%%%%%%%%%%%PLOTS%%%%%%%%%%%%%%%%%%%%%%%%%%%%%%%%%%%%%%%%%%%%%%
fignum = 0;

%%%%%%%%%%%%%%%%%%%%%%%%%%%MASS PLOTS%%%%%%%%%%%%%%%%%%%%%%%%%%%%%%%%%%%%%%%
fignum = fignum + 1;
filename = ['fig',num2str(fignum)];
eval([filename,'=figure(',num2str(fignum),');'])

 xposmin = 0.05;
 yposmin = 0.05;
 width = 0.425;
 height = 0.425;
 xoffset = 0.075;
 yoffset = 0.0625;
 %Waterbalance plot

 set(gcf, 'Units', 'inches', 'Position', [0 0 9 6.5])
 set(gcf, 'PaperPositionMode', 'auto')

 subplot('Position',[xposmin yposmin+yoffset+height width height])
 plot(t,100*(Y(:,1)-Y(1,1))/Y(1,1),'r-','LineWidth',1.5);
 hold on
 plot(t,100*(Y(:,2)-Y(1,2))/Y(1,2),'b-','LineWidth',1.5);
 plot(t,100*(Y(:,3)-Y(1,3))/Y(1,3),'k-','LineWidth',1.5);
 plot([t(1) t(end)],[0 0],'k','LineWidth',0.5)
 legend('Groundwater',...
     'Waimaluhia Reservoir',...
     'Southern KBay','Location','SouthWest');
 ylabel('Water volume (% change)');
 set(gca,'FontSize',8)
 title('Water Reservoir Volumes (% change)');
 xlim([1 85]),set(gca,'Xtick',[5:10:85]),set(gca,'XTickLabel',[2020:10:2100])
 ylim([-40 15]),set(gca,'Ytick',[-40:5:15])
 hold off

 %Phosphate mass plot
 subplot('Position',[xposmin+xoffset+width yposmin+yoffset+height width
height])
 plot(t,100*(Y(:,4)-Y(1,4))/Y(1,4),'r-','LineWidth',1.5);
 hold on
 plot(t,100*(Y(:,5)-Y(1,5))/Y(1,5),'b-','LineWidth',1.5);
 plot(t,100*(Y(:,6)-Y(1,6))/Y(1,6),'k-','LineWidth',1.5);
 plot([t(1) t(end)],[0 0],'k','LineWidth',0.5)
 ylabel('Total Phosphate (% change)');
 legend('Groundwater',...
     'Waimaluhia Reservoir',...
     'Southern KBay','Location','SouthWest');
 set(gca,'FontSize',8)
 title('Reservoir Phosphate Mass (\mumol)');
 xlim([1 85]),set(gca,'Xtick',[5:10:85]),set(gca,'XTickLabel',[2020:10:2100])
 hold off

  %N+N mass plot
```

```
 subplot('Position',[xposmin yposmin width height])
 plot(t,100*(Y(:,7)-Y(1,7))/Y(1,7),'r-','LineWidth',1.5);
 hold on
 plot(t,100*(Y(:,8)-Y(1,8))/Y(1,8),'b-','LineWidth',1.5);
 plot(t,100*(Y(:,9)-Y(1,9))/Y(1,9),'k-','LineWidth',1.5);
 plot([t(1) t(end)],[0 0],'k','LineWidth',0.5)
 xlabel('Year'); ylabel('Total N+N (% change)');
 legend('Groundwater',...
     'Waimaluhia Reservoir',...
     'Southern KBay','Location','SouthWest');
 set(gca,'FontSize',8)
 title('Reservoir N+N Mass (% change)');
 xlim([1 85]),set(gca,'Xtick',[5:10:85]),set(gca,'XTickLabel',[2020:10:2100])
 hold off

  %Ammonia mass plot
 subplot('Position',[xposmin+xoffset+width yposmin width height])
 plot(t,100*(Y(:,10)-Y(1,10))/Y(1,10),'r-','LineWidth',1.5);
 hold on
 plot(t,100*(Y(:,11)-Y(1,11))/Y(1,11),'b-','LineWidth',1.5);
 plot(t,100*(Y(:,12)-Y(1,12))/Y(1,12),'k-','LineWidth',1.5);
 plot([t(1) t(end)],[0 0],'k','LineWidth',0.5)
 xlabel('Year'); ylabel('Total Ammonia (% changel)');
 legend('Groundwater',...
     'Waimaluhia Reservoir',...
     'Southern KBay','Location','SouthWest');
 set(gca,'FontSize',8)
  title('Reservoir Ammonia Mass (% change)');
  xlim([1
85]),set(gca,'Xtick',[5:10:85]),set(gca,'XTickLabel',[2020:10:2100])
 hold off

print('-dpng','-r150',[filename,'.png'])



%%%%%%%%%%%%%%%%%%%%%%%%Concentration Plots%%%%%%%%%%%%%%%%%%%%%%%%%%%%%%%%%%%%
 %Waterbalance plot
fignum = fignum + 1;
filename = ['fig',num2str(fignum)];
eval([filename,'=figure(',num2str(fignum),');'])


 set(gcf, 'Units', 'inches', 'Position', [0 0 9 6.5])
 set(gcf, 'PaperPositionMode', 'auto')

 subplot('Position',[xposmin yposmin+yoffset+height width height])
 plot(t,Y(:,1)/1e10,'r-','LineWidth',1.5);
 hold on
 plot(t,Y(:,2)/1e5,'b-','LineWidth',1.5);
 plot(t,Y(:,3)/1e7,'k-','LineWidth',1.5);
 legend('Groundwater (x10^1^0)',...
     'Waimaluhia Reservoir (x10^5)',...
     'Ocean (x10^7)');
 ylabel('Water volume (m^3)');
 set(gca,'FontSize',8)
 title('Water Reservoir Volumes (m^3)');
```

```
 xlim([1 85]),set(gca,'Xtick',[5:10:85]),set(gca,'XTickLabel',[2020:10:2100])
 hold off

 %Phosphate concentration plot
 subplot('Position',[xposmin+xoffset+width yposmin+yoffset+height width
height])
 plot(t,Y(:,4)./Y(:,1),'r-','LineWidth',1.5);
 hold on
 plot(t,Y(:,5)./Y(:,2),'b-','LineWidth',1.5);
 plot(t,Y(:,6)./Y(:,3),'k-','LineWidth',1.5);
 ylabel('Total Phosphate (\mumol/m^3)');
 legend('Groundwater',...
     'Waimaluhia Reservoir',...
     'Ocean');
 set(gca,'FontSize',8)
 title('Reservoir Phosphate Concentrations (\mumol/m^3)');
 xlim([1 85]),set(gca,'Xtick',[5:10:85]),set(gca,'XTickLabel',[2020:10:2100])
 hold off

  %N+N concentration plot
 subplot('Position',[xposmin yposmin width height])
 plot(t,Y(:,7)./Y(:,1),'r-','LineWidth',1.5);
 hold on
 plot(t,Y(:,8)./Y(:,2),'b-','LineWidth',1.5);
 plot(t,Y(:,9)./Y(:,3),'k-','LineWidth',1.5);
 xlabel('Year'); ylabel('Total N+N (\mumol/m^3)');
 legend('Groundwater',...
     'Waimaluhia Reservoir',...
     'Ocean');
 set(gca,'FontSize',8)
 title('Reservoir N+N Concentrations (\mumol/m^3)');
 xlim([1 85]),set(gca,'Xtick',[5:10:85]),set(gca,'XTickLabel',[2020:10:2100])
 hold off

  %Ammonia concentration plot
 subplot('Position',[xposmin+xoffset+width yposmin width height])
 plot(t,Y(:,10)./Y(:,1),'r-','LineWidth',1.5);
 hold on
 plot(t,Y(:,11)./Y(:,2),'b-','LineWidth',1.5);
 plot(t,Y(:,12)./Y(:,3),'k-','LineWidth',1.5);
 xlabel('Year'); ylabel('Total Ammonia (\mumol/m^3)');
 legend('Groundwater',...
     'Waimaluhia Reservoir',...
     'Ocean');
 set(gca,'FontSize',8)
  title('Reservoir Ammonia Concentrations (\mumol/m^3)');
  xlim([1
85]),set(gca,'Xtick',[5:10:85]),set(gca,'XTickLabel',[2020:10:2100])
 hold off

  print('-dpng','-r150',[filename,'.png'])


 %%%%%%%%%%%%%%%%%%%%%%%%%%%%%%%%Flux Plots%%%%%%%%%%%%%%%%%%%%%%%%%%%%%%%%%%%%
 %%Water fluxes plot
fignum = fignum + 1;
filename = ['fig',num2str(fignum)];
```

```
eval([filename,'=figure(',num2str(fignum),');'])


 set(gcf, 'Units', 'inches', 'Position', [0 0 9 6.5])
 set(gcf, 'PaperPositionMode', 'auto')

 subplot('Position',[xposmin yposmin+yoffset+height width height])
 plot((t(2:end)+t(1:end-1))/2,1e-6*(Y(2:end,13)-Y(1:end-1,13)),'r-
','LineWidth',1.5);
 hold on
 plot((t(2:end)+t(1:end-1))/2,1e-6*(Y(2:end,14)-Y(1:end-1,14)),'g-
','LineWidth',1.5);
 plot((t(2:end)+t(1:end-1))/2,1e-6*(Y(2:end,15)-Y(1:end-1,15)),'c-
','LineWidth',1.5);
 plot((t(2:end)+t(1:end-1))/2,1e-6*(Y(2:end,16)-Y(1:end-1,16)),'m-
','LineWidth',1.5);
 plot((t(2:end)+t(1:end-1))/2,1e-6*(Y(2:end,17)-Y(1:end-1,17)),'b-
','LineWidth',1.5);
 plot((t(2:end)+t(1:end-1))/2,1e-3*(Y(2:end,18)-Y(1:end-1,18)),'k-
','LineWidth',1.5);
 plot((t(2:end)+t(1:end-1))/2,1e-3*(Y(2:end,19)-Y(1:end-1,19)),'k--
','LineWidth',1.5);
 legend('Infliltration (x10^6)',...
     'Groundwater Seepage (x10^6)',...
     'Reservoir Input (x10^6)', ...
     'Reservoir Output (x10^6)', ...
     'KB Ocean Export (x10^6)',...
     'Sediment Reservoir Input (x10^3)',...
     'Sediment Stream Input (x10^3)', 'Location','NorthWest');
 ylabel('Water volume flux (m^3/yr)');
 set(gca,'FontSize',8)
 title('Water Reservoir Volumes Fluxes (m^3/yr)');
 xlim([1 85]),set(gca,'Xtick',[5:10:85]),set(gca,'XTickLabel',[2020:10:2100])
 hold off

 %Phosphate flux concentration plot
 subplot('Position',[xposmin+xoffset+width yposmin+yoffset+height width
height])
 plot((t(2:end)+t(1:end-1))/2,...
     1e-8*PPrecip*(Y(2:end,13)-Y(1:end-1,13)),'r-','LineWidth',1.5);
 hold on
 plot((t(2:end)+t(1:end-1))/2,...
     1e-9*(Y(2:end,4)+Y(1:end-1,4)).*(Y(2:end,14)-Y(1:end-
1,14))./(Y(2:end,1)+Y(1:end-1,1)),...
     'g-','LineWidth',1.5);
 plot((t(2:end)+t(1:end-1))/2,...
     1e-8*PPrecip*(Y(2:end,15)-Y(1:end-1,15)),'c-','LineWidth',1.5);
 plot((t(2:end)+t(1:end-1))/2,...
     1e-8*(Y(2:end,5)+Y(1:end-1,5)).*(Y(2:end,16)-Y(1:end-
1,16))./(Y(2:end,2)+Y(1:end-1,2)),...
     'm-','LineWidth',1.5);
 plot((t(2:end)+t(1:end-1))/2,...
     1e-9*(Y(2:end,6)+Y(1:end-1,6)).*(Y(2:end,17)-Y(1:end-
1,17))./(Y(2:end,3)+Y(1:end-1,3)),...
     'b-','LineWidth',1.5);
 plot((t(2:end)+t(1:end-1))/2,SoilContentP*1e-8*(Y(2:end,18)-Y(1:end-
1,18)),'k-','LineWidth',1.5);
```

```
 plot((t(2:end)+t(1:end-1))/2,FreshWaterReleaseP*1e-8*(Y(2:end,19)-Y(1:end-
1,19)),'k--','LineWidth',1.5);
 legend('Infliltration (x10^8)',...
     'Groundwater Seepage (x10^9)',...
     'Reservoir Input (x10^8)', ...
     'Reservoir Output (x10^8)', ...
     'KB Ocean Export (x10^9)',...
     'Sediment Reservoir (x10^8)',...
     'Sediment Stream (x10^8)','Location','NorthWest');
 set(gca,'FontSize',8)
 title('Phosphate Fluxes (\mumol/yr)');
 xlim([1 85]),set(gca,'Xtick',[5:10:85]),set(gca,'XTickLabel',[2020:10:2100])
 hold off

  %N+N concentration plot
 subplot('Position',[xposmin yposmin width height])

 plot((t(2:end)+t(1:end-1))/2,...
     1e-8*NNPrecip*(Y(2:end,13)-Y(1:end-1,13)),'r-','LineWidth',1.5);
 hold on
 plot((t(2:end)+t(1:end-1))/2,...
     1e-9*(Y(2:end,7)+Y(1:end-1,7)).*(Y(2:end,14)-Y(1:end-
1,14))./(Y(2:end,1)+Y(1:end-1,1)),...
     'g-','LineWidth',1.5);
 plot((t(2:end)+t(1:end-1))/2,...
     1e-8*NNPrecip*(Y(2:end,15)-Y(1:end-1,15)),'c-','LineWidth',1.5);
 plot((t(2:end)+t(1:end-1))/2,...
     1e-8*(Y(2:end,8)+Y(1:end-1,8)).*(Y(2:end,16)-Y(1:end-
1,16))./(Y(2:end,2)+Y(1:end-1,2)),...
     'm-','LineWidth',1.5);
 plot((t(2:end)+t(1:end-1))/2,...
     1e-9*(Y(2:end,9)+Y(1:end-1,9)).*(Y(2:end,17)-Y(1:end-
1,17))./(Y(2:end,3)+Y(1:end-1,3)),...
     'b-','LineWidth',1.5);
 legend('Infliltration (x10^8)',...
     'Groundwater Seepage (x10^9)',...
     'Reservoir Input (x10^8)', ...
     'Reservoir Output (x10^8)', ...
     'KB Ocean Export (x10^9)','Location','NorthWest');
 set(gca,'FontSize',8)
 title('Nitrate Fluxes (\mumol/yr)');
 xlim([1 85]),set(gca,'Xtick',[5:10:85]),set(gca,'XTickLabel',[2020:10:2100])
 hold off

  %Ammonia concentration plot
 subplot('Position',[xposmin+xoffset+width yposmin width height])

 plot((t(2:end)+t(1:end-1))/2,...
     1e-8*AmmoniaPrecip*(Y(2:end,13)-Y(1:end-1,13)),'r-','LineWidth',1.5);
 hold on
 plot((t(2:end)+t(1:end-1))/2,...
     1e-9*(Y(2:end,10)+Y(1:end-1,10)).*(Y(2:end,14)-Y(1:end-
1,14))./(Y(2:end,1)+Y(1:end-1,1)),...
     'g-','LineWidth',1.5);
 plot((t(2:end)+t(1:end-1))/2,...
     1e-8*AmmoniaPrecip*(Y(2:end,15)-Y(1:end-1,15)),'c-','LineWidth',1.5);
 plot((t(2:end)+t(1:end-1))/2,...
```

```
     1e-8*(Y(2:end,11)+Y(1:end-1,11)).*(Y(2:end,16)-Y(1:end-
1,16))./(Y(2:end,2)+Y(1:end-1,2)),...
     'm-','LineWidth',1.5);
 plot((t(2:end)+t(1:end-1))/2,...
     1e-9*(Y(2:end,12)+Y(1:end-1,12)).*(Y(2:end,17)-Y(1:end-
1,17))./(Y(2:end,3)+Y(1:end-1,3)),...
     'b-','LineWidth',1.5);
 legend('Infliltration (x10^8)',...
     'Groundwater Seepage (x10^9)',...
     'Reservoir Input (x10^8)', ...
     'Reservoir Output (x10^8)', ...
     'KB Ocean Export (x10^9)','Location','NorthWest');
 set(gca,'FontSize',8)
 title('Ammonia Fluxes (\mumol/yr)');
  xlim([1
85]),set(gca,'Xtick',[5:10:85]),set(gca,'XTickLabel',[2020:10:2100])
 hold off

  print('-dpng','-r150',[filename,'.png'])

  %%%%%%%%%%%%%%%%%%%%%%%%%%%%%%Ratio plots%%%%%%%%%%%%%%%%%%%%%%%%%%%%%%%%%%
 %%Water fluxes plot
fignum = fignum + 1;
filename = ['fig',num2str(fignum)];
eval([filename,'=figure(',num2str(fignum),');'])


 set(gcf, 'Units', 'inches', 'Position', [0 0 9 6.5])
 set(gcf, 'PaperPositionMode', 'auto')

%   subplot('Position',[xposmin yposmin width height])
%  plot(t,(Y(:,7) + Y(:,10))./Y(:,4),'r-','LineWidth',1.5);
%  hold on
%  plot(t,(Y(:,8)+Y(1,10))./Y(:,5),'b-','LineWidth',1.5);
 plot(t,(Y(:,9)+Y(1,12))./Y(:,6),'k-','LineWidth',1.5);
 xlabel('Year'); ylabel('Total N+N + NH_3 / Total P');
 legend('Ocean');
 set(gca,'FontSize',8)
 title('Nutrient Ratios in Kāne‘ohe Bay');
 xlim([1 85]),set(gca,'Xtick',[5:10:85]),set(gca,'XTickLabel',[2020:10:2100])
 hold off


  print('-dpng','-r150',[filename,'.png'])



%%%%%%%%%%%%%%%%%%      Kāne‘ohe Bay Concentration Plots %%%%%%%%%%%%%%%%%%%%

xposmin = 0.1125;
yposmin = 0.1125;
width = 0.85;
height = 0.825;


fignum = fignum + 1;
```

```
filename = ['fig',num2str(fignum)];
eval([filename,'=figure(',num2str(fignum),');'])


set(gcf, 'Units', 'inches', 'Position', [0 0 9 6.5])
set(gcf, 'PaperPositionMode', 'auto')

%Phosphate concentration plot
subplot('Position',[xposmin yposmin width height])
plot(t,1e-2*Y(:,6)./Y(:,3),'r-','LineWidth',1.5);
hold on
plot(t,1e-3*Y(:,9)./Y(:,3),'b-','LineWidth',1.5);
plot(t,1e-3*Y(:,12)./Y(:,3),'k-','LineWidth',1.5);
xlabel('Year'),ylabel('Total Phosphate (\mumol/m^3)');
legend('Phosphate (x10^2)',...
    'N+N (x10^3)',...
    'Ammonia (x10^3)',...
    'Location','NorthWest');
set(gca,'FontSize',14)
title('Concentrations in Kāneʻohe Bay (\mumol/m^3)','FontSize',16);
xlim([1 85]),set(gca,'Xtick',[5:10:85]),set(gca,'XTickLabel',[2020:10:2100])
hold off

 print('-dpng','-r150',[filename,'.png'])
```

Appendix 5.3.3 SKWANEM Model Code: Mass Balance Differential Equations

```
function dydt = MassBalance_derivs(t,y)
global GW WR KB NPland NPOcean kgw kwr PPrecip NNPrecip AmmoniaPrecip...
    k1 k2 k3 k4 Precip0
global SoilContentP SoilContentNN SoilContentAmmonia FreshWaterReleaseP ...
    FreshWaterReleaseNN FreshWaterReleaseAmmonia
global ResSedRelease
global CO2run
global Preciprun

%Atmospheric CO2 content of atmosphere at t0 (in ppmv)
ACO20=399;
ACO2=CO2run(floor(t));

Pland = NPland * Preciprun(floor(t));
POcean = NPOcean * Preciprun(floor(t));


%Fco2 equation
FCO2=1.0+0.252*log(ACO2/ACO20) + 0.0156*(log(ACO2/ACO20))^2;

%Suspended sediment to WR
k1=1.25*10^-4 * FCO2;

%Suspended sediment to KS
k2=9.31*10^-4 * FCO2;

Infiltration=Pland*(2.98/12.8);                %Flux of Infiltration through
land surface
InputWR=Pland*(8.8/12.8);                      %Flux of input to Waimaluhia
Reservoir
InputWR0 = NPland * Precip0 * (8.8/12.8);
LandRunoff=Pland*(1.02/12.8);                  %Flux of runoff from land
surface
LandRunoff0 = NPland * Precip0 * (1.02/12.8);
OutputWR=kwr*y(2);                             %Flux of output from
Waimaluhia Reservoir
StreamDischarge=LandRunoff+OutputWR;           %Flux of stream water
entering ocean
SGWSeepage=kgw*y(1);                           %Flux of ground water
entering ocean
OcnExport = StreamDischarge+SGWSeepage+POcean; %Flux of water exiting S KBay
PGW = y(4);
PWR = y(5);
PKB = y(6);
NNGW = y(7);
NNWR = y(8);
NNKB = y(9);
AmmoniaGW = y(10);
AmmoniaWR = y(11);
AmmoniaKB = y(12);
sed_lin_fac = 0.6570; %Linear rate of change (dsed/dx)/dsed0

SedInputWR=k1*InputWR0*(1 + sed_lin_fac*(InputWR - InputWR0)/InputWR0);
```

```
SedInputKS=k2*LandRunoff0*(1 + sed_lin_fac*(LandRunoff -
LandRunoff0)/LandRunoff0);

%Water balance differential equations
dGWdt = Infiltration - SGWSeepage;
dWRdt = InputWR - OutputWR;
dKBdt = KB(floor(t+1)) - KB(floor(t));

%Phosphate balance differential equations
Pderivs = Nut_derivs(y(1), y(2), y(3), ...
        PGW, PWR, PKB, PPrecip,...
        Infiltration, SGWSeepage,...
        InputWR, OutputWR,...
        ResSedRelease, SedInputWR, SedInputKS, FreshWaterReleaseP,
SoilContentP,...
        POcean, LandRunoff, OcnExport);
dPGWdt = Pderivs(1);
dPWRdt = Pderivs(2);
dPKBdt = Pderivs(3);


%N+N balance differential equations
NNderivs = Nut_derivs(y(1), y(2), y(3), ...
        NNGW, NNWR, NNKB, NNPrecip,...
        Infiltration, SGWSeepage,...
        InputWR, OutputWR,...
        ResSedRelease, SedInputWR, SedInputKS, FreshWaterReleaseNN,
SoilContentNN,...
        POcean, LandRunoff, OcnExport);
dNNGWdt = NNderivs(1);
dNNWRdt = NNderivs(2);
dNNKBdt = NNderivs(3);


%Ammonia balance differential equations
Ammoniaderivs = Nut_derivs(y(1), y(2), y(3), ...
        AmmoniaGW, AmmoniaWR, AmmoniaKB, AmmoniaPrecip,...
        Infiltration, SGWSeepage,...
        InputWR, OutputWR,...
        ResSedRelease, SedInputWR, SedInputKS, FreshWaterReleaseAmmonia,
SoilContentAmmonia,...
        POcean, LandRunoff, OcnExport);
dAmmoniaGWdt = Ammoniaderivs(1);
dAmmoniaWRdt = Ammoniaderivs(2);
dAmmoniaKBdt = Ammoniaderivs(3);


dydt = [  dGWdt, dWRdt, dKBdt,...
          dPGWdt, dPWRdt, dPKBdt,...
          dNNGWdt, dNNWRdt, dNNKBdt,...
          dAmmoniaGWdt, dAmmoniaWRdt, dAmmoniaKBdt,...
          Infiltration, SGWSeepage, InputWR, OutputWR, OcnExport,...
          SedInputWR, SedInputKS]';
```

Appendix 5.3.4 SKWANEM Model Code: Data Load File

```
%%MassBalancecode_dataload


%Water Fluxes
NPland=1.28e7;                  %Flux of net precip into watershed in m^3/yr
NPOcean=9.47e6;                 %Flux of net precip into Southern Bay in
m^3/yr

%Reservoirs
GW=1.13e10;                     %Groundwater Reservoir volume in m^3
WR=2.1e5;                       %Waimaluhia Reservoir volume in m^3
KB=79.59e6;                     %Southern Kāne‘ohe Bay volume in m^3

%Rate constants for steady state first order fluxes
kgw=(2.98e6)/(1.13e10);                 %rate constant for SGWSeepage flux
kwr=(8.8e6)/(2.1e5);                    %rate constant for OutputWR flux


Infiltration=NPland*(2.98/12.8);    %Flux of Infiltration through land surface
InputWR=NPland*(8.8/12.8);            %Flux of input to Waimaluhia Reservoir
LandRunoff=NPland*(1.02/12.8);      %Flux of runoff from land surface
OutputWR=kwr*WR;                %Flux of output from Waimaluhia Reservoir
StreamDischarge=LandRunoff+OutputWR;    %Flux of stream water entering ocean
SGWSeepage=kgw*GW;              %Flux of ground water entering ocean



%Nutrient concentrations from experiments and literature
%multiply each value by 1000 to convert from \mumol/L to \mumol/m^3 and by
%volume to get mass in \mumol
PPrecip=0;                      %Precipitation phosphate mass
PWR=0.6 * 1000 * WR;            %Waimaluhia Reservoir phosphate mass
PGW=1.5 * 1000 * GW;            %Groundwater phosphate mass
PKB=0.07 *1000 * KB(1);            %Kāne‘ohe Bay phosphate mass

NNPrecip=3.6 * 1000;          %Precipitation N+N mass
NNWR=20.8 * 1000 * WR;            %Waimaluhia Reservoir N+N mass
NNGW=10 * 1000 * GW;            %Groundwater N+N mass
NNKB=0.19 * 1000 * KB(1);          %Kāne‘ohe Bay N+N mass

AmmoniaPrecip=0.05 * 1000;      %Precipitation Ammonia mass
AmmoniaWR=2.5 * 1000 * WR;      %Waimaluhia Reservoir Ammonia mass
AmmoniaGW=10 * 1000 * GW;       %Groundwater Ammonia mass
AmmoniaKB=0.1 * 1000 * KB(1);      %Kāne‘ohe Bay Ammonia mass


%%%%%%%%%%%%%%%%%%%%Suspended Sediment stuff%%%%%%%%%%%%%%%%%%%%%%%%%%%%%

%Values to relate suspended sediment value to water value (based on steady
%state)

%Atmospheric CO2 content of atmosphere at t0 (in ppmv)
ACO20=399;
ACO2=399;
```

```
%Fco2 equation
FCO2=1.0+0.252*log(ACO2/ACO20) + 0.0156*(log(ACO2/ACO20))^2;

%Suspended sediment to WR
k1=1.25*10^-4 * FCO2;

%Suspended sediment to KS
k2=9.31*10^-4 *FCO2;

%Suspended sediment out of WR
k3=2.27*10^-7 * FCO2;

%Suspended Sdiment KS to KBay
k4=9.8*10^-5 * FCO2;

%Soil Analysis values
%lab values reported in ug/g
%multiply by mw and 10^6 g/metric tons to get correct units
%mw in g/mol
%final product in \mumol/metric tons
SoilContentP=6 * 10^6 * (1/30.974);                 %phosporous mw
SoilContentNN=15 * 10^6 * (1/62.0049);              %nitrate mw
SoilContentAmmonia=1.4 * 10^6 * (1/18.03846);       %ammonium mw

%Nutrient Release Experiment Values
%experimental values in \mumol/L
%multiply by 10^6g/metric tons to convert g to metric tons
%multiply by 1L/1g since those were experimental conditions
%final product is \mumol/metric tons
FreshWaterReleaseP=0.05 * 10^6;
FreshWaterReleaseNN= 15.2 * 10^6;
FreshWaterReleaseAmmonia= 234 * 10^6;


%%
% Create the time variable for plotting
time = 1:85;
dtime = (time(2:end)+time(1:end-1))/2;

%Load steady state and forcing data
%Steady state data
SS_data = csvread('SteadyStateValues.csv',1,1);
CO2SS = SS_data(:,1);
PrecipSS = SS_data(:,2);
KBSS = SS_data(:,3);

%RCP 4.5 forcing data
Forcing45_data = csvread('IPCCforcings45.csv',1,1);
CO245 = Forcing45_data(:,1);
Precip45 = Forcing45_data(:,2);
KB45 = Forcing45_data(:,3);

%RCP 8.5 forcing data
Forcing85_data = csvread('IPCCforcings85.csv',1,1);
CO285 = Forcing85_data(:,1);
Precip85 = Forcing85_data(:,2);
KB85 = Forcing85_data(:,3);
```

```
% Load the Steady State data file
SS_data = matfile('SS_data.mat');

% Look at the data in the loaded file
SS_data

% Load the 4.5 scenario data file
IP45_data = matfile('IP45_data.mat');

% Look at the data in the loaded file
IP45_data

% Load the 4.5 scenario data file
IP85_data = matfile('IP85_data.mat');

% Look at the data in the loaded file
IP85_data

%% Plot one variable in the data, for test
fignum = 0;


%%
fignum = fignum + 1;
filename = ['fig',num2str(fignum)];
eval([filename,'=figure(',num2str(fignum),');'])

xposmin = 0.1;
yposmin = 0.1125;
width = 0.85;
height = 0.825;

set(gcf, 'Units', 'inches', 'Position', [0 0 8 6])
set(gcf, 'PaperPositionMode', 'auto')

subplot('Position',[xposmin yposmin width height])
plot(dtime,(IP45_data.SedInputKS(2:end,1)-IP45_data.SedInputKS(1:end-
1,1)),'r',...
    dtime,(IP85_data.SedInputKS(2:end,1)-IP85_data.SedInputKS(1:end-1,1)),'r-
-',...
    dtime,(IP45_data.SedInputWR(2:end,1)-IP45_data.SedInputWR(1:end-
1,1)),'b',...
    dtime,(IP85_data.SedInputWR(2:end,1)-IP85_data.SedInputWR(1:end-1,1)),'b-
-',...
    'LineWidth',2)
legend('SedInputKS 4.5','SedInputKS 8.5','SedInputWR 4.5','SedInputWR
8.5','FontSize',11,'Location','NorthWest')
xlim([1 85]),set(gca,'Xtick',[5:10:85]),set(gca,'XTickLabel',[2020:10:2100])
ylim([900 1200])
hold off
set(gca,'FontSize',14)
xlim([0 85])
xlabel('Year'),ylabel('metric tons/yr')
title('Sediment Fluxes','FontSize',16)
```

```
%%
fignum = fignum + 1;
filename = ['fig',num2str(fignum)];
eval([filename,'=figure(',num2str(fignum),');'])

xposmin = 0.0875;
yposmin = 0.1125;
width = 0.9;
height = 0.825;

set(gcf, 'Units', 'inches', 'Position', [0 0 8 6])
set(gcf, 'PaperPositionMode', 'auto')

subplot('Position',[xposmin yposmin width height])

plot(dtime,1e-7*(IP45_data.Infiltration(2:end,1)-
IP45_data.Infiltration(1:end-1,1)),'r',...
    dtime,1e-7*(IP85_data.Infiltration(2:end,1)-IP85_data.Infiltration(1:end-
1,1)),'r--',...
    dtime,1e-7*(IP45_data.InputWR(2:end,1)-IP45_data.InputWR(1:end-
1,1)),'b',...
    dtime,1e-7*(IP85_data.InputWR(2:end,1)-IP85_data.InputWR(1:end-1,1)),'b--
',...
    dtime,1e-7*(IP45_data.OcnExport(2:end,1)-IP45_data.OcnExport(1:end-
1,1)),'m',...
    dtime,1e-7*(IP85_data.OcnExport(2:end,1)-IP85_data.OcnExport(1:end-
1,1)),'m--',...
    time,1e-7*NPland*Precip45(2:end),'g',...
    time,1e-7*NPland*Precip85(2:end),'g--',...
    dtime,1e-7*(NPland*(Precip45(3:end)+Precip45(2:end-1))/2 +
(IP45_data.OutputWR(2:end,1)-IP45_data.OutputWR(1:end-1,1))),'k',...
    dtime,1e-7*(NPland*(Precip85(3:end)+Precip85(2:end-1))/2 +
(IP85_data.OutputWR(2:end,1)-IP85_data.OutputWR(1:end-1,1))),'k--',...
    'LineWidth',2)
h_legend = legend('Infiltration RCP 4.5','Infiltration RCP 8.5',...
    'InputWR/OutputWR RCP 4.5','InputWR/OutputWR RCP 8.5',...
    'OcnExport RCP 4.5','OcnExport RCP 8.5',...
    'LandRunoff RCP 4.5','LandRunoff RCP 8.5',...
    'StreamDischarge RCP 4.5','StreamDischarge RCP 8.5',...
    'FontSize',11,'Location','EastOutside');
set(h_legend,'FontSize',10)
xlim([1 85]),set(gca,'Xtick',[5:10:85]),set(gca,'XTickLabel',[2020:10:2100])
hold off
set(gca,'FontSize',14)
xlim([0 85])
xlabel('Year'),ylabel('10^7 m^3/yr')
title('Water Fluxes','FontSize',16)


%%
fignum = fignum + 1;
filename = ['fig',num2str(fignum)];
eval([filename,'=figure(',num2str(fignum),');'])

xposmin = 0.1;
yposmin = 0.1125;
```

```
width = 0.8;
height = 0.825;

set(gcf, 'Units', 'inches', 'Position', [0 0 8 6])
set(gcf, 'PaperPositionMode', 'auto')

subplot('Position',[xposmin yposmin width height])
plot(time,(IP45_data.AmmWR + IP45_data.NNWR)./IP45_data.PWR,'r',...
    time,(IP85_data.AmmWR + IP85_data.NNWR)./IP85_data.PWR,'r--',...
    time,(IP45_data.AmmKB + IP45_data.NNKB)./IP45_data.PKB,'b',...
    time,(IP85_data.AmmKB + IP85_data.NNKB)./IP85_data.PKB,'b--',...
    'LineWidth',2)
legend('Waimaluhia Reservoir 4.5','Waimaluhia Reservoir 8.5',...
    'Kāne‘ohe Bay 4.5','Kāne‘ohe Bay 8.5',...
    'FontSize',11,'Location','SouthWest')
set(gca,'FontSize',14)
xlim([1 85]),set(gca,'Xtick',[5:10:85]),set(gca,'XTickLabel',[2020:10:2100])
xlim([0 85]),ylim([0 160])
xlabel('Year')
title('N:P Ratio','FontSize',16);

%%

% Phosphate fluxes

% N+N fluxes
PInfiltration_initflux = PPrecip*(IP45_data.Infiltration(2,1)-
IP45_data.Infiltration(1,1));
PSGWSeepage_initflux = (IP45_data.PGW(2,1)+IP45_data.PGW(1,1)).*...
    (IP45_data.SGWSeepage(2,1)-IP45_data.SGWSeepage(1,1))./...
    (IP45_data.GW(2,1)+IP45_data.GW(1,1));
PInputWR_initflux = PPrecip*(IP45_data.InputWR(2,1)-IP45_data.InputWR(1,1));
POutputWR_initflux = (IP45_data.PWR(2,1)+IP45_data.PWR(1,1)).*...
    (IP45_data.OutputWR(2,1)-IP45_data.OutputWR(1,1))./...
    (IP45_data.WR(2,1)+IP45_data.WR(1,1));
POcnExport_initflux = (IP45_data.PKB(2,1)+IP45_data.PKB(1,1)).*...
    (IP45_data.OcnExport(2,1)-IP45_data.OcnExport(1,1))./...
    (IP45_data.KB(2,1)+IP45_data.KB(1,1));
PLandRunoff_initflux = PPrecip*NPland*(Precip45(end)+Precip45(end-1))/2;
PStreamDischarge_initflux = PPrecip*NPland*(Precip45(end)+Precip45(end-1))/2
+ ...
    POutputWR_initflux;
PSedInputWR_initflux = SoilContentP*(IP45_data.SedInputWR(2,1)-
IP45_data.SedInputWR(1,1));
PSedInputKS_initflux = FreshWaterReleaseP*(IP45_data.SedInputKS(2,1)-
IP45_data.SedInputKS(1,1));

P_initflux = [PInfiltration_initflux, PSGWSeepage_initflux,
PInputWR_initflux,...
    POutputWR_initflux, POcnExport_initflux, PLandRunoff_initflux,...
    PStreamDischarge_initflux, PSedInputWR_initflux, PSedInputKS_initflux];

PInfiltration_45flux = PPrecip*(IP45_data.Infiltration(end,1)-
IP45_data.Infiltration(end-1,1));
PSGWSeepage_45flux = (IP45_data.PGW(end,1)+IP45_data.PGW(end-1,1)).*...
    (IP45_data.SGWSeepage(end,1)-IP45_data.SGWSeepage(end-1,1))./...
    (IP45_data.GW(end,1)+IP45_data.GW(end-1,1));
```

```
PInputWR_45flux = PPrecip*(IP45_data.InputWR(end,1)-IP45_data.InputWR(end-
1,1));
POutputWR_45flux = (IP45_data.PWR(end,1)+IP45_data.PWR(end-1,1)).*...
    (IP45_data.OutputWR(end,1)-IP45_data.OutputWR(end-1,1))./...
    (IP45_data.WR(end,1)+IP45_data.WR(end-1,1));
POcnExport_45flux = (IP45_data.PKB(end,1)+IP45_data.PKB(end-1,1)).*...
    (IP45_data.OcnExport(end,1)-IP45_data.OcnExport(end-1,1))./...
    (IP45_data.KB(end,1)+IP45_data.KB(end-1,1));
PLandRunoff_45flux = PPrecip*NPland*(Precip45(end)+Precip45(end-1))/2;
PStreamDischarge_45flux = PPrecip*NPland*(Precip45(end)+Precip45(end-1))/2 +
...
    POutputWR_45flux;
PSedInputWR_45flux = SoilContentP*(IP45_data.SedInputWR(end,1)-
IP45_data.SedInputWR(end-1,1));
PSedInputKS_45flux = FreshWaterReleaseP*(IP45_data.SedInputKS(end,1)-
IP45_data.SedInputKS(end-1,1));

P_45flux = [PInfiltration_45flux, PSGWSeepage_45flux, PInputWR_45flux,...
    POutputWR_45flux, POcnExport_45flux, PLandRunoff_45flux,...
    PStreamDischarge_45flux, PSedInputWR_45flux, PSedInputKS_45flux];

PInfiltration_85flux = PPrecip*(IP85_data.Infiltration(end,1)-
IP85_data.Infiltration(end-1,1));
PSGWSeepage_85flux = (IP85_data.PGW(end,1)+IP85_data.PGW(end-1,1)).*...
    (IP85_data.SGWSeepage(end,1)-IP85_data.SGWSeepage(end-1,1))./...
    (IP85_data.GW(end,1)+IP85_data.GW(end-1,1));
PInputWR_85flux = PPrecip*(IP85_data.InputWR(end,1)-IP85_data.InputWR(end-
1,1));
POutputWR_85flux = (IP85_data.PWR(end,1)+IP85_data.PWR(end-1,1)).*...
    (IP85_data.OutputWR(end,1)-IP85_data.OutputWR(end-1,1))./...
    (IP85_data.WR(end,1)+IP85_data.WR(end-1,1));
POcnExport_85flux = (IP85_data.PKB(end,1)+IP85_data.PKB(end-1,1)).*...
    (IP85_data.OcnExport(end,1)-IP85_data.OcnExport(end-1,1))./...
    (IP85_data.KB(end,1)+IP85_data.KB(end-1,1));
PLandRunoff_85flux = PPrecip*NPland*(Precip85(end)+Precip85(end-1))/2;
PStreamDischarge_85flux = PPrecip*NPland*(Precip85(end)+Precip85(end-1))/2 +
...
    POutputWR_85flux;
PSedInputWR_85flux = SoilContentP*(IP85_data.SedInputWR(end,1)-
IP85_data.SedInputWR(end-1,1));
PSedInputKS_85flux = FreshWaterReleaseP*(IP85_data.SedInputKS(end,1)-
IP85_data.SedInputKS(end-1,1));

P_85flux = [PInfiltration_85flux, PSGWSeepage_85flux, PInputWR_85flux,...
    POutputWR_85flux, POcnExport_85flux, PLandRunoff_85flux,...
    PStreamDischarge_85flux, PSedInputWR_85flux, PSedInputKS_85flux];


% N+N fluxes
NNInfiltration_initflux = NNPrecip*(IP45_data.Infiltration(2,1)-
IP45_data.Infiltration(1,1));
NNSGWSeepage_initflux = (IP45_data.NNGW(2,1)+IP45_data.NNGW(1,1)).*...
    (IP45_data.SGWSeepage(2,1)-IP45_data.SGWSeepage(1,1))./...
    (IP45_data.GW(2,1)+IP45_data.GW(1,1));
NNInputWR_initflux = NNPrecip*(IP45_data.InputWR(2,1)-
IP45_data.InputWR(1,1));
NNOutputWR_initflux = (IP45_data.NNWR(2,1)+IP45_data.NNWR(1,1)).*...
```

```
    (IP45_data.OutputWR(2,1)-IP45_data.OutputWR(1,1))./...
    (IP45_data.WR(2,1)+IP45_data.WR(1,1));
NNOcnExport_initflux = (IP45_data.NNKB(2,1)+IP45_data.NNKB(1,1)).*...
    (IP45_data.OcnExport(2,1)-IP45_data.OcnExport(1,1))./...
    (IP45_data.KB(2,1)+IP45_data.KB(1,1));
NNLandRunoff_initflux = NNPrecip*NPland*(Precip45(end)+Precip45(end-1))/2;
NNStreamDischarge_initflux = NNPrecip*NPland*(Precip45(end)+Precip45(end-
1))/2 + ...
    NNOutputWR_initflux;
NNSedInputWR_initflux = SoilContentNN*(IP45_data.SedInputWR(2,1)-
IP45_data.SedInputWR(1,1));
NNSedInputKS_initflux = FreshWaterReleaseNN*(IP45_data.SedInputKS(2,1)-
IP45_data.SedInputKS(1,1));

NN_initflux = [NNInfiltration_initflux, NNSGWSeepage_initflux,
NNInputWR_initflux,...
    NNOutputWR_initflux, NNOcnExport_initflux, NNLandRunoff_initflux,...
    NNStreamDischarge_initflux, NNSedInputWR_initflux,
NNSedInputKS_initflux];

NNInfiltration_45flux = NNPrecip*(IP45_data.Infiltration(end,1)-
IP45_data.Infiltration(end-1,1));
NNSGWSeepage_45flux = (IP45_data.NNGW(end,1)+IP45_data.NNGW(end-1,1)).*...
    (IP45_data.SGWSeepage(end,1)-IP45_data.SGWSeepage(end-1,1))./...
    (IP45_data.GW(end,1)+IP45_data.GW(end-1,1));
NNInputWR_45flux = NNPrecip*(IP45_data.InputWR(end,1)-IP45_data.InputWR(end-
1,1));
NNOutputWR_45flux = (IP45_data.NNWR(end,1)+IP45_data.NNWR(end-1,1)).*...
    (IP45_data.OutputWR(end,1)-IP45_data.OutputWR(end-1,1))./...
    (IP45_data.WR(end,1)+IP45_data.WR(end-1,1));
NNOcnExport_45flux = (IP45_data.NNKB(end,1)+IP45_data.NNKB(end-1,1)).*...
    (IP45_data.OcnExport(end,1)-IP45_data.OcnExport(end-1,1))./...
    (IP45_data.KB(end,1)+IP45_data.KB(end-1,1));
NNLandRunoff_45flux = NNPrecip*NPland*(Precip45(end)+Precip45(end-1))/2;
NNStreamDischarge_45flux = NNPrecip*NPland*(Precip45(end)+Precip45(end-1))/2
+ ...
    NNOutputWR_45flux;
NNSedInputWR_45flux = SoilContentNN*(IP45_data.SedInputWR(end,1)-
IP45_data.SedInputWR(end-1,1));
NNSedInputKS_45flux = FreshWaterReleaseNN*(IP45_data.SedInputKS(end,1)-
IP45_data.SedInputKS(end-1,1));

NN_45flux = [NNInfiltration_45flux, NNSGWSeepage_45flux, NNInputWR_45flux,...
    NNOutputWR_45flux, NNOcnExport_45flux, NNLandRunoff_45flux,...
    NNStreamDischarge_45flux, NNSedInputWR_45flux, NNSedInputKS_45flux];

NNInfiltration_85flux = NNPrecip*(IP85_data.Infiltration(end,1)-
IP85_data.Infiltration(end-1,1));
NNSGWSeepage_85flux = (IP85_data.NNGW(end,1)+IP85_data.NNGW(end-1,1)).*...
    (IP85_data.SGWSeepage(end,1)-IP85_data.SGWSeepage(end-1,1))./...
    (IP85_data.GW(end,1)+IP85_data.GW(end-1,1));
NNInputWR_85flux = NNPrecip*(IP85_data.InputWR(end,1)-IP85_data.InputWR(end-
1,1));
NNOutputWR_85flux = (IP85_data.NNWR(end,1)+IP85_data.NNWR(end-1,1)).*...
    (IP85_data.OutputWR(end,1)-IP85_data.OutputWR(end-1,1))./...
    (IP85_data.WR(end,1)+IP85_data.WR(end-1,1));
NNOcnExport_85flux = (IP85_data.NNKB(end,1)+IP85_data.NNKB(end-1,1)).*...
```

```
    (IP85_data.OcnExport(end,1)-IP85_data.OcnExport(end-1,1))./...
    (IP85_data.KB(end,1)+IP85_data.KB(end-1,1));
NNLandRunoff_85flux = NNPrecip*NPland*(Precip85(end)+Precip85(end-1))/2;
NNStreamDischarge_85flux = NNPrecip*NPland*(Precip85(end)+Precip85(end-1))/2
+ ...
    NNOutputWR_85flux;
NNSedInputWR_85flux = SoilContentNN*(IP85_data.SedInputWR(end,1)-
IP85_data.SedInputWR(end-1,1));
NNSedInputKS_85flux = FreshWaterReleaseNN*(IP85_data.SedInputKS(end,1)-
IP85_data.SedInputKS(end-1,1));

NN_85flux = [NNInfiltration_85flux, NNSGWSeepage_85flux, NNInputWR_85flux,...
    NNOutputWR_85flux, NNOcnExport_85flux, NNLandRunoff_85flux,...
    NNStreamDischarge_85flux, NNSedInputWR_85flux, NNSedInputKS_85flux];


% Ammonia fluxes
AmmInfiltration_initflux = AmmoniaPrecip*(IP45_data.Infiltration(2,1)-
IP45_data.Infiltration(1,1));
AmmSGWSeepage_initflux = (IP45_data.AmmGW(2,1)+IP45_data.AmmGW(1,1)).*...
    (IP45_data.SGWSeepage(2,1)-IP45_data.SGWSeepage(1,1))./...
    (IP45_data.GW(2,1)+IP45_data.GW(1,1));
AmmInputWR_initflux = AmmoniaPrecip*(IP45_data.InputWR(2,1)-
IP45_data.InputWR(1,1));
AmmOutputWR_initflux = (IP45_data.AmmWR(2,1)+IP45_data.AmmWR(1,1)).*...
    (IP45_data.OutputWR(2,1)-IP45_data.OutputWR(1,1))./...
    (IP45_data.WR(2,1)+IP45_data.WR(1,1));
AmmOcnExport_initflux = (IP45_data.AmmKB(2,1)+IP45_data.AmmKB(1,1)).*...
    (IP45_data.OcnExport(2,1)-IP45_data.OcnExport(1,1))./...
    (IP45_data.KB(2,1)+IP45_data.KB(1,1));
AmmLandRunoff_initflux = AmmoniaPrecip*NPland*(Precip45(end)+Precip45(end-
1))/2;
AmmStreamDischarge_initflux =
AmmoniaPrecip*NPland*(Precip45(end)+Precip45(end-1))/2 + ...
    AmmOutputWR_initflux;
AmmSedInputWR_initflux = SoilContentAmmonia*(IP45_data.SedInputWR(2,1)-
IP45_data.SedInputWR(1,1));
AmmSedInputKS_initflux = FreshWaterReleaseAmmonia*(IP45_data.SedInputKS(2,1)-
IP45_data.SedInputKS(1,1));

Amm_initflux = [AmmInfiltration_initflux, AmmSGWSeepage_initflux,
AmmInputWR_initflux,...
    AmmOutputWR_initflux, AmmOcnExport_initflux, AmmLandRunoff_initflux,...
    AmmStreamDischarge_initflux, AmmSedInputWR_initflux,
AmmSedInputKS_initflux];

AmmInfiltration_45flux = AmmoniaPrecip*(IP45_data.Infiltration(end,1)-
IP45_data.Infiltration(end-1,1));
AmmSGWSeepage_45flux = (IP45_data.AmmGW(end,1)+IP45_data.AmmGW(end-1,1)).*...
    (IP45_data.SGWSeepage(end,1)-IP45_data.SGWSeepage(end-1,1))./...
    (IP45_data.GW(end,1)+IP45_data.GW(end-1,1));
AmmInputWR_45flux = AmmoniaPrecip*(IP45_data.InputWR(end,1)-
IP45_data.InputWR(end-1,1));
AmmOutputWR_45flux = (IP45_data.AmmWR(end,1)+IP45_data.AmmWR(end-1,1)).*...
    (IP45_data.OutputWR(end,1)-IP45_data.OutputWR(end-1,1))./...
    (IP45_data.WR(end,1)+IP45_data.WR(end-1,1));
AmmOcnExport_45flux = (IP45_data.AmmKB(end,1)+IP45_data.AmmKB(end-1,1)).*...
```

```
    (IP45_data.OcnExport(end,1)-IP45_data.OcnExport(end-1,1))./...
    (IP45_data.KB(end,1)+IP45_data.KB(end-1,1));
AmmLandRunoff_45flux = AmmoniaPrecip*NPland*(Precip45(end)+Precip45(end-
1))/2;
AmmStreamDischarge_45flux = AmmoniaPrecip*NPland*(Precip45(end)+Precip45(end-
1))/2 + ...
    AmmOutputWR_45flux;
AmmSedInputWR_45flux = SoilContentAmmonia*(IP45_data.SedInputWR(end,1)-
IP45_data.SedInputWR(end-1,1));
AmmSedInputKS_45flux = FreshWaterReleaseAmmonia*(IP45_data.SedInputKS(end,1)-
IP45_data.SedInputKS(end-1,1));

Amm_45flux = [AmmInfiltration_45flux, AmmSGWSeepage_45flux,
AmmInputWR_45flux,...
    AmmOutputWR_45flux, AmmOcnExport_45flux, AmmLandRunoff_45flux,...
    AmmStreamDischarge_45flux, AmmSedInputWR_45flux, AmmSedInputKS_45flux];

AmmInfiltration_85flux = AmmoniaPrecip*(IP85_data.Infiltration(end,1)-
IP85_data.Infiltration(end-1,1));
AmmSGWSeepage_85flux = (IP85_data.AmmGW(end,1)+IP85_data.AmmGW(end-1,1)).*...
    (IP85_data.SGWSeepage(end,1)-IP85_data.SGWSeepage(end-1,1))./...
    (IP85_data.GW(end,1)+IP85_data.GW(end-1,1));
AmmInputWR_85flux = AmmoniaPrecip*(IP85_data.InputWR(end,1)-
IP85_data.InputWR(end-1,1));
AmmOutputWR_85flux = (IP85_data.AmmWR(end,1)+IP85_data.AmmWR(end-1,1)).*...
    (IP85_data.OutputWR(end,1)-IP85_data.OutputWR(end-1,1))./...
    (IP85_data.WR(end,1)+IP85_data.WR(end-1,1));
AmmOcnExport_85flux = (IP85_data.AmmKB(end,1)+IP85_data.AmmKB(end-1,1)).*...
    (IP85_data.OcnExport(end,1)-IP85_data.OcnExport(end-1,1))./...
    (IP85_data.KB(end,1)+IP85_data.KB(end-1,1));
AmmLandRunoff_85flux = AmmoniaPrecip*NPland*(Precip85(end)+Precip85(end-
1))/2;
AmmStreamDischarge_85flux = AmmoniaPrecip*NPland*(Precip85(end)+Precip85(end-
1))/2 + ...
    AmmOutputWR_85flux;
AmmSedInputWR_85flux = SoilContentAmmonia*(IP85_data.SedInputWR(end,1)-
IP85_data.SedInputWR(end-1,1));
AmmSedInputKS_85flux = FreshWaterReleaseAmmonia*(IP85_data.SedInputKS(end,1)-
IP85_data.SedInputKS(end-1,1));

Amm_85flux = [AmmInfiltration_85flux, AmmSGWSeepage_85flux,
AmmInputWR_85flux,...
    AmmOutputWR_85flux, AmmOcnExport_85flux, AmmLandRunoff_85flux,...
    AmmStreamDischarge_85flux, AmmSedInputWR_85flux, AmmSedInputKS_85flux];
```

Appendix 5.3.5 SKWANEM Model Code: Data Save File

```
%SKOANEM:Southern Kāne‘ohe Offshore and Watershed Nutrient Export Model
clear all

curdir = pwd;

% cd('c:\Users\Sara\Desktop')

global GW WR KB NPland NPOcean kgw kwr PPrecip NNPrecip AmmoniaPrecip...
    k1 k2 k3 k4 Precip0

global CO2run
global Preciprun

%Load steady state and forcing data
%Steady state data
SS_data = csvread('SteadyStateValues.csv',1,1);
CO2SS = SS_data(:,1);
PrecipSS = SS_data(:,2);
KBSS = SS_data(:,3);
Precip0 = PrecipSS(1);

%RCP 4.5 forcing data
Forcing45_data = csvread('IPCCforcings45.csv',1,1);
CO245 = Forcing45_data(:,1);
Precip45 = Forcing45_data(:,2);
KB45 = Forcing45_data(:,3);

%RCP 8.5 forcing data
Forcing85_data = csvread('IPCCforcings85.csv',1,1);
CO285 = Forcing85_data(:,1);
Precip85 = Forcing85_data(:,2);
KB85 = Forcing85_data(:,3);

%Water Fluxes
NPland=1.28e7;                  %Flux of net precip into watershed in m^3/yr
NPOcean=9.47e6;                 %Flux of net precip into Southern Bay in
m^3/yr
Infiltration=NPland*(2.98/12.8);    %Flux of Infiltration through land surface
InputWR=NPland*(8.8/12.8);            %Flux of input to Waimaluhia Reservoir
LandRunoff=NPland*(1.02/12.8);      %Flux of runoff from land surface
OutputWR=kwr*WR;                %Flux of output from Waimaluhia Reservoir
StreamDischarge=LandRunoff+OutputWR;   %Flux of stream water entering ocean
SGWSeepage=kgw*GW;              %Flux of ground water entering ocean

%First run at steady state for 85 years
CO2run=CO2SS;
Preciprun=PrecipSS;
KB = KBSS;

%Reservoirs
GW=1.13e10;                     %Groundwater Reservoir volume in m^3
WR=2.1e5;                       %Waimaluhia Reservoir volume in m^3
% KB=79.59e6;                     %Southern Kāne‘ohe Bay volume in m^3
```

```
%Rate constants for steady state first order fluxes
kgw=(2.98e6)/(1.13e10);                 %rate constant for SGWSeepage flux
kwr=(8.8e6)/(2.1e5);                    %rate constant for OutputWR flux

%Nutrient concentrations from experiments and literature
%multiply each value by 1000 to convert from \mumol/L to \mumol/m^3 and by
%volume to get mass in \mumol
PPrecip=0;                          %Precipitation phosphate mass
PWR=0.6 * 1000 * WR;                %Waimaluhia Reservoir phosphate mass
PGW=1.5 * 1000 * GW;                %Groundwater phosphate mass
PKB=0.07 *1000 * KB(1);                %Kāne‘ohe Bay phosphate mass

NNPrecip=3.6 * 1000;              %Precipitation N+N mass
NNWR=20.8 * 1000 * WR;                %Waimaluhia Reservoir N+N mass
NNGW=10 * 1000 * GW;                %Groundwater N+N mass
NNKB=0.19 * 1000 * KB(1);                %Kāne‘ohe Bay N+N mass

AmmoniaPrecip=0.05 * 1000;          %Precipitation Ammonia mass
AmmoniaWR=2.5 * 1000 * WR;          %Waimaluhia Reservoir Ammonia mass
AmmoniaGW=10 * 1000 * GW;           %Groundwater Ammonia mass
AmmoniaKB=0.1 * 1000 * KB(1);          %Kāne‘ohe Bay Ammonia mass


%%%%%%%%%%%%%%%%%%%Suspended Sediment stuff%%%%%%%%%%%%%%%%%%%%%%%%%%%%

%Values to relate suspended sediment value to water value (based on steady
%state)

%Atmospheric CO2 content of atmosphere at t0 (in ppmv)
ACO20=399;
ACO2=399;

%Fco2 equation
FCO2=1.0+0.252*log(ACO2/ACO20) + 0.0156*(log(ACO2/ACO20))^2;

%Suspended sediment to WR
k1=1.25*10^-4 * FCO2;

%Suspended sediment to KS
k2=9.31*10^-4 * FCO2;

%Suspended sediment out of WR
k3=2.27*10^-7 * FCO2;

%Suspended Sdiment KS to KBay
k4=9.8*10^-5 * FCO2;

%Sediment Nutrient release relationships
global SoilContentP SoilContentNN SoilContentAmmonia FreshWaterReleaseP ...
    FreshWaterReleaseNN FreshWaterReleaseAmmonia

global ResSedRelease
ResSedRelease = 1;

%Soil Analysis values
%lab values reported in ug/g
```

```
%multiply by mw and 10^6 g/metric tons to get correct units
%mw in g/mol
%final product in \mumol/metric tons
SoilContentP=6 * 10^6 * (1/30.974);                 %phosporous mw
SoilContentNN=15 * 10^6 * (1/62.0049);              %nitrate mw
SoilContentAmmonia=1.4 * 10^6 * (1/18.03846);       %ammonium mw

%Nutrient Release Experiment Values
%experimental values in \mumol/L
%multiply by 10^6g/metric tons to convert g to metric tons
%multiply by 1L/1g since those were experimental conditions
%final product is \mumol/metric tons
FreshWaterReleaseP=0.05 * 10^6;
FreshWaterReleaseNN= 15.2 * 10^6;
FreshWaterReleaseAmmonia= 234 * 10^6;

%%%%%%%%%%%%%%%%%%%%%%%%end Susp. Sediment%%%%%%%%%%%%%%%%%%%%%%%%%%%%%%%%

%Inital reservoir volumes of GW, WR, KB and nutrient concentrations
y0=[GW WR KB(1) PGW PWR PKB NNGW NNWR NNKB AmmoniaGW AmmoniaWR AmmoniaKB,...
    0 0 0 0 0 0 0];


%Time span 2015-2100
tspan=[1:85];

% solve the problem using ODE45
[t, Y] = ode23(@MassBalance_derivs, tspan, y0);

steadyruns = 10;
for s = 1:steadyruns
    s
y0=[GW WR KB(1) Y(end,4) Y(end,5) Y(end,6) Y(end,7) Y(end,8) Y(end,9)...
    Y(end,10) Y(end,11) Y(end,12),...
    0 0 0 0 0 0 0];
% y0=[GW WR KB 0 0 0 0 0 0 0 0 0];
clear t, clear Y
%Time span 2015-2010
tspan=[1:85];

% solve the problem using ODE45
[t, Y] = ode23(@MassBalance_derivs, tspan, y0);
end

%Now change scenario
CO2run=CO285;
Preciprun=Precip85;
KB = KB85;

%Inital reservoir volumes of GW, WR, KB and nutrient concentrations
y0=[GW WR KB(1) Y(end,4) Y(end,5) Y(end,6) Y(end,7) Y(end,8) Y(end,9)...
    Y(end,10) Y(end,11) Y(end,12),...
    0 0 0 0 0 0 0];
% y0=[GW WR KB 0 0 0 0 0 0 0 0 0];
clear t, clear Y
%Time span 2015-2010
tspan=[1:85];
```

```
% solve the problem using ODE45
[t, Y] = ode23(@MassBalance_derivs, tspan, y0);

GWdata = Y(:,1);
WRdata = Y(:,2);
KBdata = Y(:,3);
PGWdata = Y(:,4);
PWRdata = Y(:,5);
PKBdata = Y(:,6);
NNGWdata = Y(:,7);
NNWRdata = Y(:,8);
NNKBdata = Y(:,9);
AmmGWdata = Y(:,10);
AmmWRdata = Y(:,11);
AmmKBdata = Y(:,12);
Infiltration = Y(:,13);
SGWSeepage = Y(:,14);
InputWR = Y(:,15);
OutputWR = Y(:,16);
OcnExport = Y(:,17);
SedInputWR = Y(:,18);
SedInputKS = Y(:,19);
%%
SS_data = fullfile(curdir,'IP85_data.mat');
matobj = matfile(SS_data,'Writable',true);

matobj.GW = GWdata;
matobj.WR = WRdata;
matobj.KB = KBdata;
matobj.PGW = PGWdata;
matobj.PWR = PWRdata;
matobj.PKB = PKBdata;
matobj.NNGW = NNGWdata;
matobj.NNWR = NNWRdata;
matobj.NNKB = NNKBdata;
matobj.AmmGW = AmmGWdata;
matobj.AmmWR = AmmWRdata;
matobj.AmmKB = AmmKBdata;
matobj.Infiltration = Infiltration;
matobj.SGWSeepage = SGWSeepage;
matobj.InputWR = InputWR;
matobj.OutputWR = OutputWR;
matobj.OcnExport = OcnExport;
matobj.SedInputWR = SedInputWR;
matobj.SedInputKS = SedInputKS;
```

Appendix 5.3.6 SKWANEM Model Code: Temperature-Precipitation Sensitivity Analysis

```
%RCP 8.5 forcing data
Forcing85_data = csvread('IPCCforcings85.csv',1,1);
CO285 = Forcing85_data(:,1);
Precip85 = Forcing85_data(:,2);
KB85 = Forcing85_data(:,3);

Forcing45_data = csvread('IPCCforcings45.csv',1,1);
CO245 = Forcing45_data(:,1);
Precip45 = Forcing45_data(:,2);
KB45 = Forcing45_data(:,3);


Preciprun = Precip85;
CO2run = CO285;
time = [2015:2014+length((Preciprun))];
Precip0 = Preciprun(1);

% Forcing constants
NPland=1.28e7;                  %Flux of net precip into watershed in m^3/yr
NPOcean=9.47e6;                 %Flux of net precip into Southern Bay in
m^3/yr
ACO20=399;

for tCO2 = 1:length(time)
    %Atmospheric CO2 content of atmosphere at t0 (in ppmv)
    ACO2=CO2run(tCO2);

    %Fco2 equation
    FCO2=1.0+0.252*log(ACO2/ACO20) + 0.0156*(log(ACO2/ACO20))^2;

    %Suspended sediment to WR
    k1=1.25*10^-4 * FCO2;

    %Suspended sediment to KS
    k2=9.31*10^-4 * FCO2;

    for tPre = 1:length(time)
        Pland = NPland * Preciprun(tPre);
        POcean = NPOcean * Preciprun(tPre);

        sed_lin_fac = 0.6507; %Linear rate of change (dsed/dx)/dsed0

        InputWR=Pland*(8.8/12.8);                       %Flux of input to
Waimaluhia Reservoir
        InputWR0 = NPland * Precip0 * (8.8/12.8);
        LandRunoff=Pland*(1.02/12.8);                   %Flux of runoff from
land surface
        LandRunoff0 = NPland * Precip0 * (1.02/12.8);


        SedInputWR(tCO2,tPre) = k1*InputWR0*(1 + sed_lin_fac*(InputWR -
InputWR0)/InputWR0);
```

```
        SedInputKS(tCO2,tPre) = k2*LandRunoff0*(1 + sed_lin_fac*(LandRunoff -
LandRunoff0)/LandRunoff0);
    end
end


%%
offset = -5;
xposmin = 0.1;
yposmin = 0.125;
height = 0.825;
width = 0.85;
width2 = 0.4;
xoffset = 0.1;
yoffset = 0.1;


figure
set(gcf, 'Units','inches', 'Position',[0 0 8 6])
set(gcf, 'PaperPositionMode','auto')
% subplot('Position',[xposmin yposmin+yoffset+height width height])
subplot('Position',[xposmin yposmin width height])
pcolor(NPland*Preciprun*1e-7,CO2run,SedInputWR)
hold on
[C,h] = contour(NPland*Preciprun*1e-
7,CO2run,SedInputWR,[950:50:1400],'k','LineWidth',2);
clabel(C,h)
h1 = plot(NPland*Preciprun*1e-7,CO2run,'r',NPland*Precip45*1e-
7,CO245,'m','LineWidth',2);
legend([h1(1),h1(2)],'RCP 8.5','RCP 4.5')
hold off
shading interp
set(gca,'FontSize',14)
xlabel('Precipitation (10^7 m^3/yr)')
ylabel('CO_2 (ppmv)')
colorbar
title('Sediment Input in Waimaluhia Reservoir (tons/year)')
```

Appendix 5.3.7 SKWANEM Model Code: Groundwater Sensitivity Analysis

```
%SKOANEM:Southern Kāne‘ohe Offshore and Watershed Nutrient Export Model
clear all

curdir = pwd;

% cd('c:\Users\Sara\Desktop')

global GW WR KB NPland NPOcean kgw kwr PPrecip NNPrecip AmmoniaPrecip...
    k1 k2 k3 k4 Precip0

global CO2run
global Preciprun

%Load steady state and forcing data
%Steady state data
SS_data = csvread('SteadyStateValues.csv',1,1);
CO2SS = SS_data(:,1);
PrecipSS = SS_data(:,2);
KBSS = SS_data(:,3);

%RCP 4.5 forcing data
Forcing45_data = csvread('IPCCforcings45.csv',1,1);
CO245 = Forcing45_data(:,1);
Precip45 = Forcing45_data(:,2);
KB45 = Forcing45_data(:,3);

%RCP 8.5 forcing data
Forcing85_data = csvread('IPCCforcings85.csv',1,1);
CO285 = Forcing85_data(:,1);
Precip85 = Forcing85_data(:,2);
KB85 = Forcing85_data(:,3);

%Water Fluxes
NPland=1.28e7;                  %Flux of net precip into watershed in m^3/yr
NPOcean=9.47e6;                 %Flux of net precip into Southern Bay in
m^3/yr
Infiltration=NPland*(2.98/12.8);    %Flux of Infiltration through land surface
InputWR=NPland*(8.8/12.8);            %Flux of input to Waimaluhia Reservoir
LandRunoff=NPland*(1.02/12.8);      %Flux of runoff from land surface
OutputWR=kwr*WR;                %Flux of output from Waimaluhia Reservoir
StreamDischarge=LandRunoff+OutputWR;    %Flux of stream water entering ocean
SGWSeepage=kgw*GW;              %Flux of ground water entering ocean

%First run at steady state for 85 years
CO2run=CO2SS;
Preciprun=PrecipSS;
Precip0 = Preciprun(1);
KB = KB85;

%Reservoirs
GW0=1.13e10;                     %Groundwater Reservoir volume in m^3
WR=2.1e5;                       %Waimaluhia Reservoir volume in m^3
% KB=79.59e6;                     %Southern Kāne‘ohe Bay volume in m^3
```

```
%Rate constants for steady state first order fluxes
kgw=(2.98e6)/(1.13e10);                 %rate constant for SGWSeepage flux
kwr=(8.8e6)/(2.1e5);                    %rate constant for OutputWR flux

%Nutrient concentrations from experiments and literature
%multiply each value by 1000 to convert from \mumol/L to \mumol/m^3 and by
%volume to get mass in \mumol
PPrecip=0;                          %Precipitation phosphate mass
PWR=0.6 * 1000 * WR;                %Waimaluhia Reservoir phosphate mass
PGW0=1.5 * 1000 * GW0;                %Groundwater phosphate mass
PKB=0.07 *1000 * KB(1);                %Kāne‘ohe Bay phosphate mass

NNPrecip=3.6 * 1000;              %Precipitation N+N mass
NNWR=20.8 * 1000 * WR;              %Waimaluhia Reservoir N+N mass
NNGW0=10 * 1000 * GW0;                %Groundwater N+N mass
NNKB=0.19 * 1000 * KB(1);              %Kāne‘ohe Bay N+N mass

AmmoniaPrecip=0.05 * 1000;          %Precipitation Ammonia mass
AmmoniaWR=2.5 * 1000 * WR;          %Waimaluhia Reservoir Ammonia mass
AmmoniaGW0=10 * 1000 * GW0;           %Groundwater Ammonia mass
AmmoniaKB=0.1 * 1000 * KB(1);          %Kāne‘ohe Bay Ammonia mass


%%%%%%%%%%%%%%%%%%%Suspended Sediment%%%%%%%%%%%%%%%%%%%%%%%%%%%%

%Values to relate suspended sediment value to water value (based on steady
%state)

%Atmospheric CO2 content of atmosphere at t0 (in ppmv)
ACO20=399;
ACO2=399;

%Fco2 equation
FCO2=1.0+0.252*log(ACO2/ACO20) + 0.0156*(log(ACO2/ACO20))^2;

%Suspended sediment to WR
k1=1.25*10^-4 * FCO2;

%Suspended sediment to KS
k2=9.31*10^-4 * FCO2;

%Suspended sediment out of WR
k3=2.27*10^-7 * FCO2;

%Suspended Sdiment KS to KBay
k4=9.8*10^-5 * FCO2;

%Sediment Nutrient release relationships
global SoilContentP SoilContentNN SoilContentAmmonia FreshWaterReleaseP ...
    FreshWaterReleaseNN FreshWaterReleaseAmmonia

global ResSedRelease
ResSedRelease = 1;

%Soil Analysis values
%lab values reported in ug/g
```

```
%multiply by mw and 10^6 g/metric tons to get correct units
%mw in g/mol
%final product in \mumol/metric tons
SoilContentP=6 * 10^6 * (1/30.974);                 %phosporous mw
SoilContentNN=15 * 10^6 * (1/62.0049);              %nitrate mw
SoilContentAmmonia=1.4 * 10^6 * (1/18.03846);       %ammonium mw

%Nutrient Release Experiment Values
%experimental values in \mumol/L
%multiply by 10^6g/metric tons to convert g to metric tons
%multiply by 1L/1g since those were experimental conditions
%final product is \mumol/metric tons
FreshWaterReleaseP=0.05 * 10^6;
FreshWaterReleaseNN= 15.2 * 10^6;
FreshWaterReleaseAmmonia= 234 * 10^6;


%%%%%%%%%%%%%%%%%%%%%%%%end Suspended Sediment%%%%%%%%%%%%%%%%%%%%%%%%%%%%%%%%

%% Define range of groundwater initial concentrations to test
GWs = [0.1:0.1:2]*GW0;
res_nums = length(GWs);

PGWs = [0.1:0.1:2]*PGW0;
NNGWs = [0.1:0.1:2]*NNGW0;
AmmoniaGWs = [0.1:0.1:2]*AmmoniaGW0;
conc_nums = length(PGWs);

%Time span 2015-2100
tspan=[1:85];

for r = 1:res_nums
    GW = GWs(r);
    r
    for c = 1:conc_nums

    %Run to steady state
    CO2run=CO2SS;
    Preciprun=PrecipSS;
    KB = KBSS;



    %Inital reservoir volumes of GW, WR, KB and nutrient concentrations
    y0=[GW WR KB(1) PGWs(c) PWR PKB NNGWs(c) NNWR NNKB AmmoniaGWs(c)
AmmoniaWR AmmoniaKB,...
        0 0 0 0 0 0 0];
%     y0=[GW WR KB(1) Y(end,4) Y(end,5) Y(end,6) Y(end,7) Y(end,8)
Y(end,9)...
%     Y(end,10) Y(end,11) Y(end,12),...
%     0 0 0 0 0 0 0];

    % solve the problem using ODE45
    [t, Y] = ode23(@MassBalance_derivs, tspan, y0);

    %Now change scenario
    CO2run=CO285;
```

```
    Preciprun=Precip85;
    KB = KB85;

    %Inital reservoir volumes of GW, WR, KB and nutrient concentrations
    y0=[GW WR KB(1) Y(end,4) Y(end,5) Y(end,6) Y(end,7) Y(end,8) Y(end,9)...
        Y(end,10) Y(end,11) Y(end,12),...
        0 0 0 0 0 0 0];
    % y0=[GW WR KB 0 0 0 0 0 0 0 0 0];
    clear t, clear Y
    %Time span 2015-2010
    tspan=[1:85];

    % solve the problem using ODE45
    [t, Y] = ode23(@MassBalance_derivs, tspan, y0);

    PKBend(c,r) = Y(end,6);
    NNKBend(c,r) = Y(end,9);
    AmmoniaKBend(c,r) = Y(end,12);
    end
end

%%
%%%%%%%%%%%%%%%%%%%%%%%%%%%%PLOTS%%%%%%%%%%%%%%%%%%%%%%%%%%%%%%%%%%%%%%%%%%%
fignum = 0;
%%%%%%%%%%%%%%%%%%%%%%%%%%%MASS PLOTS%%%%%%%%%%%%%%%%%%%%%%%%%%%%%%%%%%%%%%%
 xposmin = 0.1;
 yposmin = 0.1;
 width = 0.8;
 height = 0.2125;
 xoffset = 0.075;
 yoffset = 0.1;

fignum = fignum + 1;
filename = ['fig',num2str(fignum)];
eval([filename,'=figure(',num2str(fignum),');'])

 set(gcf, 'Units', 'inches', 'Position', [0 0 6.5 9])
 set(gcf, 'PaperPositionMode', 'auto')

 subplot('Position',[xposmin yposmin+2*(yoffset+height) width height])
 pcolor(100*GWs/GW0,100*PGWs/PGW0,100*PKBend/PKBend(10,10))
 xlabel('% of GW_0'), ylabel('% of P_{GW0}')
 title('Sensitivity of model to initial groundwater phosphate')
 colorbar,caxis([0 250])

 subplot('Position',[xposmin yposmin+(yoffset+height) width height])
 pcolor(100*GWs/GW0,100*NNGWs/NNGW0,100*NNKBend/NNKBend(10,10))
 xlabel('% of GW_0'), ylabel('% of NN{GW0}')
 title('Sensitivity of model to initial groundwater nitrate')
 colorbar,caxis([50 150])

 subplot('Position',[xposmin yposmin width height])

pcolor(100*GWs/GW0,100*AmmoniaGWs/AmmoniaGW0,100*AmmoniaKBend/AmmoniaKBend(10
,10))
 xlabel('% of GW_0'), ylabel('% of Ammonia{GW0}')
 title('Sensitivity of model to initial groundwater ammonia')
```

```
colorbar,caxis([80 130])

print('-dpng','-r150',[filename,'_sensitivity.png'])
```